DOCTORAL DISSERTATION

Impacts of Various Building Parameters on Energy Consumption of Traditional Dwellings in East and Central China

CHI Fang'ai

2016DBB405

September, 2019

Graduate School of Environmental Engineering

Bart Dewancker Lab

The University of Kitakyushu (Kitakyushu, Japan)

Contents

Contents.....I

List of figures..... IX

List of tables.....XV

Nomenclature.....XVII

Abstract..... XIX

Keywords..... XX

Chapter 1 Research background

1.1 Determination of study subject..... 1

1.1.1 Substantial quantity of population in countryside and relatively low urbanization rate in China... 1

1.1.2 Increasing trend of the average rural residential building area per capita.....1

1.1.3 Increase of energy consumption and electricity use in the rural residences.....2

1.1.3.1 Increase of energy consumption in the rural residences.....2

1.1.3.2 Ascending of electricity use in the rural residences..... 3

1.1.4 Attaching importance to protection of the traditional dwellings in countryside.....4

1.1.4.1 Increasing quantity of the traditional dwellings recorded in the Chinese Traditional Villages' Catalogs..... 4

1.1.4.2 Advantages of the traditional buildings on climate adaptation..... 5

1.1.5 Research subject determination.....6

1.2 Determination of research site.....6

1.2.1 Substantial quantity of villages in East and Central China.....7

1.2.2 Substantial quantity of traditional villages recorded in the Catalogs situated in East and Central China.....7

1.2.3 Developed economy and high electricity use in East and Central China.....9

1.2.4 Complicated energy consumption pattern of buildings in East and Central China.....9

1.2.5 Research region..... 10

1.3 Scientific originality of the study..... 12

1.4 Research flow..... 12

References.....14

Chapter 2 Literature review

2.1 Passive climate-responsive strategies in traditional dwellings..... 15

2.2 Impact of building azimuth on the energy consumption..... 16
2.2.1 Impact of the building orientation on the energy consumption.....16
2.2.2 Impact of the building orientation on the natural ventilation..... 17
2.2.3 Impact of the building orientation on the natural daylighting..... 17
2.2.4 Discussion.....18
2.3 Impact of shading devices with various shading depth and building azimuth combinations on the energy consumption.....19
2.3.1 Impact of the movable shading device on the energy consumption.....19
2.3.2 Impact of the fixed shading device on the energy consumption..... 20
2.3.3 Impact of the external shading device on the energy consumption.....20
2.3.4 Impact of the internal shading device on the energy consumption..... 21
2.3.5 Impact of the shading devices' orientation on the energy consumption..... 22
2.3.6 Discussion.....22
2.4 Impact of shading devices with various window-to-wall ratio and building azimuth combinations on the energy consumption.....23
2.4.1 Impact of the climate condition on the optimum window-to-wall ratio.....23
2.4.2 Impact of the building orientation on the optimum window-to-wall ratio.....24
2.4.3 Impact of the building energy cost on the optimum window-to-wall ratio.....25
2.4.4 Discussion.....26
2.5 Impacts of walls with various construction type and building azimuth combinations on the energy consumption.....26
2.5.1 Optimum thermal insulation thickness in wall based on the criteria of energy consumption..... 26
2.5.2 Thermal performance of wall expressed by means of parameters..... 27
2.5.3 Thermal performance of Trombe wall characterized by passive heating.....28
2.5.4 Discussion.....29
References.....30
Chapter 3 Research methodology and research content
3.1 Determination of study building..... 40
3.2 Building model's dimensions used in simulation..... 40
3.3 Division of building azimuth interval..... 43
3.4 Division of shading depth interval..... 44
3.5 Division of window-to-wall ratio interval.....46
3.6 Description of various passive cooling wall types used in simulation..... 47
3.7 Design day data assumed in simulation..... 49

3.8 Selection of simulation tool....50
Appendixes....51
Appendix 1 Software used in this study....51
Appendix 2 Measurement instruments used in this study....51
References....52
Chapter 4 Investigation of the traditional dwellings' characteristics in East and Central China
4.1 Introduction....53
4.1.1 Motivation....53
4.1.2 Scientific originality....54
4.1.3 Purpose of the work....54
4.2 Research content and research methods framework....55
4.2.1 Theoretical foundations for this work....55
4.2.2 Field investigation for the traditional dwellings....55
4.2.3 In-situ measurement for the traditional dwellings....56
4.2.3.1 Description of in-situ measurement position and testing time....56
4.2.3.2 Distribution of measurement points in the traditional dwelling....56
4.2.3.3 Description of measurement tools used in this work....57
4.2.4 Dynamic simulation for the traditional dwellings....57
4.3 Descriptions of study building and climatic features....58
4.3.1 Description of study building (Thousand Pillars Dwelling)....58
4.3.2 Description of local climatic features....59
4.4 Field investigation for the traditional dwelling of Thousand Pillar Dwelling....60
4.4.1 Passive strategies of climate adaptation in traditional dwelling of Thousand Pillar Dwelling....60
4.4.2 Passive elements in the traditional dwelling of Thousand Pillar Dwelling....61
4.4.2.1 Passive strategy used in Wall of traditional dwelling....61
4.4.2.2 Passive strategy used in Roof and waist eave of traditional dwelling....65
4.4.2.3 Passive strategy used in Flooring of traditional dwelling....68
4.4.2.4 Passive strategy used in Door and window of traditional dwelling....69
4.4.3 Passive spaces in the traditional dwelling of Thousand Pillar Dwelling....73
4.4.3.1 Passive strategy used in patio of traditional dwelling....73
4.4.3.2 Passive strategy used in Corridor of traditional dwelling....75
4.4.3.3 Passive strategy used in Open-hall of traditional dwelling....77
4.5 In-situ measurement for the traditional dwellings of Thousand Pillar Dwelling....79
4.5.1 Air temperature measurement for traditional dwelling....79

4.5.2 Relative humidity measurement for traditional dwelling..... 80
4.5.3 Air velocity measurement for traditional dwelling..... 82
4.5.4 Illuminance measurement for traditional dwelling..... 83
4.6 Environment simulation for the traditional dwellings of Thousand Pillar Dwelling..... 83
4.7 Finding and discussion..... 89
References..... 92
Chapter 5 Impact of building azimuth on the energy consumption
5.1 Introduction..... 95
5.1.1 Motivation..... 95
5.1.2 Research content..... 96
5.1.3 Scientific originality..... 96
5.1.4 Research purpose..... 97
5.2 Description of simulation tool and research flow..... 97
5.2.1 Division of dwelling subdomain for Sizhai village..... 97
5.2.2 Measurement method of building azimuth for dwelling..... 98
5.2.3 Research flow descriptions..... 98
5.3 Impact of building azimuth on the electricity consumption..... 99
5.3.1 Indoor temperature and electricity consumption of air conditioning with varying building azimuth..... 99
5.3.1.1 Air temperature in the internal space with varying building azimuth..... 99
5.3.1.2 Impact of building azimuth on the energy consumption of air conditioning..... 101
5.3.2 Indoor air velocity and electricity consumption of electrical ventilation with varying building azimuth..... 102
5.3.2.1 Natural ventilation in the internal space with varying building azimuth..... 102
5.3.2.2 Impact of BA on the energy consumption of electrical ventilation..... 104
5.3.3 Indoor daylighting and electricity consumption of artificial lighting with varying building azimuth..... 105
5.3.3.1 Daylighting in the internal space with varying building azimuth..... 105
5.3.3.2 Impact of BA on the energy consumption of artificial lighting..... 106
5.4 Total annual electricity consumption and CO_2 emission..... 108
5.5 Validation of computational results: simulation tool versus real bills..... 109
5.6 Frequency distribution characteristics of BAs in Sizhai..... 112
5.6.1 Type classification of dwelling subdomain..... 112
5.6.1.1 Definition of the main uni-directional subdomain type..... 112

5.6.1.2 Definition of the main bi-directional subdomain type....113
5.6.1.3 Definition of the multi-directional subdomain type....113
5.6.2 Factors of impacting three dwelling subdomain types....113
5.6.2.1 Factors of impacting main uni-directional subdomain....113
5.6.2.2 Factors of impacting main bi-directional subdomain....114
5.6.2.3 Factors of impacting multi-directional subdomain....114
5.6.3 Building azimuth frequency distribution and assessment of energy saving potential for Sizhai village....114
5.7 Finding and discussion....117
References....119
Chapter 6 Impact of shading devices with various shading depth and building azimuth combinations on the energy consumption
6.1 Introduction....123
6.1.1 Motivation....123
6.1.2 Scientific originality....124
6.1.3 Research purpose....125
6.2 Research process and research flow....125
6.3 Impact of shading depth on SHGC and MSWR based on changes in building azimuth....127
6.3.1 Impact of shading devices with different orientations on SHGCs for windows....128
6.3.2 Impact of shading devices with different orientations on MSWRs for windows....128
6.3.3 Equation formulation of shading-to-window ratio....129
6.3.3.1 When $H_3<H_2$....130
6.3.3.2 When $H_3>H_2$....130
6.3.4 Validation of shading-to-window ratio: software versus equation....131
6.4 Impact of shading depth on the indoor daylighting and artificial lighting energy consumption based on changes in building azimuth....132
6.4.1 Impact of shading devices with different orientations on the solar radiation reception levels for windows....132
6.4.2 Impact of shading devices with different orientations on the mean indoor illuminance....133
6.4.3 Validation of illuminance data: simulation tool versus field measurements....134
6.4.4 Impact of shading devices with different orientations on the energy consumption of artificial lighting....135
6.5 Impact of shading depth on the indoor temperature and air conditioning energy cost....136
6.5.1 Impact of shading devices with different orientations on the indoor solar heat gain....137

6.5.2 Impact of shading devices with different orientations on the indoor temperature..... 137
6.5.3 Validation of air temperature data: simulation tool versus in-situ measurements..... 139
6.5.4 Impact of shading devices with different orientations on the energy consumption of air conditioning..... 139
6.6 Total energy consumption including artificial lighting and air conditioning..... 141
6.7 Validation of the energy consumption data: simulation tool versus real bills..... 143
6.7.1 Energy consumption in the real traditional dwellings obtained from bills..... 143
6.7.2 Comparison of total energy consumption obtained from simulation tool and bills..... 145
6.8 Optimal shading depths recommended for the 18 building azimuth intervals based on the energy consumption and Daylighting Standard..... 146
6.8.1 Daylight factor corresponding to 10 shading depths..... 146
6.8.2 Recommendation of the optimal shading depth to each building azimuth interval..... 147
6.9 Application of the research results..... 147
6.9.1 Definition of evaluation score of shading depth..... 147
6.9.2 Application of the evaluation score of shading depth to three courtyard dwellings..... 148
6.10 Finding and discussion..... 150
References..... 152
Chapter 7 Impact of windows with various window-to-wall ratio and building azimuth combinations on the energy consumption
7.1 Introduction..... 156
7.1.1 Motivation..... 156
7.1.2 Scientific originality..... 157
7.1.3 Research purpose..... 158
7.2 Research process and research flow..... 158
7.3 Impact of window-to-wall ratio on the indoor temperature and air conditioning energy consumption based on changes in building azimuths..... 159
7.3.1 Energy Differences between solar heat gains and indoor heat losses passing through windows with different window-to-wall ratio and building azimuth combinations..... 160
7.3.1.1 Energy differences between solar heat gains and indoor heat losses in winter..... 160
7.3.1.2 Energy differences between solar heat gains and indoor heat losses in summer..... 161
7.3.2 Impact of windows with different window-to-wall ratio and building azimuth combinations on the mean indoor temperatures..... 162
7.3.2.1 Mean indoor temperature in each of the test scenarios during winter..... 162
7.3.2.2 Mean indoor temperature in each of the test scenarios during summer..... 163

7.3.3 Impact of windows with different window-to-wall ratio and building azimuth combinations on the air conditioning energy consumption....164
7.3.3.1 Energy consumption in each of the test scenarios during winter....164
7.3.3.2 Energy consumption in each of the test scenarios during summer....165
7.3.4 Total energy consumption of air conditioning including space cooling and space heating....166
7.4 Impact of window-to-wall ratio on the solar radiation reception and energy consumption of artificial lighting based on changes in building azimuth....167
7.4.1 Impact of windows with different window-to-wall ratio and building azimuth combinations on the solar radiation reception....167
7.4.2 Impact of windows with different window-to-wall ratio and building azimuth combinations on the indoor visual comfort rate....168
7.4.3 Impact of windows with different window-to-wall ratio and building azimuth combinations on the energy consumption of artificial lighting....170
7.5 Impact of window-to-wall ratio on the total energy consumption including air conditioning and artificial lighting based on changes in building azimuth....171
7.6 Validation of the energy consumption results: simulation tool versus real bills....172
7.6.1 Energy consumption in the real traditional dwellings obtained from real bills....172
7.6.2 Comparison of the total energy consumption obtained from simulation tool and real bills....174
7.7 Optimal window-to-wall ratio recommended for each building azimuth interval....175
7.8 Application of the research results....177
7.8.1 Definition of Evaluation Score of Window-to-Wall Ratio....177
7.8.2 Application of the evaluation score of window-to-Wall ratio to three courtyard dwellings....177
7.9 Finding and discussion....179
References....181
Chapter 8 Impacts of walls with various construction type and building azimuth combinations on the energy consumption
8.1 Introduction....184
8.1.1 Motivation....184
8.1.2 Scientific originality....185
8.1.3 Aim of this study....186
8.2 Research methodology....186
8.2.1 Research subject....186
8.2.2 Description of in-situ measurement....187
8.2.3 Research flow description....189

8.3 Field measurements for walls in base building and test building.....191
8.3.1 Meteorological data of Sizhai during testing days.....191
8.3.2 Wall surface temperatures in base building and test building.....191
8.3.3 Air temperatures in cavity of base building and in vents of test building.....193
8.4 Air temperature and energy consumption obtained from simulation.....194
8.4.1 Air temperatures for four wall types based on changes in building azimuth.....194
8.4.1.1 Air temperatures in each building model during summer.....194
8.4.1.2 Air temperatures in each building model during winter.....195
8.4.2 Energy consumption for four wall types based on changes in building azimuth.....196
8.4.2.1 Energy consumption of space cooling in each building model.....196
8.4.2.2 Energy consumption of space heating in each building model.....197
8.4.2.3 Total Energy consumption including cooling and heating in each building model.....198
8.5 Validation of computational results.....199
8.5.1 Validation of air temperature: Ecotect versus filed measurement.....199
8.5.2 Validation of energy consumption: ArchiWIZARD versus real experimentation.....200
8.6 Conclusion.....201
References.....203
Chapter 9 Conclusion.....149
9.1 Research results.....204
9.2 Research findings.....206
9.2.1 Optimum building azimuth.....206
9.2.2 Optimum shading depth recommended for each building azimuth interval.....206
9.2.3 Optimum window-to-wall ratio recommended for each building azimuth interval.....206
9.2.4 Optimum wall construction type recommended for each building azimuth interval.....206
9.3 Contributions.....207
9.3.1 Application of optimum building azimuth to both newly-built buildings and existing buildings207
9.3.2 Application of optimum shading depth to both newly-built buildings and existing buildings..207
9.3.3 Application of optimum window-to-wall ratio to both newly-built buildings and existing buildings.....207
9.3.4 Application of optimum wall construction type to both newly-built buildings and existing buildings.....207
Acknowledgements.....208

List of figures

Fig. 1.1 Urban-rural population structure from 2005 to 2017 in China....1
Fig. 1.2 Urbanization rate in the range from 2010 to 2017 in China....1
Fig. 1.3 Public building area, urban residential rural area and rural residential area in China for 2017....2
Fig. 1.4 Change trends of average residential area per capita in city and countryside from 1987 to 2017 in China....2
Fig. 1.5 Percentage distribution of energy consumption for building sector in China for 2017....2
Fig. 1.6 Building energy consumption from 2001 to 2017 in China....3
Fig. 1.7 Percentage distribution of building energy consumption from 2001 to 2017 in China....3
Fig. 1.8 The quantity of household electrical appliance used in the rural residences from 2001 to 2017 in China....4
Fig. 1.9 Average electricity use per unit of building area in countryside of China from 2001 to 2017....4
Fig. 1.10 Distribution of traditional villages recorded in the Chinese Traditional Villages' Catalogs....5
Fig. 1.11 Distribution of seven regions in accordance with the geographical location in China....6
Fig. 1.12 Ten provinces and one municipality included in East and Central China....6
Fig. 1.13 Distribution of village density throughout China for 2017....7
Fig. 1.14 Quantity distribution of recorded traditional dwellings in East and Central China....8
Fig. 1.15 The quantity of recorded traditional dwellings in China depicted by bar graph....8
Fig. 1.16 Distribution of five categories for traditional dwellings in China....8
Fig. 1.17 Electricity use of buildings for each province of China in 2017....9
Fig. 1.18 Seven building climate zones' distribution in China....10
Fig. 1.19 Scope of research region (i.e., intersection area of dwelling zone with brick-wood structure and hot summer and cold winter cilmate zone in China)....11
Fig. 1.20 Details of research region and location of Zhejiang Province....11
Fig. 1.21 Villages recorded in the Chinese Traditional Villages' Catalogs and location of Sizhai traditional village in Zhejiang Province....11
Fig. 1.22 Scope of Sizhai traditional village in the map highlighted by red dotted line....11
Fig. 1.23 Lay-out and distribution of main buildings located in Sizhai traditional village....11
Fig. 1.24 Bird's-eye view of Sizhai traditional village and distribution of main buildings....11
Fig. 1.25 Research methods framework....13
Fig. 3.1 Measurement method of dwelling dimensions in Google Earth....41
Fig. 3.2 Statistics of building quantity and percentage for Sizhai village....41

Fig. 3.3 Front facade details and size description of building model in simulation..... 42
Fig. 3.4 Back facade details and size description of building model in simulation.....42
Fig. 3.5 Division of 18 building azimuth intervals for the test scenarios..... 43
Fig. 3.6 Schematic division of 18 building azimuth intervals for the test scenarios..... 44
Fig. 3.7 Shasing depth shown in front facade of the geometric model.....45
Fig. 3.8 Schematic of shading depth and window shaded by corridor roof.....45
Fig. 3.9 Schematic of various angles on solar shading used in equation formulation.....45
Fig. 3.10 Monthly and annual air temperatures in Sizhai village..... 49
Fig. 4.1 Geographic distribution of the five categories of Chinese traditional dwellings and location of Zhejiang Province..... 53
Fig. 4.2 Distribution of five categories of traditional dwelling in Zhejiang Province and location of Sizhai village.....55
Fig. 4.3 Seven measurement points in the traditional dwelling..... 56
Fig. 4.4 Research methods framework..... 58
Fig. 4.5 Position of Thousand Pillar Dwelling in Sizhai village.....59
Fig. 4.6 Bird's-eye view of Thousand Pillar Dwelling..... 59
Fig. 4.7 Layout and configuration of Thousand Pillar Dwelling..... 59
Fig. 4.8 Climate data of Sizhai village (a-left figure) and (b-right figure)..... 60
Fig. 4.9 External brick wall in TPD in traditional dwelling.....62
Fig. 4.10 Construction of external brick wall in traditional dwelling.....62
Fig. 4.11 External wooden wall in TPD in traditional dwelling..... 62
Fig. 4.12 Schematic of external brick wall in traditional dwelling.....62
Fig. 4.13 Upward view of the roof details in traditional dwelling.....65
Fig. 4.14 Schematic of the roof construction in traditional dwelling..... 65
Fig. 4.15 Schematic of diverse angles related to solar shading cast by roof eave..... 66
Fig. 4.16 Schematic of solar shading cast by roof eave and roof eave's depth..... 66
Fig. 4.17 Flooring on the first floor of traditonal dwelling covered clay bricks.....69
Fig. 4.18 A small ventilation vent near the door of traditonal dwelling 69
Fig. 4.19 Annual distribution of outdoor comfort time in Sizhai village..... 84
Fig. 4.20 Monthly distribution of outdoor comfort time in Sizhai village throughout the year.....84
Fig. 4.21 Indoor comfort time distributions based on diverse passive strategies in the whole year..... 85
Fig. 4.22 Distributions and proportions of monthly Indoor comfort time throughout the year..... 85
Fig. 5.1 Scope of building zone and division of dwelling subdomains in Sizhai village.....97
Fig. 5.2 Measurement method of building azimuth for dwelling in G.E.....98

Fig. 5.3 Schematization of the proposed research method.....99
Fig. 5.4 Electricity consumption of air conditioning in January, June, July and August and the total electricity consumption corresponding to different building azimuths..... 102
Fig. 5.5 Distribution of the three points for measuring air velocity in Sizhai village..... 103
Fig. 5.6 Hourly air velocities at three measurement points for three days..... 103
Fig. 5.7 Mean indoor air velocities in the 18 test scenarios with various building azimuth..... 104
Fig. 5.8 Electricity consumption of electrical ventilation in the 18 test scenarios..... 105
Fig. 5.9 Mean indoor illuminance at 1 hour time-step for in the 18 test scenarios..... 106
Fig. 5.10 Arrangement condition and quantity requirement of lighting fixtures over 300 lux..... 106
Fig. 5.11 Time of artificial lighting in operation and duration of visual comfort in the 18 test scenarios over a year.....107
Fig. 5.12 Total annual electricity consumption of artificial lighting in the 18 test scenarios..... 108
Fig. 5.13 Electricity consumption and CO2 emissions in the 18 test scenarios..... 108
Fig. 5.14 Positions of four reference buildings in Sizhai village.....109
Fig. 5.15 Two reference suites orientated towards S in NO. 1 dwelling subdomain 109
Fig. 5.16 Two reference suites orientated towards N in NO. 4 dwelling subdomain.....109
Fig. 5.17 Comparison of the total annual electricity consumed by air conditioning, fans and lamps from real bills and simulation.....111
Fig. 5.18 Distribution of road and stream in the Sizhai traditional village.....113
Fig. 5.19 Quantity and frequency distribution of building azimuths for all dwellings at village-scale..... 117
Fig. 6.1 Research methods framework.....127
Fig. 6.2 Impact of shading devices with various shading depth and building azimuth combinations on SHGC.... 128
Fig. 6.3 MSWRs on the summer solstice corresponding to the circle of building azimuth intervals..... 129
Fig. 6.4 MSWRs on the winter solstice corresponding to the half-circle of building azimuth intervals..... 129
Fig. 6.5 Schematic 1: windows shaded by the shading device of corridor in traditional dwelling.....130
Fig. 6.6 Schematic 2: windows shaded by the shading device corridor in traditional dwelling..... 131
Fig. 6.7 Comparison of shading-to-window ratios obtained from simulation tool and equations..... 131
Fig. 6.8 Direct and diffuse radiation receptions for windows integrated with various shading devices.....133
Fig. 6.9 Total solar radiation reception for windows integrated with various shading devices 133
Fig. 6.10 Mean indoor illuminance in the test scenarios mounted with various shading devices on the summer solstice..... 134
Fig. 6.11 Mean indoor illuminance in the test scenarios mounted with various shading devices on the winter solstice..... 134
Fig. 6.12 Comparison of illuminance obtained from simulation tool and field measurements..... 135

Fig. 6.13 Energy consumption of artificial lighting in the test scenarios mounted with different shading devices.. 136
Fig. 6.14 Indoor solar heat gains in the test scenarios mounted with different shading devices 137
Fig. 6.15 Mean diurnal indoor temperatures the in the test scenarios mounted with various shading devices on the summer solstice 138
Fig. 6.16 Mean diurnal indoor temperatures the in the test scenarios mounted with various shading devices on the winter solstice..... 138
Fig. 6.17 Comparison of air temperatures obtained from the simulation tool and real measurements.....139
Fig. 6.18 Heating energy consumption in the test scenarios mounted with different shading devices 141
Fig. 6.19 Cooling energy consumption in the test scenarios mounted with different shading devices.....141
Fig. 6.20 Energy consumption of air conditioning in the test scenarios mounted with different shading devices... 141
Fig. 6.21 Total energy consumption in the test scenarios mounted with various shading devices..... 142
Fig. 6.22 Positions of four reference buildings in Sizhai village..... 143
Fig. 6.23 Comparison of the total annual electricity use obtained from simulation tool and real bills.....145
Fig. 6.24 Daylight factor for directly south (S) based on changes in shading depth..... 146
Fig. 6.25 Recommendation of the optimum shading depth to each building azimuth interval..... 147
Fig. 6.26 Evaluation score of shading depth assigned to the 9 shading depth intervals corresponding to 18 building azimuths.....148
Fig. 6.27 Three dwellings selected to assess their building energy saving potentials by the evaluation score of shading depth..... 149
Fig. 7.1 Research methods framework..... 159
Fig. 7.2 Solar heat gains and indoor heat losses passing through windows in winter.....160
Fig. 7.3 Energy differences between solar heat gains and indoor heat losses passing through windows in winter.. 160
Fig. 7.4 Solar heat gains and indoor heat losses passing through windows in summer 161
Fig. 7.5 Energy differences between solar heat gains and indoor heat losses passing through windows in summer 161
Fig. 7.6 Mean indoor temperatures for windows with different window-to-wall ratio and building azimuth combinations in winter..... 162
Fig. 7.7 Mean indoor temperatures for windows with different window-to-wall ratio and building azimuth combinations from June to August.....163
Fig. 7.8 Heating energy consumption for windows with different window-to-wall ratio and building azimuth combinations.....165

Fig. 7.9 Cooling energy consumption for windows with different window-to-wall ratio and building azimuth combinations....165
Fig. 7.10 Energy consumption of air conditioning for windows with different window-to-wall ratio and building azimuth combinations....166
Fig. 7.11 Three kinds of solar radiation receptions for windows with different window-to-wall ratio and building azimuth combinations....168
Fig. 7.12 Visual comfort rates for windows with different window-to-wall ratio and building azimuth combinations....169
Fig. 7.13 Energy loads of artificial lighting for windows with different window-to-wall ratio and building azimuth combinations....170
Fig. 7.14 Total energy consumption for windows with different window-to-wall ratio and building azimuth combinations....171
Fig. 7.15 positions of four reference buildings in Sizhai village....173
Fig. 7.16 Comparison of the total annual electricity consumed by lamps and air conditioning obtained from simulation tool and real bills....174
Fig. 7.17 Daylight factor for directly south (S) by varying window-to-wall ratio....176
Fig. 7.18 Recommendation of the optimum window-to-wall ratio for each building azimuth interval....176
Fig. 7.19 Evaluation score of window-to-Wall ratio assigned to 8 window-to-wall ratio intervals for 18 building azimuth intervals....177
Fig. 7.20 Three dwellings selected to assess their building energy saving potentials....179
Fig. 8.1 Construction of the external cavity brick wall in Sizhai traditional dwelling....187
Fig. 8.2 Distribution of measurement walls and point as well as selected suite in Sizhai village....188
Fig. 8.3 Research methods framework of this chapter....190
Fig. 8.4 Meteorological data of solar intensity and air temperature during the testing days....191
Fig. 8.5 Inner layer and outer layer surface temperatures of cavity wall in case building and test building 192
Fig. 8.6 Air temperature in channel of base building and vents of test building during the testing days....193
Fig. 8.7 Air temperatures in each of the building models with various wall type-building azimuth combinations in summer....194
Fig. 8.8 Air temperatures in each of the building models with various wall type-building azimuth combinations in winter....195
Fig. 8.9 Cooling energy consumption in each of the building models with various wall type-building azimuth combinations in summer....197
Fig. 8.10 Heating energy consumption in each of the building models with various wall type-building azimuth combinations in winter....198
Fig. 8.11 Total energy consumption in each of the building models with various wall type-building azimuth combinations....199

Fig. 8.12 Comparison of air temperature from Ecotect and filed measurement.....200
Fig. 8.13 Details of air conditioner used in the experimental building in Sizhai village..... 201
Fig. 8.14 Temperature setting of air conditioner and data collection from electricity meter.....201
Fig. 8.15 Comparison of energy consumption from ArchiWIZARD and real experimentation.....201

List of tables

Table 3.1 Construction features and material properties of the study building.....43

Table 3.2 Building models with 10 kinds of shading depths at 0.25 m increments.....46

Table 3.3 Building models with 9 kinds of window-to-wall ratios at 0.1 of increments.....47

Table 3.4 Details of wall constructions for the building models used in simulation.....48

Table 4.1 Measurement details and conditions of each point in the traditional dwelling.....57

Table 4.2 Characteristics and types of passive elements in the traditional dwelling of Thousand Pillar Dwelling.....61

Table 4.3 Elasticity effect of wall in the traditional dwelling of Thousand Pillar Dwelling.....64

Table 4.4 Elasticity effect of eave roof in the traditional dwelling of Thousand Pillar Dwelling.....67

Table 4.5 Construction of windows and doors in the traditional dwelling of Thousand Pillar Dwelling.....71

Table 4.6 Elasticity effects of doors and windows in the traditional dwelling of Thousand Pillar Dwelling.....72

Table 4.7 Characteristics and types of passive spaces in the traditional dwelling of Thousand Pillar Dwelling 73

Table 4.8 Elasticity effect of patio in the traditional dwelling of Thousand Pillar Dwelling.....74

Table 4.9 Elasticity effect of corridor in the traditional dwelling of Thousand Pillar Dwelling.....76

Table 4.10 Elasticity effect of open-hall in the traditional dwelling of Thousand Pillar Dwelling.....78

Table 4.11 Field measurements of air temperature in summer and winter.....80

Table 4.12 Field measurements of relative humidity in summer and winter.....81

Table 4.13 Field measurements of air velocity in summer and winter.....82

Table 4.14 Field measurements of illuminance in summer and winter.....83

Table 4.15 Indoor comfort time distribution in each month throughout the year.....86

Table 4.16 Strategies and effectiveness of Passive strategies in the traditional dwelling of Thousand Pillar Dwelling.....88

Table 5.1 Mean monthly indoor temperatures in the 18 test scenarios during January, June, July and August 100

Table 5.2 List of domestic electrical appliances and details of the four reference suites.....110

Table 5.3 Total actual annual electricity consumption of 2014 and 2015 in the four reference suites.....111

Table 5.4 Quantity statistics and frequency distribution of all building azimuths scattered in the 10 dwelling subdomains 115

Table 6.1 Four reference suites in Sizhai chosen to collect the real energy bills.....144

Table 6.2 List of domestic electrical appliances and details of the four reference suites.....144

Table 6.3 Total actual annual electricity consumption of 2014 and 2015 in the four reference suites..... 144
Table 6.4 Evaluation score of shading depths calculated for the three study dwellings..... 149
Table 7.1 Four reference suites in Sizhai chosen to provide real energy bills 173
Table 7.2 List of domestic electrical appliances and details of the four reference suites.....173
Table 7.3 Total actual annual electricity consumption of 2014 and 2015 in the four reference suites..... 174
Table 7.4 Evaluation score of window-to-Wall ratios calculated for the three study dwellings.....178
Table 8.1 Details of measurement points and measurement methods in base building and test building..... 189
Table 9.1 Summary of search results based on four building parameters 205
Table 9.2 Summary of optimum building azimuth interval recommend in this work.....206

Nomenclature

1 Air Conditioners (AC)

2 Building Azimuth (BA)

3 Buffer Effect (BE)

4 Central Scientific Technological Building（CSTB）

5 Chartered Institution of Building Services Engineers (CIBSE)

6 Dynamic Passive Element (DPE)

7 Elasticity Effect (EE)

8 Evaluation Score of Shading Depth (ESSD)

9 Evaluation Score of Window-to-Wall Ratio (ESWWR)

10 Extension Level of Indoor Comfort Time (ELICT)

11 Extension of Indoor Comfort Time (EICT)

12 Geographic Information System（GIS）

13 Global Position System（GPS ）

14 Google Earth (G.E.)

15 Heating, Ventilating and Air Conditioning (HVAC)

16 Indoor Comfort Level (ICL)

17 Indoor Comfort Time (ICT)

18 Indoor Environmental Quality (IEQ)

19 Intergovernmental Panel on Climate Change Fifth Assessment Report（IPCCAR5）

20 Mean Shading-to-Window Ratio (MSWR)

21 Outdoor Comfort Time (OCT)

22 Passive Element (PE)

23 Passive Spaces (PS)

24 Photovoltaic (PV)

25 Shading Depth (SD)

26 Shading-to-Window Ratio (SWR)

27 Solar Heat Gain Coefficient (SHGC)

28 T_{al}: air temperature inside cavity wall

29 Thermal Pressure Ventilation (TPV)

30 Thousand Pillars Dwelling (TPD)

31 Wind Pressure Ventilation (WPV)

32 Window-to-Wall Ratio (WWR)

33 T_{s1}: wall surface temperature of inner layer contacted with indoor air for cavity wall without vents

34 T_{s2}: wall surface temperature of outer layer contacted with outdoor air for cavity wall without vents

35 T_{v1}: air temperature in lower vent of cavity wall

36 T_{v2}: air temperature in upper vent of cavity wall

37 T_{vs1}: wall surface temperature of inner layer contacted with indoor air for cavity wall with vents

38 T_{vs2}: wall surface temperature of outer layer contacted with outdoor air for cavity wall with vents

Abstract

The rural residences with substantial quantity and required plenty of energy cost in China were selected as the research subjects in this work. Thanks to high electricity use and village density, as well as complicated pattern of building energy consumption in East and Central China, East and Central China was chosen as the research region. The Sizhai traditional village located in the east of Zhejiang Province, included in the scope of research region, was recorded in the First Edition of Chinese Traditional Villages' Catalog, with large scale and well-protected conditions. The traditional dwellings in this village were chosen as the representative house samples for researching the energy behaviors in the rural residences.

Rather than centered on the performances of evaluation parameters based on a few number, the indoor daylighting and thermal conditions, as well as various energy behaviors were analyzed step by step. This study focuses on the impacts of building azimuth, shading device and window system, as well as wall construction on the performances of indoor daylighting, air temperatures and building energy consumption. The recommended building azimuth interval, shading devices and window-to-wall ratios, as well as wall construction type were summarized, based on the daylighting standard issued by the Ministry of Housing and Urban-Rural Development of China, and the energy consumption performance. The research results indicate that (1) Optimum building azimuth: the three building azimuth intervals with the highest energy saving potentials were observed for S, S-E20 and S-E40 in sequence. (2) Optimum shading depths recommended for each building azimuth interval: the recommended shading depths for S and S-E 20 are 1.37 m and 1.62 m respectively, and those for S-E 40, S-E 60, S-E 80, S-W 20 and S-W 40 are all 2.12 m, as well as those for the other 11 BAs are all 2.37 m. (3) Optimum window-to-wall ratios recommended for each building azimuth interval: the recommended window-to-wall ratios for 18 building azimuth intervals are all 0.2. (4) Optimum wall construction type recommended for each building azimuth interval: the recommended wall construction type for 18 building azimuth intervals are all the vented cavity wall with increased outer layer thickness.

The building energy saving can be achieved by selecting an optimum building orientation, shading device with a proper depth and appropriate glazing area on the facade, as well as suitable wall construction type. This study results aim at providing some design suggestions on building azimuth, shading device and window system, as well as wall construction type determinations to both newly-built constructions and to retrofit projects of the rural residences, as well as providing some new evaluation methods to assess the energy saving potentials of buildings and villages. (1) Application of the building azimuth statistics: for newly-built buildings, the optimum building orientation is recommended for each of them, which are located in the research region; for existing buildings, the evaluation of the

energy saving potentials at village scale can be conducted, by measuring all the existing buildings' azimuth in the target village. (2) Application of the evaluation score of shading depth: for newly-built buildings, the optimum shading depth is recommended for each of them with different building orientations, which are located in the research region; for existing buildings, the evaluation of the energy saving potentials can be conducted for them, based on the evaluation parameter of shading depth. (3) Application of the evaluation score of window-to-wall ratio: for newly-built buildings, the optimum window-to-wall ratio is recommended for each of them with different building orientations, which are located in the research region; for existing buildings, the evaluation of the energy saving potentials can be conducted for them, based on the evaluation parameter of window-to-wall ratio. (4) Application of the optimum wall construction type: for newly-built buildings, the optimum wall construction is recommended for each of them with different building orientations, which are located in the research region; for existing buildings, some suggestions on improvement of walls' thermal insulation property can be supplied for existing buildings.

The research methods can be used in any country to explore the optimum building azimuth, shading device and window system, as well as wall construction type, by using this research method and the corresponding geometric model and local climate data instead of the original ones used in simulation.

Keywords

Building azimuth; Shading depth; Window-to-wall ratio; wall construction; Traditional dwelling; Energy cost

Chapter 1

Research background

1.1 Determination of study subject

1.1.1 Substantial quantity of population in countryside and relatively low urbanization rate in China

From the viewpoint of the urban-rural population structure (Fig. 1.1), the permanent resident population of city was approximately 792.98 million in 2017, which increased by 9.6 million in comparison with 2016. On the contrary, the permanent resident population of village was roughly 589.73 million in 2017, which reduced by 5.28 million compared with 2016. Although the rural population has been experiencing a gradual reduction process, the quantity of rural population is still large. In 2017, the urbanization rate of China was about 58.45% (i.e., the percentage of urban population) (Fig. 1.2), which is comparatively low compared to Europe and North American.

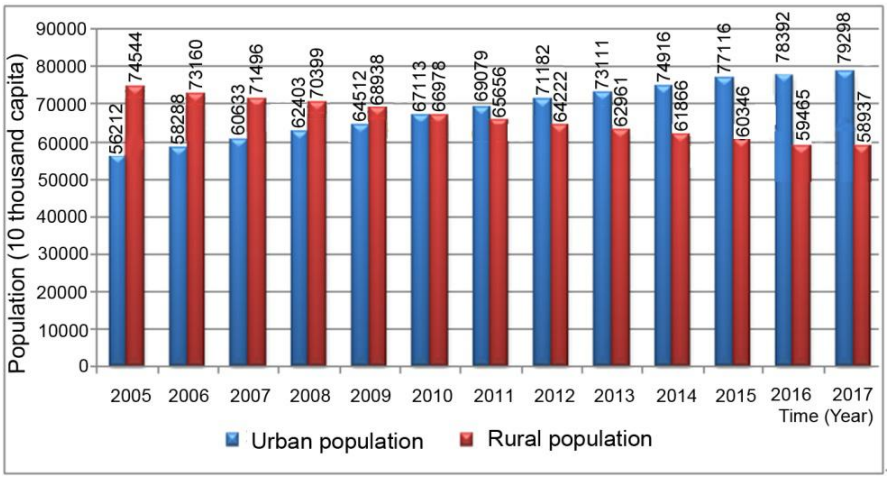

Fig. 1.1 Urban-rural population structure from 2005 to 2017 in China

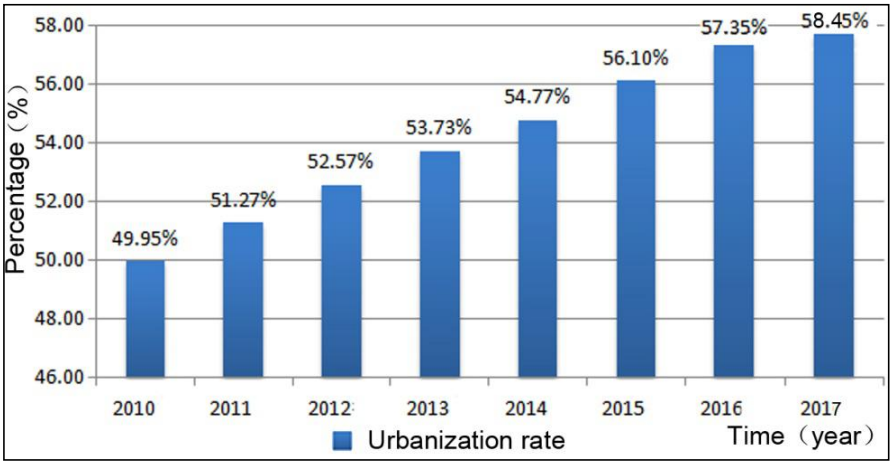

Fig. 1.2 Urbanization rate in the range from 2010 to 2017 in China

1.1.2 Increasing trend of the average rural residential building area per capita

It can be seen from Fig. 1.3 that the public building area was 10081 million m^2 in China for 2017, which accounted for 17% of the national total building area. For the residential building, the residential building areas in city and

countryside were 25969 and 24500 million m^2 respectively, responsible for 43% and 40% of the national total. The average residential area per capita was 41.8 m^2 in China for 2017, of which the average residential areas per capita in city and countryside were 37.6 m^2 and 46.8 m^2, respectively. As shown in Fig. 1.4, the average annual growths of the average residential area per capita in city and countryside were 2.6% and 2.7% respectively from 1987 to 2017. In particular for the countryside, the average residential area has been experiencing a rapid increase from 2012, due largely to the economy development and vast available land.

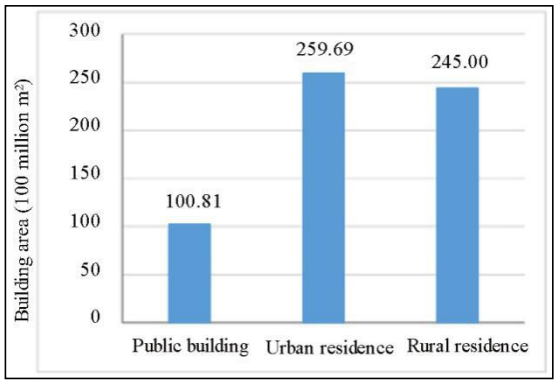

Fig. 1.3 Public building area, urban residential area And rural residential area in China for 2017

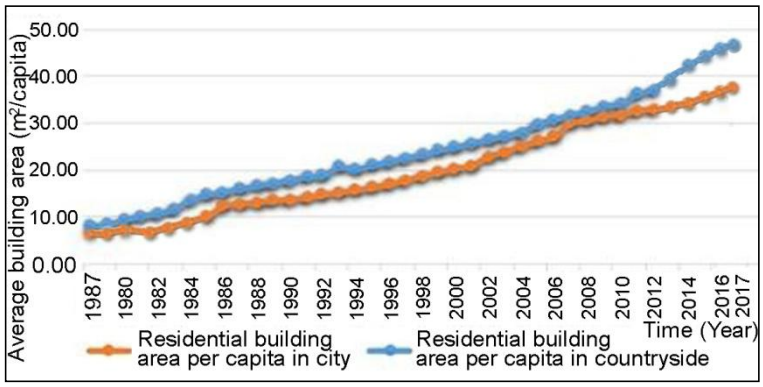

Fig. 1.4 Change trends of average residential area per capita in city and countryside from 1987 to 2017 in China

1.1.3 Increase of energy consumption and electricity use in the rural residences

1.1.3.1 Increase of energy consumption in the rural residences

As shown in Fig. 1.5, the total Chinese building energy consumption was 814 million tce in 2017, which accounted for 19.12% of the national total energy consumption [2]. In the building sector, the energy consumption in public buildings, urban residences and rural residences was 326, 301 and 187 million tce respectively, responsible for 40%, 37% and 23% of the national total building energy consumption [2].

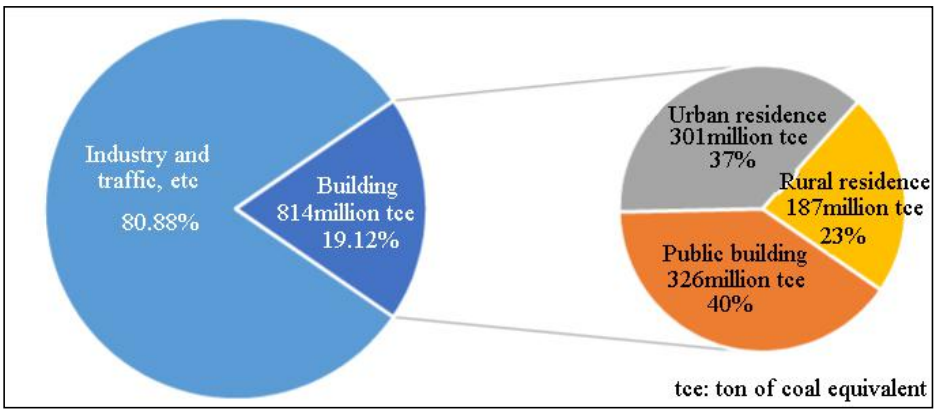

Fig. 1.5 Percentage distribution of energy consumption for building sector in China for 2017

As shown in Fig. 1.6, the energy consumption of public building, urban residence and rural residence has been experiencing a sustained growth from 2001 to 2017, of which the percentage of total energy consumption in the rural residences kept comparative steady, about 24% (Fig. 1.7). One of the driving reasons is that the quantity of household electrical appliances used in the rural residences, leading to the increase in the energy demands is increasing.

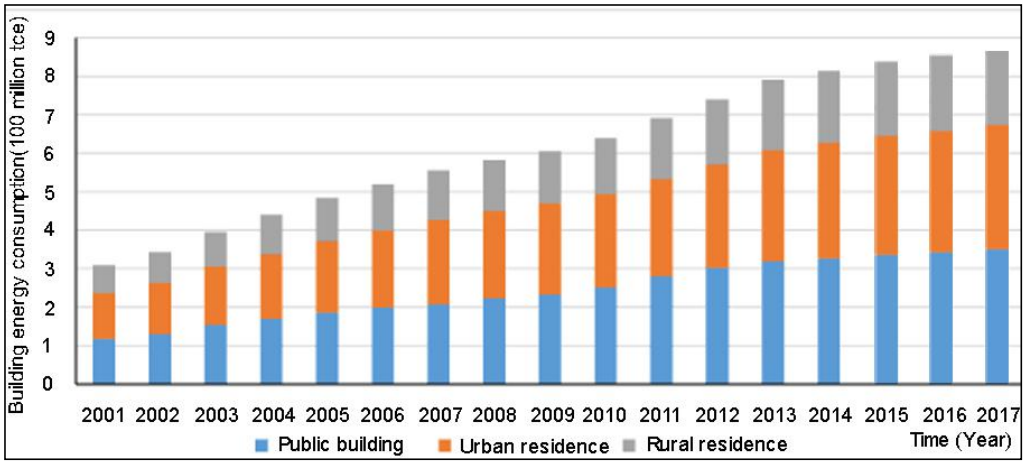

Fig. 1.6 Building energy consumption from 2001 to 2017 in China

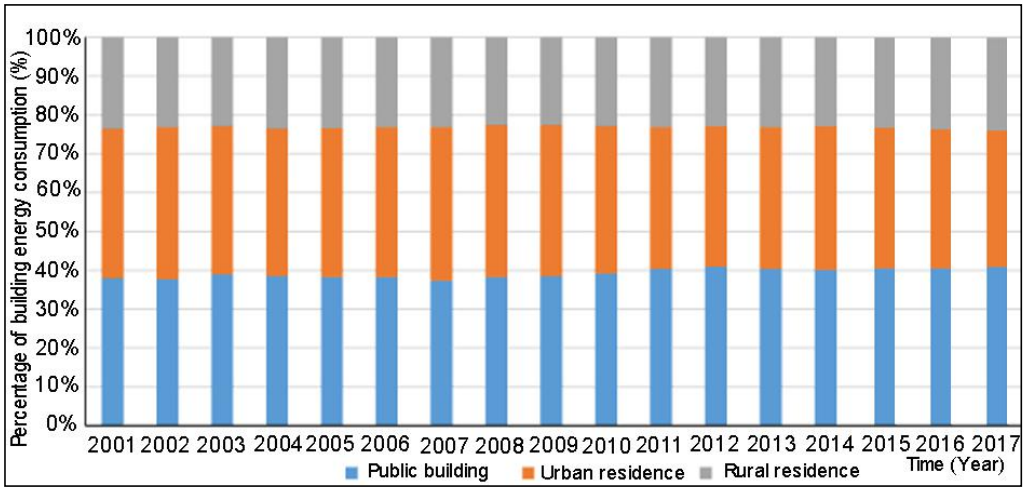

Fig. 1.7 Percentage distribution of building energy consumption from 2001 to 2017 in China

1.1.3.2 Ascending of electricity use in the rural residences

With the economy development, the living standards are significantly improved for occupants living in the countryside. There is a dramatic increase in the quantity of household electrical appliances used in the rural residences. For the air conditioner, its average quantity per 100 houses in countryside increased from 1.7 in 2001 to 64.4 in 2017, with a 37-fold growth (Fig. 1.8). The average quantities of refrigerator and television per 100 houses increased from 30.6 and 54.4 in 2001 to 90.3 and 123.9 in 2017 respectively, with 3 and 2.3-fold growths.

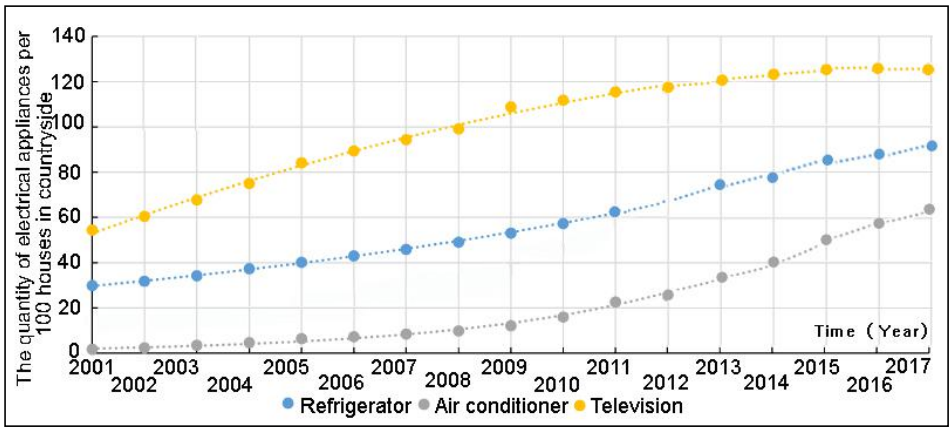

Fig. 1.8 The quantity of household electrical appliance used in the rural residences from 2001 to 2017 in China

With the increase of the average energy consumption per unit of building area in the rural residences, their average electricity use per unit of building area also was experiencing a rapid increase simultaneously. As shown in Fig. 1.9, the average electricity use per unit of rural residence area increased from 3.1 Kw·h in 2001 to 13.9 Kw·h in 2017, with an average annual growth of 4.6%.

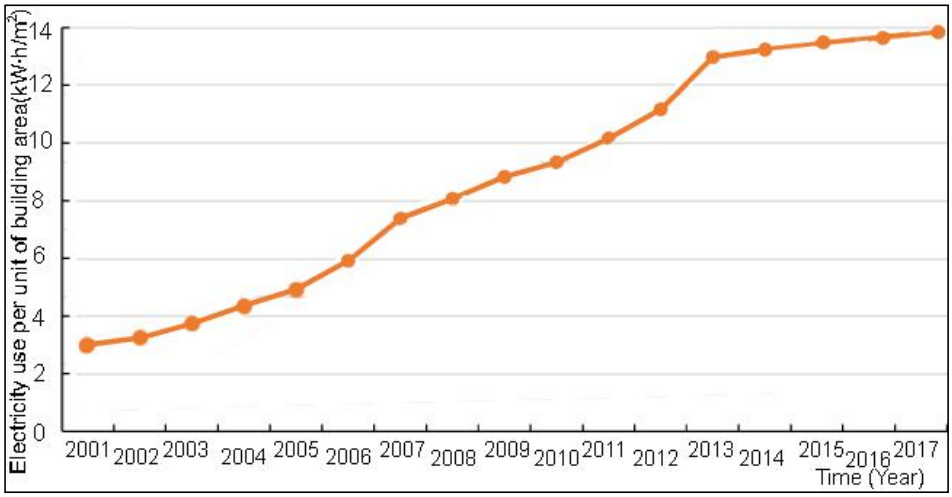

Fig. 1.9 Average electricity use per unit of building area in countryside of China from 2001 to 2017

1.1.4 Attaching importance to protection of the traditional dwellings in countryside

1.1.4.1 Increasing quantity of the traditional dwellings recorded in the Chinese Traditional Villages' Catalogs

Up to 31st Dec, 2017, the summation of the administrative village in China was 691510, which is comprised of 2617000 natural villages [1]. At present, there are approximately over 13100 of the traditional villages in China, which accounts for 1.9% of the sum of national administrative villages. Up to now, the Ministry of Housing and Urban-

Rural Development of China has issued 5 editions of the Chinese Traditional Villages' Catalogs. The First Edition of the Chinese Traditional Villages' Catalog was issued in December 2012, which records 646 villages. Then, the Second (issued in August 2013), Third (issued in November 2014), Fourth (issued in December 2016) and Fifth (issued in December 2018) Editions record 915, 994, 1598 and 2646 villages respectively. By the end of 2018, the summation of traditional villages recorded in the Catalogs is 6799. As shown in Fig. 1.10, the recorded traditional villages mainly concentrate in the south and east of China.

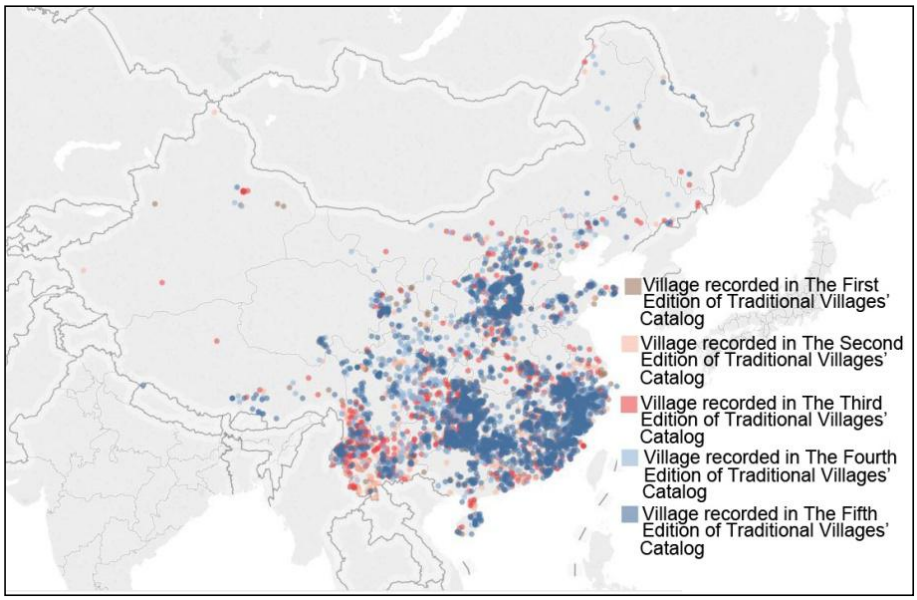

Fig. 1.10 Distribution of traditional villages recorded in the Chinese Traditional Villages' Catalogs

1.1.4.2 Advantages of the traditional buildings on climate adaptation

Not only do the architectural configurations and craft techniques of the traditional dwellings reflect the social culture, customs, and life-styles, but they are also the results of climate adaptation, which have been evolving constantly over a long period of time [3]. Furthermore, the formations and arrangements of traditional dwellings are the harmonious results of external conditions and internal replies, which rely on the medium with an effective interaction between the building components and the local climatic conditions [4]. Although the traditional dwellings are not as efficient as modern reinforced concrete buildings, in terms of the sound insulation [5] and air tightness of envelope [6], the levels of carbon emissions and energy consumption are much lower and the ability of climate adaptation is much more effective in traditional dwellings [7]. Relying on passive climate-responsive strategies, the traditional dwellings can buffer the indoor thermo-hygrometric and daylighting fluctuations, by using the favorable climatic elements like wind, solar radiation, etc [8]. Consequently, the indoor microclimate can be kept stable and

adjusted to the comfort limits, which contributes to creating the environments with relatively high levels of the thermal and visual comforts for occupants [8].

1.1.5 Research subject determination

Combined with the four afore-mentioned reasons, the rural residences in China were selected as the research subject in this work. The rural residences have diverse styles worldwide, attributing to the rural residences built by occupants in compliance with the principles of living accustom, using local building materials and adapting the residence to local climate.

With a capacious territory, the style of rural residences in China is very various. The rural residences in the mountainous areas and along with water systems are comparatively scattered. However, those located in the flatlands are very intensive. Besides, according to building configuration, the rural residences can be generally divided into two categories in China, which are the single-family detached building and courtyard building.

1.2 Determination of research site

As shown in Fig. 1.11, China has a huge territory, which is consisted of seven regions, which are Northeast China, North China, Northwest China, Southwest China, Central China, East China and South China. Central China is consisted of three provinces (i.e., Henan, Hubei and Hunan), and East China is comprised of seven provinces and one municipality (i.e., Shandong, Jiangsu, Anhui, Zhejiang, Jiangxi, Fujian, Taiwan and Shanghai respectively) (Fig. 1.12), which were chosen as the research region in this work. There are four reasons as follows for explain the reason why Central China and East China were chosen as the research site.

Fig. 1.11 Distribution of seven regions in accordance with the geographical location in China

Fig. 1.12 Ten provinces and one municipality included in East and Central China

1.2.1 Substantial quantity of villages in East and Central China

As shown in Fig. 1.13, the village densities in the west and north of China are much lower than those in the east, south and center of China. Due largely to the scattered distribution of villages and relatively uncomfortable natural environments in the west of China, resulting in comparatively low of their village densities, such as Tibet, Xinjiang, Qinghai and Inner Mongolia Provinces. In contrast, due the developed economy, the village densities in East and Central China are relatively high.

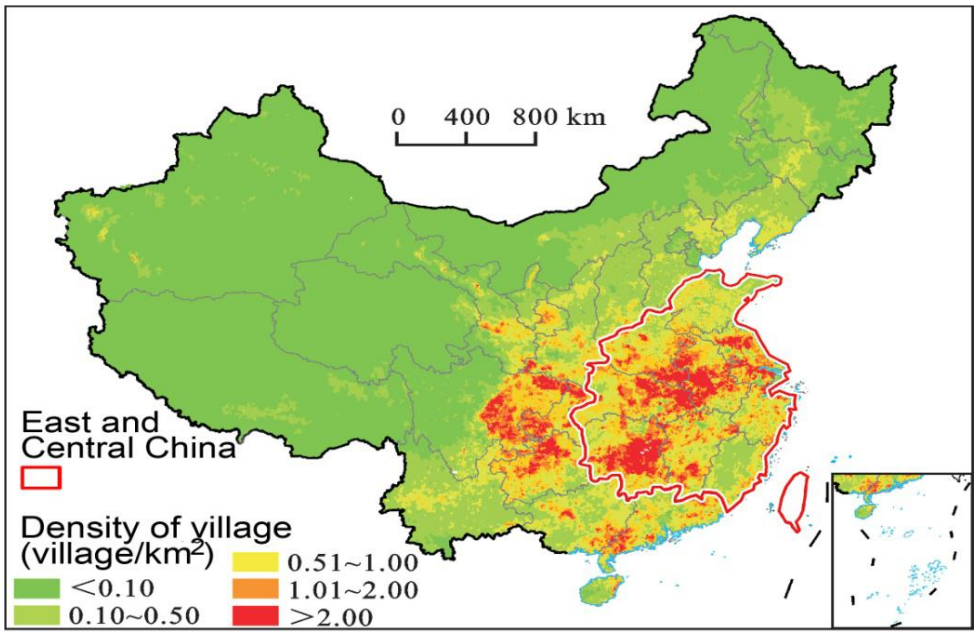

Fig. 1.13 Distribution of village density throughout China for 2017

1.2.2 Substantial quantity of traditional villages recorded in the Catalogs situated in East and Central China

It can be seen from Fig. 1.14 that the quantity of traditional villages recorded in the Catalogs in East and Central China are much greater than those in other areas. The quantities of traditional village recorded in the Catalogs in East China and Central China are 2031 and 1064, accounting for 29.9% and 15.7% of the national total, which ranks the top and third places, respectively (Fig. 1.15).

The category of traditional dwellings has seven in China as shown in Fig. 1.16, which are the brick-wood structure dwelling, wooden structure dwelling, brick-wood-clay structure dwelling, brick-stone-clay structure dwelling and felt-wood dwelling. Most traditional dwellings in East and Central China are characterized by the brick-wood structure, which are belonged to the classification of the brick-wood structure dwelling.

The common characteristics of the traditional dwellings in East and Central China are general with north-south orientation and focus on the internal daylighting. Furthermore, the tile sloped roof, bricks and stones are all borne by

the wooden beams and pillars. The configurations of traditional dwellings in East and Central China are roughly the same as those in the other places of brick-wood structure dwelling zone, which are characterized by the layouts centered by the hall, except for the scale and size (i.e., compact layouts with small courtyards, so as to adapt to East and Central China's conditions of high population density and less farmland). Besides, East and Central China have rich water resources. The river flowing through the front of the traditional dwellings not only provides drinking water resources for occupants in daily life, but also contributes to adjusting the micro-environments for buildings.

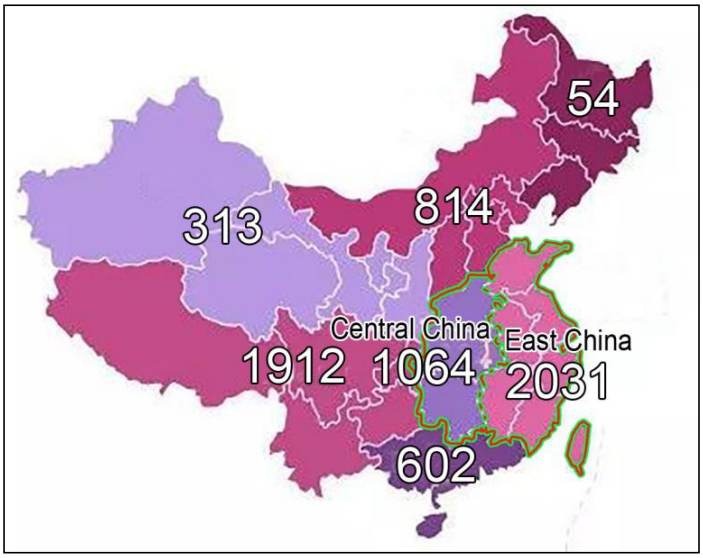

Fig. 1.14 Quantity distribution of recorded traditional dwellings in East and Central China

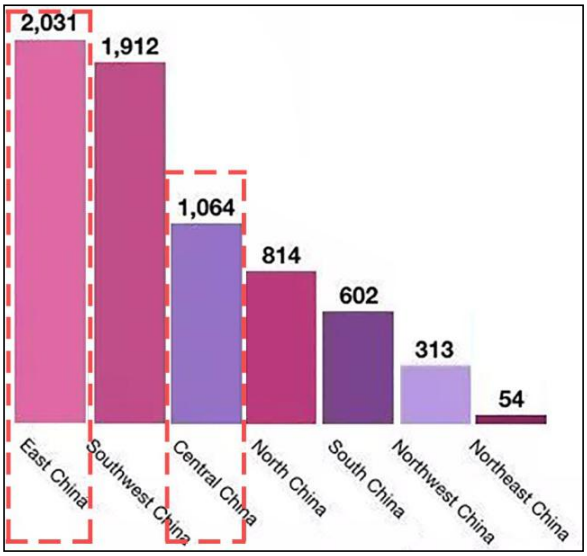

Fig. 1.15 The quantity of recorded traditional dwellings in China depicted by bar graph

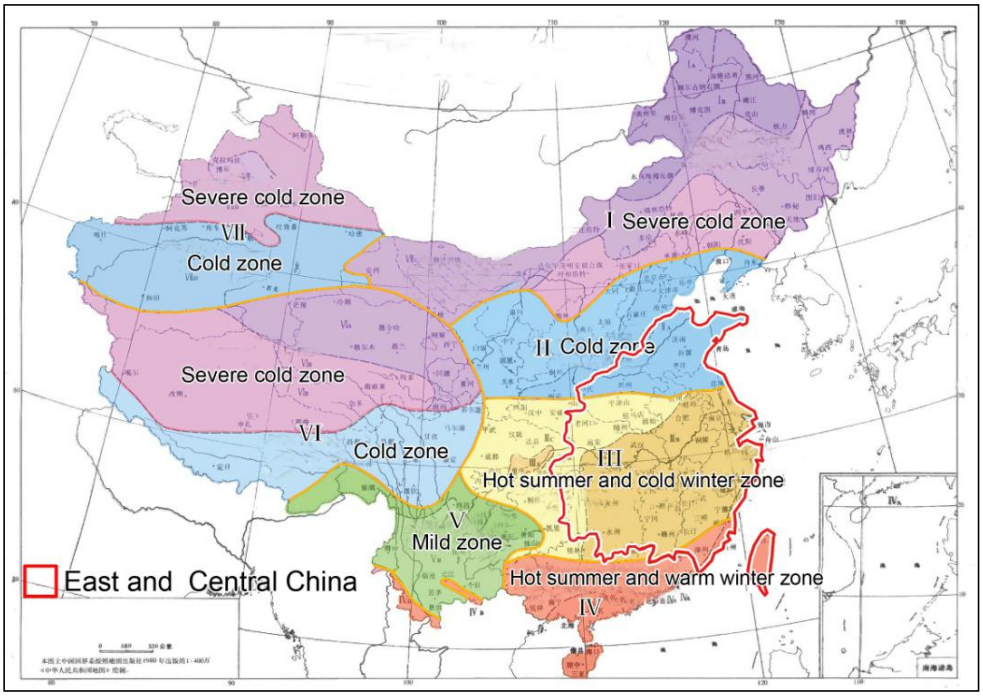

Fig. 1.16 Distribution of five categories for traditional dwellings in China

1.2.3 Developed economy and high electricity use in East and Central China

As shown in Fig. 1.17, the electricity uses of buildings had wide-ranging differences between each province. The top three provinces in terms of the building electricity use were Guangdong with 5.311 billion Kw·h, Shangdong with 5.117 billion Kw·h and Jiangsu with 5.115 billion kW·h in 2017. Besides, Zhejiang, Fujian, Henan and some maritime provinces, located in East and Central China, also had high values of electricity uses.

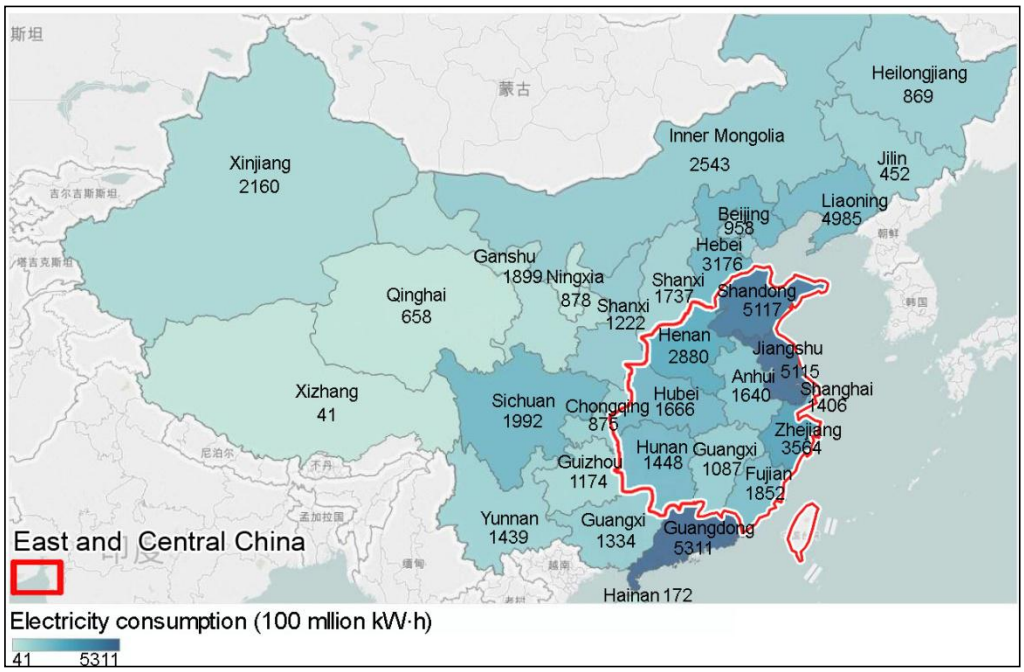

Fig. 1.17 Electricity use of buildings for each province of China in 2017

1.2.4 Complicated energy consumption pattern of buildings in East and Central China

The building energy consumption is greatly related to the climate conditions, of which the energy consumption for space cooling and heating is sensitive to the temperature variations [9]. In consideration of the impact of climate on the indoor environments, in order to provide the appropriate thermal insulation measurements for the buildings in different areas, China is divided into 7 climate zones, which are the severe cold zone (1), severe cold zone (2), clod zone (1), clod zone (2), hot summer and cold winter zone, hot summer and warm winter zone, warm zone [10] (Fig. 1.18).

In North China, the main building energy consumption is used for space heating. On the contrary, the cooling cost contributes most to the total energy consumption in South China. Apparently, most regions of East and Central China in the hot summer and cold winter climate zone is featured by the harshly hot weather conditions in summer and harshly cold weather conditions in winter, resulting in the complex energy consumption pattern in buildings, which deserves to be studied.

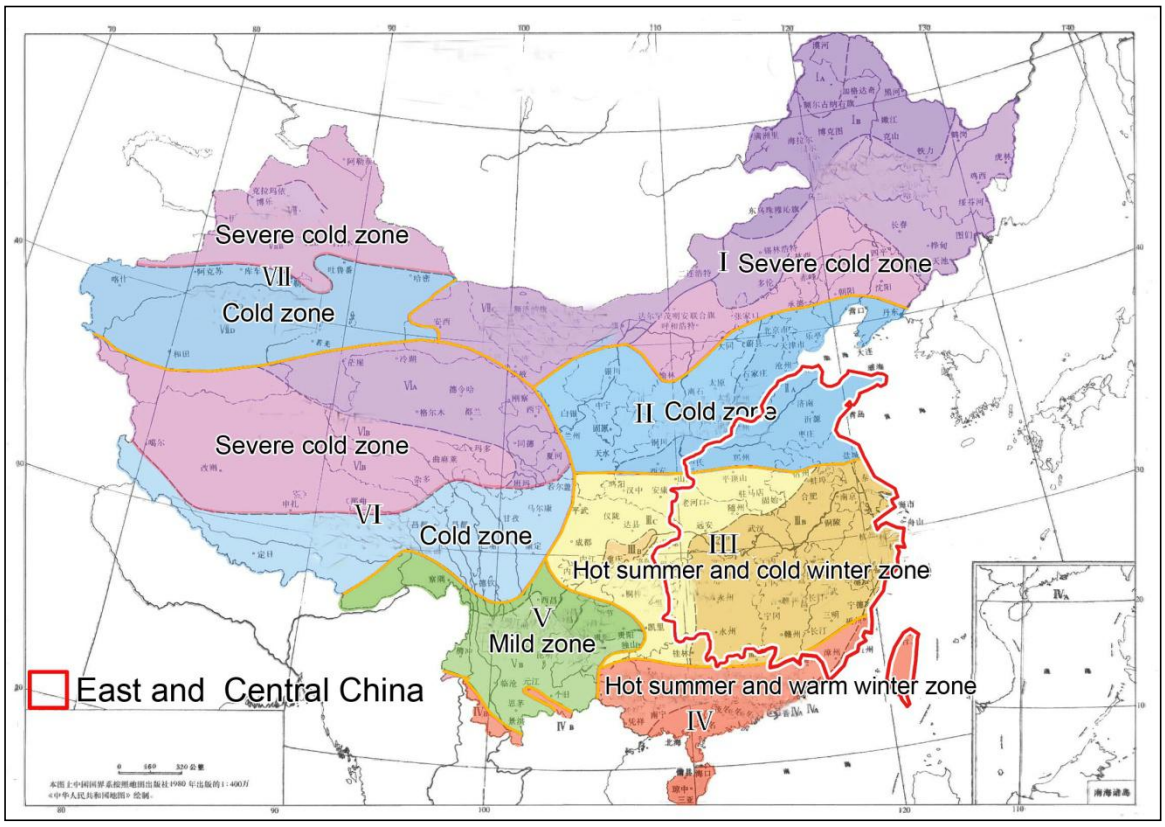

Fig. 1.18 Seven building climate zones' distribution in China

1.2.5 Research region

Due to a substantial quantity of traditional villages recorded in the Catalogs, high electricity use and complicated energy consumption pattern of buildings in East and Central China, the intersection area of East and Central China's zone, and dwelling zone with brick-wood structure, and climate zone characterized by hot summer and cold winter was selected as the research region in this work, as shown in Fig. 1.19-1.20. The research region is consisted of the whole area of Zhejiang Province, and most parts of Fujian, Jiangsu, Anhui, Hebei provinces, Jiangxi and Hunan provinces, as well as small parts of Guangdong and Henan provinces.

Thanks to the whole Zhejiang Province included in the scope of research region, and a large number of traditional villages recorded in the Catalogs (ranking the fourth place in China, with 634 villages), the building models used in simulation for the following chapters were based on the reference building from the Zhejiang traditional dwellings (Fig. 1.21-1.23). The Sizhai traditional village located in the east of Zhejiang was recorded in the First Edition of Traditional Villages' Catalogs, with large scale and well-protected conditions, was chosen as the representative house samples for researching the energy consumption in the rural residences.

The traditional dwellings in Sizhai village are characterized by the black double-sloped roofs and white brick walls (Fig. 1.24). Moreover, the rooms of buildings are usually with high storey height to facilitate the internal ventilation and expel indoor moisture.

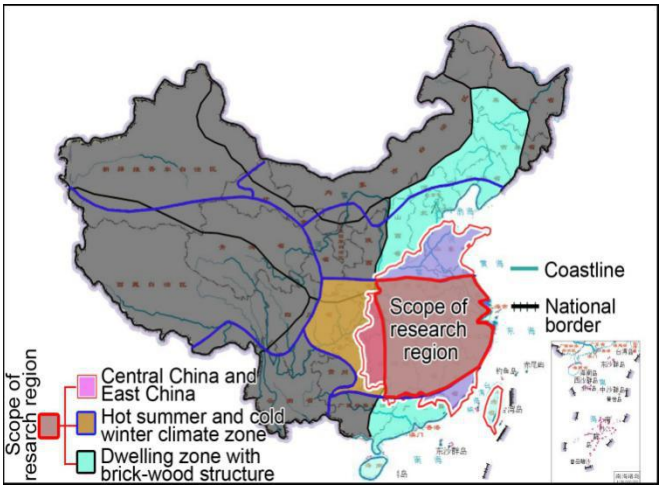

Fig. 1.19 Scope of research region (i.e., intersection area of dwelling zone with brick-wood structure and hot summer and cold winter climate zone in China)

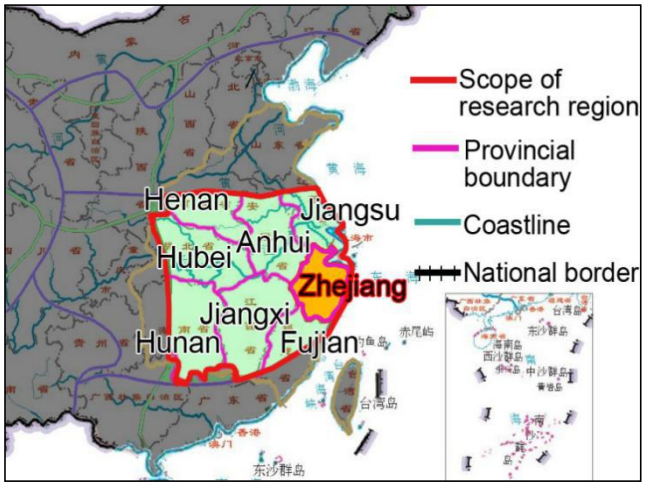

Fig. 1.20 Details of research region and location of Zhejiang Province

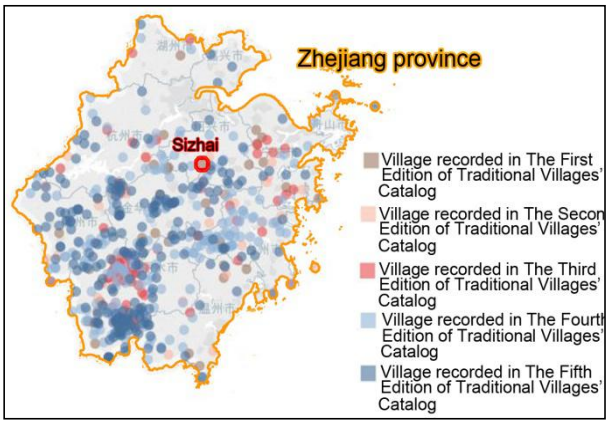

Fig. 1.21 Villages recorded in the Chinese Traditional Villages' Catalogs and location of Sizhai village in Zhejiang Province

Fig. 1.22 Scope of Sizhai traditional village in the map highlighted by red dotted line

Fig. 1.23 Lay-out and distribution of main buildings located in Sizhai traditional village

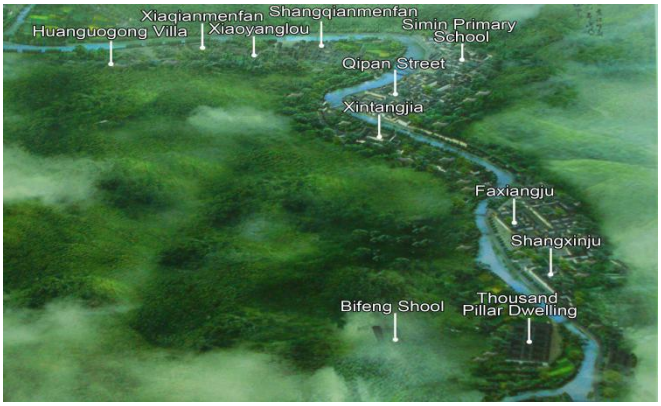

Fig. 1.24 Bird's-eye view of Sizhai traditional village and distribution of main buildings

1.3 Scientific originality of the study

Since the building orientations' determination for the traditional dwelling complies with the rule of "adapting it to building site conditions" in East and Central China, the building azimuth vary considerably depending on the building site. The present research mainly focuses on the impacts that the shading devices and windows facing a limited quantity of orientations have on the energy consumption and on indoor daylighting performances, while few studies are based on multiple orientations. In addition, many studies related to the influences of shading devices and windows on the building energy consumption are grounded on changes in shading depth and window-to-wall ratio within relatively small scopes, respectively. What's more, the related researches, in particular with regards to the impacts of shading device and window on the energy consumption, have often been neglected to get carried out in the traditional buildings up to now.

Based upon the afore-mentioned discussions, the originality of this study are that (1) estimated the solar energy management performances of building azimuth, shading device and window, as well as wall construction for the traditional dwellings, which are located in East and Central China experienced the harshly hot climates over a long period of time. (2) Rather than focus on the performances of several evaluation parameters, the indoor daylighting and thermal conditions, as well as various energy behaviors were analyzed step by step. (3) Also, the optimal building azimuth intervals, optimal shading depth for each building azimuth interval, and optimal window-to-wall ratio for each building azimuth interval, as well as optimal wall construction type for each building azimuth interval were recommended, for determining the best final designs to the traditional dwellings. (4) Furthermore, three new evaluation parameters (i.e., the building azimuth statistic, the evaluation score of shading depth, the evaluation score of window-to-wall ratio) based on the energy saving potential and visual comfort were proposed. Then the three evaluation parameters were used to assess the energy saving potentials for all existing residences in a village (at village scale) and individual buildings (at building scale). (5) On the other hand, the traditional dwellings that were adopted as case studies in this study, can supply some new body of knowledge on the shading, daylighting and energy consumption, to fill in the gap in this field. (6) The research methods can be used in any country to explore the optimum building azimuth, shading depth and window-to-wall ratio, as well as wall construction type, by using the corresponding geometric model and local climate data instead of the original ones used in simulation.

1.4 Research flow

The structure of the dissertation is divided into 8 sections: the research background was depicted in chapter 1. The chapter 2 illustrated the previous studies, including the characteristics of the traditional dwellings, impact of building

azimuth on the energy consumption, impact of shading devices with various shading depth and building azimuth combinations on the energy consumption, and impact of shading devices with various window-to-wall ratio and building azimuth combinations on the energy consumption, as well as impact of walls with various wall construction type and building azimuth combinations on the energy consumption. In chapter 3, research methodology was indicated detailedly, such as, the simulation model dimensions, division of various evaluation parameters. Chapter 4 analyzed the strategies and effectiveness of climate adaptation for the traditional dwellings in East and Central China, based on their passive elements and passive spaces, by taking the Thousand Pillars Dwelling as case study. In chapter 5, the impact of building azimuth on energy consumption in the traditional dwellings was studied. Chapter 6 analyzed the impact of shading devices with various shading depth and building azimuth combinations on energy consumption in the traditional dwellings. Chapter 7 researched the impact of windows with various window-to-wall ratio and building azimuth combinations on energy consumption. Chapter 8 studied the impact of walls with various wall construction type and building azimuth combinations on the energy consumption. The last chapter is conclusion. To facilitate understanding the research method framework, it is presented in Fig. 1.25.

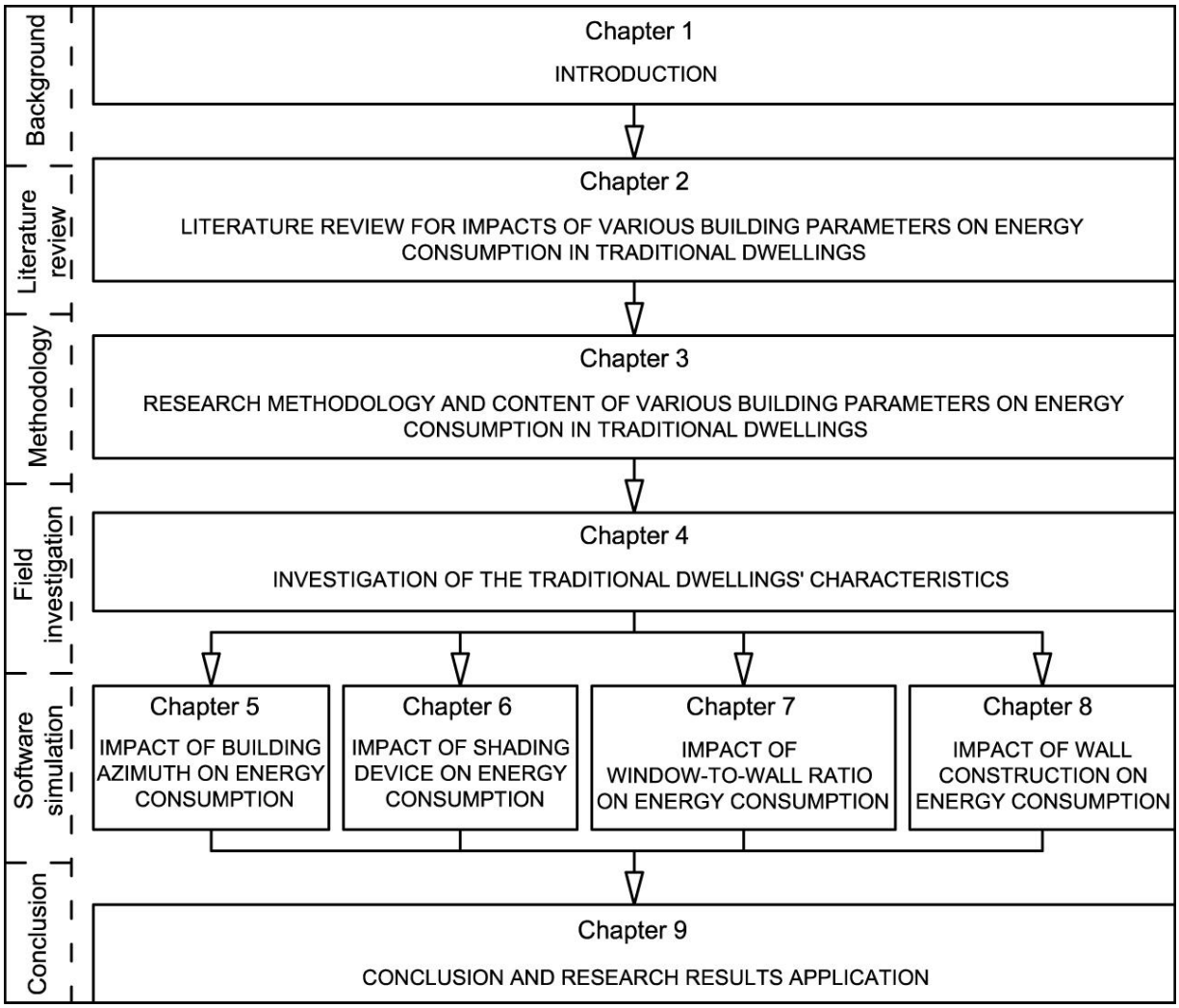

Fig. 1.25 Research methods framework

References

[1] YANG R, LIU Y S, LONG H L, et al. Spatial distribution characteristics and optimized reconstructing analysis of rural Settlement in China [J]. *Scientia Geographica Sinica*, 2016, 36(2): 170-179.

[2] MENG N. Building energy consumption of China in 2018[J]. *Architecture*, 2019(2): 26-31.

[3] McHarg I L. *Design combines nature* [M].RUI W J, Trans. Beijing: China Construction Industry Press, 1992: 57.

[4] ZHANG T. *Overall Area Building* [M]. Nanking: Southeast University Press, 2003: 25-64.

[5] JollyJohna Ash, Latha Thampuran, B.Premlet. Objective and subjective evaluation of acoustic comfort in classrooms: A comparative investigation of vernacular and modern school classroom in Kerala [J]. *Applied Acoustics*, 2016, 104(3): 33-41.

[6] H.Al-Hinai, W.J.Batty, S.D.Probert. Vernacular architecture of Oman: Features that enhance thermal comfort achieved within buildings [J]. *Applied Energ*y, 1993, 44(3): 233-244.

[7] A.S.Dili, M.A.Naseer, T.Zacharia Varghese. Passive control methods for a comfortable indoor environment: Comparative investigation of traditional and modern architecture of Kerala in summer [J]. *Energy and Buildings*, 2011, 43: 653-664.

[8] Jorge Fernandes, Carlos Pimenta, Ricardo Mateus, et al. Contribution of Portuguese Vernacular Building Strategies to Indoor Thermal Comfort and Occupants' Perception [J]. *Buildings*, 2015(5): 1242-1264.

[9] LONG W D. The sustainable development of HVAV industry in China [J]. *Heating Ventilating & Air Conditioning*, 1999, 29 (3): 25 - 30

[10] LIU J P, YANG L. *Index of Indoor Environment Design* [M]. Beijing: China machine press, 2005: 1-5.

Chapter 2

Literature review

2.1 Passive climate-responsive strategies in traditional dwellings

Relying on passive climate-responsive strategies, the traditional dwellings can effectively control the indoor thermo-hygrometric and daylighting conditions by taking advantage of some favorable climatic elements like wind, solar radiation, etc. Furthermore, the building's elements and spaces can be regulated to make the indoor microclimate reach the comfort limits, thanks to these passive strategies.

Extensive studies and efforts have been focused on exploring the passive strategies and climate adaptation of traditional dwellings for local climate up to now. Through the methodologies of field measurements and questionnaire surveys, HUANG Linjiang et al. [1] indicated that the passive strategies of Tibetan castles effectively improve the indoor thermal comfort level, where the lowest temperatures of a southerly oriented room and a northerly oriented room are 9.00 ℃ and 5.00 ℃ respectively, both above the outdoor temperature in winter. Whereas, the indoor temperatures cannot reach the comfort limits ranged from 16.40℃ to 24.00℃, if the rooms are without heaters. By investigating traditional cave dwellings in Shannxi Province of China, LIU Jiaping et al. [2] presented that due to usage of the raw clay wall in cave, with semi-infinite-thickness property, the impact of external climate variations on indoor thermal environments is buffered effectively. Consequently, the amplitude of indoor temperature fluctuation is kept negligible in the traditional cave dwellings, which is helpful for creating warm winter and cool summer environments. Field measurement data show that the mean temperatures of outdoor surface and indoor surface for the cave wall during summer are 27.70℃ and 24.00℃, respectively. Regarding winter, indoor temperatures are kept within the range of 8.50~11.00℃. LI Angui et al. [3] explored the adjustment effectiveness of Kang (a kind of heatable brick bed) on the indoor temperature in the traditional dwellings located in the countryside of Northwest China. Based on the original configuration of Kang, they proposed a new scenario for its construction and layout. According to software simulation results, the new scenario could improve and optimize energy use efficiency. Analogously, by the means of on-site investigations and in-situ measurements, GOU Shaoqing et al. [4] carried out a study on climate adaptation effectiveness of the traditional dwellings in the hot summer and cold winter climate zone of China. They indicated that the passive strategies of climate adaptation for the traditional dwellings located in this climate zone principally consist of natural ventilation, sunshade, wall insulation, etc. The field measurement data show that indoor temperatures have a 2.00~4.00℃ reduction during daytime, while the relative humidity is stable, within the range of 66~68% in summer. Giuseppe Desogus et al. [5] researched the bio-climatic strategies of raw clay vernacular buildings in the Mediterranean. By constructing patios, employing raw clay walls and creating corridors with performance of semi-open transitional space leaning against southerly oriented walls, the buildings effectively adjust the extremely hot or cold indoor temperatures, which contributes to extending the ICT by

14~17% of the whole year. A study on indoor thermal environments in the Spanish vernacular buildings ("horreo") was conducted by C. Saá et al. [6]. By using CDF software to simulate the indoor ventilation conditions, they claimed that the passive strategies of transparent stilt floors and partial wall openings, etc., are conductive to creating the internal spaces with moderate temperatures and well-ventilated environments. M. Barbero-Barrera et al. [7] indicated that a comfortable indoor environment of the cave situated in Spain can be created by utilizing natural resources, such as choosing an optimal building orientation and using local building materials reasonably, etc. A study on comparison of climate adaptation and indoor thermal comfort levels among three kinds of stone vernacular buildings situated in coast, flatland and mountainous area of Cyprus was conducted by Maria Philokyprou et al. [8]. Based on the passive strategies of semi-opening and opening spaces, etc., the indoor temperatures are remained stable contributing to a reduction in energy requirements for space cooling and space heating.

2.2 Impact of building azimuth on the energy consumption

For regulating indoor temperature, the ACs used to keep rooms cool or warm are responsible for about 40% of the overall building energy consumption around the world [9]. Whereas, the glazed facade of a building facing an optimal orientation can effectively avoid undesired solar radiation penetrating through the glazing during summer, while internal spaces can obtain sufficient solar energy as they need in winter [10]. Wang and Fam [11] stated that indoor solar radiation yields could be regulated and controlled by varying BA. Furthermore, the study indicates that a building with proper orientation is beneficial to gain sufficient solar radiation for buildings in the cold climate zones. In addition, as stated by Torreggiani et al. [12], the BA has impact on the air temperature and the amplitude of temperature change. Their research results show that the internal space in southeast facing building situated in the Mediterranean has relatively low thermal comfort level.

2.2.1 Impact of the building orientation on the energy consumption

A great quantity of researches on the well-orientated building contributing to reduction in the building energy consumption have been carried out in Kuwait [13], Nigeria [14], Ghana [15], Hongkong [16], etc. Aksoy and Inalli et al. [17] found that a building with proper building orientation and appropriate shape coefficient leads to saving up to 36% of the building energy consumption. Moreover, Acosta et al. [18] through energy simulation argued that energy consumption variations in buildings are dissimilar by varying the window to wall ratio (WWR) for different building orientations, of which the east facing buildings with varying WWR present the most dramatic variations. By adopting Green Building Studio to perform the energy cost simulation, Abanda et al. [10] found that the best orientation for buildings is directly south facing in Britain, and the worst one is the orientation with north by east 45°. Throughout the whole life cycle of 30 years, the total differences of electricity use and gas consumption between the best and

worst orientations of the buildings are 17056 kW kW·h and 27988 MJ, respectively. Brandão de Vasconcelos et al. [19] denoted that in comparison to a north-south orientation of building, the electricity consumption for space heating and cooling in a building with east-west orientation increases by 15% and 100%, respectively. Koranteng [15] took buildings located in Kumasi city of Africa as a case study to research the correlation between building orientation and energy consumption for space cooling. As the front facade of a building is orientated towards west, the indoor solar radiation yields and energy consumption both increase. On the contrary, when it faces north or south, the energy cost for space cooling reduces by 16.02%. Chan et al. [16] researched the impact of building orientation on energy cost in high-rise buildings located in Hongkong. The research results presented that the overall energy consumed for space cooling decreases by 19.76% in buildings with south-north orientation. In addition, the less glazing area on east-facing and west-facing facades, the lower cooling energy is required. Martin Marin [20] took a residence with one storey situated in the Madrid of Spain as the study building. By using software of IDA Indoor Climate and Energy (IDA ICE).4.7.1 version to compute the energy costs corresponding to different orientations, the simulation results show that the minimum overall energy demand occurs in a building facing directly south. In contrast, the building requiring the most energy is orientated towards north by west 45°. Furthermore, the total energy cost of building facing north is generally greater than that facing south. As a building is orientated towards directly south, it demands the minimum heating energy in winter compared to the buildings facing other orientations. However, the minimum cooling energy cost occurs in a building facing directly north in summer.

2.2.2 Impact of the building orientation on the natural ventilation

Natural ventilation can expel indoor heat to mitigate human thermal sensation during summer. Through incorporation of the passive strategy of natural ventilation into building, the indoor temperatures are effectively controlled in the comfort range during nighttime in summer [21-22]. Besides, a well-ventilated building contributes to indoor temperature approximately being 1.7~2.5℃ lower than exterior [23]. Almeida et al. [24] declared that the factors impacting indoor air movement are facade configuration, building shape and building orientation, etc. Hiaus et al. [25] stated that building facing an optimal orientation and configured with a proper glazing area is conducive to driving indoor air to flow, which is helpful for improving the indoor thermal comfort level. Al-Tamimi et al. [26] suggested that due to the east-facing and west-facing facades without well-ventilated conditions and covered by intense solar radiation during daytime, the glazed areas on these two facades are not suitable to be large.

2.2.3 Impact of the building orientation on the natural daylighting

With regards to the energy consumption of artificial lighting, it is responsible for approximately 19% of the total electrical energy consumed in the world and 2.4% of the world's entire primary electricity consumption [27]. What's

more, the global amount of CO_2 yielded by artificial lighting reaches approximately 130 million ton per year [28]. Using natural daylighting is widely considered as one of the most efficient strategies to reduce the reliance on artificial lighting, aiming at energy saving [29-30]. Besides, the room under natural daylighting can generate numerous desired results, which especially reflect in human health [31-37] and visual comfort [38].

The fenestration system geometry is closely related to daylighting performances for the internal spaces, which contributes to reduction in the energy consumption of artificial lighting, as a building is installed with proper area of glazing and orientated towards optimum orientation [39-40]. Spanos et al. [41] indicated that a well-orientated building is good for prolonging the indoor daylighting time, which leads to decreasing by 20% of the total building energy consumption. Marshi et al., [42] through energy simulation in Ecotect, found that the best orientation for the front facade of a building is south by west 12.5°.

With regard to the indoor daylighting performance assessment, many evaluation parameters are available so far, such as the average daylight factor, average uniformity, daylight autonomy, useful daylight illuminance, simplified daylight glare probability. Acosta et al. [18] employed DaySim 3.2 to simulate and analyze the daylighting performance for an internal space. Simulation results show that the coefficient of daylight autonomy in a space far away from windows facing south is 3 times higher than that facing north. Moreover, the coefficients of daylight autonomy in the same space with windows facing east and west are both 2 times higher than that facing north. Jovanović et al. [38] took a student dormitory in the University of Nis situated in Serbia as a study building. Using the research methodology of questionnaire, they suggested that the rooms facing northeast got the highest satisfaction rates from students in terms of the indoor natural daylighting, approximately 71%. In contrast, the students expressed the lowest satisfaction with rooms facing northwest, approximately 50%. In addition, through software simulation to analyze the indoor daylighting performances, the results illustrate that the visual comfort levels in the north orientated rooms are the highest during summer. In spring and autumn, the rooms with the most outstanding daylighting performances are facing southeast.

2.2.4 Discussion

Based on the previous literature reviews and discussions, it is not difficult to draw a conclusion that the building orientation has a significant impact on the building energy consumption. However, taking into account the research methodology and technique strategy, numerous researchers just focused on the impact of building orientation on the total building energy consumption. Unfortunately, less of in-depth studies were conducted to compute the energy consumption of various active systems at the same time in a building. What's more, the aforementioned researches in terms of the impact of building orientation on energy consumption were based on a limited number of orientation

variations. The interval division of BA in most studies is not clear enough, in which the building facades are generally just defined as four categories, consisting of east-facing, west-facing, north-facing and south-facing.

2.3 Impact of shading devices with various shading depth and building azimuth combinations on the energy consumption

2.3.1 Impact of the movable shading device on the energy consumption

There are numerous studies and efforts focused on the impact of shading devices on the building energy consumption up to now. According to the device configuration, performing a static or dynamic shading effect on the given glazing, they are categorized into two categories, namely the movable shading device and the fixed shading device. The movable shading device is operated with the aim of improving indoor daylighting and thermal environment, by means of preventing the glare and overheating from reaching the occupants [43], while the window can still receive a large quantity of solar irradiation when the internal space needs it [44]. Therefore, the movable shading device is usually deemed to be better than the fixed one in terms of shading performance [45]. However, the movable shading device, under the manually operated control, is greatly correlated with the occupants' living customs and the function of the room, resulting in the energy consumption and daylighting performances varying from person to person [46].

The growing attention has been given to the incorporation of Photovoltaic (PV) into the movable shading systems recently. A test scenario equipped with sun-tracking PV was modeled by Gao et al. [47] to analyze the average energy efficiency and annual energy generation, which are improved by 19.17% and 27.40%, respectively. Furthermore, the optimum sun-tracking shading device reveals a greater ability to protect from solar glare. Using the similar method, Hong et al. [48] proposed a slat control approach for the bi-directional PV blind. The results show that the average power generation in room shaded by a uni-directional PV blind is a 85.05-110.88% of that shaded by a bi-directional PV blind control. Li et al. [49] researched a special PV module used to intercept the solar radiation in multi-story buildings. By analyzing benefits in terms of the energy saving, the optimum widths and angles of PV modules for buildings located in various cities of China, were recommended. Furthermore, the use of the movable shading devices is one of the methods to efficiently improve the building's energy saving potential. Lee et al. [50] demonstrated that by using a movable venetian blind, a significant energy saving can be achieved in an office building equipped with the dimmable electric lighting system. Firlag et al. [51] analyzes the impact of shading device controlled by a smart automated system on the energy consumption in a case study in Poland. The smart automation control system includes five algorithms that are the simple rules, heating/cooling, perfect citizen, predictive weather

and heat flow. The results show that use of the movable shading devices with proposed control algorithms can cut off energy consumption by 11.6~13.0%.

2.3.2 Impact of the fixed shading device on the energy consumption

With regards to the fixed shading device, it is consisted of a conventionally static shading configuration that is generally installed on the external facade horizontally or vertically. There are also numerous sections focused on the incorporation of the PV into the fixed shading systems so far. An investigation on the shading performances of 13 types of the fixed shading devices was conducted by Mandalaki et al. [52]. Using integrated PV on the south facing walls, the energy costs of lighting, cooling and heating were computed for an office building situated in the Mediterranean. Furthermore, the daylight glare index, useful daylight illuminance and daylight autonomy were selected as the evaluation parameters to estimate the indoor visual comfort level. Stamatakis et al. [53] incorporated the monocrystalline PV panel into various patterns of the fixed shading devices. The results revealed that the “brise soleil full facade” is the recommended shading device type, when the proposed shading devices are mounted on a south facing office building in the Mediterranean. While, the “louvers horizontal inwards inclined” or “simple window” or “canopy inclined double” are observed for the most unsuitable for the study building. Using the mathematical algorithm model is another approach to evaluate the shading performances for the fixed shading devices. F. Mazzichi et al. [54] proposed a new research method based on the genetic algorithm to study the performances of indoor daylighting and energy consumption in buildings integrated with the fixed shading device. By installing the fixed venetian blinds on external facade, these two parameters have both been improved. Saelens et al. [55] used both the ray-tracing calculation method and simplified calculation method to evaluate the impact of the external fixed louver on the building energy consumption. An analogy between the energy costs shows that the simplified model underestimates the peak cooling power and cooling requirements by up to 25% and 43%, respectively.

2.3.3 Impact of the external shading device on the energy consumption

According to the installation position, the shading devices are classified into the external shading device and the internal shading device [56]. The external shading device is an energy-efficient component in buildings, which protects the internal spaces from intense solar radiation before it reaches the glazing. With the assistance of the external shading device, the cooling energy load is cut down significantly, as well as a reduction in equipment costs of active air conditioning systems, are obtained [57]. Besides, a series of simulations and investigations have validated the fact that integration of the external shading device into buildings contributes to notable advantages in terms of the indoor visual and thermal comfort and energy saving [58]. From the viewpoint of the aesthetics, a building mounted with external shading devices can produce rich shadow changes on the facades.

Extensive studies and efforts have been placed on the building energy performance correlated with the external shading devices up to now, by means of the dynamic energy simulation. A study on the impact of five evaluation parameters consisting of the glazing type, shading device, building area, color of the external surface, and building orientation on indoor daylighting performances for 35 buildings located in the subtropical area of Hong Kong was performed by Li and Tsang [59]. Furthermore, according to the simulation results, they indicated that approximately a 20%-25% of the lighting energy is saved in the study buildings. Alhuwayil et al. [60] researched the energy saving potential for a hotel building in the hot-humid climate zone of Saudi Arabia, where the external shading device was incorporated with a self-shading envelope. The results show that the proposed shading system could reduce the annual building energy consumption by 20.5%, in comparison with the baseline case. Poirazis et al. [61] indicated that the external shading device is used with the purpose of minimizing energy consumption for buildings. A building integrated with the external shading devices contributes to a reduction in the primary energy consumption by up to 30% in Rome and 19% in Trieste, compared with the alternatives with unshaded windows, respectively. Niu [62] pointed out that the external shading device can lower the direct solar exposure for windows, which is helpful for dropping the solar heat gain by a maximum of 80% for the internal space. Moreover, some additional energy savings are obtained in terms of the cooling load and heat rejection, since the time of artificial lighting fittings being in operation is shortened, leading to a reduction in heat contribution. Oleskowicz-Popiel et al. [63] stated that approximately 44% of the heat loss is saved by the windows with double glazing with low emissivity coatings, and 45% of that is saved by the external roller blinds during nighttime.

2.3.4 Impact of the internal shading device on the energy consumption

Many papers have stated that the energy saving potential of internal shading devices is lower than that of the external shading devices [64]. For instance, according to the research results from Ye et al. [65], the amount of energy saved in a building configured with the blinds on the interior wall surface is much lower than that with the blinds outside. Moreover, the internal shading device can decrease visual discomfort and glare more efficiently and effectively in comparison with the external one [66]. In addition, as a result of the internal shading device being mounted on the inside surface of the wall, the construction expenses can be reduced and the building's appearance can be free of constraints and easier to design [65].

Some studies, which are related to the impacts of internal shading devices of different kinds on the indoor daylighting and thermal performances, have been conducted [67-68]. Yao [69] indicated that the shading performance of internal shading device for the internal spaces is superior to that of pane windows. Moreover, a comparison of daylighting and energy performances between four types of the internal rollers was investigated by Tzempelikos and

Shen. [70]. The results show that the rollers can effectively reduce the risk of visual discomfort and solar heat gain, contributing to improving the daylighting quality and decreasing the energy costs. However, the energy consumption of buildings varies by shading device type, leading to the differences in annual energy consumption between them ranging from 10.1% to 34.4%. Gratia et al. [71] stated that by selecting the appropriate type, color and dimensions for the internal shading device, as well as mounting it on a optimal position in building, the energy costs for space cooling can be cut off up to 14% during a sunny day in summer.

2.3.5 Impact of the shading devices' orientation on the energy consumption

Apart from the shading device's type and shape, as well as its installation position, building orientation is also a significant factor influencing the shading performance and building energy cost. Lai et al. [72] researched the impacts of shading devices facing different orientations on the energy costs in two target buildings, which located in Detroit (with high latitude) and Miami (with low latitude), respectively. As windows are covered by full shading, the buildings in the two locations requiring the maximum and minimum total energy loads are both orientated towards the east and south, respectively. Li et al. [73] presented that the energy saving potential varies according to the building orientation, which means that 1.4%, 1.8% and 2.1% of energy savings can be obtained by installing the shading devices on south, east and west walls, respectively. Singh et al. [74] indicated that there are big differences in the visual performances and energy costs for office buildings with the shading devices facing various orientations. The research results show that the reductions in lighting energy for southwest and west are greater than those for north and northeast. Concerning the energy consumption of Heating, Ventilating and Air Conditioning (HVAC), the maximum energy cost is observed for the office building facing east, while the alternative facing north has the lowest energy demand.

Many of the aforementioned studies have demonstrated that the shading devices have a significant impact on the energy requirements due to artificial lighting and air conditioning in buildings [75-76]. A substantial quantity of shading and glazing options have been proposed by researchers to regulate and adjust the indoor visual and thermal environments [77]. In addition, the energy efficient buildings can be achieved, by incorporating the suitable shading device into them [78].

2.3.6 Discussion

In the research field of residential buildings, there are also numerous studies focused largely on the influence of solar shading on the building energy consumption and daylighting performances conducted by O'Brian et al. [79], Arasteh et al. [80], Mavrogianni et al. [81], J. Karlsson [82], Sullivan et al. [83], S. Firlag et al. [84], Kim et al. [85], Vanhoutteghem [86]. Besides, the shading system also plays an important role in improving the occupants'

productivity and health [87]. Due to the shading device having many advantages, it has become a passive strategy commonly applied in both newly-built construction and in retrofit projects. On the other hand, the total energy cost consumed by heating, cooling and lighting systems is responsible for a large proportion of the total in buildings [88]. Thus, the topic of improving the energy saving potential by means of the shading devices has become a major issue for buildings at present, where the internal environment and the energy consumption need to be coupled together to be analyzed in depth [89].

The present research mainly focuses on the impacts that the shading devices facing a limited amount of orientations have on the energy consumption and on indoor daylighting performance, while few studies are based on the study of multiple orientations [74]. In addition, many studies related to the influences of shading devices on the building energy consumption are based on changes in shading depth within a relatively small scope [72]. Whereas, the studies about the impact on the energy consumption performance at a series of SDs, from providing full shading to no shading for glazing, are rather scarce. What's more, the related researches, in particular with regards to the impact of shading device on the energy consumption, have often been neglected to get carried out in the traditional buildings up to now [90].

2.4 Impact of shading devices with various window-to-wall ratio and building azimuth combinations on the energy consumption

2.4.1 Impact of the climate condition on the optimum window-to-wall ratio

There are extensive researches and efforts focused on the Window-to-Wall Ratio (WWR) up to now. Climate conditions have been validated as a vital impact factor on the WWR optimization from many studies [91]. Ghisi and Tinker [92] carried out a study on exploring the appropriate glazing areas for buildings located in two climate zones (Cfb and Cfa), in accordance with the indoor daylighting performances and lighting energy behaviors. The research results show that the optimal glazing ratios were estimated to be in the scope of 20-86% and 10-44% under the Cfa and Cfb climate, respectively. Kheiri et al. [93] researched the optimum window areas for four study buildings situated in diverse climate zones respectively, based on the dynamic energy behaviors of lighting and HVAC. The research results release that the optimum WWRs, which can contribute to lowering the energy requirement, under these four climates are all ranged from 0.2 to 0.32. F. Goia et al. [94] took a highly insulated building under the representative Europe climate as study case to research its energy consumption behaviors. The minimum total energy demand including lighting, cooling and heating is achieved in this building, as its WWR is assigned within a range from 35% to 45%, regardless of building orientation. Using a model of room in office building located in the United States, the impact of WWR on the energy consumption performance under six various climates was researched by Susorova et

al. [95]. In the warm climate zone, a facade with WWR of 0.5-0.8 has the maximum energy saving potential, while a comparatively low WWR ranged from 0.20 to 0.60 is recommended for the Dfa climate zone. In severely cold climate zone, the highest energy saving potential was observed for a building whose south wall has the WWR within range of 0.50-0.80 and north wall is configured with small dimensions of glazing. Chow TT et al. [96] incorporation a daylight simulation module and power output equation into EnergyPlus to investigate the solar management performances for a semi-transparent window in office building located in Hong Kong. The outcome shows that the maximum energy saving was observed for the building with 0.33 of WWR, when the visible transmittance of glazing system is ranged from 0.45 to 0.55. Peng Xue et al. [97] studied the optimal value range of WWR for buildings with different shading device and building orientation combinations situated in a low latitude region of China. They presented that the comprehensive sunshade configuration has the most distinguished performance in terms of energy saving. By mounting this configuration with 1.8 m of shading depth, the acceptable upper limits of WWRs for west-, east-, north- and south-facing facades can be increased up to 0.56, 0.6, 0.6 and 0.78, respectively. In order to explore the optimum WWRs for official buildings located in different climatic zones of Europe, Francesco Goia et al. [98] used the energy simulation tool of Energy Plus to analyze their internal thermal and daylighting performances. The research results reveal that although the optimum WWR varies depending on the building orientation and local climate, the WWRs ranged from 30% to 45% have the highest energy saving potentials in the study buildings in general, regardless of building orientation. Moreover, in comparison with unreasonable WWR, a building with proper WWR contributes to reduction in the building energy consumption by 5~25%. Inanici and Demirbilek [99] investigated the impacts of the north- and south-facing facade's WWRs on the thermal performances in the mid-size residences located in five positions of Turkish within a limited latitude range, which are characterized by different weather conditions. They stated that the optimum WWRs recommended to the residences are dissimilar with varying the location, which are ranged from an upper limit of 0.9 to lower limit of 0.25.

2.4.2 Impact of the building orientation on the optimum window-to-wall ratio

Building orientation is another driving variable affecting the optimum WWRs of buildings cover a wide range of types. CHANG Jing et al. [100] analyzed the correlation between WWR and building energy consumption for residences situated in China. The energy simulation tool of DeST was used to compute the energy requirements of heating and cooling in buildings facing different orientations throughout a year. The research results demonstrate that the total building energy consumption has an increasing trend in relation to increase in the glazing areas on the east-, west- and north- facades. While, as the south-facing facade is mounted with an external shading device and the internal spaces under well-ventilated conditions, increasing glazing area is beneficial to improving the building

energy saving potential during nighttime in summer. Johnosn et al. [101] researched the optimal WWRs and best orientations for buildings located in America. The outcomes indicate that the energy saving could be achieved in buildings with WWRs of less than 20%, but the north-facing facades are suitable to be configured with a large area of glazing. Liwei WEN et al. [102] recommended the optimal WWRs for south-, north-, east- and west-facing facades in 10 prefectures of Japan, based on the evaluation parameter of CO_2 emission. By using Energy Plus to conduct the CO_2 emissions simulation, the results identify that (1) the magnitudes of CO_2 emissions from buildings decrease with increase in WWRs of the four facades in Hokkaido prefecture and the north-facing facade in 10 prefectures; (2) excluding Hokkaido prefecture, the CO_2 emissions in the other 9 prefectures decrease with reduction in WWR of the east facing facade; (3) except for Hokkaido prefecture, the CO_2 emissions reach the minimum values, when the WWRs of south-facing and north-facing facades are both within the range of 30-50%. Feng et al. [103] investigated the impact of WWR on the energy consumption in a nearly zero energy building. The results show that the impact level order of WWR corresponding to different orientations on the energy consumption is east = west > south > north.

2.4.3 Impact of the building energy cost on the optimum window-to-wall ratio

Some researches and efforts have been placed on exploring the optimum WWRs for various types of buildings, based on the evaluation parameter of the energy consumption. Pino et al. [104] indicated that the total annual energy use including cooling and heating in a totally glazed facade building located in Santiago of Chile is 155 $kW \cdot h/m^2$. In a building with WWR of 20%, the total annual energy use is reduced up to 25 $kW \cdot h/m^2$ at maximum. If the night ventilation is available during cooling season, an additional decrease of approximately 37% in the total annual building energy use can be achieved. Moreover, a 20% of WWR is enough to keep the internal spaces having a useful daylight during 80% of the time throughout the year. Goia et al. [105] researched the optimal WWRs for office buildings located in the mild maritime climate zone of Italy, based on the evaluation parameter of energy consumption. According to the research results, when the WWRs of four facades are all within the optimal range of 35-45% in an office building, its energy load is minimal. For none of the four WWRs within the optimal range, the indoor environment experienced the most dramatic shift by varying the glazing sizes is observed for a northerly oriented building. Instead, the variation in WWR for a south facing building has the most negligible impact on the indoor environment. Yanyi Sun et al. [106] integrated the photovoltaics (CdTe solar cells with 10% transparency) into a window system to investigate the annual energy performances in office buildings located in China under five typical climates. The result indicates that the application of PV window can achieve an evident energy saving potential, as the buildings have comparatively large WWRs (i.e., WWR≥45%), in comparison to those mounted with the conventional windows with double glazed system. Touraj Ashrafian et al. [107] researched the impacts of windows

with different WWR and orientation (west and east) combinations on the energy demands and visual comforts in a classroom. Through simulation with the aid of EnergyPlus 8.9, DesignBuilder 5.5 and DIALux Evo 6.0, the results show that a glazing ratio of 50% can reduce the lighting energy consumption by at least 15%, and improve the visual comfort level effectively. Silvia Cesari et al. [108] evaluated the impacts of different glazing sizes on the cooling and heating energy needs in a hospital patient room located in Bologna (Italy). Comparing with the base case (i.e., a room with 25% of WWR), a dramatic decrease in the cooling and heating energy demands achieved attributes to the adoption of larger WWR with proper glazing system.

2.4.4 Discussion

The present research mainly focuses on the impacts that the windows facing a limited quantity of orientations or based on changes in WWR at large increments have on the energy consumption and indoor daylighting performances, while few studies are on the basis of the multiple combinations of WWR and orientation [109-110]. What's more, the related researches, in particular with regards to the impact of window on the energy consumption, have often been neglected to get carried out in the traditional buildings up to now [90].

2.5 Impacts of walls with various construction type and building azimuth combinations on the energy consumption

2.5.1 Optimum thermal insulation thickness in wall based on the criteria of energy consumption

Up to now, extensive efforts and researches were devoted to improve the thermal property of walls in the world. Using an optimum thermal insulation thickness is an effective way to achieve the building energy conservation and save building material cost. Alsayed, et al. [111] used a method of degree-day to research the optimum thermal insulation thicknesses of the external walls with different wall structures (five categories) and insulation types (two categories) combinations in a building. The results show that the optimal thickness of thermal insulation ranges from 0.4 cm to 9 cm, varying by the wall structure and thermal insulation type. Furthermore, Sagbansua, et al. [112] employed the same research method (i.e., degree-day) to determine the optimum thermal insulation thickness, based on the criteria of heating load. The results of this study show that the optimum thicknesses are between 8.7 cm and 18.5 cm, which contribute to the amount of 0.755-9836 $/m^2 in terms of energy saving. M. Ozel [113] studied the impact of glazing with various layers mounted in wall on the optimum thicknesses of thermal insulation materials. In this section, the heat transmission loads passing through wall were analyzed, on the basis of a dynamic energy simulation. In consideration of the different wall orientations, the results indicate that the optimum thicknesses of insulation materials used in a south-facing wall with single glazing and double glazing are within the range of 4-8.5 cm and 2.5-8.5 cm, respectively. In M. Ouzel's [114] study, a transient heat transfer model, based on the implicit finite

difference, has been adopted to calculate the thermal load flowing through walls with various thermal insulation material types. The results state that the optimum thermal insulation thicknesses range from 5.4 cm to 19.2 cm, depending upon the insulation material type. When the optimum thickness insulation materials are employed, the SO_2 and CO_2 emissions are decreased to 0.013-0.040 kg/m^2 per year and 6.37-19.55 kg/m^2 per year, respectively. Based on time-dependent implicit and finite-volume procedures, Al-Sanaa et al. [115] proposed a numerical model to evaluate the thermal transmission load passing through the exterior wall in a building. The results revealed that the optimum thicknesses of polystyrene used as insulation material are between 4.8 cm and 16 cm. Furthermore, Daouas et al. [116] proposed an analytical transient method to estimate the thermal transfer magnitudes through two different walls with different structures (i.e., brick-brick sandwich wall and stone-brick sandwich wall). Rockwool and polystyrene were used as the walls' insulating materials in their study. The results indicate that the payback period for a building integrated with thermal insulation material with an optimum thickness of 5.7 cm is 3.11 years, in synchronicity with 58% of energy saving during this period of time. Using the thermodynamic optimization method, Ucar [117] studied the optimum thicknesses of insulation materials that were employed in the external walls of buildings situated in four cities under different climate conditions. The incorporation of optimum thickness in buildings under the humid continental climate conditions has a 79% higher rate of energy saving potential, in comparison with the alternatives in the other three climate zones.

2.5.2 Thermal performance of wall expressed by means of parameters

Quite often, the thermal performances of building envelope systems are expressed by means of parameter, such as the thermal transfer coefficient (i.e., U-value), w/(m^2·k) and thermal conductivity, w/(m·k), which are commonly applied to the building design standards. Evangelisti et al. [118] carried out an in-situ measurement to evaluate the U-value of building envelope system, based on the uni-directional thermal flow theory. Walker et al. [119] performed a field study on the utilization of the heat flux sensors to conduct a measurement of brick walls' U-values, and validation their U-values through investigation of the thermal images. A study on the thermal property of adobe wall was performed by Zhang et al. [120]. and Berardi et al. [121] to investigate the correlation between the operating temperatures and measured thermal conductivity of wall insulation materials. The research results were validated through the laboratory tests, which revealed that there is dependence between the indoor temperature and wall's thermal conductivity. A similar study was conducted by Abdou et al. [122], and pointed out that variation in the humidity and operating temperature will dramatically impact the thermal conductivity of insulation material (fibrous) used in wall. Kontoleon et al. [123] and Zhang et al. [124], according to the tested results of walls' thermal inertia, stated that increase in the heat storage capacity for a masonry wall will lead to increase in the time lag of thermal

transmission. However, an opposite effect will occur, as the thermal conductivity of insulation material was increased in a masonry wall. Aste et al. [125] adopted the parametric numerical analysis method to study the impact of walls' thermal inertia on the building energy performance. They found that an outstanding energy consumption performance can be realized, by incorporating the proper admittance value and optimal thermal transmittance coefficient value into wall system.

2.5.3 Thermal performance of Trombe wall characterized by passive heating

Many researchers have investigated the impact of Trombe walls, known as passive heating wall, on the energy consumption in buildings. Through the solar design for Trombe wall, the building energy conservation and thermal comfort can be achieved in the internal spaces [126-127], especially in reducing heating energy need [128]. Abbassi et al. [129] researched the influence of Trombe wall area on the building energy consumption. The research results based on an energy simulation show that roughly 77% of the total heating requirement can be cut off in a Tunisian building, by installing Trombe wall with 8 m^2 in a non-insulated wall with the total area of 16 m^2. Through the experimental analysis method, Rabani et al. [130] conducted a study on the heating performance for a newly proposed Trombe wall, which can be covered by solar irradiance from east, south and west orientations. The results revealed that the new Trombe wall can achieve a maximum 10 °C of the indoor temperature rise, in comparison with the conventional Trombe wall. Yu et al. [131] conducted a study on the heating performance of Trombe wall. The results indicated that the outer layer insulated Trombe wall has a better performance in terms of energy efficiency than the conventional Trombe wall, which achieves the energy saving up to 56%. Mohamed et al. [132] carried out a series of experimentation and simulations to research the thermal performances of Trombe walls in Tunisia. The research results demonstrated that during the period of time with highest solar intensity, the air temperatures in a room with single glazed Trombe wall can reach 25 °C, but below 22 °C in an alternative with double glazed Trombe wall. Ma et al. [133] used the software of THERB to research the heating efficiency of Trombe wall with assistance of fan. The results showed that the Trombe wall assisted by a fan can reduce the heating need by 0.6 $kW \cdot h/m^3$ in building interiors. Burek et al. [134] carried out an experimental study about the heat transfer performance and mass flow rate in a Trombe wall. They found that the mass flow rate is directly proportional to the air cavity depth and heat input. However, when the heat input is over 1000 W/m^2, increase in the air cavity depth no longer improves the energy efficiency of Trombe wall. Rabani et al. [135] researched the heating duration of building installed with Trombe wall made of different materials under overcast weather conditions. The results showed that the heating duration corresponding to the brick Trombe wall, concrete Trombe wall and paraffin wax Trombe wall are 8 h 11 min, 7 h 12 min and 8 h 55 min, respectively. Furthermore, Rabani et al. [136] researched the thermal performance of a newly proposed Trombe wall during summer in Iran, integrated with the water spraying system and solar chimney. They

state that using the water spraying system can improve the thermal efficiency of wall by up to 30%. Furthermore, the air movement driven by sunlight in solar chimney contributes to the indoor natural ventilation.

2.5.4 Discussion

The afore-mentioned studies on the thermal performance of cavity wall mainly focus on the heating performances of the glazed cavity walls (i.e., Trombe wall). Moreover, most of the previous studies are related to the thermal insulation property of wall, in terms of in the indoor temperature rise and energy saving during the heating season, while few of them are referred to the heat dissipation performance of the wall during the cooling season. What's more, extensive emphases have been placed in the buffer effectiveness of cavity walls in the traditional dwellings under the harshly outdoor weather conditions, whose target is to improve the thermal comfort levels, while lots of studies are generally neglected to perform the analysis of the building energy consumption up to now [90].

References

[1] HUANG Lingjiang, HAMZA Neveen, LAN Bing, ZAHI Dava. Climate-responsive design of traditional dwellings in the cold-arid regions of Tibet and a field investigation of indoor environments in winter [J]. *Energy and Buildings*, 2016, 128(7): 697-712.

[2] LIU Jianping, WANG Lijuan, YOSHINO Yasuko, et al.The thermal mechanism of warm in winter and cool in summer in China traditional vernacular dwellings [J]. *Building and Environment*, 2011, 46(2): 1709-1715.

[3] LI Angui, GAO Xiaopan, YANG Lehui. Field measurements, assessments and improvement of Kang: case study in rural northwest China [J]. *Energy and Buildings*, 2016, 111(12): 497-506.

[4] GUO Shaoqing, LI Zhengrong, ZHAO Qun, et al. Climate responsive strategies of traditional dwellings located in an ancient village in hot summer and cold winter region of China [J]. *Building and Environment*, 2015, 86(12): 151-165.

[5] DESOGUS Giuseppe, CANNAS Leonardo Giuseppe Felice, SANNA Antonello. Bioclimatic lessons from Mediterranean vernacular architecture: The Sardinian case study [J]. *Energy and Buildings*, 2016, 129(6): 574-588.

[6] SAÁ C., M ÍGUEZ J.L, MORÁN J.CC. A study of the influence of solar radiation and humidity in a bioclimatic traditional Galician agricultural dry storage structure (horreo) [J]. *Energy and Buildings*, 2012, 55(5): 109-117.

[7] BARBERO-BARRERA M.M., GIL-CRESPO I.J., MALDONADO-RAMOS L.. Historical development and environment adaption of the traditional cave-dwellings in Tajuña's vally, Madrid, Spain [J]. *Building and Environment*, 2014, 82(10): 536-545.

[8] Maria Philokyprou, Aimilios Michael, Eleni Malaktou. Environmentally responsive design in Eastern Mediterranean-the case of vernacular architecture in the coastal, lowland and mountainous regions of Cyprus [J]. *Building and Environment*, 2007, 111(1): 91-109.

[9] DianaÜrge-Vorsatz, Luisa F.Cabeza, SusanaSerrano. Heating and cooling energy trends and drivers in buildings [J]. *Renewable and Sustainable Energy Reviews*, 2015, 41(1): 85-98.

[10] F.H. Abanda, L. Byers. An investigation of the impact of building orientation on energy consumption in a domestic building using emerging BIM (Building Information Modelling) [J], *Energy*. 2016, 97(2): 517-527.

[11] Wang KD, Fan Q. Building information modelling (BIM) for sustainable building design [J]. *Facilities*, 2013, 31(3/4): 138-57.

[12] Daniele Torreggiani, Alberto Barbaresi, Francesca Dallacasa, et al. Effects of different architectural solutions on the thermal behaviour in an unconditioned rural building. The case of an Italian winery [J]. *Journal of Agricultural Engineering*, 2018, 49 (1): 52-63.

[13] A. Al-Anzi, O. Khattab, Solar conscious house design in Kuwait [J]. *Kuwait Journal of Science & Engineering*, 2010, 37(2): 59-72.

[14] K.M. Odunfa, T.O. Ojo, V.O. Odunfa, O.S. Ohunakin. Energy efficiency in building: case of buildings at the University of Ibadan [J]. *Journal of Building Construction and Planning Researc*h, 2015 (3): 18-26.

[15] O. Koranteng, E.G. Abaitey. Simulation based analysis on the effects of orientation on energy performance of residential buildings in Ghana [J]. *Journal of Science and Technology (Ghana)*, 2009, 29 (3): 86-101.

[16] A.L.S. Chan, Effect of adjacent shading on the thermal performance of residential buildings in a subtropical region [J]. *Applied Energy*, 2012, 92 (4): 516-522.

[17] Aksoy U, Inalli M. Impacts of some building passive design parameters on heating demand for a cold region [J]. *Building and Environment*, 2006, 12(41): 1742-54.

[18] Ignacio Acosta, Miguel Ángel Campano, Juan Francisco Molina. Window design in architecture: Analysis of energy savings for lighting and visual comfort in residential spaces [J], *Applied Energy*. 2016, 168(2): 493-506.

[19] Ana Brandãode Vasconcelos, António Cabaço , Manuel Duarte Pinheiro, et al. The impact of building orientation and discount rates on a Portuguese reference building refurbishment decision [J], *Energy policy*. 2016, 91(1): 329-340.

[20] Daniel Martin Marin. The impact on building orientation on energy use [D].Gavle: University of Gavle, 2017: 20-24.

[21] Valeria Vitale, Ginevra Salerno. A numerical prediction of the passive cooling effects on thermal comfort for a historical building in Rome [J]. *Energy and Buildings*, 2017, 157(6): 1-10.

[22] M. Humphreys, F. Nicol. Derivation of the Adaptive Equations for Thermal Comfort in Free-running Buildings in European Standard EN15251 [J]. *Building and Environment*, 2010, 45(1): 11-17.

[23] Ma X W, Fan Y Y, Hou Y B. Experiment of natural ventilation for residential buildings during summer time in Shenzhen [J]. *Journal Heating Ventilating and Air conditioning*, 2003, 33(5): 115-118.

[24] M. Almeida, E. Maldonado, M. Santamouris, G. Guarracino. The design of optimal openings in: Natural Ventilation in the Urban Environment: Assessment and Design, 2005: 168-194.

[25] C. Ghiaus, F. Allard. Natural Ventilation in the Urban Environment: Assessment and Design, Earthscan, London, 2005.

[26] N.A.M. Al-Tamimi, S.F.S. Fadzil, W.M.W. Harun. The effects of orientation, ventilation, and varied WWR on the thermal performance of residential rooms in the tropics [J]. *Journal of Sustainable Development*, 2011, 4 (2):142-149.

[27] Hans-peter Brikhofer. SSL lighting hype or the only solution in future lighting with respect to specification and application, Proceedings, Balkan Light 5th International Banlkan Conference on Lighting, October 3-6, 2012: 8-13.

[28] Hans-Peter Birkhofer. SSL Lighting Hype or the only solution in future lighting with respect to specification and application, Proceedings, Balkan Light 5th International Balkan Conference on Lighting, October 3-6, 2012, Belgrade, Serbia, pp. 8-13.

[29] A. Nabil, J. Mardaljevic. Useful daylight illuminance: A replacement for daylight factors [J]. *Energy and Buildings*. 2006, 38 (7): 721-727.

[30] F.C. Winkelmann, S. Selkowitz. Daylighting simulation in the DOE-2 building energy analyses program [J]. *Energy and Buildings*, 1985, 8: 271-286.

[31] M.C. Singh, S.N. Garg. Illumination estimation and daylighting energy savings for Indian regions [J]. *Renewable Energy*, 2010, 35 (3): 703-711.

[32] G.C. Brainard, J.P. Hanafin. The effects of light on human health and behaviour: relevance to architectural lighting, in: Proceedings of the Symp.'04 Light and Health: Non-Visual Effects, CIE, Vienna, 2004.

[33] E. Rautkyla, M. Puolakka. Alerting effects of daytime light exposure- a proposed link between light exposure and light mechanisms [J]. *Lighting Research and Technology* 2012, 44 (9): 238-252.

[34] H. Fischer, H. Freymuth, P. Haeupl, M. Homann, R. Jeninsch, E. Richter, M.Stoehrer. Theory of Building Physics, Vieweg and Taubner Verlag, Germany, 2008.

[35] S. J. Gochenour, M. Andersen. Circadian effects of daylighting in a residential environment, Proceedings Lux Europa 2009-Istanbul, Sept 9-11, 2009.

[36] K.M.J. Farley, J.A. Veitch. A room with a view: A review of the effects of windows on Work and Well-being [D]. Ottawa: Institute for Research in Construction, 2001.

[37] H. Alzoubi, S. Al-Rqaibat, R.F. Bataineh. Preversus post-occupancy evaluation of daylight quality in hospitals [J]. *Building and Environment*, 2010, 45(12): 2652-2665.

[38] A. Jovanović, P. Pejić, S. Djorić-Veljković, Importance of building orientation in determining daylighting quality in student dorm rooms: Physical [J]. *Energy and Buildings*, 2014, 77(3): 158-170.

[39] M. Santamouris. Cooling the buildings-past, present and future [J]. *Energy and Buildings*. 2016, 128 (9): 617-638.

[40] I. Farrou, M. Kolokotroni, M. Building envelope design for climate change mitigation: a case study of hotels in Greece [J]. *International Journal of Sustainable Energy*, 2016, 35 (10): 944-967.

[41] Spanos I, Simons M, Holmes K. Cost savings by application of passive solar heating [J]. *Structural Survey*, 2005, 23(2):111-130.

[42] A. Marsh, Autodesk®Ecotect TM v5.6 Licence Managment, Autodesk, Inc., 2008 ([Visited 06.11.2016]).

[43] F. Gugliermetti, F. Bisegna. Saving energy in residential buildings: the use of fully reversible windows [J]. *Energy*, 2007, 32 (7): 1235-1247.

[44] A. Gasparella, G. Pernigotto, F. Cappelletti, P. Romagnoni, P. Baggio. Analysis and modelling of window and glazing systems energy performance for awell-insulated residential building [J]. *Energy Build.*, 2011, 43: 1030-1037.

[45] Freewan AAY. Impact of external shading devices on thermal and daylighting performance of offices in hot climate regions [J]. *Sol. Energy*, 2014, 102: 14-30.

[46] Yao, J. Determining the energy performance of manually controlled solar shades: a stochastic model based co-simulation analysis [J]. *Appl. Energy*, 2014, 127: 64-80.

[47] Yuan Gao, Jianfei Dong, Olindo Isabella, Rudi Santbergen, Hairen Tan, Miro Zemana, Guoqi Zhang. A photovoltaic window with sun-tracking shading elements towards maximum power generation and non-glare daylighting [J]. *Applied Energy*, 2018, 228: 1454-1472.

[48] Seongkwan Hong, An-Seop Choi, Minki Sung. Development and verification of a slat control method for a bi-directional PV blind [J]. *Applied Energy*, 2017, 206: 1321-1333.

[49] Xue Li, Jinqing Peng, Nianping Li, Yupeng Wu, Yueping Fang, Tao Lie, Meng Wang, Chunlei Wang. Optimal design of photovoltaic shading systems for multi-story buildings [J]. *Journal of Cleaner Production*, 2019, 220: 1024-1038.

[50] Lee ES, DiBartolomeo DL, Selkowitz SE. Thermal and daylighting performance of an automated venetian blind and lighting system in a full-scale private office [J]. *Energy Build.*, 1998, 29: 47-63.

[51] Szymon Firlag, Mehrangiz Yazdanian, Charlie Curcija, Christian Kohler, Simon Vidanovic, Robert Hart, Stephen Czarnecki. Control algorithms for dynamic windows for residential buildings [J]. *Energy Build.*, 2015, 109: 157-173.

[52] M. Mandalaki, K. Zervas, T. Tsoutsos, A. Vazakas. Assessment of fixed shading devices with integrated PV for efficient energy use [J]. *Sol. Energy*, 2012, 86: 2561-2575.

[53] A.Stamatakis, M.Mandalaki, T.Tsoutsos. Multi-criteria analysis for PV integrated in shading devices for Mediterranean region [J]. *Energy and Buildings*, 2016, 117: 128-137.

[54] F. Mazzichi, M. Manzan. Energy and daylight interaction in offices with shading devices, in: Proc. of 1st IBPSA Italy Conference, Bolzano, IT, 2013,

[55] D. Saelens, W. Parys, J. Roofthooft , A.T. De la Torre. Assessment of approaches for modeling louver shading devices in building energy simulation programs [J]. *Energy Build.*, 2013, 60: 286-297.

[56] Bellia L, Marino C, Minichiello F, Pedace A. An overview on solar shading systems for buildings [J]. *Energy Procedia*, 2014, 62: 309-17.

[57] Kim G, Lim H, Lim TS, Schaefer L, Kim JT. Comparative advantage of an exterior shading device in thermal performance for residential buildings [J]. *Energy Build.*, 2012, 46: 105-11.

[58] Cho J, Yoo C, Kim Y. Viability of exterior shading devices for high-rise residential buildings: case study for cooling energy saving and economic feasibility analysis [J]. *Energy Build.*, 2014, 82: 771-785.

[59] Li DHW, Tsang EKW. An analysis of daylighting performance for office buildings in Hong Kong [J]. *Build Environ.*, 2008, 43: 1446-1458.

[60] Waleed Khalid Alhuwayil, Muhammad Abdul Mujeebu, Ali Mohammed M.Algarny. Impact of external shading strategy on energy performance of multi-story hotel building in hot-humid climate [J]. *Energy*, 2019, 169: 1166-1174.

[61] Poirazis H, Blomsterberg A, Wall M. Energy simulations for glazed office buildings in Sweden [J]. *Energy Build.*, 2008, 40: 1161-70.

[62] J. Niu. Some significant environmental issues in high-rise residential building design in urban areas [J]. *Energy and Buildings*, 2004, 36(12): 1259-1263.

[65] Oleskowicz-popiel C, Sobczak M. Effect of the roller blinds on heat losses through a double-glazing window during heating season in Central Europe [J]. *Energy Build.*, 2014, 73: 48-58.

[64] China Architecture & Building Press, Sunshade and Energy Efficiency in Buildings, China Architecture & Building Press, 2009 (in Chinese).

[65] Yunyang Ye, Peng Xu, Jiachen Mao, Ying Ji. Experimental study on the effectiveness of internal shading [J]. *Energy and Buildings*, 2016, 111(12): 154-163.

[66] Grynning Steinar, Time Berit, Matusiak B. Solar shading control strategies in cold climates-heating, cooling demand and daylight availability in office spaces [J]. *Sol. Energy,* 2014, 107: 182-94.

[67] Sanati L, Utzinger M. The effect of window shading design on occupant use of blinds and electric lighting [J]. *Build Environ.*, 2013, 64: 67-76.

[68] Yao J. An investigation into the impact of movable solar shades on energy, indoor thermal and visual comfort improvements [J]. *Build Environ.*, 2014, 71: 24-32.

[69] Yao J. Determining the energy performance of manually controlled solar shades: a stochastic model based co-simulation analysis [J]. *Appl. Energy*, 2014, 127: 64-80.

[70] Tzempelikos A, Shen H. Comparative control strategies for roller shades with respect to daylighting and energy performance [J]. *Build Environ.*, 2013, 67:179-92.

[71] E. Gratia, A. De Herde. The most efficient position of shading devices in a double skin facade [J]. *Energy and Buildings*, 2007, 39(3): 364-373.

[72] Kun Lai, Wen Wang, Harry Giles. Solar shading performance of window with constant and dynamic shading function in different climate zones [J]. *Solar Energy*, 2017, 147(3): 113-125.

[73] Li Li, Ming Qu, Steve Peng. Performance evaluation of building integrated solar thermal shading system: Building energy consumption and daylight provision [J]. *Energy and Buildings*, 2016, 113(12):189-201.

[74] Ramkishore Singh, I.J. Lazarus, V.V.N. Kishore. Uncertainty and sensitivity analyses of energy and visual performances of office building with external venetian blind shading in hot-dry climate [J]. Applied Energy, 2016, 184(10):155-170.

[75] Liu M, Wittchen KB, Heiselberg PK. Control strategies for intelligent glazed facade and their influence on energy and comfort erformance of office buildings in Denmark [J]. *Appl. Energy*, 2015, 145: 43-51.

[76] Goia F, Haase M, Perino M. Optimizing the configuration of a facade module for office buildings by means of integrated thermal and lighting simulations in a total energy perspective [J]. *Appl. Energy*, 2013, 108: 515-527.

[77] O'Brien W, Kapsis K, Athienitis AK. Manually-operated window shade patterns in office buildings: a critical review [J]. *Build Environ.*, 2013, 60: 319-38.

[78] Shen H, Tzempelikos A. Sensitivity analysis on daylighting and energy performance of perimeter offices with automated shading [J]. *Build Environ.*, 2013, 59: 303-314.

[79] W. O'Brian, A. Athienitis, T. Kesik. Thermal zoning and inter zonal airflow in the design and simulation of solar houses: a sensitivity analysis [J]. *J. Build. Perform. Simul.*, 2011,4: 239-256.

[80] J. Apte, D. Arasteh, Y.J. Huang. Future Advanced Windows for Zero-Energy Homes. ASHRAE Transactions 109 Part 2 (2003). Lawrence Berkeley National Laboratory Report LBNL-51913.

[81] A. Mavrogianni, M. Davies, J. Taylor, Z. Chalabi, P. Biddulph, E. Oikonomou, P.Das, B. Jones. The impact of occupancy patterns: occupant-controlled ventilation and shading on indoor overheating risk in domestic environments [J]. *Build. Environ.*, 2014, 78: 183-198.

[82] J. Karlsson, B. Karlsson, A. Roos. Control strategies and energy saving potentials for variable transmittance windows versus static windows, in: Proceedings of Euro sun, 19-22 June, Copenhagen, Denmark, 2000.

[83] R. Sullivan, F. Beck, D. Arasteh, W. Selkowitz. Energy Performance of Evacuated Glazings in Residential Buildings. Report LBL-37130, Lawrence Berkeley Laboratory, 1995.

[84] S. Firlag, M. Yazdanian, C. Curcija, C. Kohler, S. Vidanovic, R. Hart, S. Czarnecki. Control algorithms for dynamic windows for residential buildings [J]. *Energy Build.*, 2015, 109: 157-173.

[85] G. Kim, H.S. Lim, T.S. Lim, L. Schaefer, J.T. Kim. Comparative advantage of an exterior shading device in thermal performance for residential buildings [J]. *Energy Build.*, 2012, 46: 105-111.

[86] L. Vanhoutteghem, S. Svendsen, Modern insulation requirements change the rules of architectural design in low-energy homes [J]. *Renew. Energy*, 2014, 72: 301-310.

[87] M.C. Dubios. Solar Shading and Building Energy Use, Lund University, Lund, 1997.

[88] Goyal S, Ingley HA, Barooah P. Occupancy-based zone-climate control for energy-efficient buildings: complexity vs. performance [J]. *Appl. Energy*, 2013, 106: 209-221.

[89] S. Citherlet, J.A. Clarke, J. Hand. Integration in building physics simulation [J]. *Energy Build.*, 2001, 33: 451-461.

[90] Sonia Longo, Francesco Montana, Eleonora Riva Sanseverino. A review on optimization and cost-optimal methodologies in low-energy buildings design and environmental considerations [J]. *Sustainable Cities and Society*, 2019, 45 (1): 87-104.

[91] Marino C, Nucara A, Pietrafesa M. Does window-to-wall ratio have a significant effect on the energy consumption of buildings? A parametric analysis in Italian climate conditions [J]. *J Build Eng*, 2017, 13: 169-83.

[92] Ghisi, E., Tinker, J.A.. An Ideal Window Area concept for energy efficient integration of daylight and artificial light in buildings [J]. *Build. Environ*, 2005, 40: 51-61.

[93] Farshad Kheiri, M Arch. The relation of orientation and dimensional specifications of window with building energy consumption in four different climates of Koppen classification [J]. *Researcher*, 2013, 5: 107-115.

[94] F. Goia, M. Haase, M. Perino, Optimizing the configuration of a facade module for office buildings by means of integrated thermal and lighting simulations in a total energy perspective[J]. *Appl. Energy*, 2013, 108: 515-527.

[95] Susorova, I., Tabibzadeh, M., Rahman, A., Clack, H.L., Elnimeiri, M.. The effect of geometry factors on fenestration energy performance and energy savings in office buildings [J]. *Energy Build.*, 2013, 57: 6-13.

[96] Chow TT, et al. Performance evaluation of a PV ventilated window applying to office building of Hong Kong [J]. *Energy Build*., 2007, 39(6): 643-50.

[97] Peng Xue, Qian Li, Jingchao Xie. Optimization of window-to-wall ratio with sunshades in China low latitude region considering daylighting and energy saving requirements [J]. *Applied Energy*, 2019, 62: 233-234.

[98] FrancescoGoia. Search for the optimal window-to-wall ratio in office buildings in different European climates and the implications on total energy saving potential [J]. *Solar Energy*, 2016, 132 (7): 467-492.

[99] Inanici, M., Demirbilek, F.. Thermal performance optimization of building aspect ratio and south window size in five cities having different climatic characteristics of Turkey [J]. *Build. Environ.*, 2000, 35: 41-52.

[100] CHANG J, LI Y A. Study on the influence of window area ratio of residential building on heating energy consumption [J]. *Journal Heating Ventilating and Air conditioning*, 2008, 38(5): 109-113.

[101] C. A. Johnson, R. W. Besant, G. J. Schoenau. “Economic preferred window orientation and optimum fenestration design of a non-daylit and daylit large office building for different climate conditions and different billing structures.” [J]. *ASHRAE Transactions*, 1990, 96(1): 23-33.

[102] Liwei Wen, Kyosuke Hiyama, Makoto Koganei. A method for creating maps of recommended window-to-wall ratios to assign appropriate default values in design performance modeling: A case study of a typical office building in Japan [J]. *Energy and Buildings*, 2017, 145 (4): 304-317.

[103] Feng G, Chi D, Xu X, Dou B, Sun Y, Fu Y. Study on the influence of window-wall ratio on the energy consumption of nearly zero energy buildings [J]. *Proc Eng*, 2017, 205: 730-737.

[104] Pino A, Bustamante W, Escobar R, Pino FE. Thermal and lighting behavior of office buildings in Santiago of Chile [J]. *Energy Build*., 2012, 47: 441-449.

[105] F. Goia, M. Haase, M. Perino. "Optimizing the configuration of a facade module for office buildings by means of integrated thermal and lighting simulations in a total energy perspective." [J]. *Applied Energy*, 2013, 108(4): 515-527.

[106] Yanyi Sun, Katie Shank, Hasan Baig. Integrated CdTe PV glazing into windows: energy and daylight performance for different window-to-wall ratio [J]. *Energy Procedia*, 2019, 158: 3014-3019.

[107] Touraj Ashrafian, Nazanin Moazzen. The impact of glazing ratio and window configuration on occupants' comfort and energy demand: The case study of a school building in Eskisehir, Turkey [J]. *Sustainable Cities and Society*, 2019, 47: 101483.

[108] Silvia Cesari, Paolo Valdiserri, Maddalena Coccagn, et al. Energy savings in hospital patient rooms: the role of windows size and glazing properties [J]. *Energy Procedia*, 2018, 148: 1151-1158.

[109] Ramkishore Singh, I.J. Lazarus, V.V.N. Kishore. Uncertainty and sensitivity analyses of energy and visual performances of office building with external venetian blind shading in hot-dry climate [J]. *Applied Energy*, 2016, 184(10): 155-170.

[110] Peizheng MA, Linshu WANG, Nianhua GUO. Maximum window-to-wall ratio of a thermally autonomous building as a function of envelop U-value and ambient temperature amplitude [J]. *Applied Energy*, 2015, 146: 84-91.

[111] M.F. Alsayed, R.A. Tayeh. Life cycle cost analysis for determining optimal insulation thickness in palestinian buildings [J]. *J. Build. Eng.*, 2018, 22(11): 101-112.

[112] L. Sagbansua, F. Balo. Ecological impact & financial feasibility of Energy Recovery (EIFFER) Model for natural insulation material optimization [J]. *Energy Build.*, 2017, 148 (5): 1-14.

[113] M. Ozel. Influence of glazing area on optimum thickness of insulation for different wall orientations [J]. *Appl. Therm. Eng.*, 2019, 147 (10) 770-780.

[114] M. Ozel. Cost analysis for optimum thicknesses and environmental impacts of different insulation materials [J]. *Energy Build.*, 2012, 49 (3) 552-559.

[115] S.A. Al-Sanea, M.F. Zedan, S.A. Al-Ajlan. Effect of electricity tariff on the optimum insulation-thickness in building walls as determined by a dynamic heat-transfer model [J]. *Appl. Energy*, 2005, 82 (10): 313-330.

[116] N. Daouas, Z. Hassen, H. Ben, Aissia. Analytical periodic solution for the study of thermal performance and optimum insulation

thickness of building walls in Tunisia [J]. *Applied Thermal Engineering*, 2010 30(4): 319-326.

[117] A. Ucar. Thermoeconomic analysis method for optimization of insulation thickness for the four different climatic regions of Turkey [J]. *Energy*, 2010, 35 (12) 1854-1864.

[118] Evangelisti L, Guattari C, Gori P, Vollaro RD. In situ thermal transmittance measurements for investigating differences between wall models and actual building performance [J]. *Sustainability*, 2015, 7(8): 10388-10398.

[119] Walker R, Pavía S. Thermal performance of a selection of insulation materials suitable for historic buildings [J]. *Build. Environ.*, 2015, 31(12): 94:155-165.

[120] Zhang J, Xu W, Li A, Zheng K, Zhang J. Study on improving thermal environment and energy conservation of quadrangle adobe dwelling [J]. *Energy Build.*, 2016, 129(10): 92-101.

[121] Berardi U, Tronchin L, Manfren M, Nastasi B. On the effects of variation of thermal conductivity in buildings in the Italian construction sector [J]. *Energies*, 2018, 11(4): 1-17.

[122] Abdou A, Budaiwi I. The variation of thermal conductivity of fibrous insulation materials under different levels of moisture content [J]. *Construct Build. Mater.*, 2013, 43(6): 533-544.

[123] Kontoleon KJ, Theodosiou TG, Tsikaloudaki KG. The influence of concrete density and conductivity on walls' thermal inertia parameters under a variety of masonry and insulation placements [J]. *Appl. Energy*, 2013, 122(12): 325-337.

[124] Zhang L, Zhang J, Wang F, Wang Y. Effects of wall masonry layer's thermophysical properties and insulation position on time lag and decrement factor [J]. *Indoor Built. Environ.*, 2016, 25(2):371-377.

[125] Aste N, Angelotti A, Buzzetti M. The influence of the external walls thermal inertia on the energy performance of well insulated buildings [J]. *Energy Build.*, 2009, 41(11): 1181-1187.

[126] A. Chel, J.K. Nayak, G. Kaushik, Energy conservation in honey storage building using Trombe wall [J], *Energy Build.*, 2008, 40 (9): 1643-1650.

[127] K. Hami, B. Draoui, O. Hami, The thermal performances of a solar wall [J]. *Energy*, 2012, 39 (1): 11-16.

[128] A. Briga-Sa, A. Martins, J. Boaventura-Cunha, J.C. Lanzinha, A. Paiva, Energy performance of Trombe walls: adaptation of ISO 13790:2008(E) to the Portuguese reality [J]. *Energy Build.*, 2014, 74: 111-119.

[129] F. Abbassi, N. Dimassi, L. Dehmani. Energetic study of a Trombe wall system under different Tunisian building configurations [J]. *Energy Build.*, 2014, 80: 302-308.

[130] Rabani M, Kalantar V, Dehghan AA, Faghih AK. Experimental study of the heating performance of a Trombe wall with a new design [J]. *Sol. Energy*, 2015, 118:359-374.

[131] Yu B, He W, Li N, Wang L, Cai J, Chen H, et al. Experimental and numerical performance analysis of a TC-Trombe wall [J]. *Appl. Energy*, 2017, 206: 70-82.

[132] Mohamed L, Dehmani L, Gagliano A. Effect of glazing type on the performance of a Trombe wall in Tunisia [C]. Renewable

Energy Congress (IREC), 2015 6th International: IEEE; 2015: 1-6.

[133] Ma Q, Fukuda H, Kobatake T, Lee M. Study of a double-layer Trombe wall assisted by a temperature-controlled DC fan for heating seasons [J]. *Sustainability*, 2017, 9: 2179.

[134] Burek SAM, Habeb A. Air flow and thermal efficiency characteristics in solar chimneys and Trombe Walls [J]. *Energy Build.*, 2007, 39: 128-135.

[135] Rabani M, Kalantar V, Faghih AK, Rabani M, Rabani R. Numerical simulation of a Trombe wall to predict the energy storage rate and time duration of room heating during the non-sunny periods [J]. *Heat Mass Transfer/Waerme-und Stoffuebertragung*, 2013, 49: 1395-1404.

[136] Rabani M, Kalantar V, Dehghan AA, Faghih AK. Empirical investigation of the cooling performance of a new designed Trombe wall in combination with solar chimney and water spraying system [J]. *Energy Build.*, 2015, 102: 45-57.

Chapter 3

Research methodology and research content

3.1 Determination of study building

With a substantial quantity of 131000 villages, the traditional villages in China constitute a 1.9% of the national administrative villages. Aiming at a better protection of the traditional dwellings, the Ministries of Housing and Urban-Rural Development, Culture and Finance of China have published five editions of the Chinese Traditional Villages' Catalogs, which have recorded the quantity of 6799 villages. There are 646 villages recorded in the first edition, and the other three editions recorded 915, 994 and 1598 villages, respectively. In 2017, the Fifth Traditional Village Survey has been performed, which leads to the sum of protected villages, recorded in the 5 editions of the Chinese Traditional Villages' Catalogs, exceeding 6000.

The protection of traditional dwellings has been getting increasing attention, and their energy consumption and indoor comfort levels are very important factors for the sustainable development of traditional villages. The Sizhai traditional village is recorded in the first edition of the Chinese Traditional Villages' Catalogs, where the dwellings are regarded as the typical and representative house sample among the rural residences. Furthermore, taking into consideration the little research on the energy consumption in the traditional buildings, the traditional dwellings located in Sizhai village with latitude 29°34' North and 120°26' East, were chosen to be the study buildings in this study.

3.2 Building model's dimensions used in simulation

Google Earth (G.E.) is incorporated with GIS (Geographic Information System), aerial photography and satellite photos in a three-dimensional earth model, as well as supplies functionality of distance measurement and GPS (Global Position System), with relatively high accuracy.

The building areas of all dwellings (i.e., 437 buildings) in Sizhai village, were calculated in G.E. by utilizing the distance measurement tool to measure their lengths and widths, respectively (Fig. 3.1). The building areas were divided into 7 intervals at 100 m^2 of increments, and the statistics of building quantity and percentage distribution for each 100 m^2 interval are shown in Fig. 3.2. According to equation (3.1), the average value of all dwelling areas (S) is 158.5 m^2, which was chosen as the reference of plane dimensions for the building model of test scenario in the building energy consumption simulation.

$$S = \sum [50 + 100 \times (n - 1)] \times f_n = 158.5 \quad (3.1)$$

Where, n is the number of the building area interval; f_n is the percentage of dwelling quantity within the number n interval.

By field investigation, the gable wall lengths of Sizhai traditional dwellings were determined to be generally within the range of 6-8 m. The front facades are mostly comprised of three or five bays (i.e., suites), among which the middle bay width is 4-5 m and other bay widths are 3-4 m. In this study, the traditional dwelling with 5 bays was selected as the layout pattern for the test scenario, whose dimensions of middle bay are 8 m×5 m and the other four are 8 m×3.7 m.

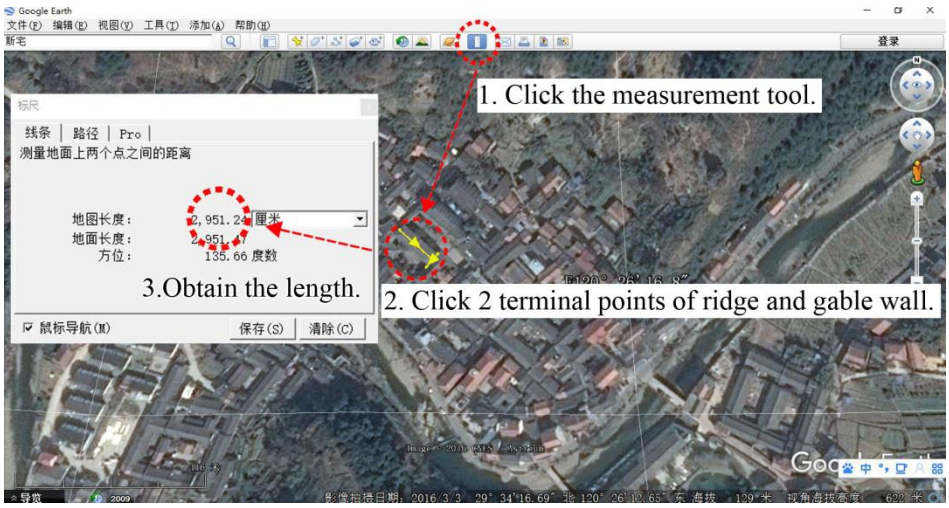

Fig. 3.1 Measurement method of dwelling dimensions in Google Earth

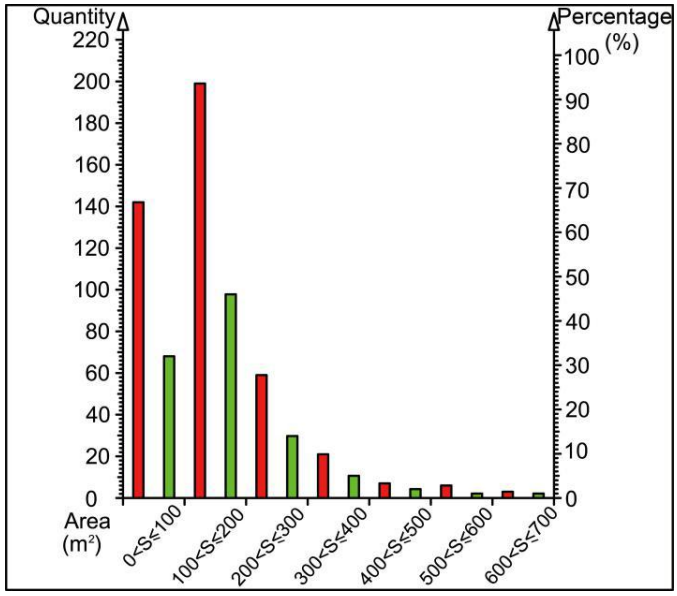

Fig. 3.2 Statistics of building quantity and percentage for Sizhai village

The traditional dwellings in Sizhai village generally have 2 storeys, of which the heights of the first and second floor are approximately 4 m and 2.1 m, respectively. The front facade openings are configured with lots of lattice doors and lattice windows. However, the back facade is comparatively opaque, and there are no windows in the two gable walls. In this work, the front facade equipped with glazing is used as the reference to determine BA of dwelling.

In order to avoid the impact of windows in other walls on the simulation results, the building model of the test scenario is created as shown in Fig. 3.3 and Fig. 3.4. The visible transmittance and solar heat gain coefficient of single glazed window used in the test scenario is 0.83 and 0.8 respectively, and the other details are listed in Table 3.1. Since the second floors in Sizhai traditional dwellings are usually used as storage spaces for grain, farming tools, etc., and the first floors are living spaces, the first floor was chosen as the simulation scene in the software to conducted various parameters predictions.

The heat transfer coefficient (K, W/(m^2·k)) is applied to express the thermal property of the wall, since it widely used in many other researched as described in section 2. When the direction of heat flow parallel to the envelope structure composed of several layers with different materials, the equation of total thermal resistance (R, m^2·k/w) was derived as Eq. (3.2).

$$R = \sum R_n = \frac{d_n}{\lambda_n} \tag{3.2}$$

$$R_n = \sum \frac{d_n}{\lambda_n} + R_i + R_o \tag{3.3}$$

Where, R_n is thermal resistance of each layer, m^2·k/w. d_n is thickness of each layer, m. λ_n is heat conductivity coefficient of each layer, W/(m·k). R_i is the heat exchange resistance of the inner layer surface contacted with the indoor air, which was assumed to be 0.11 according to the *Thermal design code for civil building* (GB50176-2016) issued in China, m^2·k/ W. R_o is the heat exchange resistance of the outer layer surface contacted with the outdoor air, which was assumed to be 0.05 according the code, m^2·k/ W. Based on Eq. (3.2), the K was formulated as Eq. (3.4).

$$K = \frac{1}{R} \tag{3.4}$$

The solar heat gain coefficient and visible transmittance of single glazed windows installed in the building models are 0.8 and 0.83, respectively. In accordance with Eq. (3.4), the U-values of envelopes and the detailed description of the building constructions are listed in Table 3.1.

Fig. 3.3 Front facade details and size description of building model in simulation

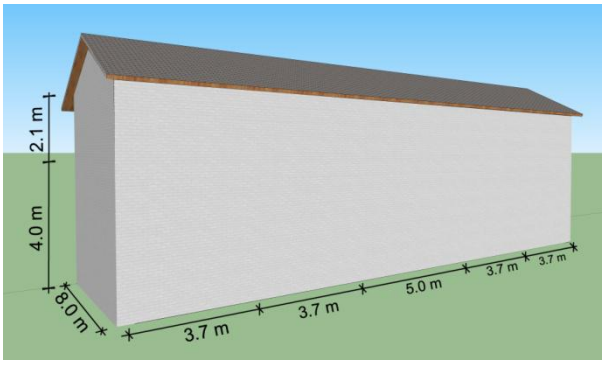

Fig. 3.4 Back facade details and size description of building model in simulation

Table 3.1 Construction features and material properties of the study building

Designation	External brick wall	External timber wall	Tile roof	Lattice window
Picture				
Construction	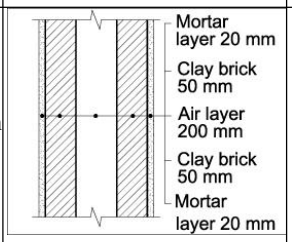	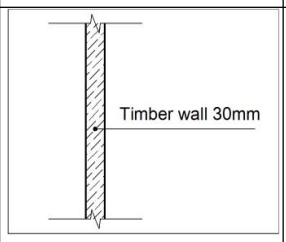	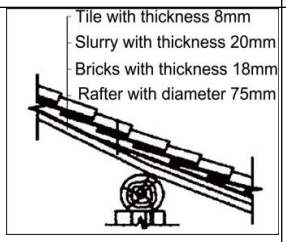	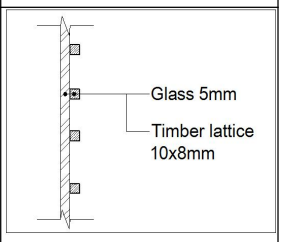
U-value	2.72 W/(m^2·K)	4.33 W/(m^2·K)	3.87 W/(m^2·K)	5.24 W/(m^2·K)

3.3 Division of building azimuth interval

The BA is a parameter that measures and expresses the building orientation. Aiming at performing an in-depth research of the impact of building orientation on the indoor environment and energy cost, the building model was rotated at 20° increments clockwise to create a total of 18 BA intervals (Fig. 3.5, 3.6). Each building azimuth (BA) interval is marked by a different color in order to facilitate the follow-up statistics. To simplify the simulation process, the intermediate value of each BA interval is chosen as a representative parameter in software. For example, the representative parameter for BA interval of [350°, 10°] marked red, is 0°(i.e., S), which represents the BA scope of test scenario ranging from south by east 10° to south by west 10°. Consequently, there are 18 test scenarios corresponding to a certain SD, as the intermediate value of each interval is chosen.

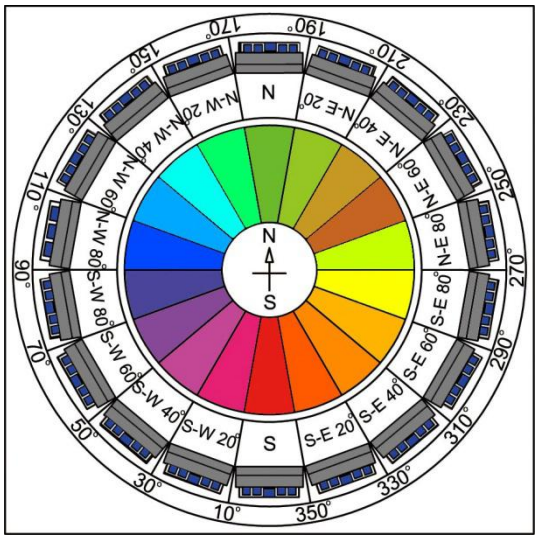

Fig. 3.5 Division of 18 building azimuth intervals for the test scenarios

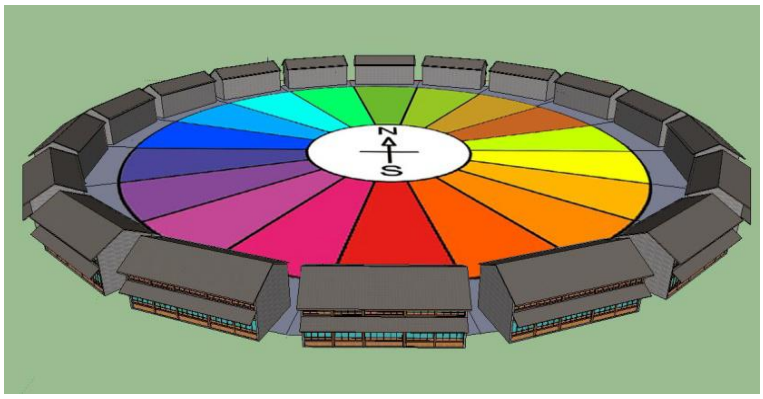

Fig. 3.6 Schematic division of 18 building azimuth intervals for the test scenarios

3.4 Division of shading depth interval

Based on the criterion of typology, the shading devices can be divided into shutter, roller, venetian blind and overhang. Indoor daylighting and energy consumption performances in building vary greatly depending on the shading device type [1]. Roof eaves and corridors mounted on the facades of Shizai traditional dwellings belong to the overhang type, which are again regarded as the horizontal shading devices. Furthermore, according to the shading device is movable or not, it can has two classifications (i.e., the movable shading device and fixed shading device). Obviously, roof eaves and corridors in traditional dwellings are categorized as the movable shading device.

The shading depth (SD) is a key factor impacting the performance of the shading device [2]. In this study, the SD (i.e., L_1 as shown in Fig. 3.7-3.8) is defined as the distance between the outer terminal of shading device and the external surface of the wall. The included angle of a_3 can be derived by the following equation:

$$a_3 = |180° - a_1| \tag{3.5}$$

Where, a_3 (Fig. 3.9) is the included angle between the normal of south-facing wall and horizontal projection line of solar radiation, °; a_1 is the solar azimuth, °. According to the trigonometric functions, the b_1 (Fig. 3.8-3.9) is formulated as equation (3.6).

$$\tan b_1 = \frac{\tan a_2}{\cos a_3} = \frac{\tan a_2}{\cos|180° - a_1|} \tag{3.6}$$

Where, b_1 is the included angle between the wall normal and vertical projection line of solar ray, °; a_2 is the solar altitude, °. The correlation between L_1 and H_3 is formulated as equation (3.7):

$$L_1 = \frac{H_3 + H_4}{\tan b_1} \tag{3.7}$$

Where, H_1 is the height of the corridor roof, m; H_3 is the shadow height on the window, m; H_4 is the height from the bottom of the corridor roof to the top of the window, m.

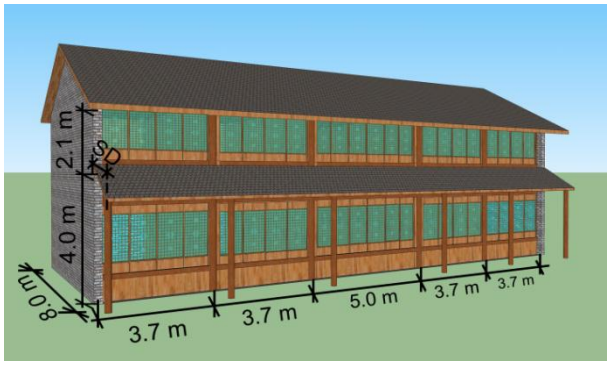

Fig. 3.7 Shading depth shown in front facade of the geometric model

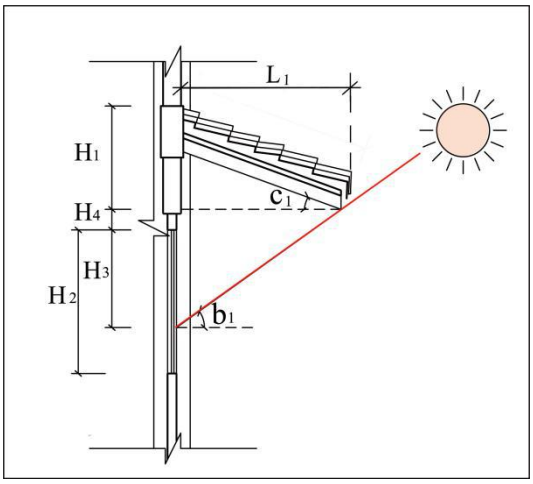

Fig. 3.8 Schematic of shading depth and window shaded by corridor roof

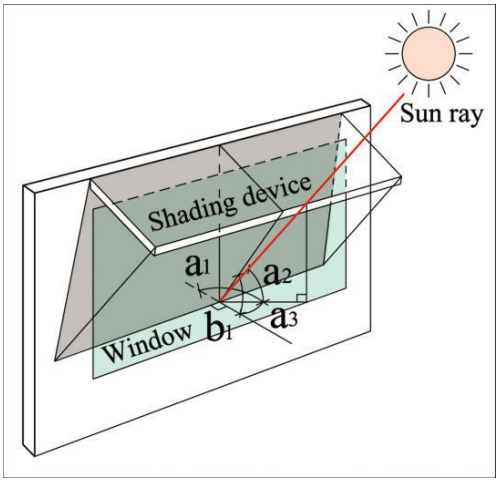

Fig. 3.9 Schematic of various angles on solar shading used in equation formulation

The sun on the summer solstice and winter solstice is located at the highest and lowest points in the sky at noon, on the longest and shortest days of the year respectively, whose solar altitudes are 83°43’ and 36°56’ in Sizhai. Due largely to the Sizhai village being located in the climate zone of humid subtropical climate (Cfa) according to the Köppen-Geiger Climate Classification [3], it is characterized by the pluvial climate here. The constructions of traditional dwellings in East and Central China are erected by complying with the professional standard of *Ying Zao Fa Yuan* (a book on elaborating the construction methods of the traditional dwellings in East and South China). Thus, the tilt angles of the roof and overhang are both quite large, about 30° (i.e., c_1). The bottom edge of the window is 0.9 m above the floor. Thanks to the particularity of the brick-timber construction, the overhang needs to be combined with wooden parts to ensure its solidity and safety, as shown in Fig. 3.8. The window heights (H_2) are generally equivalent to 2 m in the Sizhai traditional dwellings, so the H_4 can be calculated, which is equivalent to 1.1 m. Based on the information above, the L_1 can be determined by substituting the given data into equation (3.7). The maximum and minimum SDs providing no shading and full shading to the window are 0.125 m on the summer solstice and

2.334 m on the winter solstice, respectively. For simplification, the chosen SD range varies from 0.12 m to 2.37 m, at 0.25 m increments which divide it into 9 intervals (Table 3.2). By adopting the terminal values of each interval, the building model corresponding to a certain BA generates 10 test scenarios.

Table 3.2 Building models with 10 kinds of shading depths at 0.25 m increments

SD of 0.12 m	SD of 0.37 m	SD of 0.62 m
WWR of 0.87 m	WWR of 11.2 m	SD of 1.37 m
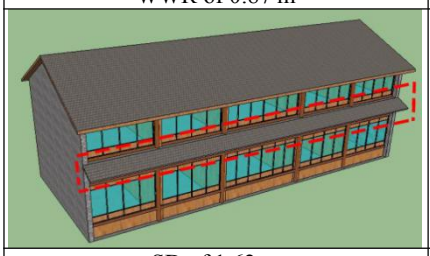	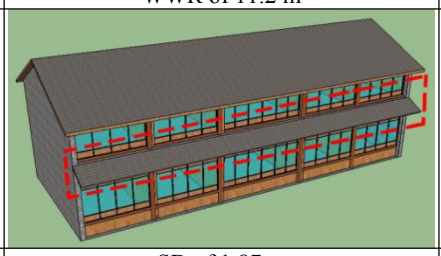	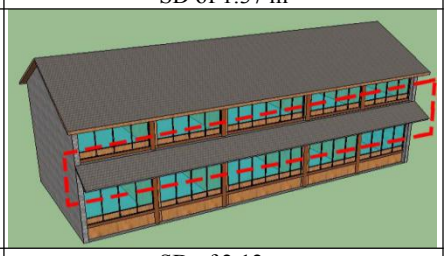
SD of 1.62 m	SD of 1.87 m	SD of 2.12 m
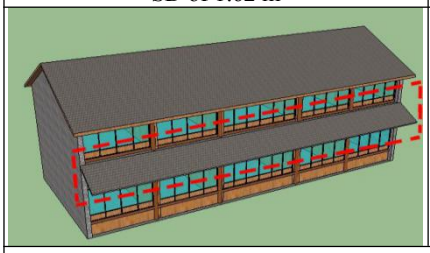	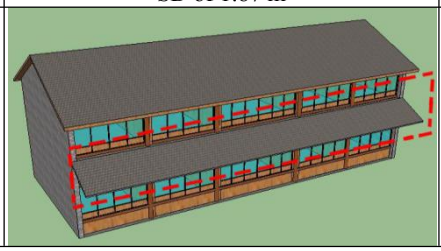	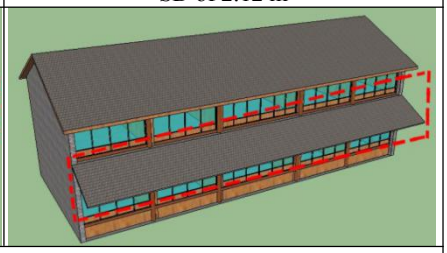
SD of 2.37 m		
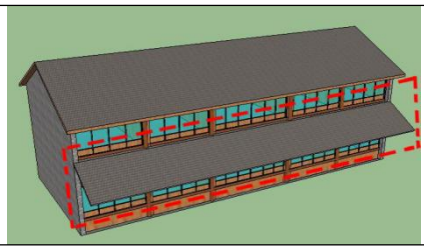		

3.5 Division of window-to-wall ratio interval

WWR is defined as the ratio of glazing area (S_g) to facade area (S_f) or the percentage of facade area installed with glazing (equation 3.8). Since the indoor environments and energy costs are varied by changing Window-to-Wall Ratio (WWR), the WWR of front facade was divided into 10 intervals at increments of 0.1. Deleting two terminal intervals of [0~0.1] and [0.9~1] that are not applied to dwellings commonly, the variable scope of WWR was ranged from [0.1~0.2] to [0.8~0.9] in this work. By adopting the terminal values of each interval, there are total 9 test scenarios corresponding to a certain BA (Table 3.3).

$$WWR=S_g/S_f \qquad (3.8)$$

Table 3.3 Building models with 9 kinds of window-to-wall ratios at 0.1 of increments

WWR of 0.1		WWR of 0.2		WWR of 0.3	
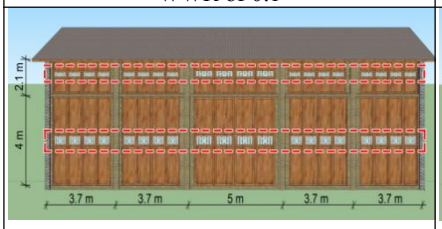		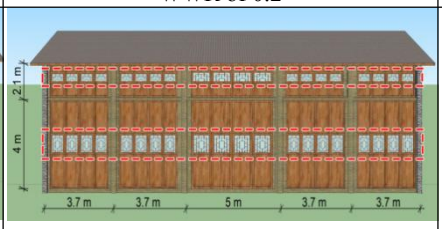		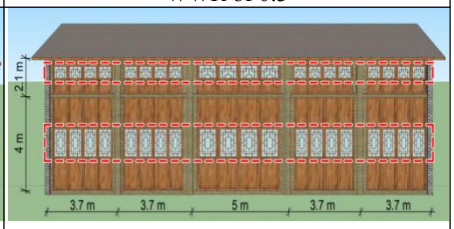	
Window area (m^2)	1F: 7.92, 2F: 4.16	Window area (m^2)	1F: 15.84, 2F: 8.32	Window area (m^2)	1F: 23.76, 2F: 12.48
WWR of 0.4		WWR of 0.5		WWR of 0.6	
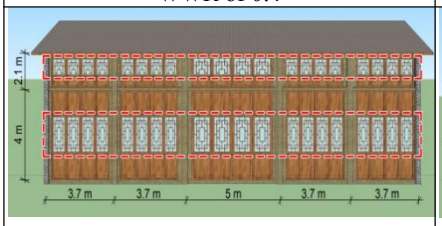		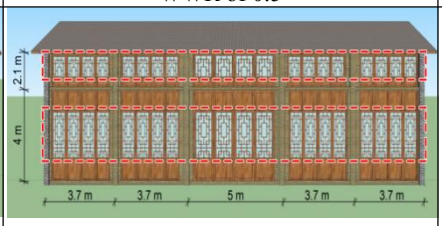		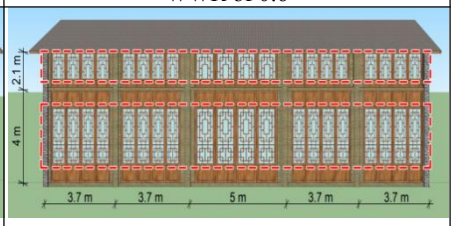	
Window area (m^2)	1F: 31.58, 2F: 16.64	Window area (m^2)	1F: 39.6, 2F: 20.8	Window area (m^2)	1F: 47.52, 2F: 24.96
WWR of 0.7		WWR of 0.8		WWR of 0.9	
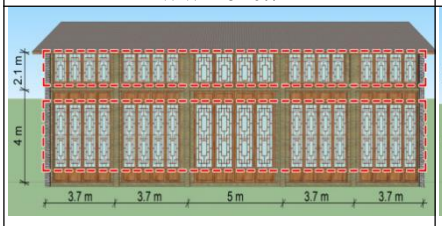		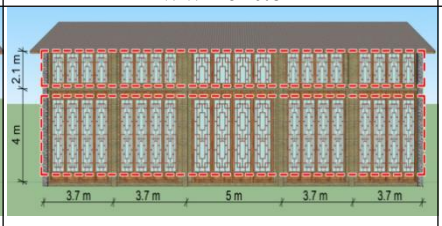		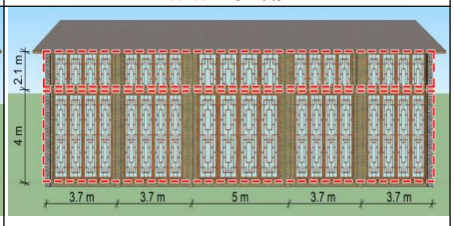	
Window area (m^2)	1F: 55.44, 2F: 29.12	Window area (m^2)	1F: 63.36, 2F: 33.28	Window area (m^2)	1F: 71.28, 2F: 37.44

3.6 Description of various passive cooling wall types used in simulation

With the ever-increasing demands of energy conservation, the thermal insulation performance of traditional cavity brick walls is not satisfied with the currently new energy saving codes yet. To this end, based on the two test scenarios (i.e., base building and testing building) (Table 3.4.1-3.4.2), another two novel types of vented cavity brick walls were proposed in this work, to create an air circulation condition for walls for decreasing the heat flowing through walls. The novelly-designed scenario 1 is the building model with doubled inner layer thickness of vented cavity brick wall (see Table 3.4.3), and the novelly-designed scenario 2 is the alternative with doubled layer thickness in outer layer (see Table 3.4.4). The lower vent and upper vent were created for each bay of the test building, the novelly-designed scenario 1 and the novelly-designed scenario 2, as shown in Table 3.4.

Through field investigation, the heights of traditional dwellings in Sizhai are generally 4 m. The centers of lower vent and upper vent, whose dimensions are both 0.24 m (Height) × 0.24 m (Width) equivalent to the sum of two bricks' area on the facade, were assumed to be placed 0.36 m and 3.64 m above the flooring on the first floor, respectively. In cooling season, the two vents in test building, novel scenarios were opened, for the sake of passive cooling. In contrast, all of the vents in each of the building models were sealed by bricks during winter, aiming at heat insulation.

Table 3.4 Details of wall constructions for the building models used in simulation

3.4.1 Base building		
Schematic	Summer	Winter
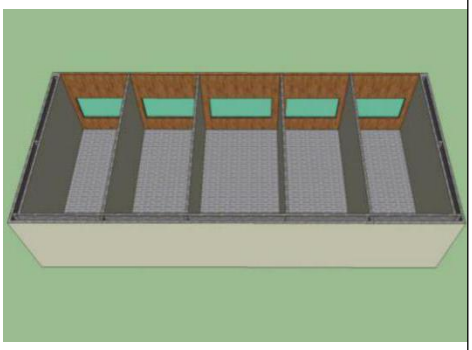	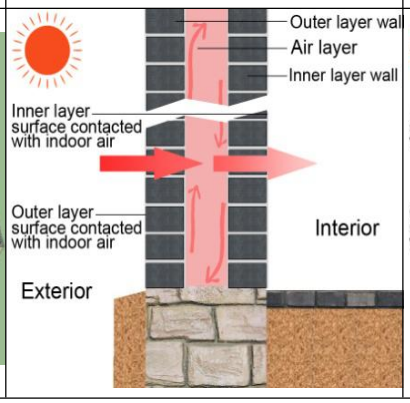	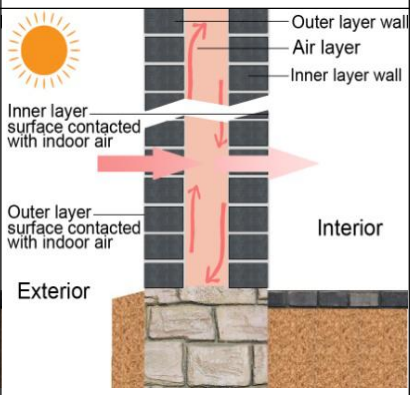
3.4.2 Test building		
Schematic	Summer (vents opened)	Winter (vents closed)
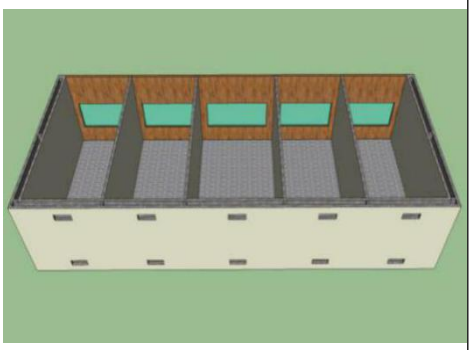	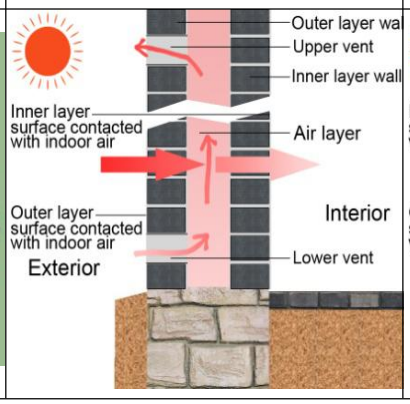	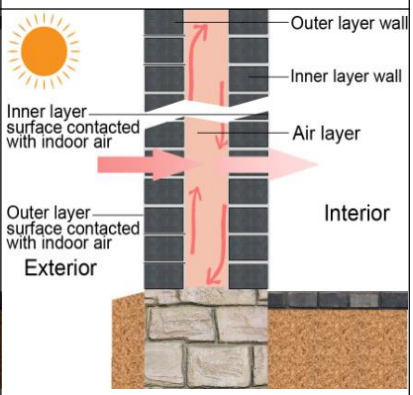
3.4.3 Novelly-designed scenario 1		
Schematic	Summer (vents opened)	Winter (vents closed)
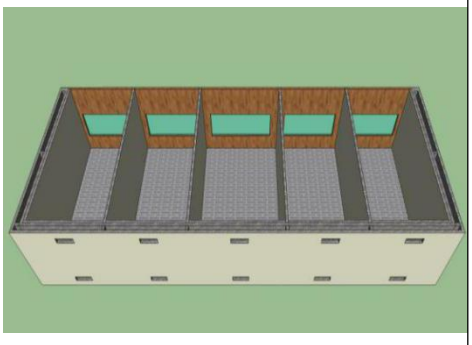	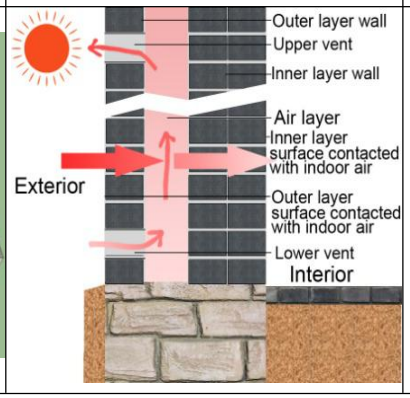	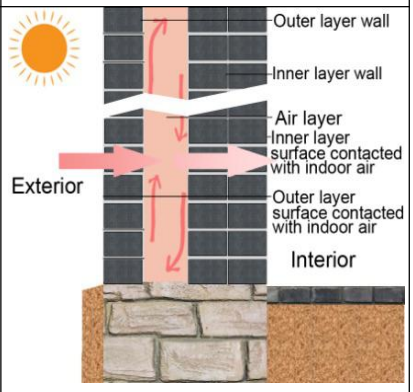
3.4.4 Novelly-designed scenario 2		
Schematic	Summer (vents opened)	Winter (vents closed)
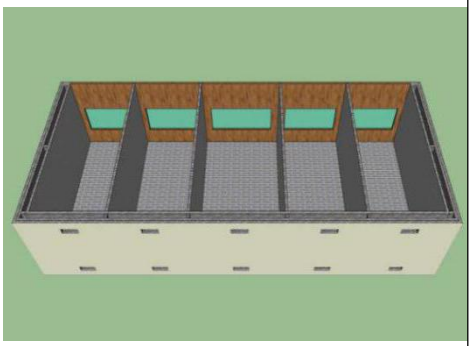	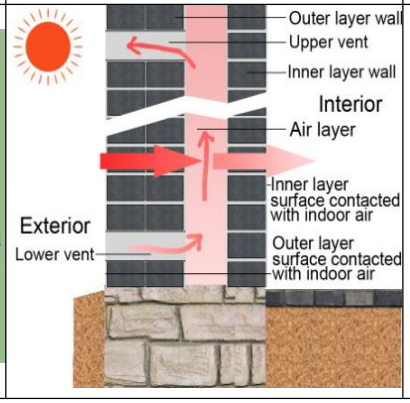	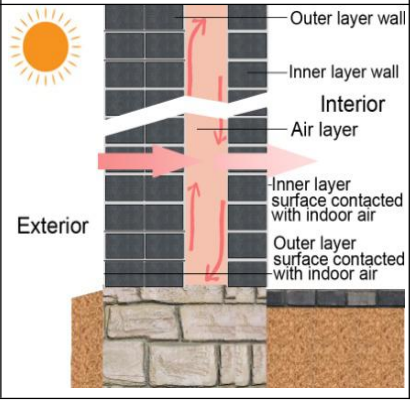

By means of increase in the thickness of inner layer or outer layer for the cavity wall, it can succeed in efficiently blocking the heat transmission. As afore-mentioned, the heat transfer coefficient of the traditional cavity brick wall is 2.72 W/(m^2·K), which can not meat the currently new codes in China. Here, the heat transfer coefficient of two novelly-designed brick walls is 1.34 W/(m^2·K), by using the Eq. (3.4), which is lower the upper limit of 1.5 W/(m^2·K).

3.7 Design day data assumed in simulation

According to human sensations, the upper limit of temperature within thermal comfort ranges from 28 ℃ to 29 ℃, and the lower limit of that ranges from 5 ℃ to 10 ℃. The climate in Sizhai is characterized by high air temperature and high humidity in summer, while sunny weather conditions are prevailing in winter. Taking into consideration the actual working conditions of Air Conditioning (AC) being controlled by occupants, hence, the criteria of turning on the AC, according to the exterior temperature in this study, are that the mean monthly temperature is greater than or equivalent to 28℃ in summer and lower than or equivalent to 5℃ in winter. According to the meteorological data in Sizhai throughout the year (Fig. 3.10), the internal spaces need to be air-conditioned for four months (i.e., three months need cooling and one month needs heating). Therefore, the cooling season in summer is consisted of June, July and August, and the period of time needing heating in winter is January.

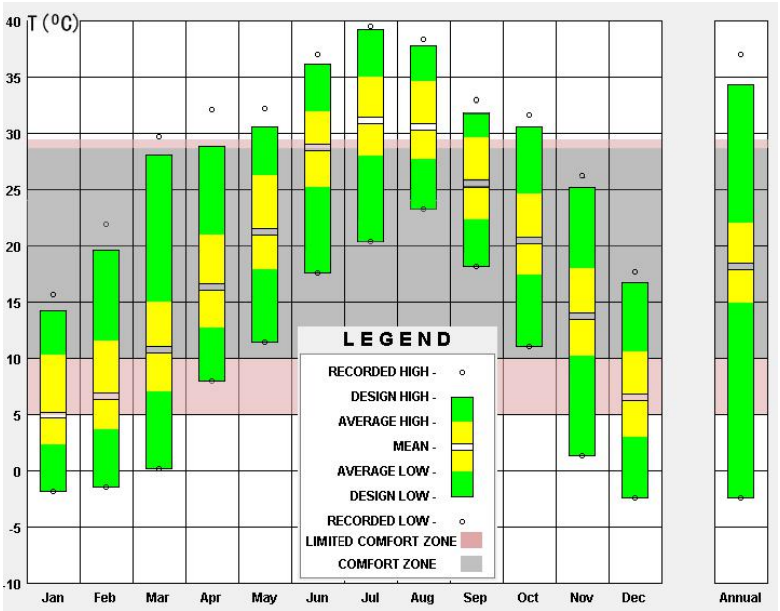

Notes: 1. Record High and Low Temperatures (round dots) note what are probably not the all-time record high and low temperatures for that zone but rather represent the average record high and low temperatures. 2. Design High and Low Temperatures (top and bottom of green bars) are used to calculate the sizes of the heating and cooling equipment. 3. Average High and Low Temperature (top and bottom of yellow bars) are the averages of the highest and lowest dry bulb temperatures for each day during a month or a year. 4. Mean Temperature (open slot) is the average of all dry bulb temperatures.

Fig. 3.10 Monthly and annual air temperatures in Sizhai village

3.8 Selection of simulation tool

The building energy performances can be computed by numerous energy simulation tools, such as EnergyPlus, IES-VE, ESP-r, TRNSYS, etc. However, through the review study on applying different tools to simulate energy costs in buildings by varying WWR, Energy Plus is the most widely adopted, due to it with high accuracy of computational results [4]. Moreover, the incorporation of DOE-2 and BLAST programs into this tool can conduct the energy simulation of cooling, heating, lighting and ventilating for different types of buildings [5]. The ArchiWIZARD is a piece of building energy assessment software integrated with the Energy Plus plug-in, especially worked for the BIM models [6]. As obvious, the solar heat gain and solar radiation reception will influence the indoor air temperatures and illuminance, respectively [7]. To this end, the ArchiWIZARD integrated with the EnergyPlus in-plug, characterized by time saving during running, is suitable to be adopted in this work. The weather data file with format type of typical meteorological year 2 (TMY2) was used for computing the building energy demand [8], which can be converted by the DOE-2 program to make it compatible with Energy Plus [9]. On the other hand, the TMY2 format data were created by the National Renewable Energy Laboratory's Analytic Studies Division under the Resource Assessment Program, which can be downloaded freely from the U.S. National Renewable Energy Laboratory.

Besides, the other two simulation tools of VELUX Daylight Visualizer 2 and Ecotect 2012 were used in this work. The VELUX Daylight Visualizer 2 [10] is a professional lighting simulation tool for the analysis of daylight conditions in buildings, which was used to analyze the visual comfort rate in each of the test scenarios in this work. Besides, the Ecotect 2012 [11] is a piece of whole building simulation tool, which can be used to predict the thermal, acoustic and visual performances in buildings. The thermal performance analysis method in this tool based on the Chartered Institution of Building Services Engineers (CIBSE) is fitted to perform indoor air temperature simulation in this study. Since the indoor illuminance and air temperature can impact the energy demands of artificial lighting and AC [12], the software of ArchiWIZARD (version 3.1.1) was adopted again to research their correlations.

Appendixes

Appendix 1 Software used in this study

Designation	Legend	Functionality	Application in this study
1.1 Ecotect 2012		The Ecotect produced by the Autodesk® .With a powerful function in fields of simulation and analysis, can be used to simulate the indoor daylighting conditions, variation tendencies of time-to-time temperatures and thermal environments. The data and charts of simulation results are with concise and accurate characteristics.	Simulation of daylighting and temperature
1.2 PHOENICS 2009		It was launched commercially in 1981 by Concentration Heat and Momentum Limited in Wimbledon, London, UK as the world's first general-purpose CFD code. An assessment software for building energy conservation simulates and analyzes the conditions of indoor and outdoor ventilation. The velocity, amplification coefficients of air velocity, wind pressure, etc., can be accurately simulated.	Simulation of indoor natural ventilation
1.3 VELUX Daylight Visualizer 2	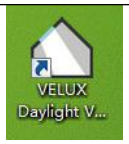	It was produced by the company of the VELUX Group. It is a professional daylighting simulation tool for buildings that intends to promote the use of daylighting and to aid professionals during realization of the building design. From small investigations to full project evaluations, it lets you calculate the performance of daylight in users' designs.	Simulation of IDF
1.4 Climate Consultant 6.0		It was created by Building Technology and Urban Systems Division, U.S. Department of Energy. It contains detailed climatic data of different regions all over the world. The data include solar radiation, temperature, humidity, atmospheric pressure, etc., which can be transferred to EPW file directly.	Simulation of ICT
1.5 ArchiWIZARD 3.1.1		It was created by the French company of GRAITEC. The tool is a real-time 3D analysis software based on BIM model directly. ArchiWIZARD provides accurate air temperature, thermal, light, solar gains and shadows analysis, renewable energy simulation.	Simulation of energy consumption
1.6 Google Earth		It was created by the Google company in U.S.. Google Earth is incorporated with GIS (Geographic Information System), aerial photography and satellite photos in a three-dimensional earth model, as well as supplies functionality of distance measurement and GPS (Global Position System), with relatively high accuracy.	Measuring building azimuth and distance

Appendix 2 Measurement instruments used in this study

Designation	Synopsis	Picture
2.1 Infrared camera	Type: FLIR T460 T632; accuracy: ±2℃; range of the measurement: -20~1500℃; thermal sensitivity/NETD: <0.03℃ @+30.	
2.2 Illuminometer	Type: 061206363; Accuracy: ±3%; Range of the measurement: 1~100000lux.	
2.3 Hygrothermograph	Type: 20100117; Accuracy of temperature measurement: ±1℃; Accuracy of relative humidity measurement: ±3% (30~99%) ±5% (5%~30%); Range of the temperature measurement: -10℃~50℃; Range of the relative humidity measurement: 5%RH~99%RH.	
2.4 Infrared thermometer	Type: AS530; Accuracy of temperature measurement: ±2% or ±2℃; Range of the temperature measurement: -32℃~320℃.	
2.5 Anemograph	Type: 20100110; Pattern: hot ball anemometer; Distinguish ability: 0.01; Range of the measurement: 0.01~30 m/s.	

References

[1] Li Li, Ming Qu, Steve Peng. Performance evaluation of building integrated solar thermal shading system: Building energy consumption and daylight provision [J]. *Energy and Buildings*, 2016, 113(12):189-201.

[2] Jinkyun Cho, Changwoo Yoo, Yundeok Kim. Viability of exterior shading devices for high-rise residential buildings: Case study for cooling energy saving and economic feasibility analysis [J]. *Energy and Buildings*, 2014, 82(8): 771-785.

[3] M. Kottek, J. Grieser, C. Beck, B. Rudolf, F. Rubel, World map of the Köppen-Geiger climate classification updated, Meteorol. Z. 2006, 15 (3): 259-263.

[4] Ramos G, Ghisi E. Analysis of daylight calculated using the Energy Plus programme [J]. *Renew Sust Energy Rev*, 2010, 14: 1948-1958.

[5] Seo D, Ihm P, Krarti M. Development of an optimal daylighting controller [J]. *Build Environ*, 2011, 46(10): 1011-1022.

[6] Fumo N, Mago P, Luck R. Methodology to estimate building energy consumption using Energy Plus Benchmark Models [J]. *Energy Build*, 2010, 42(7): 2331-2347.

[7] F. Mazzichi, M. Manzan. Energy and daylight interaction in offices with shading devices, in: Proc. of 1st IBPSA Italy Conference, Bolzano, IT, 2013.

[8] Kun Lai, Wen Wang, Harry Giles. Solar shading performance of window with constant and dynamic shading function in different climate zones [J]. *Solar Energy*, 2017, 147(3): 113-125.

[9] Ramkishore Singh, I.J. Lazarus, V.V.N. Kishore. Uncertainty and sensitivity analyses of energy and visual performances of office building with external venetian blind shading in hot-dry climate [J]. *Applied Energy*, 2016, 184(10): 155-170.

[10] Ignacio Acosta, Carmen Munoz, Miguel Angel Campano, Jaime Navarro. Analysis of daylight factors and energy saving allowed by windows under overcast sky conditions [J]. *Renewable Energy*, 2015, 77(5): 194-207.

[11] Jinkyun Cho, Changwoo Yoo, Yundeok Kim. Viability of exterior shading devices for high-rise residential buildings: Case study for cooling energy saving and economic feasibility analysis [J]. *Energy and Buildings*, 2014, 82(8): 771-785.

[12] Reeves T, Olbina S, Issa R. Validation of building energy modeling tools: Ecotect™, Green Building Studio™ and IES™. In: Laroque C, Himmelspach J, Pasupathy R, Rose O, Uhrmacher AM, editors. Proceedings of the 2012 Winter Simulation Conference. Berlin: Germany; 2012.

Chapter 4

Investigation of the traditional dwellings' characteristics in East and Central China

4.1 Introduction

4.1.1 Motivation

China has a vast territory with various landform and large latitudinal extension resulting in a diversity of climates. Climate is a major factor that impacts the energy consumption of a building. Without the influence of climate, it is difficult to generate and explain diverse building styles [1]. The climate adaptation strategies of traditional dwellings vary greatly depending on local climate, since the building materials and techniques are different in each climate zone. The traditional dwellings in China are classified into five categories in accordance with the criteria of building materials and structural types (Fig. 4.1) [2]. With a substantial quantity of 131000 villages, the traditional villages in China constitute 1.9% of the national administrative villages. Aiming at a better protection for the traditional dwellings, the Ministries of Housing and Urban-Rural Development, Culture and Finance of China have published five editions of Chinese Traditional Villages' Catalogs, which include the total quantity of 6799 villages.

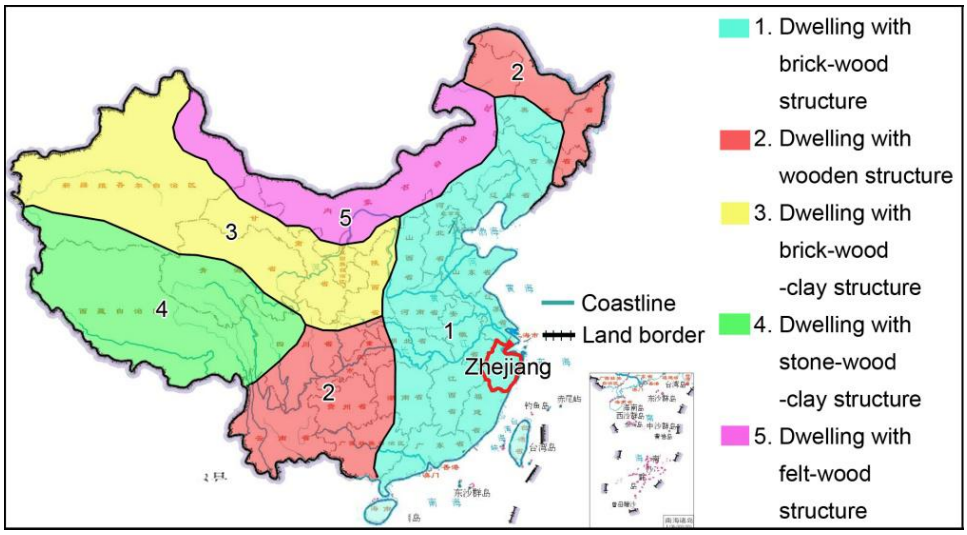

Fig. 4.1 Geographic distribution of the five categories of Chinese traditional dwellings and location of Zhejiang Province

Victor Olgyay, in his Climate Balanced Theory, indicated that buildings should merge with outdoor environments and comply with the principle of preservation of the natural environment. At the same time, architects need to take full advantage of natural resources and try to balance the relationship between buildings and nature [3]. Not only do the architectural configurations and craft techniques of traditional dwellings reflect the social culture, customs, and life-styles, but they also are the results of climate adaptation, which have been evolving constantly over a long period of time [4]. Furthermore, the formations and arrangements of traditional dwellings are the harmonious results of external conditions and internal replies, which rely on the medium with an effective interaction between the components of building and the local climatic conditions [5]. Although traditional dwellings are not as efficient as modern reinforced concrete buildings, in terms of sound insulation [6] and air tightness of envelope [7], the levels of

carbon emissions and energy consumption are much lower and the climate adaptation is much more effective in traditional dwellings [8]. Relying on passive climate-responsive strategies, traditional dwellings can buffer the indoor thermo-hygrometric and daylighting fluctuations by using the favorable climatic elements like wind, solar radiation, etc [9]. Consequently, the indoor microclimate can be kept stable and adjusted to the comfort limits, which provides the environments with thermal and visual comfort for the occupants [9].

The thermal performances in traditional dwellings are considered in the design and construction phase, contributing to creation of internal spaces with a good thermal comfort [10], so the active strategies of indoor temperature regulation systems are almost never applied [11]. The total energy consumption per unit of traditional dwelling area, with 18.0 kWh/m^2-yearly is much lower than that of urban residences with 27.0 kWh/m^2-yearly (exclusion of heating and cooling energy cost in both cases as there are no heating or cooling systems in traditional dwellings for a fair comparison) in China. Especially in the case of electricity cost, the average electricity cost of traditional dwelling with 6.24 kWh/m^2-yearly just accounts for 40% of the energy used in urban residences [12-13]. Low energy consumption and comfortable indoor environment are the major factors for a sustainable development of traditional villages, so these topics are worthy of being studied.

4.1.2 Scientific originality

Many studies used the methodologies of field measurements and software simulations to assess the degree of climate adaptation for traditional dwellings/vernacular buildings to local climate. Nonetheless, the passive climate-responsive strategies of traditional dwellings for indoor environments have not been classified systematically, and the Extension Level of Indoor Comfort Time (ELICT) with assistance of Buffer Effects (BEs) generated by passive strategies has also not been researched qualitatively and quantitatively so far. In this chapter, the passive climate-responsive strategies are categorized into PE and PS. In addition, an intensive study on ELICT corresponding to each BE of PEs and PSs is carried out.

4.1.3 Purpose of the work

Zhejiang Province is located in East China (Fig. 4.1), where climate is characterized by hot summer and cold winter. According to the diverse climatic and topographic conditions there, the Zhejiang traditional dwellings are classified into five categories (Fig. 4.2) [14]. The dwellings in Sizhai traditional village belong to the category of Eastern Zhejiang traditional dwelling, which are included in the first edition of Chinese Traditional Villages' Catalog, were chosen as the research topic in this chapter. The research results of passive strategies are summarized from the study case of Thousand Pillars Dwelling (TPD) and its effectiveness of climate adaptation can provide some methods and implications to create more comfortable indoor environments for rural residences.

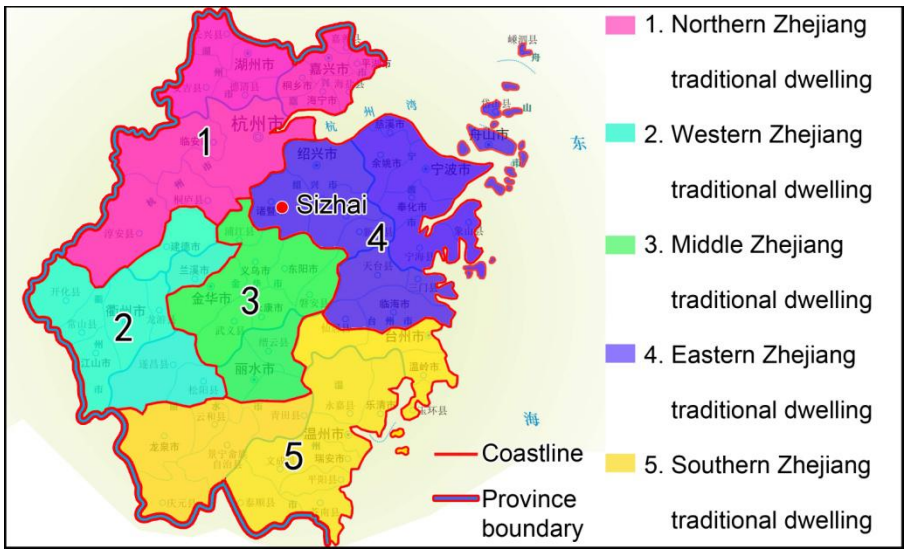

Fig. 4.2 Distribution of five categories of traditional dwelling in Zhejiang Province and location of Sizhai village

4.2 Research content and research methods framework

4.2.1 Theoretical foundations for this work

In the early 1970s, American scholar Holling was first to introduce the elasticity theory [15]. He applied it to ecology for researching the quantity of external disturbance that an ecosystem can bear [16]. Gradually, this theory was applied to other fields. Although the definitions of elasticity theories defined in each field are different [17], the various definitions have a common meaning that the Elasticity Effects (EEs) have a capability to buffer and mitigate outside impingement [18]. Currently, the definition scope of elasticity theory in architecture field is broad. The buildings with the properties of flexibility, adaptability and changeability are all regarded as elasticity buildings [19-20]. As for the traditional dwellings, the elasticity theory states that under the condition of meeting structural performances and spatial requirements, the EEs of passive climate-responsive strategies could improve the indoor comfort level [21].

4.2.2 Field investigation for the traditional dwellings

By means of literature reviews and field investigations, the Passive Elements (PEs) and Passive Spaces (PSs) in TPD were researched, and each EE's characteristics of PEs and PSs were concluded as well. The PEs in TPD consist of door, window, brick wall, wooden wall, perforated window, waist eave, roof and flooring, and the PSs include patio, corridor and open-hall. Based on the field survey, both the material performances of PEs and configuration features of PSs are analyzed. Besides, an infrared camera (Type FLIR T460 T632) was used to take photos of PEs and PSs, aiming at researching the effectiveness of climate adaptation for TPD. Combined with some software analyses, the characteristics of the traditional dwelling were explored.

4.2.3 In-situ measurement for the traditional dwellings

4.2.3.1 Description of in-situ measurement position and testing time

Filed measurement is the assignment of a number to a characteristic of an object or event, which can be compared with other objects or events. The scope and application of field measurement are dependent on the context and discipline. In architecture field, the filed measurement refers to obtain the desired data through directly contact with the respective subject, such as wind velocity, air temperature, relative humidity, as opposed to remote sensing instruments (e.g., weather radar or satellites).

The field measurements were performed to research the degree of TPD's climate adaptation to local climate conditions. In this research, the climatic parameters were adopted to measure include air temperature, relative humidity, air velocity, illuminance and wall surface temperature. The measurements of the air temperature, relative humidity, air velocity and illuminance in both summer and winter were taken 3 days in a row from Aug 4 to Aug 6 and from Dec 29 to Dec 31 in 2015. Regarding the measurements of wall surface temperatures, it was conducted on July 20, 2018 from 6:00 a.m. to 18:00 p.m.

4.2.3.2 Distribution of measurement points in the traditional dwelling

To study the indoor thermo-hygrometric and daylighting conditions quantitatively, we took measurements in three main rooms of TPD. In addition, the point in an outer square outside the building was also selected to measure for comparison. The measurement positions in the traditional dwellings of TPD are shown in Fig. 4.3.

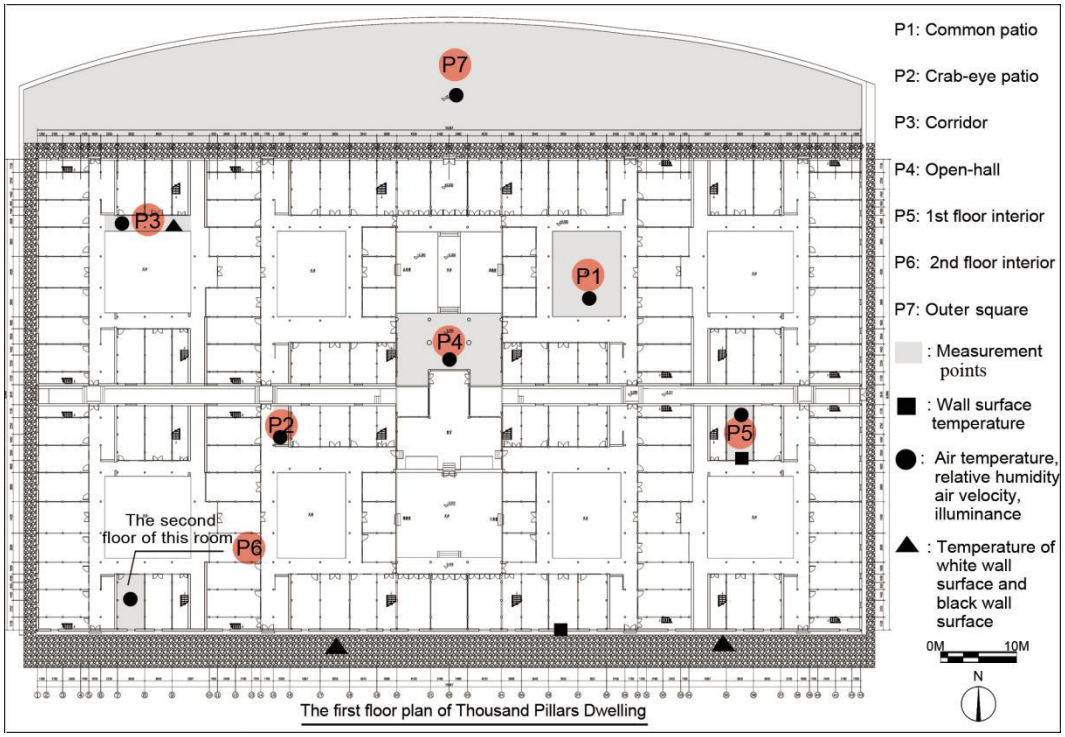

Fig. 4.3 Seven measurement points in the traditional dwelling

The selection principle of measurement points is to use non-occupied spaces and to spread collection points throughout the mansion as much as possible. In detail, (1) P1 is a common patio; (2) P2 is a crab-eye patio; (3) P3 is a corridor; (4) P4 is an open-hall; (5) P5 is a room on the first floor; (6) P6 is a room on the second floor; (7) P7 is an outer square. The measurement details and conditions are depicted in Table 4.1.

Table 4.1 Measurement details and conditions of each point in the traditional dwelling

No.	Location and orientation	Function	Area (m^2)	Window-to-wall ratio (%)		Condition during the measurement
				South-facing wall	North-facing wall	
P1	1st floor	Large patio	104.45			Non-occupied
P2	1st floor	Small patio	11.56			Non-occupied
P3	1st floor, south-facing	Corridor	25.38			Non-occupied
P4	1st floor, south-facing	Open-hall	124.08	1	0.10	Non-occupied, non-heated or non-cooled, no artificial lighting, no electric ventilation
P5	1st floor, south-facing	Suite	27.29	0.46	0.14	Non-occupied, non-heated or non-cooled, no artificial lighting, no electric ventilation
P6	2nd floor, north-facing	Storeroom	27.29	0.46	0.14	Non-occupied, non-heated or non-cooled, no artificial lighting, no electric ventilation
P7	1st floor	Square	1018.05			Non-occupied

4.2.3.3 Description of measurement tools used in this work

Data loggers used to measure the air temperature, relative humidity and illuminance were all placed in shaded spaces in both interiors and exteriors. These climatic parameters were recorded by data loggers of illuminometer (Type 061206363) and hygrothermograph (Type 20100117). Besides, the infrared thermometer (Type AS530) and anemograph (Type 20100110) were used to measure the external and internal surface temperatures for both wooden and brick walls and air velocities, respectively. All data loggers were operated at a height of 0.9 m above ground and all data were recorded at 1 h intervals.

4.2.4 Dynamic simulation for the traditional dwellings

Climate Consultant 6.0 is a simple-to-use, graphic-based computer program that helps architects, builders, contractor, homeowners, and students understand their local climate, which can suggest the most appropriate passive design strategies for buildings in each climate zone and calculate the ICT corresponding to diverse passive strategies. Besides, it uses annual 8760 hour EPW format climate data that is made available at no cost by the Department of Energy for thousands of weather stations around the world. In this work, the tool of Climate Consultant 6.0 was employed to analyze the passive strategy performance of traditional dwellings.

The California's 2013 Energy Code embedded in this software was chosen as comfort model in the simulation. The comfort parameters are the indoor dry bulb temperature that should be between 20℃ and 23.9℃. But the relative humidity limits are not specified in the code, a relative humidity with 80% and 66 ℉ (18.9℃) wet bulb is used for upper limit and 27 ℉ (-2.8℃) dew point is used for lower limit. Based on different EEs of PEs and PSs in TPD, the distributions and proportions of ICT in each month were simulated and computed. Following the preceding qualitative and quantitative analysis, the study on ways and effectiveness of EEs are concluded. To facilitate understanding, the research methods framework is shown in Fig. 4.4.

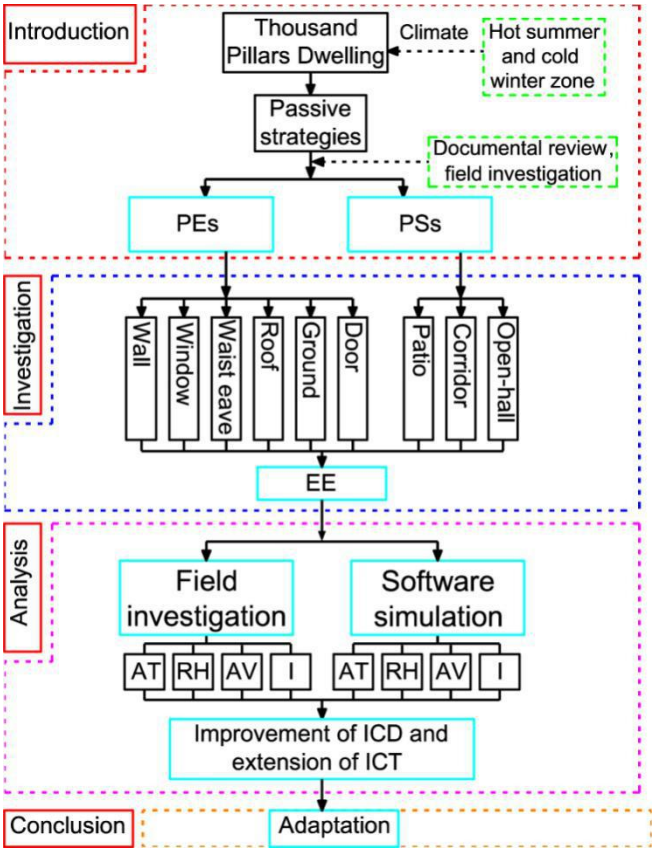

Note: AT: air temperature, RH: relative humidity, AV: air velocity, I: illuminance.

Fig. 4.4 Research methods framework

4.3 Descriptions of study building and climatic features

4.3.1 Description of study building (Thousand Pillars Dwelling)

The Sizhai traditional village is located in the mountainous area of western Zhuji city, Zhejiang Province, China (Fig. 4.2). The terrain of the village slopes down from east to west forming a valley with an exit on the west side. According to the village geography and building typology, Sizhai village is considered as a typical mountainous traditional village. The TPD (Fig. 4.5- 4.6) with 852 pillars, situated in the western part of the village is also called as

"Si Sheng Mansion", which was selected as the study building in this work.

With magnificent momentum and antique beauty, it was built by the 32nd descendant named Si Yuanru in 1798. The total area of the building base for TPD is 6850.14 m^2, with 108.56 m length and 63.10 m width. The layout of this mansion is divided into 8 quadrangle dwellings, 10 large patios, 36 small patios, 32 corridors and 118 rooms, as shown in Fig. 4.7. The layout of the TPD is present a symmetrical distribution with the south-north axis and east-west axis located in the middle of the building.

Fig. 4.5 Position of Thousand Pillar Dwelling in Sizhai village

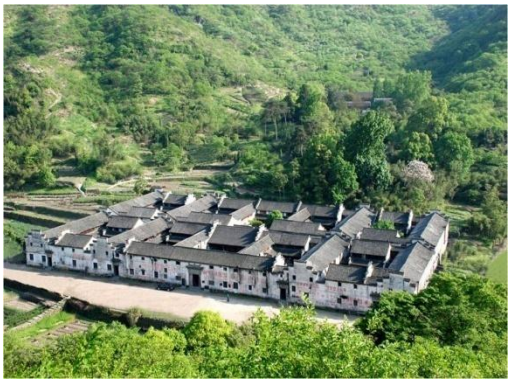

Fig. 4.6 Bird's-eye view of Thousand Pillar Dwelling

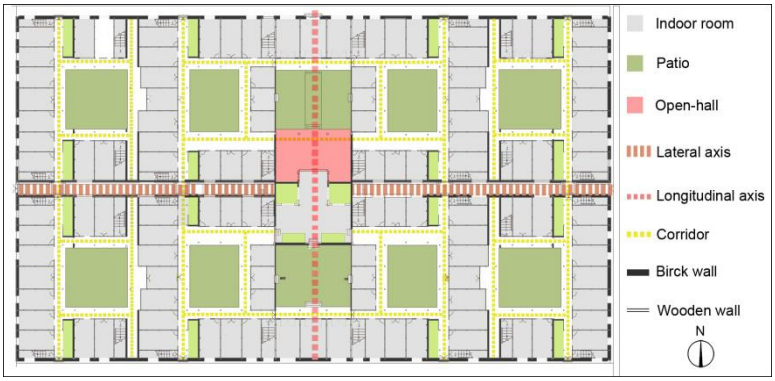

Fig. 4.7 Layout and configuration of Thousand Pillar Dwelling

4.3.2 Description of local climatic features

According to the *Code for Design of Civil Buildings* (GB50352-2005) [22], Sizhai village is in the predominantly hot summer and cold winter area, with latitude 29°43' North and longitude 120°14' East. Moreover, in compliance with the Köppen-Geiger Climate Classification [23], the climate zone of Sizhai belongs to humid subtropical climate (Cfa). Influenced by marine moist air flows and southeastern monsoon simultaneously in May, cool and warm airflow converge here resulting in turbulent weather. Beginning from June, the subtropical high-pressure with warm

and humid airflow from the Pacific Ocean meets the cold airflow from northern China leading to intense rains (plum rains). From July to October, Sizhai experiences the high relative humidity and harshly hot weather conditions. As cold northern air moves to the south of China constantly from December to February, the winter season is characterized by the minimum temperatures and a dry climate. Then air temperature rises gradually during the period from March to April. July is the hottest month throughout the whole year with mean temperature of 31.7℃, while January is the coldest month with an average of 5.4℃. The mean annual temperature is slightly above 15.0℃ (Fig. 4.8-a), and the annual precipitation, precipitation days, average relative humidity and sunshine duration per year are 1373.60 mm, 158.30 d, 82%, and 1887.60 h, respectively. In addition, the southeasterly and northwesterly winds prevail in summer and winter respectively (Fig. 4.8-b), and the mean annual air velocity is approximately 1.90 m/s.

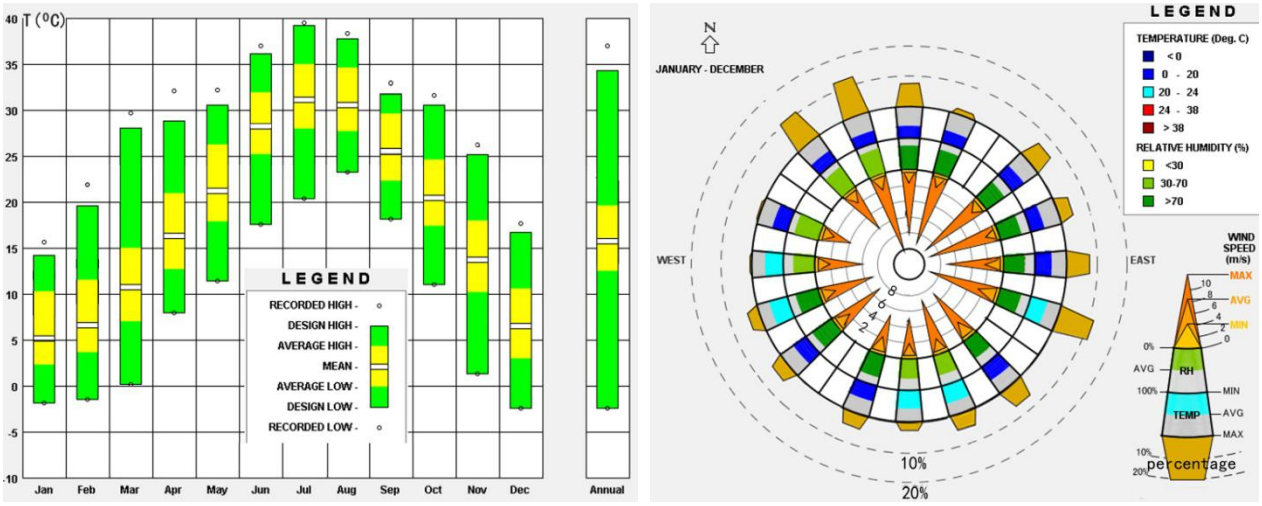

Fig. 4.8 Climate data of Sizhai village (a-left figure) and (b-right figure)

4.4 Field investigation for the traditional dwelling of Thousand Pillar Dwelling

4.4.1 Passive strategies of climate adaptation in traditional dwelling of Thousand Pillar Dwelling

Climatic conditions consist of wind environment and thermal environment, which, in turn, can be described by the measurements of air velocity, air temperature, humidity and radiation, etc [24]. A considerable quantity of elements impact ICL, but most of them are correlated with climate, for instance, air temperature, average radiant temperature, relative humidity and air velocity, etc. Taking into consideration the climatic features of Sizhai with "long summer and short winter", the most challenging issue to solve is to successfully adapt to the weather of summer period. So, the predominant design principle for TPD is "consideration of heat insulation in summer as a priority and thermal preservation in winter as a minor" [25].

To utilize some favourable factors existing in natural climate adequately and to prolong the ICT to the maximum, the passive strategies need to be used. The ancient craftsmen usually regarded buildings as facilities used for

adjusting and regulating indoor environments. By applying a variety of passive strategies like PEs and PSs, they aimed at adapting buildings to local climate and improving ICL [26].

4.4.2 Passive elements in the traditional dwelling of Thousand Pillar Dwelling

The PE of TPD is comprised of Dynamic Passive Element (DPE) and Static Passive Element (SPE) (Table 4.2). The DPEs have open-close function controlled by occupants. Reversely, the SPEs are the static building components.

Table 4.2 Characteristics and types of passive elements in the traditional dwelling of Thousand Pillar Dwelling

Designation		DPE				SPE					
Element		Door in brick wall	Door in wooden wall	Window in brick wall	Window in wooden wall	External brick wall	External wooden wall	Perforated window	Waist eave	Roof	Flooring
Picture											
Main material		Wood	Wood, single-glazing	Stone, wood, single-glazing	Wood, single-glazing	Clay brick, stone	Wood	Stone	Tile, wood	Tile, wood, clay brick	Clay brick
U-value W/(m^2·K)		2.83	3.11	2.72	3.11	0. 68	2.33	7.53	0.88	0.88	0.82
Characteristics	Double-layered construction		●	●	●	●				●	
	Deep overhang								●	●	
	Low thermal conductivity	●	●	●	●	●	●	●	●	●	●
	Closing	●	●	●	●						
	Opening	●	●	●	●			◎			
Position	Vertical interface	●	●	●	●	●	●	●			
	Top interface								●	●	
	Bottom interface										●

Note: 1. ● represents an element with strong performance, ◎ represents an element with medium performance. 2. The U-values of building elements are generated from software of ArchiWIZARD 3.1.1.

The DPEs can exert the adjustment and modification effects to mitigate the impacts of outdoor climate variations on interiors. Besides, those elements are a kind of medium connecting buildings with nature to create a mutual relation between them. By opening or closing the DPEs, the ICL can be effectively improved in TPD. The SPEs are characterized by a closed envelope that creates a comparatively independent space, which can buffer or mitigate the adverse impact of outdoor climate on indoor environments.

4.4.2.1 Passive strategy used in Wall of traditional dwelling

The material of gable walls and back walls in TPD is sintered clay brick (Fig. 4.9). Stones are employed as plinths for the external brick walls with height of 500 mm aiming at reinforcing the foundation and damp-proofing (Fig. 4.9).

The thickness of external brick wall is 340 mm, 300 mm of which corresponds to a rowlock cavity wall composed of 2 single 50 mm brick walls with 200 mm of air layer between them. Besides, 20 mm layers of mortar are brushed on both outer surfaces of the rowlock cavity wall (Fig. 4.10).

The walls of TPD orientated towards patios are made of wood (Chinese torreya and pine) with 30 mm thickness (Fig. 4.11). Timber is characterized by high heat storing capacity and low heat conductivity, so it does not allow its surface to gain a large amount of heat throughout the day, and resulting in poor heat transfer performance [27].

Fig. 4.9 External brick wall in TPD in traditional dwelling

Fig. 4.10 Construction of external brick wall in traditional dwelling

Fig. 4.11 External wooden wall in TPD in traditional dwelling

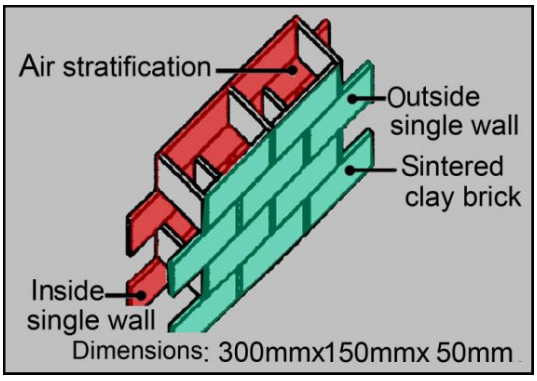

Fig. 4.12 Schematic of external brick wall in traditional dwelling

(1) Heat insulation and thermal preservation strategies

The brick walls in TPD are a kind of compound walls which employ the rowlock cavity pattern aiming at creating an insulating layer of air inside (Fig. 4.12). When the air temperatures between interior and exterior are different, the outer layer of the wall gains heat, resulting in its inner surface temperature differing from the temperature of air inclosed in the wall inside. With slow changes of air temperatures in the airtight space, the heat transfer between two single brick walls turns into a process of conduction, convection and radiation. Subsequently, the heat is gradually transferred to internal spaces (Table 4.3.1.1). The heat transfer coefficients of brick walls with different constructions can be calculated in compliance with equations formulated by DI Peng [28]. Under the condition of a single layer wall

and a compound wall with the same solid thickness of 240 mm, the process of heat transfer in compound wall (with heat transfer coefficient of 3.17 $W\cdot(m^2\cdot K)^{-1}$) is more complicated and difficult than that in single wall (with heat transfer coefficient of 2.57 $W\cdot(m^2\cdot K)^{-1}$). Therefore, the compound wall is more appropriate to keep the indoor temperatures stable [29].

Several infrared photographs of the wall were taken on Aug 5, 2015, in sunny condition. Based on the infrared photographs shown in Table 4.3.1.1, an analogy was drawn between the two surface temperatures of an external brick wall. The results show that the indoor surface temperature with 31.40 ℃, is 6.4℃ lower than that of the outdoor surface. Regarding an external wooden wall, the indoor surface temperature with 30.9 ℃, is 4.8 ℃ lower than that of outdoor surface (Table 4.3.1.1). In addition, the in-situ measurements of surface temperatures for the external brick wall and external wooden wall were conducted on July 20, 2018, in sunny condition. As shown in Table 4.3, the average temperature differences between the two surfaces of external brick wall and external wooden wall are 7.49 ℃ and 3.00℃ respectively during daytime from 6 a.m. to 17 p.m. on July 20, 2018.

(2) Solar shading and ventilation mechanisms

Shading devices can improve internal environment in order to provide greater comfort for occupants. Furthermore, the shading devices can reduce the heat gains during summer. Thus, use of shading device can improve building energy performance. On the other hand, ventilation is the intentional introduction of outdoor air into a space and is mainly used to control indoor air quality, as well as aims at improving thermal comfort or dehumidification.

The gable walls in TPD are “Matou wall” or “Guanyin dou wall”, covered with tiles on their tops and presenting double pitched patterns. The configuration characteristics of gable walls are that their tops protrude above the roofs, which can provide solar shading in summer so that delays the temperature rises of tiles and decreases the thermal gains for internal spaces (Table 4.3.1.2).

(3) Solar radiation reflection

In Sizhai village, the total annual solar radiation and sunshine duration are approximately 4607.04 MJ/m^2 and 1887.6 h, accounting for 45% and 22% of the whole year, respectively. The months with maximum solar radiation and sunshine duration are both in July with about 553.60 MJ/m^2 and 222.53 h, while February and January are the months with minimum solar radiation and sunshine duration respectively, approximately 216.21 MJ/m^2 and 102.73 h.

The external brick walls in TPD with elegant and clear colour, so the solar radiations can be reflected efficiently to reduce solar heat gains for internal spaces [30]. The reflection ratio of near-infrared rays on light walls exceeds 80%, and that of global solar radiation is greater than 65% [31]. As shown in Table 4.3.1.3, the temperature of white surface is approximately 1.45℃ lower than that of black surface on the same wall in a summer afternoon.

Table 4.3 Elasticity effect of wall in the traditional dwelling of Thousand Pillar Dwelling

<table>
<tr><td rowspan="8">4.3.1 Temperature adjustment</td><td rowspan="4">4.3.1.1 Heat insulation</td><td colspan="3">External brick wall</td></tr>
<tr><td>Heat transfer</td><td colspan="2">Temperature difference between two wall surfaces</td></tr>
<tr><td> 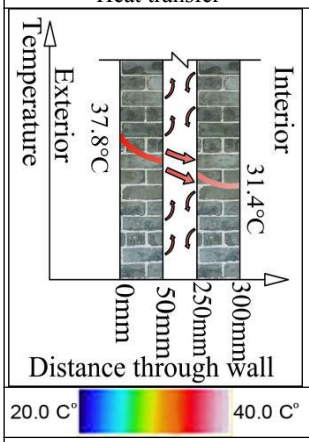
</td><td> 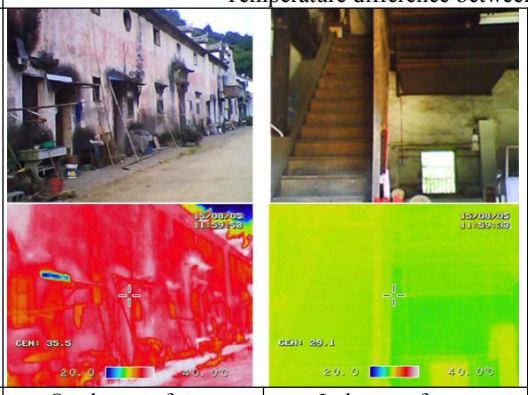
</td><td> 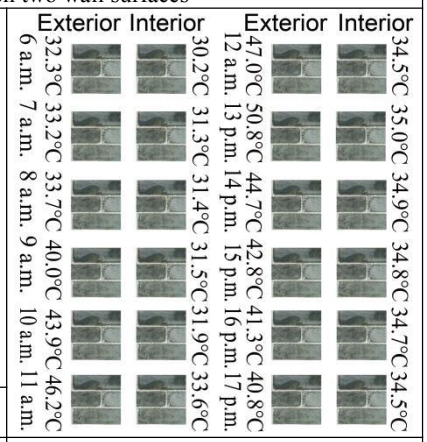
</td></tr>
<tr><td>Aug 5, 2015, 11:59 a.m.</td><td>July 20, 2018, from 6 a.m. to 17 p.m.</td></tr>
<tr><td rowspan="4">4.3.1.2 Solar shading</td><td colspan="3">External wooden wall</td></tr>
<tr><td>Heat transfer</td><td colspan="2">Temperature difference between two wall surfaces</td></tr>
<tr><td> 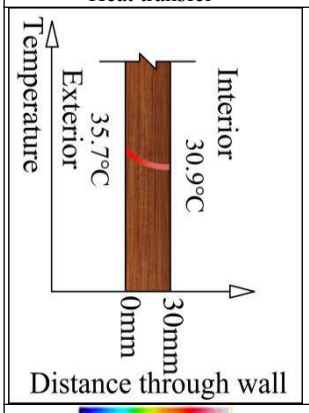
</td><td> 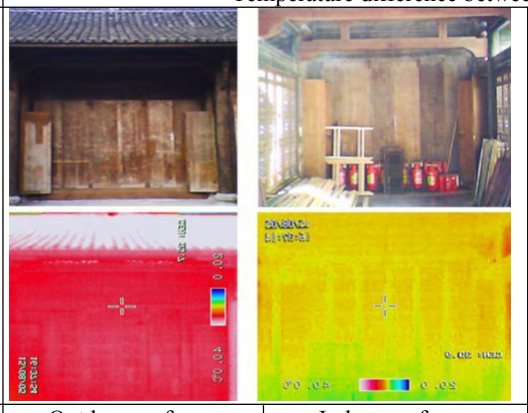
</td><td> 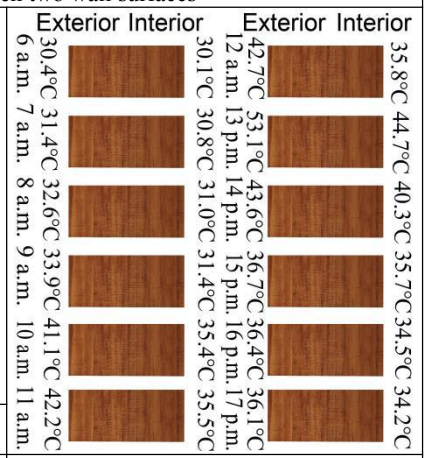
</td></tr>
<tr><td>Aug 5, 2015, 16:57 p.m.</td><td>July 20, 2018, from 6 a.m. to 17 p.m.</td></tr>
<tr><td>4.3.1.2 Solar shading</td><td colspan="3">Shading formed by “Guanyin dou wall”

Shading formed by “Matou wall”
 </td></tr>
<tr><td rowspan="3">4.3.1.3 Radiation reflection</td><td colspan="3">Temperature difference between white wall and dark wall</td></tr>
<tr><td> 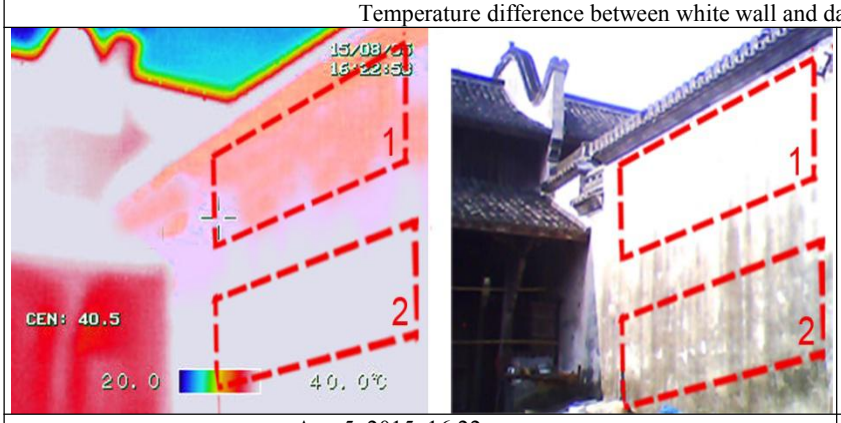
</td><td> 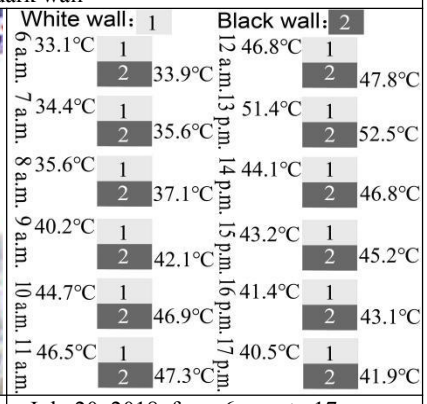
</td></tr>
<tr><td>Aug 5, 2015, 16:22 p.m.</td><td>July 20, 2018, from 6 a.m. to 17 p.m.</td></tr>
</table>

4.4.2.2 Passive strategy used in Roof and waist eave of traditional dwelling

The construction of roof in TPD (Fig. 4.13) is shown in Fig. 4.14. With low thermal conductivity and high thermal inertia, the sintered clay tiles employed as a surface layer in the roof can effectively mitigate the impact of external climate variations on indoor temperatures. The overlap length between cover tile and bottom tile accounts for approximately two-thirds of a tile length, that is the tiling method of "covering 70% and exposing 30%".

Fig. 4.13 Upward view of the roof details in traditional dwelling

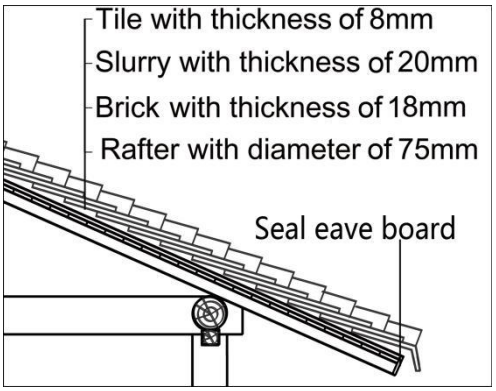

Fig. 4.14 Schematic of the roof construction in traditional dwelling

(1) Heat insulation and thermal preservation

Since the heat exchange in a top floor space takes place in roof and walls, and that in a ground floor spaces just takes place in walls, it results in that the indoor temperatures of the top floor are approximately 2 ℃ higher than that of the ground floor during summer [32].

The TPD with 2 storeys, occupants are living in the lower floors during summer, and the upper floors are generally used as storerooms for sundries. The windows of upper floors are all opened to expel the indoor heat to the exterior by natural ventilation so that creates a thermal buffer zone for the lower floors. The tiles covered on the roofs and waist eaves are used the tiling method of "up and down superposition" to create an air layer between tiles and red mud slurry. To take away the heat of the slurry and tiles through airflow generated by wind pressure and thermal pressure in the air layer, the seal eave boards are dismantled during summer (Table 4.4.1.2). According to an infrared photograph presented in Table 4.4.1.1, the indoor temperature on the second floor is 32.9℃, which is 2.5℃ lower than outside near high noon in summer.

In winter, the seal eave boards are configured back on roof edges to improve the thermal preservation performance of roof (Table 4.4.1.2). Synchronously, the upper floors are used as a bedroom and windows are all closed to enjoy a greenhouse effect, where the solar radiations are passed through windows and solar gains are transmitted from roofs (Table 4.4.1.2).

(2) Solar shading

Roof eaves installed on facades are an effective passive strategy to minimize indoor temperatures and control the transmission of sunlight permeability into internal spaces. In the hot summer and cold winter climate zone of China, a building with the horizontal external shading devices can achieve a 3.2% reduction in energy consumption during summer [33]. The roof eaves and waist eaves, characterized by deeply extended overhang of 0.90 m, provide solar shadings for windows to avoid intense solar radiations, which is helpful for a reduction in heat gains for internal spaces [27]. The evaluation parameter of shading rate (SR) is adopted to estimate the solar shading effects on upper floor windows for a south-facing facade during daytime from sunrise to sunset, which was taken as the study case in this section. As shown in equations (4.1-4.6), the processes of equation formulation for SR were conducted to analyze the EEs of roof eave.

$$a_3 = |180° - a_1| \quad (4.1)$$

Where, a_3 (Fig. 4.15) is the angle between the normal of south-facing wall and horizontal projection line of solar radiation, °; a_1 is solar azimuth, °; b_1 is the angle between the wall normal and vertical solar projection line. According to the trigonometric function, the equation of tangent b_1 is formulated as following:

$$\tan b_1 = \frac{\tan a_2}{\cos a_3} \quad (4.2)$$

Where, a_2 is solar altitude, °. The equation of H_3 (the shadow height on window shown in Fig. 4.16) is formulated as following:

$$H_3 = L_1 \times \cos c_1 \times \tan b_1 - H_1 \quad (4.3)$$

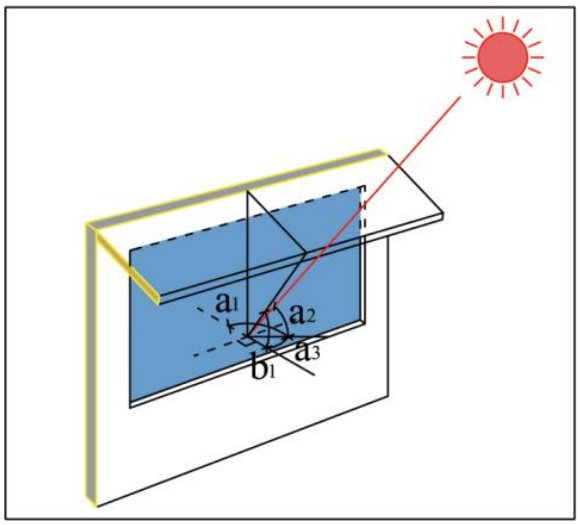

Fig. 4.15 Schematic of diverse angles related to solar shading cast by roof eave

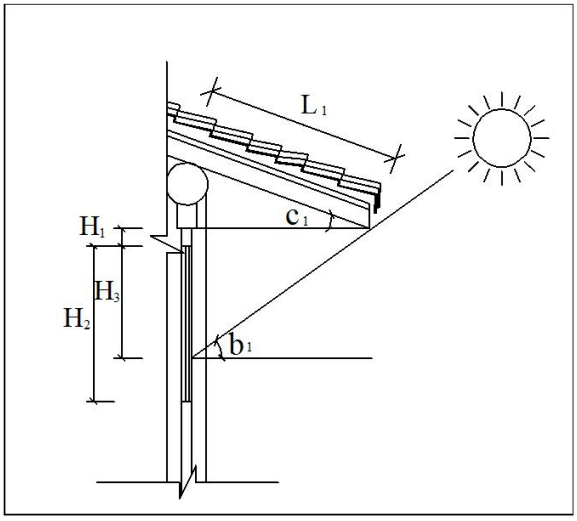

Fig. 4.16 Schematic of solar shading cast by roof eave and roof eave's depth

Table 4.4 Elasticity effect of eave roof in the traditional dwelling of Thousand Pillar Dwelling

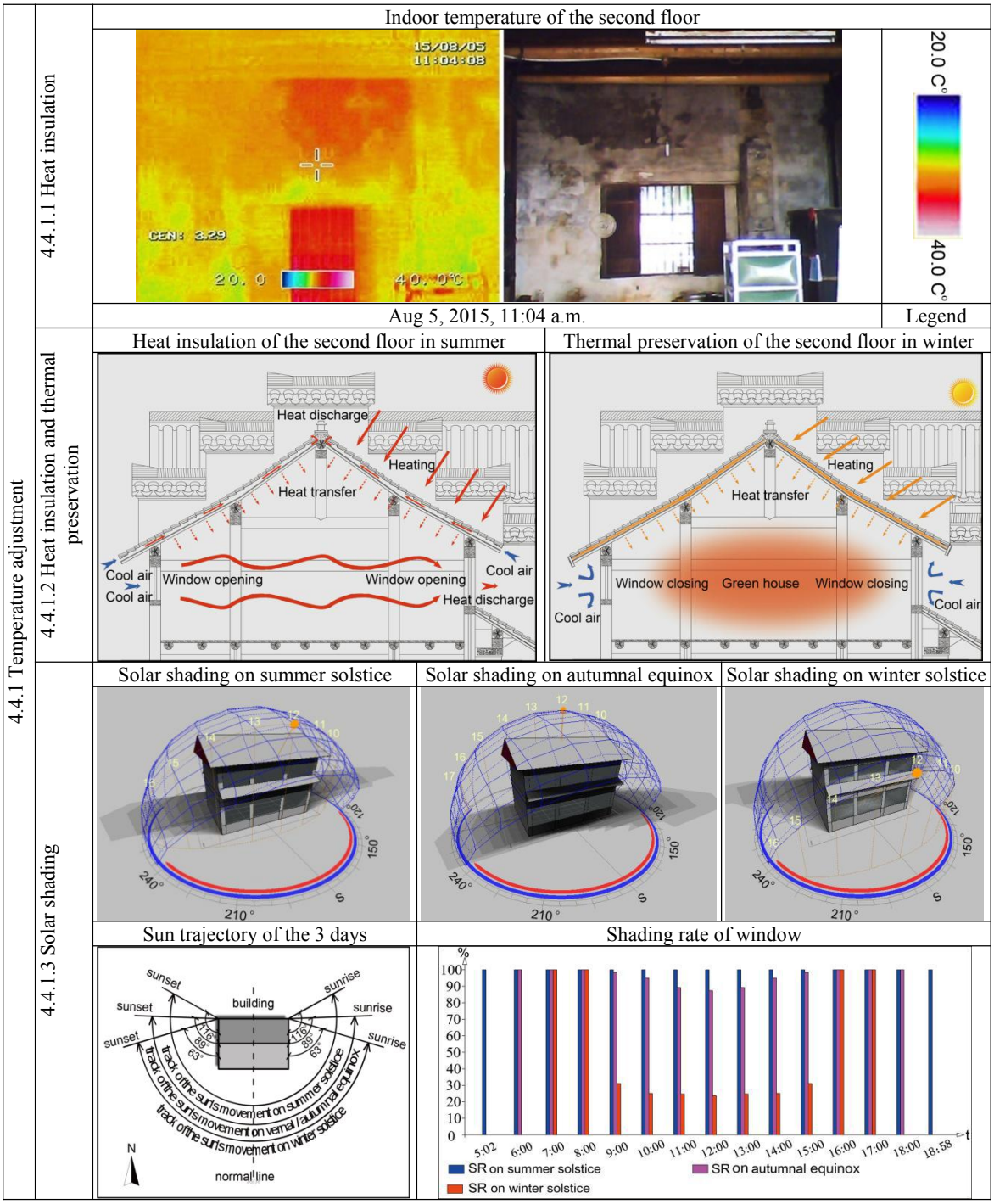

Where, L_1 is the depth of roof eave, 0.9 m; c_1 is the tilt angle of roof eave, 30°; H_1 is the height from bottom roof eave to the top of window, 0.3 m; H_2 is the height of window, 1.2 m. The equation of shading area (S_S) is formulated as following:

$$S_s = B \times H_3 = B \times (L_1 \times \cos c_1 \times \tan b_1 - H_1) \qquad (4.4)$$

Where, B is the length of window, m. The equation of window area (S_w) is formulated as following:

$$S_w = B_1 \times H_3 = B_1 \times H_2 \qquad (4.5)$$

Finally, the equation of SR is formulated as Eq. 6.

$$SR = (L_1 \times \cos c_1 \times \tan b_1 - H_1)/H_2 \qquad (4.6)$$

The data of solar altitude angles for the three days of the summer solstice, autumnal equinox and winter solstice (the data of solar altitude angles for the vernal equinox and that for the autumnal equinox are the same) with representative characteristics are selected as the calculation conditions (Table 4.4.1.3). In terms of calculation results shown in Table 4.4.1.3, the SR is 100% throughout the whole daytime on the summer solstice, so the radiation penetration into interiors is blocked completely, which is helpful for reduction in the solar heat gain for the internal spaces and indoor air temperature stabilization. Regarding the autumnal equinox, there is slight amount of direct sunlight covering the windows. In spring and autumn seasons, the outdoor air temperatures are high in Sizhai, outstanding shading is conducive to improving thermal comfort. In contrast, the windows are with comparatively low SR during daytime on the winter solstice, which contributes to solar heat gains and daylighting for interiors.

4.4.2.3 Passive strategy used in Flooring of traditional dwelling

(1) Construction of flooring pavement in TPD

The practice of flooring on the first floors is made by forming a subcrust layer with 200 mm thickness pressed on foundation firstly. The materials of subcrust are “mixed earth” consisting of sand, ash and clay that forms an aquiclude for indoor grounds. Then the cement sand layer with 40 mm thickness is paved over the subcrust to create a screed-coat. Finally, the clay bricks with dimensions of 300 mm length, 300 mm width and 50 mm thickness are paved over the screed-coat.

(2) Damp-proofing

The construction of flooring on the first floors in TPD employed a compromise practice that leads to the flooring with high thermal stability, so the thermal performance of heat insulation in summer is almost equivalent to that of thermal preservation in winter. Due to the usage of clay brick (Fig. 4.17) with low heat storage coefficient, just a small amount of coolness can be stored in its interior in winter, so the surface temperatures are generally higher than its dew point temperatures. Furthermore, the heat transfer from indoor air to the foundation is blocked effectively, because of the clay bricks with high thermal resistance. Therefore, damp-related phenomena generally do not occur on the indoor ground surfaces, even during the transitional season between spring and summer experienced heavy rains and great temperature fluctuations. The damp-proofing property of flooring on the first floor in the traditional dwellings is helpful for remaining the indoor humidity stable.

The clay bricks with numerous micro-pores on their surfaces can absorb water droplets, which coagulate on their surfaces occasionally. When outside humidity decreases, the moisture contained in clay bricks is evaporated and expelled to exterior by natural ventilation. That's why the clay brick is also called as "a breathing building material". Integrating with moisture-proof strategy of indoor pavement, both south-facing and north-facing facades of each room in TPD are configured with a small ventilation vent (Fig. 4.18) for dehumidifying. Whereas, the ventilation vents are stuffed by wood blocks in winter to enhance the thermal preservation performance of walls.

Fig. 4.17 Flooring on the first floor of traditional dwelling covered clay bricks

Fig. 4.18 A small ventilation vent near the door of traditional dwelling

4.4.2.4 Passive strategy used in Door and window of traditional dwelling

(1) Doors and windows installed in the external brick walls

To improve the heat insulation and thermal preservation capabilities of the external brick walls, the passive strategy of "no opening or less opening" is adopted, resulting in the window-wall-ratios (WWRs) lower than 15% (Table 4.5.1). In summer, the brick walls effectively prevent solar radiations from permeating into the building's interiors, which is helpful for keeping the indoor temperature low and stable. In winter, the thermal preservation performance of the walls can be improved by closing these small windows. Moreover, the property of main entrance in TPD is featured by transitional space, which exerts a noticeable EE to keep cold and wind out in winter.

(2) Doors and windows installed in the external wooden walls

Under the conditions of natural ventilation, the indoor temperature is approximately 1.7~2.5℃ lower than outside temperature [34]. The patio-facing walls in TPD are made of timbers distributed into three bays usually. Differing from brick walls, the external wooden walls are employed an opening strategy with high proportion of WWR about 46% (Table 4.5.2). All wooden walls for three bays are usually configured with doors, or the middle bay is configured with doors and the other two are equipped with windows, in order to facilitate the cross-ventilation for internal spaces. According to outdoor climatic conditions, a different number of doors and windows are opened to

adjust and improve the ICL.

(3) Construction and open-close mechanisms of doors and windows

Solar radiation is the unique source for indoor natural lighting. Natural light is not only helpful in energy conservation for buildings, but it also provides visual comfort, as well as is important for human health [35-38], etc. Artificial lighting costs amounts to approximately 19% of the total electricity consumption in the world, resulting in the CO_2 emissions of about 1.3 billion ton per year [39]. The storey height of the first floors in TPD is high (approximately 4 m), so the "heng pi window" (Table 4.5.3) is configured in the space between windows and beam to improve the indoor daylighting levels.

The functionality of door and window not only provide daylighting for the building interiors, but also contribute to create an indoor environment with desired thermal comfort. Door and window closing and opening mechanism are the important factor impacting indoor environments in the internal spaces. The opening and closing mechanism should be controlled in an appropriate arrangement to adjust the indoor thermal comfort level. During the different period of time throughout the year, the arrangements of opening and closing for door and window are dissimilar, due largely to the various climate conditions.

The doors and windows in TPD are characterized by a double-layered construction, which the outdoor layer is window pane consisting of wooden lattice frames and glazing, and the indoor layer is a wooden shutter (Table 4.5.4, 4.5.5). Due to the solar shading provided by roofs and corridor eaves, both two layers of windows and doors in south-facing and north-facing walls are kept opened for the sake of creating a well-ventilated environment during daytime in summer.

Taking into consideration security and occupants' living habits, both two layers of doors and windows in the south-facing walls of the first floor are closed, but in other positions are both opened during nighttime in summer. By closing window panes and opening wooden shutters in the south-facing walls, the internal spaces can gain solar radiation that penetrates through the glazing parts of the window panes during daytime in winter. Regarding the north-facing walls, the two layers are both closed to improve the thermal preservation of walls. During winter nighttime, the two layers are closed in both the south-facing and north-facing walls. By varying the open and closed conditions of two layers in different walls depending on time and outdoor climate conditions, the CIL can be effectively extended (Table 4.6.1-4.6.2).

By using PHOENICS 2009, the conditions of indoor natural ventilation were simulated. The parameter of inflow air velocity is set at 2.30 m/s with south by east 45° orientation. Since the space located within 2.00 m from the ground is where the most human activities are performed, the wind environment planes at a height of 1.50 m from

the flooring are chosen as the research objectives. The computational results show that the mean indoor air velocity on the first floor is 3.53 m/s and 1.02 m/s during daytime and nighttime in summer, respectively (Table 4.6.3). Both values meet the *Assessment Standard for Green Building* (GB/T 50378-2014) that stipulates the ideal range of air velocity for an interior from 1.00 to 5.00 m/s.

Ecotect 2012 was used to simulate the internal daylighting conditions. The sky illuminance of simulation environment in the software is set at 5000.00 lux. The simulation results show that the mean illuminance at a height of 1.5 m on the first floor and second floor are 824.63 lux and 805.31 lux during daytime in summer, respectively. Regarding winter daytime, the mean illuminance on the first floor is equivalent to that on the second floor, with approximately 742.06 lux (Table 4.6.4). The mean illuminance values are both greater than 300 lux, which is the minimum requirement for a bedroom, living room and kitchen, etc. in accordance with the *Chinese Standard for Daylighting Design of Buildings* (GB 50033-2013).

Table 4.5 Construction of windows and doors in the traditional dwelling of Thousand Pillar Dwelling

<table>
<tr><td colspan="2">Configuration principle</td><td colspan="3">Construction</td></tr>
<tr><td rowspan="2">4.5.1 External brick wall</td><td rowspan="2"> </td><td rowspan="2">4.5.4 Door</td><td> 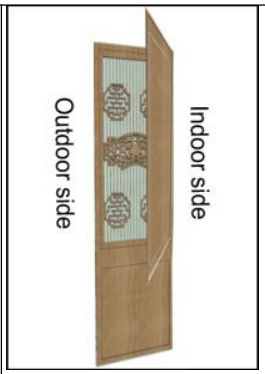
</td><td> </td></tr>
<tr><td>Less and small</td><td>Schematic</td><td>Picture</td></tr>
<tr><td rowspan="2">4.5.2 External wooden wall</td><td rowspan="2"> </td><td rowspan="2">4.5.5 Window</td><td> 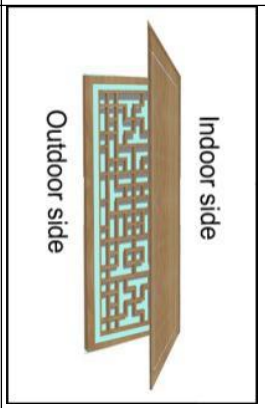
</td><td> </td></tr>
<tr><td>Numerous and large</td><td>Schematic</td><td>Picture</td></tr>
<tr><td>4.5.3 “Heng pi window”</td><td colspan="3"> </td></tr>
</table>

Table 4.6 Elasticity effects of doors and windows in the traditional dwelling of Thousand Pillar Dwelling

Time		Summer daytime				Summer nighttime				Winter daytime				Winter nighttime			
Diagram		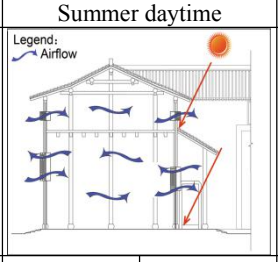				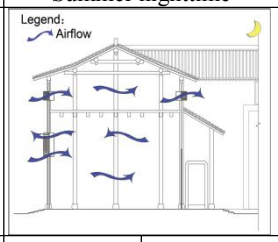				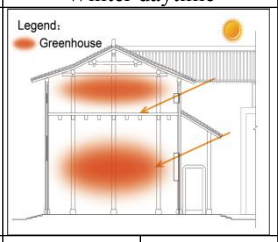				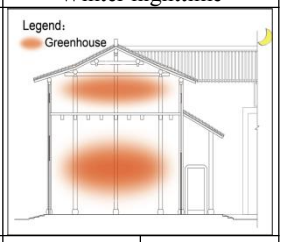			
Wall		South wall		North wall		South wall		North wall		South wall		North wall		South wall		North wall	
4.6.1 Door		WP	WS			WP	WS			WP	WS			WP	WS		
	1 F	●	●			○	○			○	●			○	○		
4.6.2 Window		WP	WS	WP	WS	WP	WS	WP	WS	WP	WS	WP	WS	WP	WS	WP	WS
	1 F	●	●	●	●	●	●	●	●	○	●	○	○	○	○	○	○
	2 F	●	●	●	●	●	●	●	●	○	●	○	○	○	○	○	○
4.6.3 Ventilation adjustment	1 F	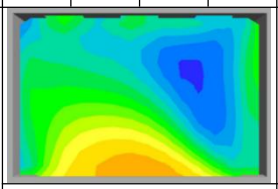 Average value: 3.53 m/s				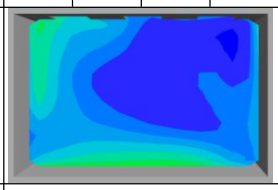 Average value: 1.02 m/s								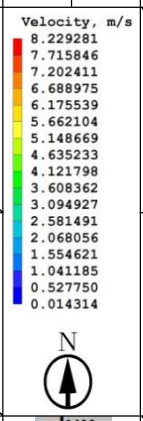		
	2 F	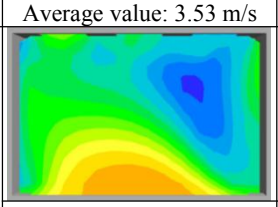 Average value: 4.21 m/s				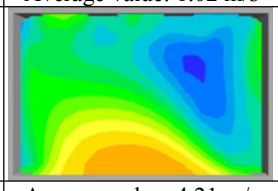 Average value: 4.21 m/s											
4.6.4 Daylighting adjustment	4.6.4.1 Illuminance 1 F	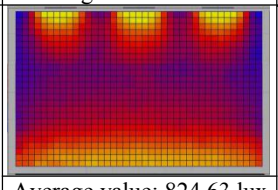 Average value: 824.63 lux								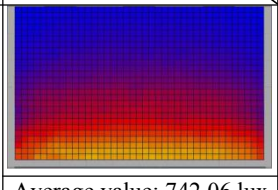 Average value: 742.06 lux				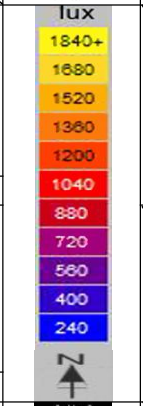			
	4.6.4.1 Illuminance 2 F	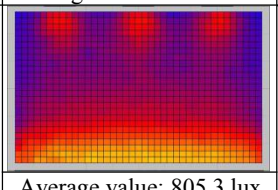 Average value: 805.3 lux								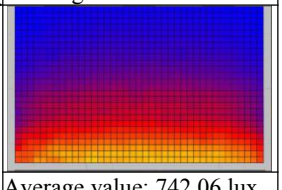 Average value: 742.06 lux							
	4.6.4.2 Illumination	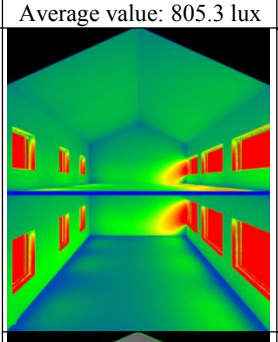								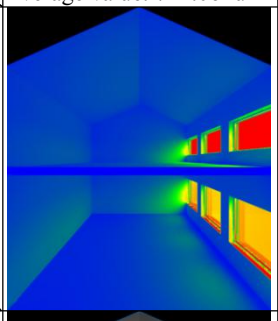				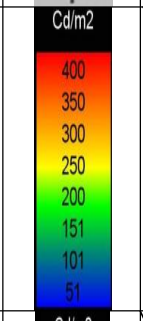			
		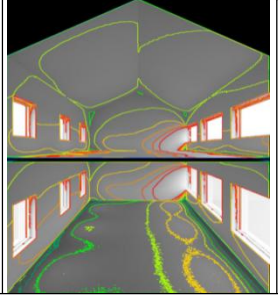								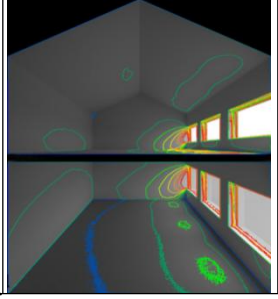				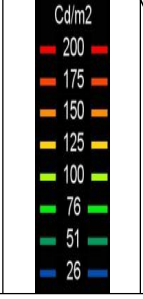			

Note: 1. ● represents opening, ○ represents closing; 2. WP: window pane, WS: wooden shutter.

4.4.3 Passive spaces in the traditional dwelling of Thousand Pillar Dwelling

Possessing a certain spaciousness with semi-open space feature, PSs are regarded as the third space between the interiors and exteriors. In TPD, the PSs composed of patios, corridors and open-hall create a climate gradient in their own spaces to provide a thermal buffer zone for internal spaces (Table 4.7).

Patio is an outdoor space generally used for dining or recreation that adjoins a residence and is typically paved, which is characterized by small dimensions in TPD. The corridor in TPD is a long passage under sloped roof with doors and rooms on one side. In contrast, the open-hall in TPD is huge and spacial.

Table 4.7 Characteristics and types of passive spaces in the traditional dwelling of Thousand Pillar Dwelling

Designation		Patio		Corridor	Open-hall
		Normal patio	Crab-eye patio		
Picture					
Space property	Semi-open	●	●	●	●
Open position	Vertical direction	●	●		
	Horizontal direction			●	●
Characteristics	Large opening	●	●	●	●
	Small size	○	●	◎	○
	Double-layered construction			●	●
	Deep overhang	●	●	●	●
	Introducing natural elements	●	○		

Note: ● represents a element with strong performance, ◎ represents a element with medium performance, ○ represents a element with weak performance.

4.4.3.1 Passive strategy used in patio of traditional dwelling

(1) Humidity regulation and cooling strategy

The dimensions of patios in TPD are comparatively small, whose proportions of length and height are approximately 1:1. Thus, the internal spaces of patios cannot receive lots of solar contribution during summer, which contributes to delay the rise of air temperature. Sizhai experiences high air temperatures in summer, but wooden fabrics are easy to crack in the hot or dry environment. So, as a precaution, occupants usually plant some trees or dig a well in the patios aiming at a reduction in direct solar radiation gains and cooling the air by means of evapotranspiration [40].

Table 4.8 Elasticity effect of patio in the traditional dwelling of Thousand Pillar Dwelling

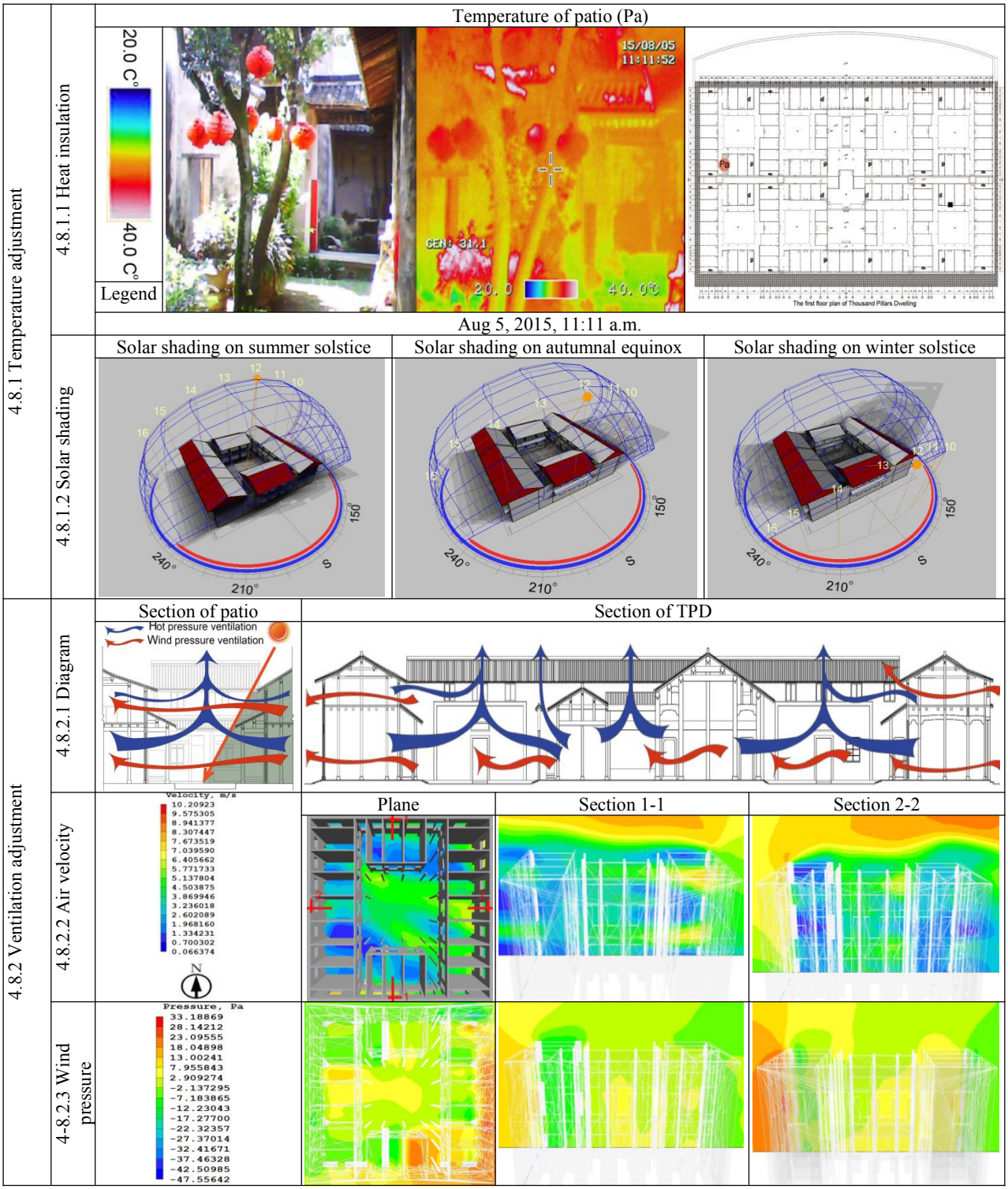

Due to water possessing higher specific heat than the wall materials, the temperature fluctuation amplitude of water is much slighter when they absorb or release the same amount of heat [41]. That's why having water elements in patios contributes to lowering air temperature in their closer to the ground portions [27]. Furthermore, water and plants in patios have a cooling effect which keeps their ambient microclimate comfortable and stable. Based on the infrared photographs presented in Table 4.8.1.1, the mean air temperature of patio is approximately 30.1℃ that is 5.1℃

lower than outdoor temperature. The hot air from outside will lose heat when it enters into patios, which is helpful for cooling the internal spaces.

(2) Daylighting and solar shading

From the view of architectural typology, patio provides sunshine distance and daylighting conditions for buildings arranged around it. Whereas, the patios in TPD are characterized by small dimensions, which can lower solar radiation exposures for walls and windows aiming at a reduction in heat gains for internal spaces [42]. Moreover, the patios can uniform the indoor daylight distributions, where the main light source is diffuse radiation generated by the envelope reflections around patios (Table 4.8.1.2).

(3) Natural ventilation

Due to the lower space of patio being shaded by its adjacent and opposite buildings, the ventilation at the bottom of patio is mostly generated by thermal pressure. Regarding its upper space, the heat dissipation primarily is performed by airflow created by both wind pressure and thermal pressure (Table 4.8.2). In addition, the stack effect in patios integrated with outdoor wind pressure is beneficial to generate cross-ventilation for internal spaces. As shown in Table 4.8.2.2, the mean air velocity in patio space is approximately 3.82 m/s.

4.4.3.2 Passive strategy used in Corridor of traditional dwelling

From the viewpoint of spatial configuration, the corridor with a deep eave also possesses the property of semi-open space. During the transitional season between spring and summer, the plum rain weather conditions in Sizhai remains uninterrupted about one month. The corridors provide a shelter for occupants avoiding splashing and getting wet, when they walk in this mansion. Furthermore, by taking the climate adaptation into account, the corridors can create an adjustable and controllable climatic buffer zone to reduce the adverse impacts of the outside climate on interior environments.

(1) Heat insulation

To improve the heat insulation, the suspended ceiling is configured under the corridor roof in TPD. The closed air layer between roof and ceiling delays the heat transfer, resulting in taking more time to heat up the air in corridor [27]. The thermal energy contained in this air layer can be expelled by natural ventilation to keep corridor space cool. In addition, the roofs of corridors intercept the solar radiations for internal spaces, which contributes to a reduction in peak heat flux. According to the infrared photograph shown in Table 4.9.1.1, the mean temperature near the flooring of corridor is 28.5℃ that is 6.7℃ lower than outside. Meanwhile, it also is distinct from that of the upper space with 29.4℃.

Table 4.9 Elasticity effect of corridor in the traditional dwelling of Thousand Pillar Dwelling

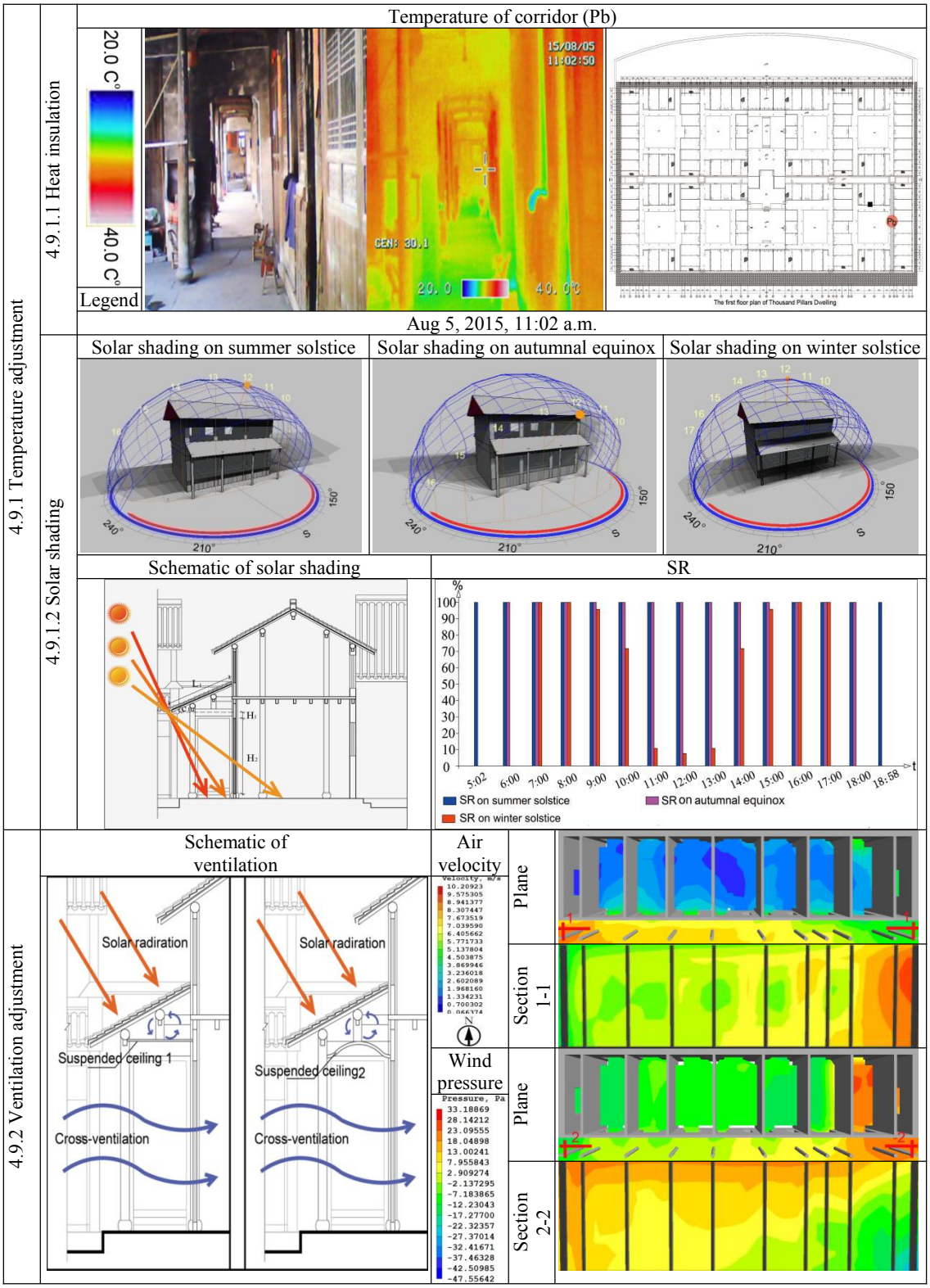

(2) Solar shading and daylighting

The passive strategy of solar shading is vital for TPD in summer characterized by harshly hot weather conditions. Corridors leaning against the wooden walls can minimize the indoor temperature fluctuations by means of solar

shading. The solar shading mechanism of corridor is consistent with that of the roof eave, which both belong to the external horizontal shading systems. By substituting the given data of corridor into the equations (4.1-4.6), the SR can be determined for south-facing windows on the first floor shaded by corridor during the three representative days. Where, the L_1 is 1.8 m; c_1 is 30°; H_1 is 0.3 m and H_2 is 2 m.

The calculation results show that the SR is 100% during the whole daytime on the summer solstice providing an effective shading performance for interiors. There is also no solar radiation reaching the windows during the whole daytime on the autumnal equinox, due largely to the fact that the corridor has a deeper overhang than roof. In contrast, windows receive comparatively high solar contributions during daytime on the winter solstice, especially near high noon, which contributes to heat gains and temperature increase for internal spaces (Table 4.9.1.2).

(3) Natural ventilation

The configuration of corridor is like a narrow lane, which also has the function of inducing ventilation. For one thing, the airflow from outside is guided into each patio and room through the corridors. For another, the patios as cool source spaces and the rooms as hot source spaces can form thermal pressure. The thermal pressure integration of inducing ventilation function of corridor, all rooms arranged around patios can be driven to ventilate, which forms a self-ventilation system to cool internal spaces in summer. As shown in Table 4.9.2, the mean air velocity in corridor exceeds 5 m/s.

4.4.3.3 Passive strategy used in Open-hall of traditional dwelling

The open-hall is one of the most important spaces in Zhejiang traditional dwellings. With both features of practicality and decorum, it is not only the public communication and reception room, but also the ceremony room and sacrifice space, etc. Moreover, it is also the most significant symbol that represents the identity and status of the host and hostess of the building. Regarding its space characteristic, the open-hall in TPD with a property of transitional space is transparent and high.

(1) Heat insulation and daylighting

The open-hall in TPD has three bays presenting completely open plan for the south-facing facade, which is helpful for improving indoor daylighting and accelerates internal heat discharge. Whereas, the north-facing walls are relatively closed, of which the middle bay is enveloped by a wooden wall and two side bays are enveloped by brick walls with small doors and windows. Based on infrared photograph, the mean temperature of the open-hall is 32.7℃, which is 2.5℃ lower than outside (Table 4.10.1.1). Additionally, the mean illuminance levels according to the computational results are 784.34 and 742.58 lux during daytime in summer and winter, respectively (Table 4.10.3.1).

Table 4.10 Elasticity effect of open-hall in the traditional dwelling of Thousand Pillar Dwelling

4.10.1 Temperature adjustment	4.10.1.1 Heat insulation	Temperature of open-hall (Pc)		
			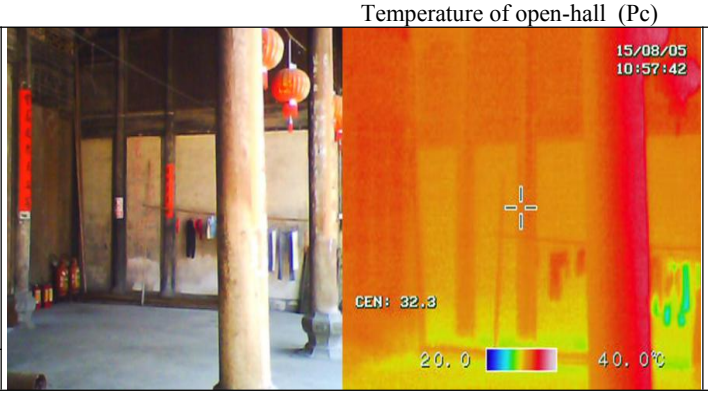	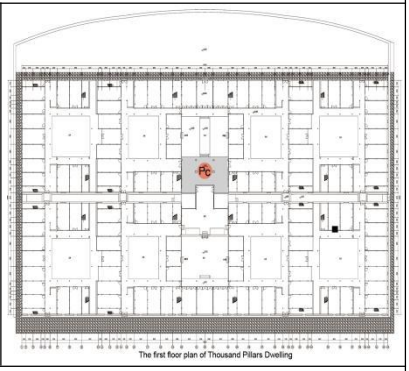
		Legend	Aug 5, 2015, 10:57 a.m.	
4.10.2 Ventilation adjustment in summer	4.10.2.1 Diagram	Schematic of Ventilation	Legend	
		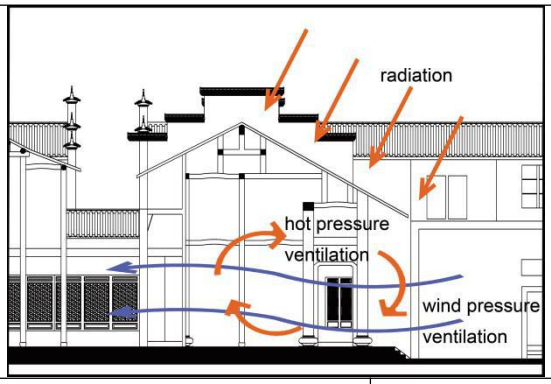	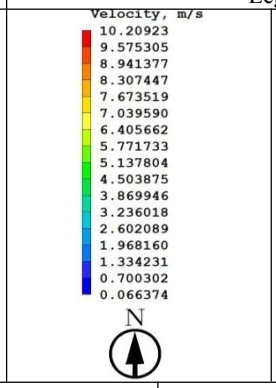	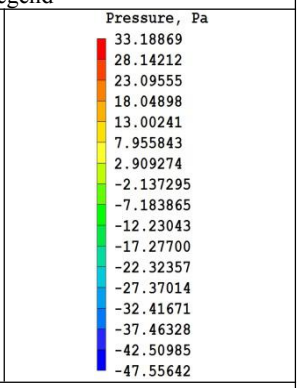
	4.10.2.2 Air velocity	Plane	Section 1-1	Section 2-2
		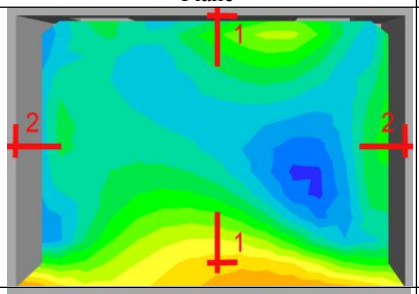	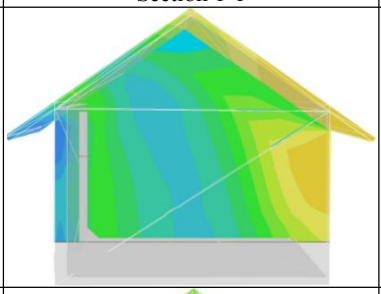	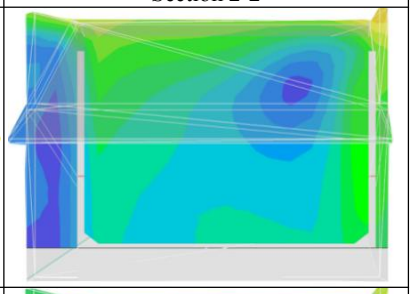
	4.10.2.3 Wind pressure	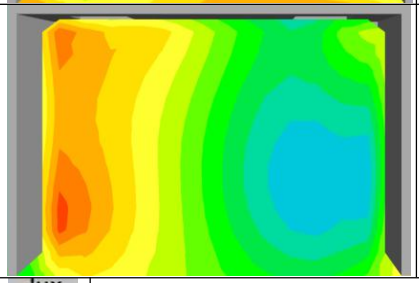	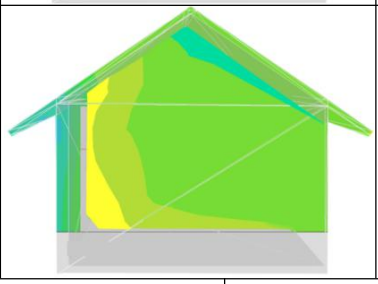	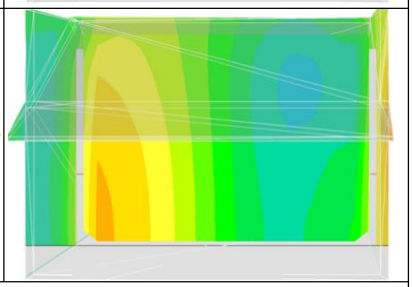
4.10.3 Daylighting adjustment	4.10.3.1 Natural daylighting		Illuminance in summer	Illuminance in winter
			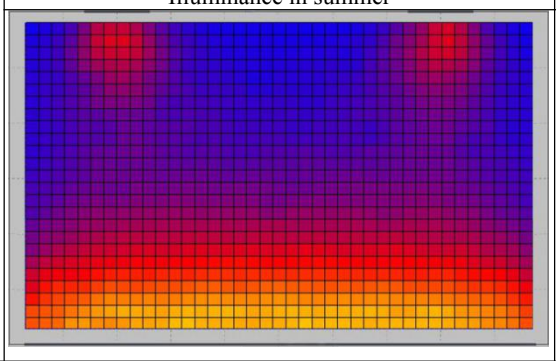	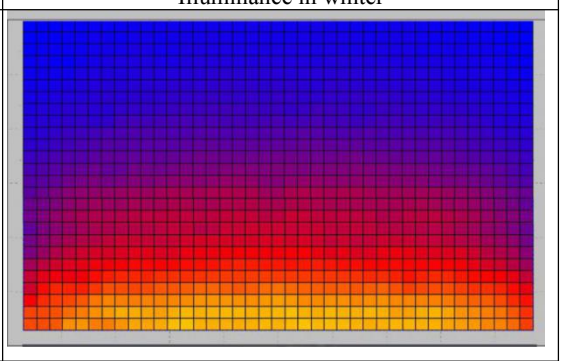
		Legend	Average value: 784.34 lux	Average value: 742.58 lux

(2) Natural ventilation

There are two ventilation patterns existing in the open-hall, namely the Wind Pressure Ventilation (WPV) and Thermal Pressure Ventilation (TPV). During summer, the doors and windows in the back wall are opened to reduce resistance of airflow so that keeps the room well-ventilated. Furthermore, the open-hall can be regarded as the TPV system with a single vent, where the air inlet and outlet are on the same side (Table 4.10.2). When the indoor temperature is higher than the outside, the outdoor cool airflow enters into the bottom of open-hall and the indoor hot air is expelled from upper space to exteriors. In contrast, the doors and windows are usually closed during winter to block cross-ventilation, in order to improve occupants' comfort sensation. In accordance with the computational results presented in Table 4.10.2.2, the mean indoor air velocity in open-hall is approximately 3.5 m/s under assistance of WPV and TPV during summer.

4.5 In-situ measurement for the traditional dwellings of Thousand Pillar Dwelling

Through on-site measurements, the climatic parameters of air temperature, air velocity, relative humidity and illuminance in the common patio (P1), crab-eye patio (P2), corridor (P3), open-hall (P4), interior of the first floor (P5), interior of the second floor (P6) and outer square (P7) in TPD were measured to analyze the EEs quantitatively (Fig. 4.3). The thermo-hygrometric and daylighting monitoring were conducted in TPD during summer and winter, which are the two most demanding seasons when the thermal comfort is considered. The measurement time in summer was from Aug 4, 2015 to Aug 6, 2015; and that in winter was from Dec 29, 2015 to Dec 31, 2015.

Based on the EEs of PEs and PSs to control and adjust the indoor microclimate, the climatic parameters of internal spaces are kept stable and close to the thermal comfort range. Thus, the measurements support the assumption that the internal spaces can achieve thermal and visual comfort by the passive strategies.

4.5.1 Air temperature measurement for traditional dwelling

The passive strategies in TPD, such as the rowlock cavity walls with an enclosed air layer, the wooden walls with low heat conductivity, the double-layered roofs, doors and windows, the compact patios, etc., all contribute to create a comfortable thermal environment for the occupants. The EN 15251:2007 Thermal Comfort Standard stipulates that the most comfortable indoor temperature for thermal sensation ranges from 26.50℃ to 30.8℃ in summer and from 21.8℃ to 24.1℃ in winter for a room without the use of heating and cooling systems. It is significant to note that with the significant daily fluctuations of outside temperatures, the indoor temperatures remain comparatively stable. The interiors of TPD can avoid the extreme high temperatures during summer daytime and extreme low temperatures during winter night, and keep the indoor temperatures much closer to the comfort limits (Table 4.11).

Table 4.11 Field measurements of air temperature in summer and winter

Season	Summer	
Time	Aug 4, 2015, sunny	Aug 5, 2015, sunny
Temperature	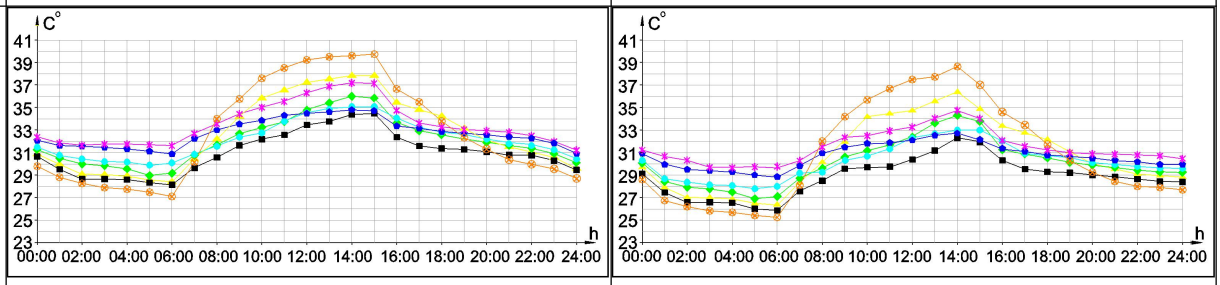	
Season	Summer	Winter
Time	Aug 6, 2015, cloudy	Dec 29, 2015, sunny
Temperature	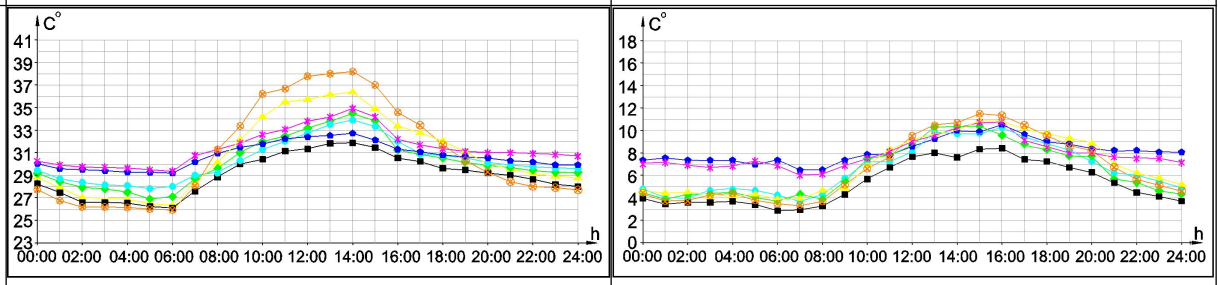	
Season	Winter	
Time	Dec 30, 2015, sunny	Dec 31, 2015, sunny
Temperature	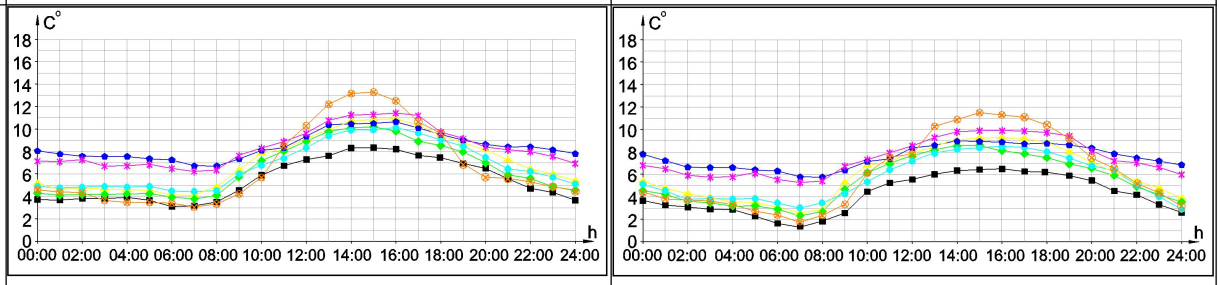	
Legend	P1 Common patio; P2 Crab-eye patio; P3 Corridor; P4 Open-hall; P5 Interior of first floor; P6 Interior of second floor; P7 Outdoor square	

4.5.2 Relative humidity measurement for traditional dwelling

The EN 15251:2007 stipulates that both the most comfortable relative humidity levels for human beings range from 20% to 70% in summer and winter for a room without air conditioning. By configuring ventilation vents, constructing patios, substantial number of windows and doors in the wooden wall, etc., the internal spaces are kept well ventilated in summer, which is helpful for expelling the heat and humidity to outside. Although the outdoor relative humidity experience dramatic fluctuation, especially in the summertime, the indoor relative humidities are kept stable under the control of these passive strategies. The profiles of measurement results show that the indoor relative humidity remains in the range of 57%~68% in summer and 57%~65% in winter, which are both within the comfortable range (Table 4.12).

Table 4.12 Field measurements of relative humidity in summer and winter

Season	Summer	
Time	Aug 4, 2015, sunny	Aug 5, 2015, sunny
Relative humidity	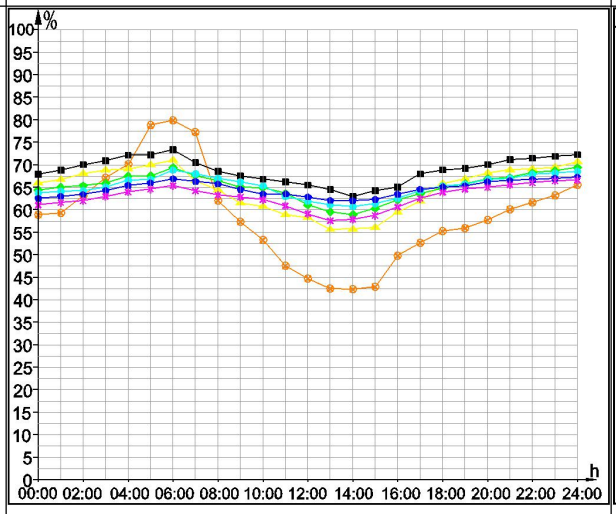	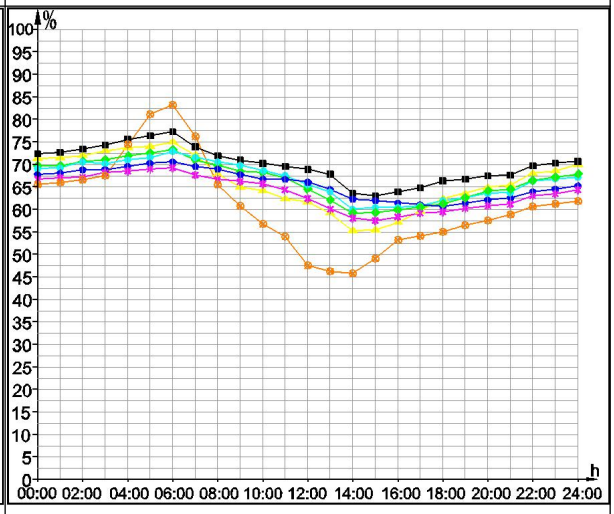
Season	Summer	Winter
Time	Aug 6, 2015, cloudy	Dec 29, 2015, sunny
Relative humidity	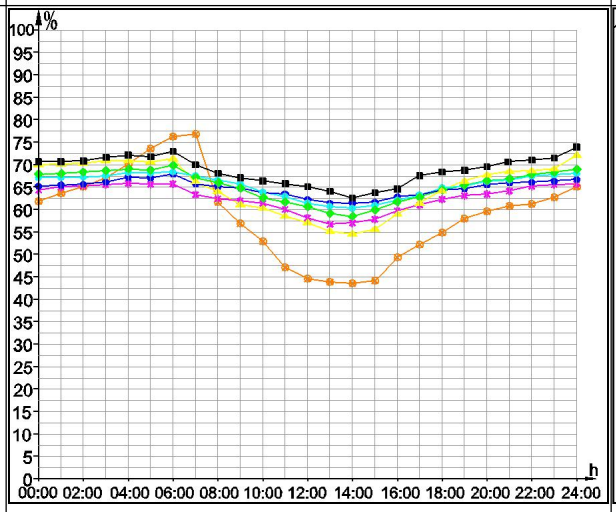	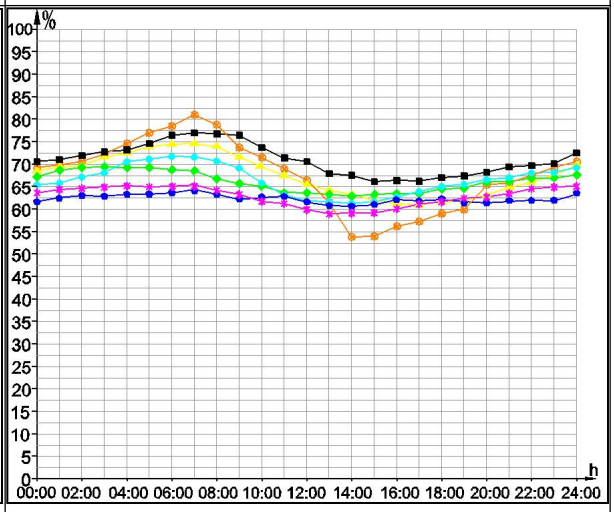
Season	Winter	
Time	Dec 30, 2015, sunny	Dec 31, 2015, sunny
Relative humidity	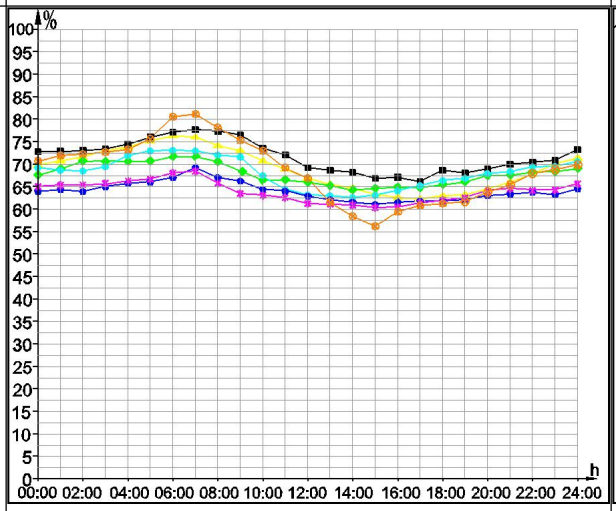	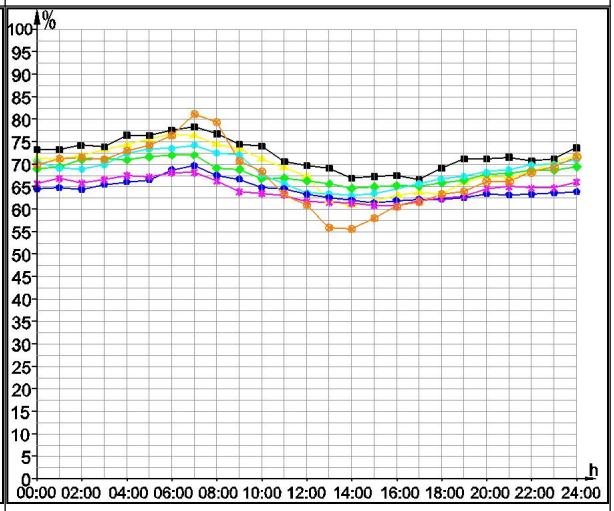
Legend	P1 Common patio; P2 Crab-eye patio; P3 Corridor; P4 Open-hall; P5 Interior of first floor; P6 Interior of second floor; P7 Outdoor square	

4.5.3 Air velocity measurement for traditional dwelling

Integrated with the ventilation strategies provided by patios and corridors, a considerable quantity of openable doors and windows are located in the wooden walls, in order to facilitate a well-ventilated condition for all rooms in the mansion. During summer, the average air velocities are comparatively high in common patios and corridors, approximately 0.3 m/s (Table 4.13), due large to with the space property of semi-open. In contrast, the mean indoor air velocities are below 0.025 m/s in winter (Table.13), since the windows and doors are usually closed aiming at a reduction in thermal energy loss.

Table 4.13 Field measurements of air velocity in summer and winter

Season	Summer	
Time	Aug 4, 2015, sunny	Aug 5, 2015, sunny
Air velocity	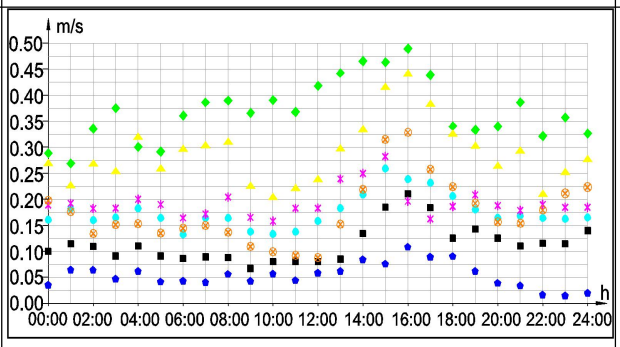	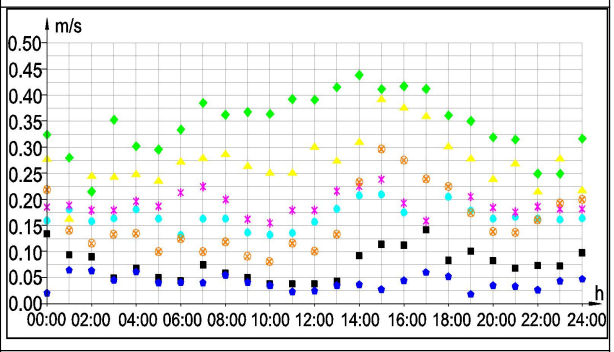
Season	Summer	Winter
Time	Aug 6, 2015, cloudy	Dec 29, 2015, sunny
Air velocity	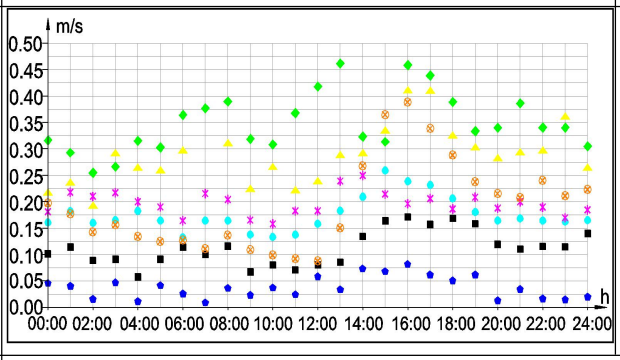	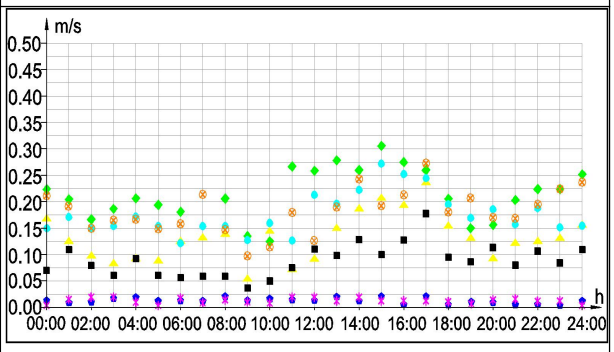
Season	Winter	
Time	Dec 30, 2015, sunny	Dec 31, 2015, sunny
Air velocity	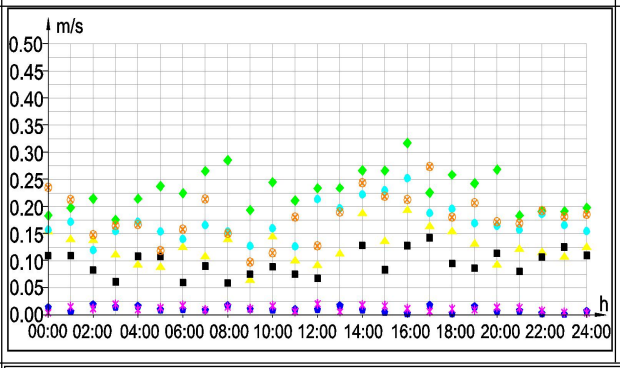	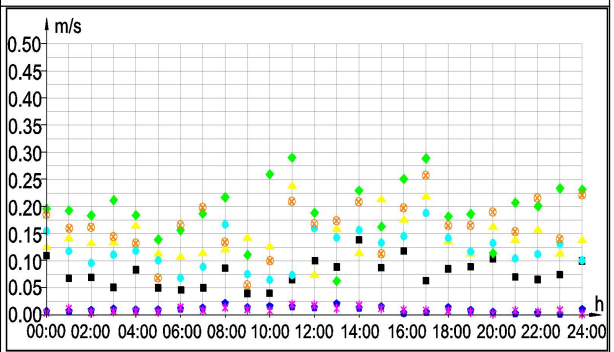
Legend	P1 Common patio; P2 Crab-eye patio; P3 Corridor; P4 Open-hall; P5 Interior of first floor; P6 Interior of second floor; P7 Outdoor square	

4.5.4 Illuminance measurement for traditional dwelling

By constructing patios and installing openable doors and windows, the indoor daylighting levels can be controlled and regulated efficiently. With assistance of PSs and PEs, the daylight factors of internal spaces are improved by means of indirect and direct daylighting. As data of field measurements shown in Table 4.14, the indoor illuminance ranges from 500 lux to 1300 lux in summer and from 350 lux to 1100 lux in winter.

Table 4.14 Field measurements of illuminance in summer and winter

Season	Summer	
Time	Aug 4, 2015, sunny	Aug 5, 2015, sunny
Illuminance	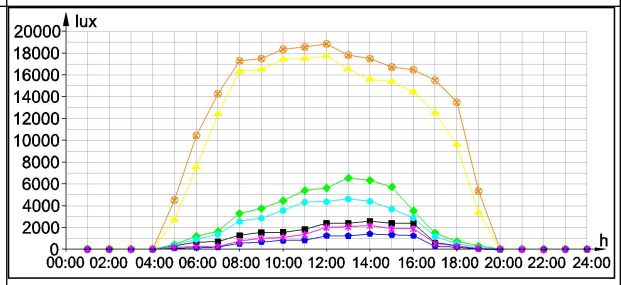	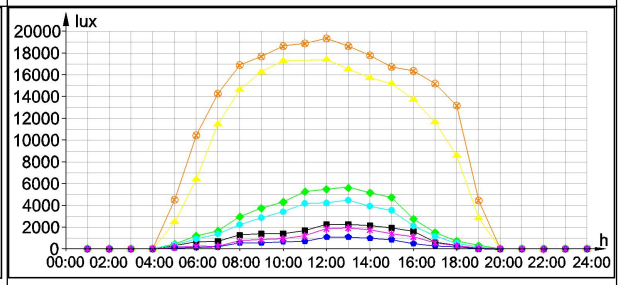
Season	Summer	Winter
Time	Aug 6, 2015, cloudy	Dec 29, 2015, sunny
Illuminance	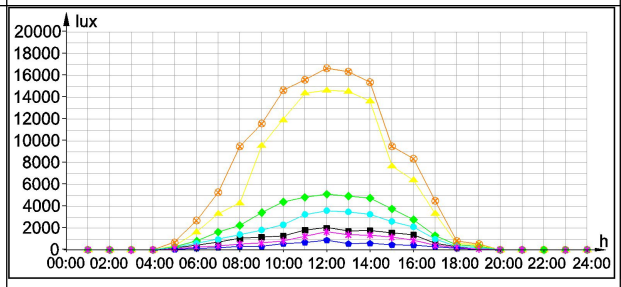	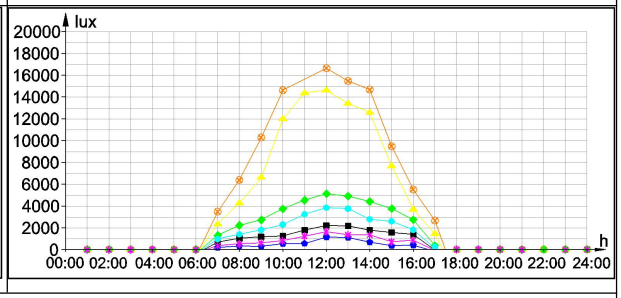
Season	Winter	
Time	Dec 30, 2015, sunny	Dec 31, 2015, sunny
Illuminance	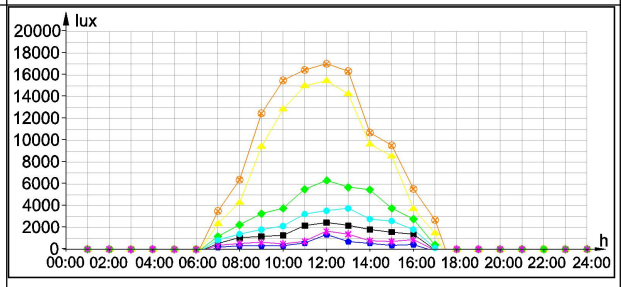	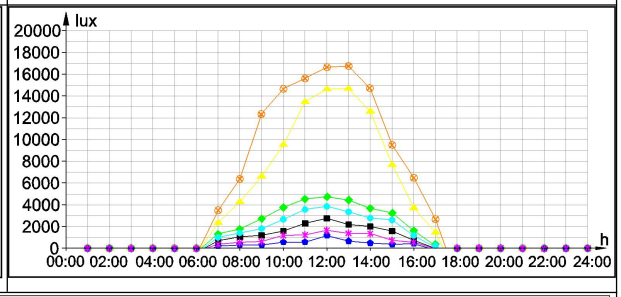
Legend	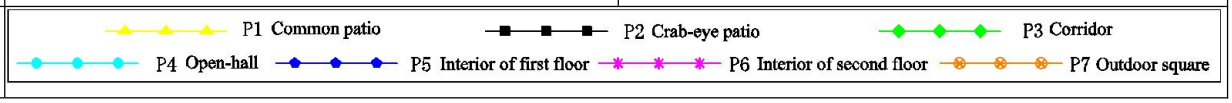	

4.6 Environment simulation for the traditional dwellings of Thousand Pillar Dwelling

As shown in Fig. 4.19, the computational results generated by Climate Consultant 6.0 display that the total outdoor comfort time amounts to 380 h in Sizhai, accounting for 4.3% of the whole year. With air temperature rising up gradually form April, the Outdoor Comfort Time (OCT) also becomes longer daily. Nonetheless, the OCT is

transitory during the period from late May to mid-October, since the zone experiences a hot and humid summer. In contrast, the cool and fresh autumn lasts from mid-October to mid-November, so the time within thermal comfort limits is extended again. From late December to early March the climate is characterized by low temperatures, and the OCT is shortened (Fig. 4.20).

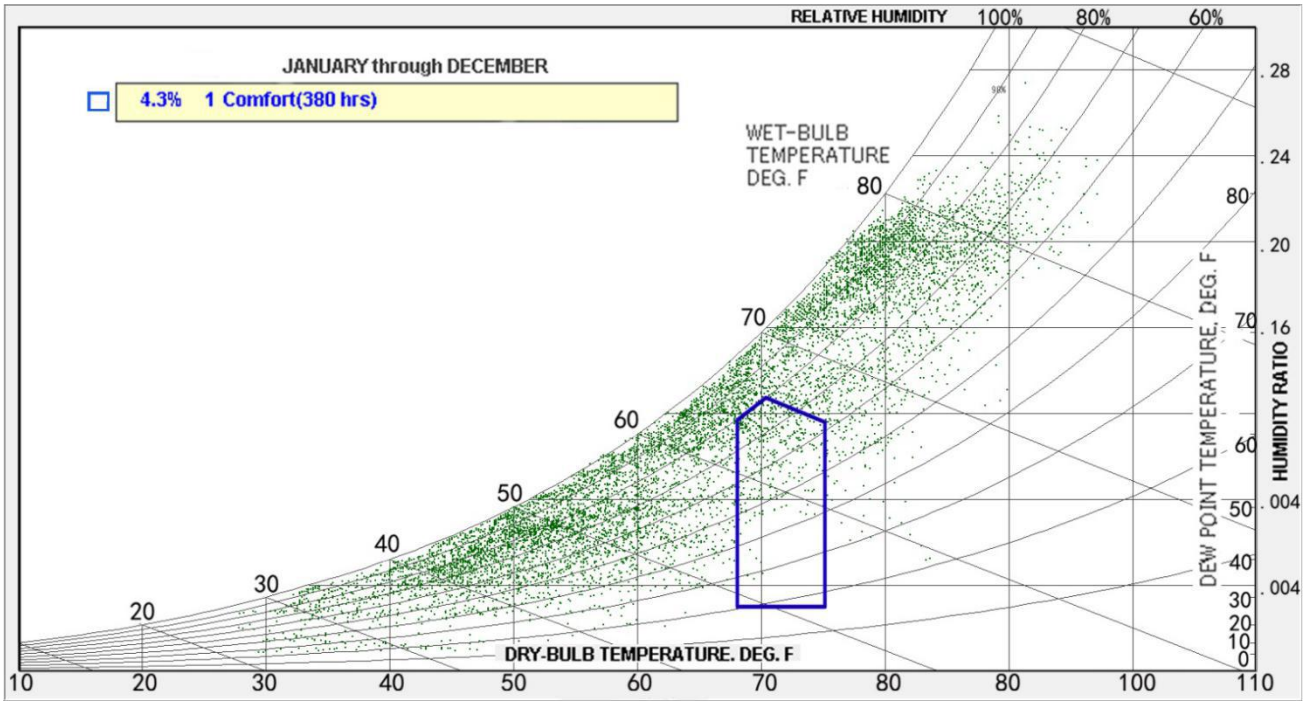

Fig. 4.19 Annual distribution of outdoor comfort time in Sizhai village

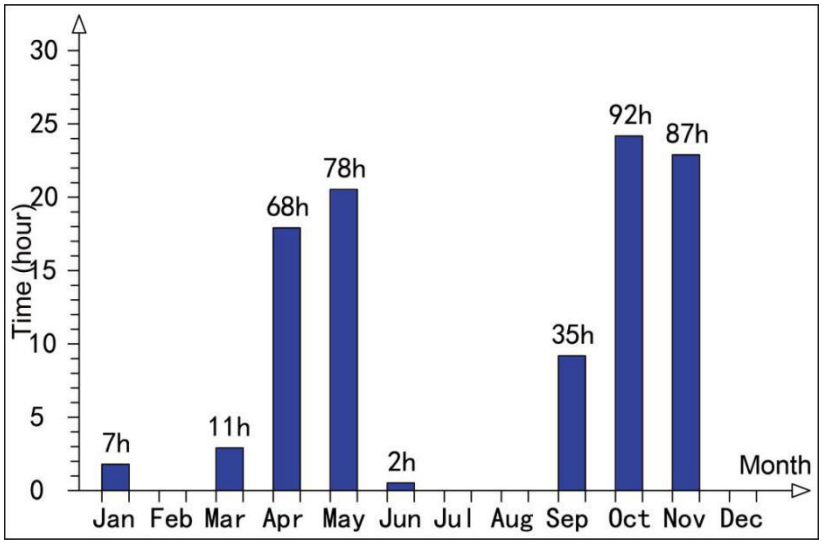

Fig. 4.20 Monthly distribution of outdoor comfort time in Sizhai village throughout the year

Based on PEs and PSs in TPD, the ELICT is simulated monthly by the software of Weather Consultant 6.0 to analyze the effectiveness of each EE. In accordance with computational results, the total ICT is extended from the original 380 h to 3852 h at present, accounting for 44.58% of the whole year (Fig. 4.21). The EEs are much more effective in May, June, September and October, in which ICT accounts for 18.1%, 11.5%, 14.2% and 22.1% of the

whole year, respectively (Fig. 4.22). Among these passive strategies, the EEs of solar shading, natural ventilation and dehumidification contribute notably to extend ICT, accounting for 10.2%, 8.3% and 9.9%, respectively. Comparing to winter, the EEs are more effective in summer, accounting for 38.4% from June to September vs. 4.6% from December to February, which validates the design principle of "consideration of heat insulation in summer as priority and thermal preservation in winter as minor" in TPD. Table 15 indicates that during the six months of a year from January to April and from November to December, the EEs principally exert heating function. On the contrary, it predominantly plays a role on cooling for interiors from June to September.

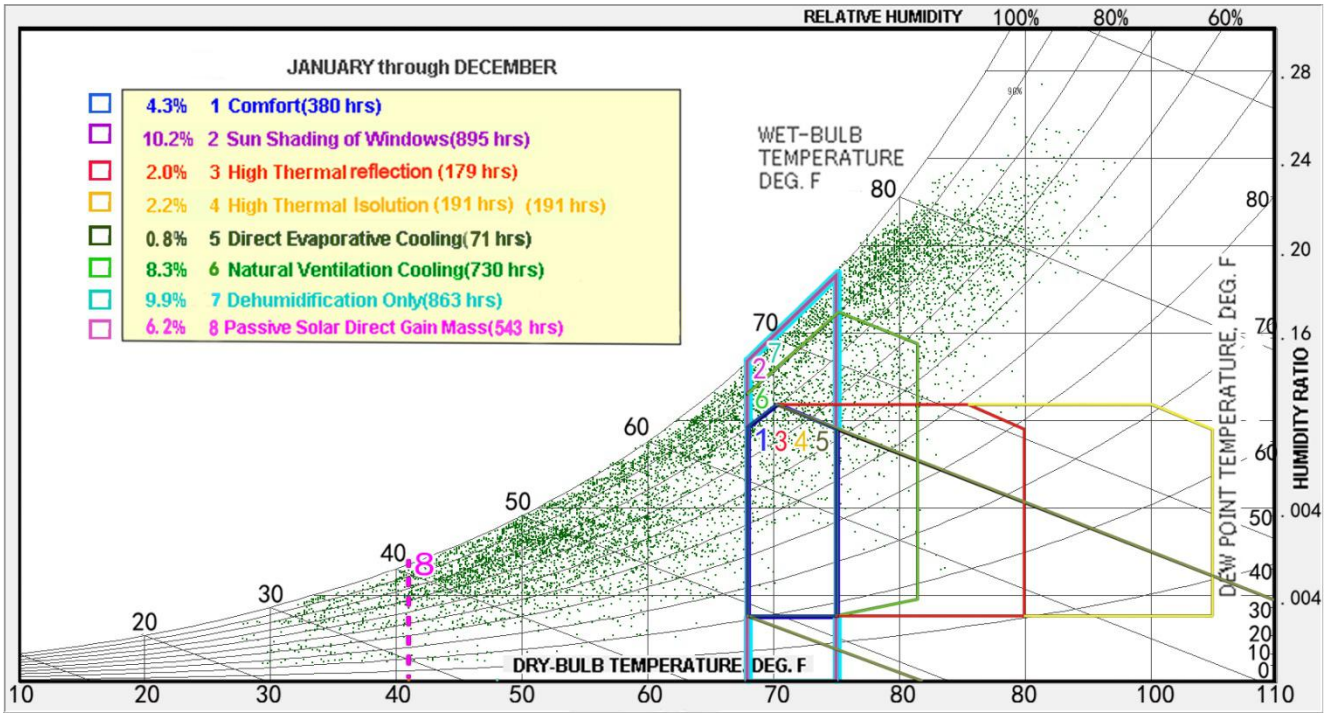

Fig. 4.21 Indoor comfort time distributions based on diverse passive strategies in the whole year

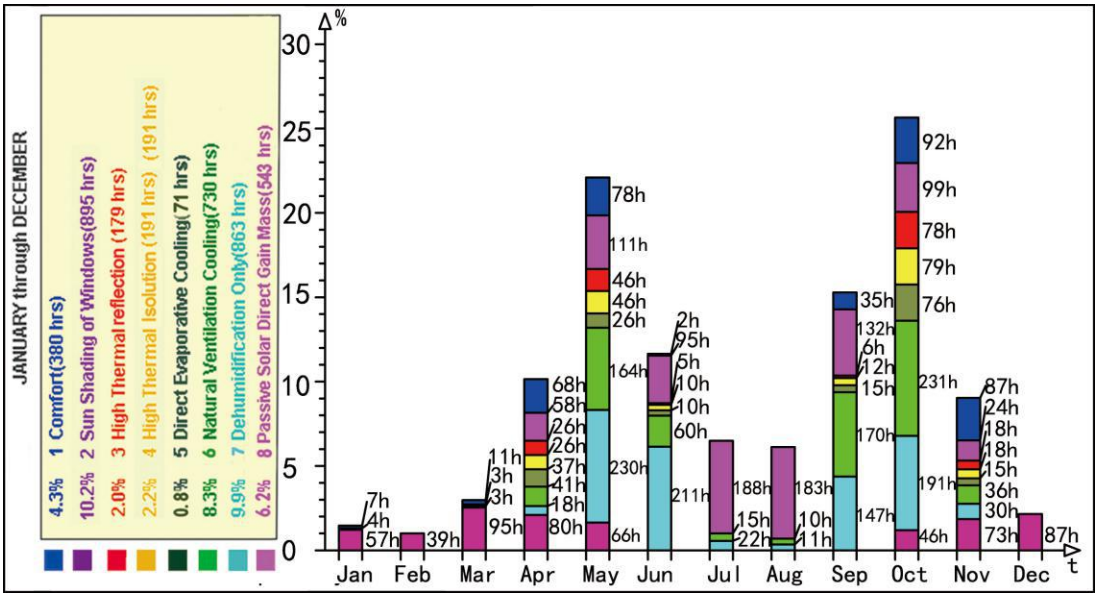

Fig. 4.22 Distributions and proportions of monthly Indoor comfort time throughout the year

Table 4.15 Indoor comfort time distribution in each month throughout the year

M	January	February
Diagram	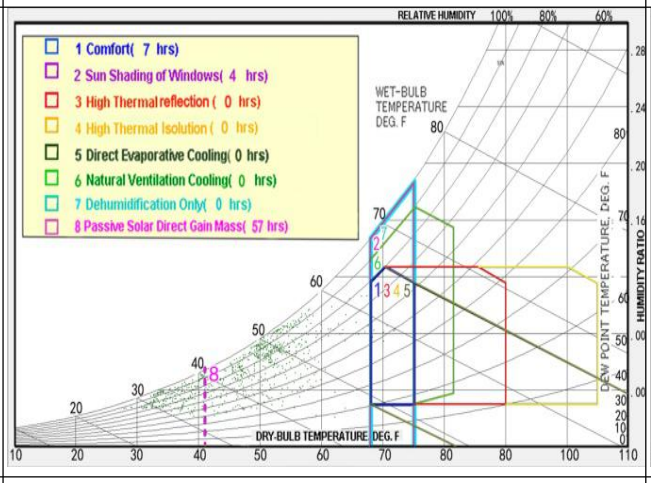	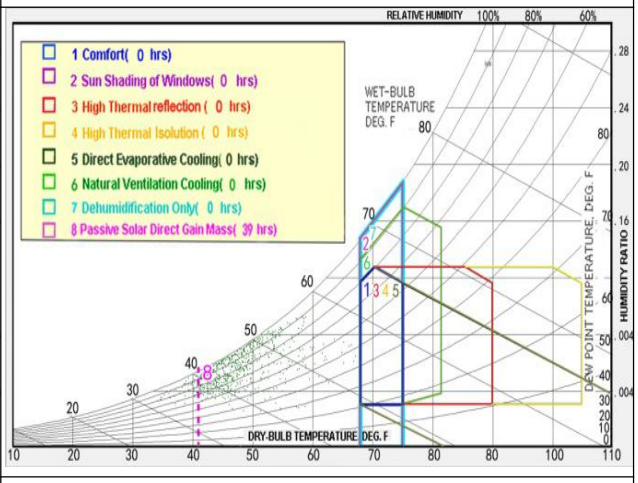
M	March	April
Diagram	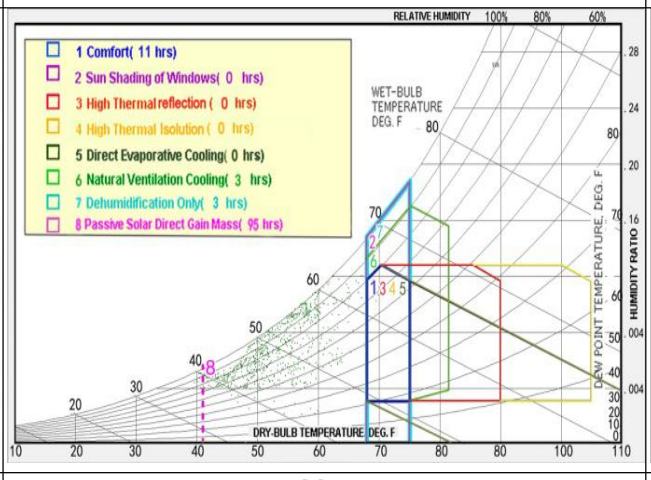	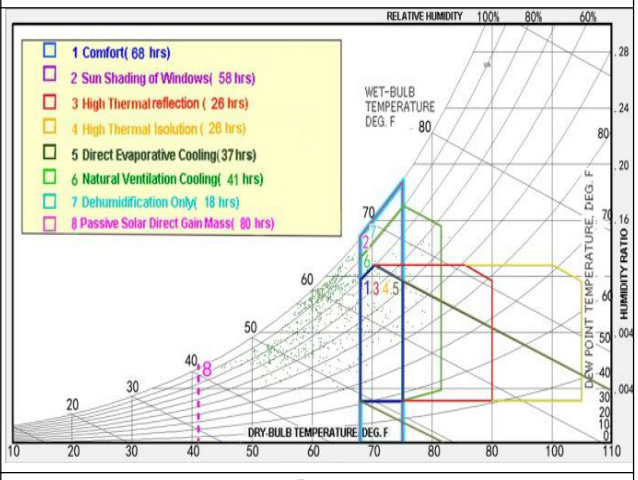
M	May	June
Diagram	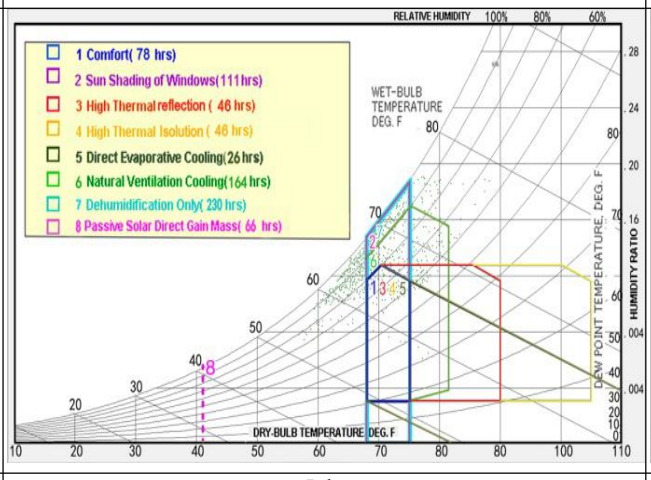	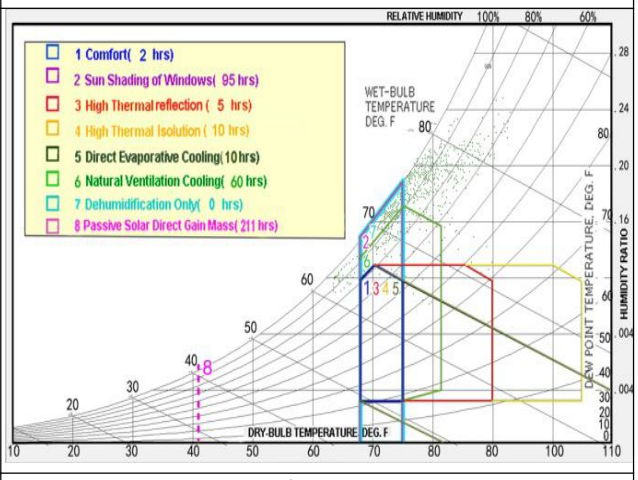
M	July	August

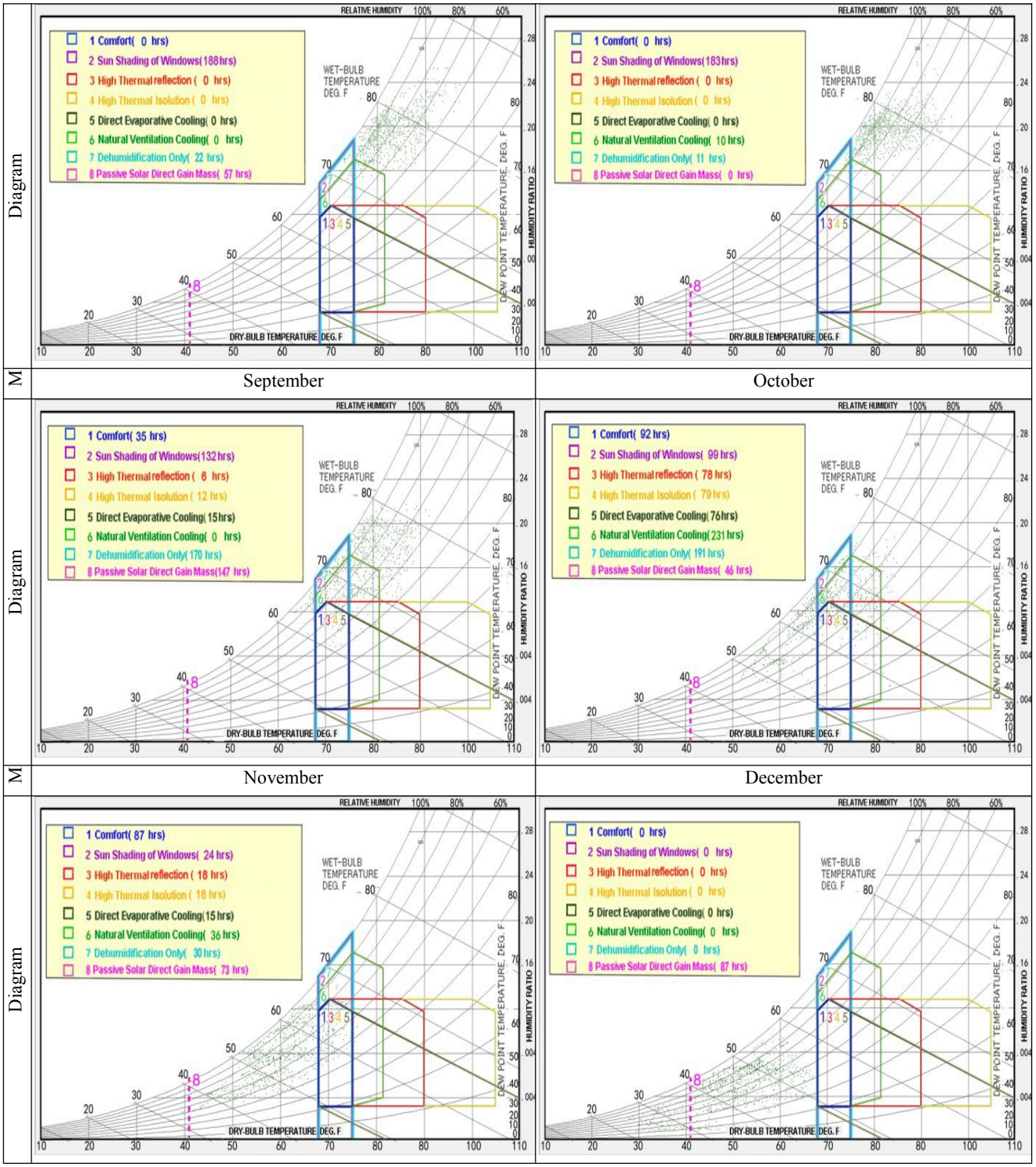

Note: M is the abbreviation of month.

Based on the above-mentioned analyses, the DPEs, SPEs and transitional spaces in TPD all perform positive EEs for both outside climate and indoor environments, contributing to creating a more comfortable indoor environment for the occupants. Each PE and PS does not exist alone, but by means of mutual connection and collaboration, they exert more efficient EEs, which contribute to improvement of the ICL and extension of ICT. The EEs of each PE and PS are concluded in Table 4.16, of which the passive strategy of solar shading has the most significant impact on the

ICL in TPD, contributing to 895 h accounted for 10.2%, and that of cooling through evaporation leads to the minimum ICL with 71 h accounted for 0.8%.

Table 4.16 Strategies and effectiveness of Passive strategies in the traditional dwelling of Thousand Pillar Dwelling

Elastic Effect		Passive strategy	Effectiveness	PE or PS	ICT (h) and proportion (%)
Temperature adjustment	Cooling adjustment	**Strengthening heat insulation performance**			191 (2.2)
		Rowlock cavity wall with a closed air layer	●	◇	
		Double-layered Roof	●	◇	
		Wooden wall with low heat-conductivity	◎	◇	
		Double-layered window and door	●	◇	
		Solar shading			895 (10.2)
		"Matou wall" and "Guanyin dou wall"	○	◇	
		Roof eave	●	◇	
		Waist eave	●	◇	
		Corridor	●	■	
		Reflection of solar radiation			179 (2.0)
		Light color wall	◎	◇	
		Cooling through evaporation			71 (0.8)
		Well and plants in the patio	◎	■	
	Heating adjustment	**Strengthening thermal preservation performance**			543 (6.2)
		Rowlock cavity walls with a closed air layer	●	◇	
		Double-layered Roof	●	◇	
		Wooden wall with low heat-conductivity	◎	◇	
		Double-layered window and door	●	◇	
Humidity adjustment		**Humidity reduction**			863 (9.9)
		Using stone wall base as damp-proof layer	◎	◇	
		Small ventilation vent near the door	◎	◇	
		Prevention wall from damp through eave	●	◇	
		Humidity adjustment			
		Ground surface used clay brick	◎	◇	
		Well and plants in the patio	◎	■	
Ventilation adjustment		**WPV**			730 (8.3)
		Ornamental perforated window	○	◇	
		Door and window	●	◇	
		Patio	●	■	
		Corridor	●	■	
		Open-hall	◎	■	
		TPV			
		Patio	●	■	
		Open-hall	○	■	
Daylighting adjustment		**Direct daylighting**			
		Door and window	●	◇	
		Indirect daylighting			
		Patio	●	■	

Note: 1. ● represents a element with strong performance, ◎ represents a element with medium performance, ○ represents a element with weak performance; 2. ■ represents PS, ◇represents PE.

4.7 Finding and discussion

Based on the passive climate-responsive strategies of PEs and PSs, the ICT is increased to 3852 h with the assistance of EEs, accounting for 43.9% of the whole year. It shows that the passive strategies in TPD provide effective EEs for internal spaces. Taking into consideration the research results of this study, it can be concluded that the traditional dwellings in Sizhai village adapt to the local climate and mitigate the impacts of outdoor climate on internal spaces effectively, which contributes to reduction in the building's energy consumption. Nevertheless, some studies with similar conclusions have been carried out in Portugal and other European countries, highlighting the fact that techniques used in traditional dwellings as being effective for use in contemporary buildings [43-45]. Most of them just focus on the passive strategies rather than the improvement on the level for indoor comfort.

Even though the aforementioned adaptive strategies of TPD are effective and improve the living conditions in this dwelling, the perfect thermal conditions, according to modern standards, are not reached without modern heating and cooling systems. So, during the 56.1% of the year, the thermal conditions in the dwelling are not within the comfort ranges. Also, the extreme amplitudes of temperatures at the location of the dwelling is outside the range of applicability of the comfort standards referred to this study. The winter temperatures sometimes can go below 5℃ and the summer temperatures rise up to 39.5℃, while the comfort model is designed for weather above 15℃ and below 30℃ in EN15251:2007. This means that although the degree of sophistication of the design for the dwelling elements is high, it is still not able to cope with local climate perfectly well.

The passive climate-responsive strategy in TPD consists of PEs and PSs, of which the PEs are composed of doors, windows, roofs, flooring, etc. and the PSs are composed of patios, corridors and open-hall. The EEs of PEs and PSs depend on adapting the local weather conditions and adjusting indoor microclimate rather than counteract the outdoor climate. According to the season alternation and external climate variation, the EEs in TPD can exert different buffer effects for internal spaces to create a comfortable indoor environment.

(1) The rowlock cavity walls with an air layer and the wooden walls with low heat conductivity have effective EEs on heat insulation and thermal preservation for the building's interiors.

(2) The tiles covered on the roofs and waist eaves adopted the pavement method of "up and down superposition" create an air layer between tiles and red mud slurry, conducing to improving heat insulation and thermal preservation

(3) performances. Moreover, the roof eaves and waist eaves are both the effective passive strategies to minimize indoor temperatures by decreasing solar exposures for walls, windows and doors.

(3) The construction of flooring for the first floors in TPD employed a compromise principle that leads to the floorings with high thermal stability. Due to usage of the clay brick with low heat storage coefficient, just a small

amount of coolness can be stored in its interior in winter, so the surface temperatures of the flooring in TPD are generally higher than their dew point temperature.

(4) The construction of doors and windows in TPD are double-layered, which the outdoor layer is window pane consisting of wooden lattice frames and glazing and the indoor layer is wooden shutter. By varying the open and closed conditions of two layers and the degrees of their opening in different walls depending on time and outdoor climate conditions, the CIL can be effectively extended.

(5) The patios in TPD with property of semi-open spaces are the important roles to play in humidity adjustment, daylighting, solar shading and natural ventilation for building's interiors.

(6) The corridors, together with suspended ceilings under the roof, create an air layer, which leads to the improvement in heat insulation performance. Furthermore, the corridor eaves are also deep, aiming at maximizing the solar shading covered wooden walls. Through induced air currents in corridors, all rooms arranged around patios can be well ventilated.

(7) The open-hall in TPD is transparent and high, which has noticeable EEs in natural ventilation and daylighting for indoor environments.

(8) An additional study on field measurements for air temperature, relative humidity, air velocity and illuminance in diverse parts of TPD were carried out to research its climate-adapting effectiveness quantitatively. The measurement results reveal that the ICL is improved effectively with the assistance of EEs.

(9) The results of qualitative and quantitative analyses show that based on the EEs, the total ICT is prolonged from original 380 h to 3852 h at present, accounting for 44.58% of the whole year.

In conclusion, the research results indicate that the passive climate-responsive strategies of TPD located in Sizhai village are examples of solutions able to adapt the hot summer and cold winter climate zone in China. Furthermore, the strategies of climate adaptation based on the case study of TPD can provide some methods and implications to rural residences for creating the comfortable indoor environments. Although the adaptation is not perfect, it is coping effectively with the extreme local climate during almost the half of the duration of the year, which is a remarkable achievement for a traditional dwelling. The standard comfort models are also not very suitable for studying this type of building without the modern heating and cooling systems, so an effective quantitative analysis on the effectiveness of all the aforementioned strategies can be performed only relatively well. Anyways, the study of the design features made with local materials, effective passive climate-responsive strategies and high durability can be useful as verified reference points for modern bio-climatic buildings in China.

The research results in this chapter attempts to provide a contribution in the passive building field by presenting

the research results on thermo-hygrometric and daylighting performances of a traditional dwelling with assistance of EEs. Even though all the advantages of passive strategies are evident in the traditional dwelling, there is a lack of quantitative analyses and quantitative data to support the effectiveness of these approaches on improving ICL in the hot summer and cold winter climate zone of China up to now. This chapter raises the significance of passive strategies in traditional dwellings for improving their comfort levels of indoor environments. The research results provide new opportunities for buildings using the traditional passive strategies aiming at climate adaptation at the present day.

References

[1] Xi'an University of Architecture and Technology. *Architectural Physics (fourth edition)* [M]. Beijing: China Construction Industry Press, 2009: 12-13.

[2] LIU Su. The types and geographical distribution of Chinese traditional dwellings [J]. *Chinese and Overseas Architecture*, 1996 (6): 27-28

[3] Olgyay V. *Design with Climate: Bioclimatic Approach to Architectural Regionalism* [M]. Princeton: Princeton University Press, 1963: 10.

[4] McHarg I L. *Design combines nature* [M].RUI W J, Trans. Beijing: China Construction Industry Press, 1992: 57.

[5] ZHANG T. *Overall Area Building* [M]. Nanking: Southeast University Press, 2003: 25-64.

[6] JollyJohna Ash, Latha Thampuran, B.Premlet. Objective and subjective evaluation of acoustic comfort in classrooms: A comparative investigation of vernacular and modern school classroom in Kerala [J]. *Applied Acoustics*, 2016, 104(3): 33-41.

[7] H.Al-Hinai, W.J.Batty, S.D.Probert. Vernacular architecture of Oman: Features that enhance thermal comfort achieved within buildings [J]. *Applied Energ*y, 1993, 44(3): 233-244.

[8] A.S.Dili, M.A.Naseer, T.Zacharia Varghese. Passive control methods for a comfortable indoor environment: Comparative investigation of traditional and modern architecture of Kerala in summer [J]. *Energy and Buildings*, 2011, 43: 653-664.

[9] Jorge Fernandes, Carlos Pimenta , Ricardo Mateus, et al. Contribution of Portuguese Vernacular Building Strategies to Indoor Thermal Comfort and Occupants' Perception [J]. *Buildings*, 2015(5): 1242-1264.

[10] D.G. Leo Samuel, K. Dharmasastha, S.M. Shiva Nagendra, et al. Thermal comfort in traditional buildings composed of local and modern construction materials [J]. *International Journal of Sustainable Built Environment*, 2017(6), 463-475.

[11] Ahmadreza, Foruzanmehr, Fergus Nicol. Towards new approaches for integrating vernacular passive-cooling systems into modern buildings in warm-dry climates of Iran [J]. *Journal of Forensic Psychiatry*, 2008, 13 (13): 329-344.

[12] Building Energy Conservation Research Center of Tsinghua University. *Research report on the annual development of energy conservation in China* [M]. Beijing: China Building Industry Press, 2008, 1-279.

[13] HE J Q. The improvement of residential property by the way of green industry [J]. *Development of Small Cities*, 2006, 22(1): 70-74.

[14] DING J Q, et al. *Zhejiang Traditional Dwelling* [M]. Beijing: China Architecture & Building Press, 2009.

[15] HOLING C S. Resilience and stability of ecological systems [J]. *Annual Review of Ecology and Systematics*, 1973(4): 1-23.

[16] GUNDERSON L H, HOLING C S: *Understanding Transformations in Human and Natural Systems* [M]. Washington D C: Island Press, 2002.

[17] ZHOU H J, WANG J A, WAN J H, et al. Resilience to natural hazards: A geographic perspective [J]. *Natural Hazards*, 2010, 53(1): 21-41.

[18] BRUNEARU M, STEPHAINE E C, RONALD T E, et al. A framework to quantitatively assess and enhance the seismic resilience of communities [J]. *Earthquake Spectra*, 2003, 19(4): 733-752.

[19] LIU Q. The creation of persistent and flexible-the research of architectural elastic design theory and practice [D]. Tianjin: Tianjin University.

[20] DESOUZA. Designing, planning, and managing resilient cities: a conceptual framework [J]. *Cities*, 2013, 35: 89-99.

[21] LI T T, NIU P Y, GU C L. The summarized research framework of elastic urban [J]. *Journal of Urban Planning*, 2014 (5): 23-31.

[22] P.R.C. Ministry of Construction, *Code for Design of Civil Buildings* (GB50352-2005), Beijing: China Architecture & Building Press, 2005.

[23] M. Kottek, J. Grieser, C. Beck, B. Rudolf, F. Rubel, World map of the Köppen-Geiger climate classification updated, Meteorol. Z. 2006, 15 (3): 259-263.

[24] HUANG J H, ZHANG Y, ZHENG W F. Jiangsu and Zhejiang area traditional residential energy conservation technology research [J]. *Architectural Journal*, 2005 (9): 22-23.

[25] GUO H F, ZHANG G T. Norganic light aggregate system common defects and the cause analysis of insulation mortar [J]. *Zhonghua Local-style Dwelling*, 2012 (3): 439-43.

[26] LIU X J. *Ecological Architecture* [M]. Beijing: China Architecture Industry Press, 2009: 21-34.

[27] R. Shanthi Priya, M.C. Sundarraja, S. Radhakrishnan, L. Vijayalakshmi. Solar passive techniques in the vernacular buildings of coastal regions in Nagapattinam, TamilNadu-India a qualitative and quantitative analysis [J]. *Energy and Buildings*, 2012, 49: 50-61.

[28] DI Peng, WANG Zhen-zhen. Analysis on thermal performance of Wannan residential wall [J]. *Journal of Xi'an University of Science and Technology,* 2014, 34(3): 279-283.

[29] Manoj Kumar Singh, Sadhan Mahapatra, S.K. Atreya, Thermal performance study and evaluation of comfort temperatures in vernacular buildings of North-East India [J]. *Building and Environment*, 2010, 45:320-329.

[30] Jorge Fernandes, Ricardo Mateus, Luís Bragança, et al. Portuguese vernacular architecture: the contribution of vernacular materials and design approaches for sustainable construction [J]. *Architectural Science Review*, 2015(10): 324-336.

[31] Ministry of Housing and Urban-Rural Development of the People's Republic of China. Architectural reflective thermal insulation coatings (JG-T 235-2014) [Z]. Beijing: Industrial Architecture Press, 2014: 2.

[32] Francisco Salamanca, Andrea Krpo, Alberto Martilli, Alain Clappier. A new building energy model coupled with an urban canopy parameterization for urban climate simulations part I. formulation, verification, and sensitivity analysis of the model [J]. *Theoretical and Applied Climatology*, 2010 (1): 99-133.

[33] DONG K, LA Y J, QIAN X Q, et al. Energy efficiency of residential buildings with horizontal external shading in hot summer and cold winter zone [J]. *Journal of Zhejiang University (Engineering Science)*, 2016, 50(8): 1431-1437.

[34] YMA X W, FAN Y Y, HOU Y B. Experiment of natural ventilation for residential buildings during summer time in Shenzhen [J]. *Journal Heating Ventilating and Air conditioning*, 2003, 33(5): 115-118.

[35] A. Jovanovića, P. Pejićb, S. Djorić-Veljkovićb, et al. Importance of building orientation in determining daylighting quality in student dorm rooms: Physical and simulated daylighting parameters' values compared to subjective survey results [J]. *Energy and Buildings*, 2014, 77(3): 158-170

[36] G.C. Brainard, J.P. Hanafin. The effects of light on human health and behaviour: relevance to architectural lighting, in: Proceedings of the Symp.'04 Light and Health: Non-Visual Effects, CIE, Vienna, 2004.

[37] E. Rautkyla, M. Puolakka. Alerting effects of daytime light exposure a pro-posed link between light exposure and light mechanisms [J]. *Lighting Research and Technology*, 2012, 44: 238-252.

[38] H. Fischer, H. Freymuth, P. Haeupl, et al. Theory of Building Physics, Vieweg and Taubner Verlag [Z], Germany, 2008.

[39] Hans-Peter Birkhofer, SSL. Lighting Hype or the only solution in future lighting with respect to specification and application, Proceedings, Balkan Light 5th International Balkan Conference on Lighting, October 3-6, 2012, Belgrade, Serbia, 8-13.

[40] Fernandes, Jorge, and José Correia da Silva. 2007. "Passive Cooling in Évora's Traditional Architecture." In 2nd PALENC Conference and 28th AIVC Conference on Building Low Energy Cooling and Advanced Ventilation Technologies in the 21st Century, edited by M. Santamouris and P. Wouters, 1: 341-345. Heliotopos, Greece: Heliotopos Conferences.

[41] ZHOU H M, HUA Y X. Low-tech ecological applications in water of Chinese traditional architectural environment [J]. *Huazhong Architecture*, 2012, 29 (9): 10-17, 689.

[42] HU Y, WANG H D, ZHANG L. Zhejiang xianju comparison and analysis of traditional local-style dwelling houses and has been gloriously enrolled architecture [J]. *Zhejiang Architecture*, 2012, 29 (9): 10-17, 689.

[43] Fernandes, J., Mateus, R., Bragança, L., Correia da Silva, J.J. Portuguese vernacular architecture: The contribution of vernacular materials and design approaches for sustainable construction [J]. *Archit. Sci. Rev*. 2015, 58: 324-336.

[44] Cardinale, N., Rospi, G., Stefanizzi, P. Energy and microclimatic performance of Mediterranean vernacular buildings: The Sassi district of Matera and the Trulli district of Alberobello [J]. *Building and Environment*. 2013, 59: 590-598.

[45] Martín, S., Mazarrón, F.R., Cañas, I. Study of thermal environment inside rural houses of Navapalos (Spain): The advantages of reuse buildings of high thermal inertia [J]. *Constr. Build. Mater*. 2010, 24: 666-676.

Chapter 5

Impact of building azimuth on the energy consumption

5.1 Introduction

5.1.1 Motivation

In accordance with IPCCAR5 (Intergovernmental Panel on Climate Change Fifth Assessment Report), the world buildings were responsible for approximately 32% of the total energy consumption in 2010, which resulted in emission of 19% of energy-related greenhouse gases. Based on some research predictions, the global building energy consumption will continue increasing at the average growth rate of 15% from 2012 to 2040 [1]. The entire building area of rural residences in China has reached roughly 24 billion m^2 in recent years, accounting for over 60% of the national building area [2]. Furthermore, the energy cost per unit of floor area in rural residence grows continually as well, which rises from 3.02 $kW \cdot h/m^2$ in 2001 to 13.23 $kW \cdot h/m^2$ in 2017, with an increasing rate of 3.4 [3]. The data from the State Statistics Bureau indicate that the total annual electricity consumed in rural residences is approximately 90 billion $kW \cdot h$, which accounts for about 26% of the national electricity cost of buildings [4]. Moreover, China is the largest CO_2 emitting country in the world currently, of which the building sector is one of the main energy consuming industries. The proportion of energy cost in buildings has reached up to 27.6% of the total in China, with an evolving trend of continuous growth [4].

Energy consumption in rural residences is principally used for heating, cooling, lighting, cooking and appliances in China, of which Air Conditioning (AC) (with inclusion of heating and cooling) and artificial lighting are responsible for 20% and 7~8% of the total energy cost, respectively [5]. Additionally, taking into account the use of electrical ventilators and humidifiers, etc., the energy used for regulating and adjusting indoor thermal and daylighting environments accounts for approximately 30% of the total building energy consumption [5]. Besides, with growing severity of global warming, more attention should be given to the construction industry to research low carbon emission and the energy efficiency for buildings [6].

There are many factors influencing the building energy consumption, but some of them can be managed and adjusted by using passive strategies. For instance, by incorporating the measures of thermal insulation [7-8] and shading configurations [9-12] into buildings, as well as choosing a suitable building typology [13-16], optimum building orientation [17] and appropriate fenestration system [18-19] for them, the indoor comfort level will be improved, which can lead to the reduction in the building energy consumption and CO_2 emissions. The passive strategy of selecting an optimal building orientation is efficient to cut off energy consumption by means of taking advantage of the renewable resources from nature[20], such as solar radiation and wind, which in turn decreases the reliance on the power grid. Especially for a building with a rectangular configuration, the influence of its orientation on the energy consumption is more evident [21-22].

5.1.2 Research content

Building orientation is a sensitive factor influenced and restrained by ambient conditions frequently and easily by constraints, such as the building base, roads and rivers. Especially, the selecting principle of building site for Chinese traditional dwellings, “adaptation to local conditions”, makes building orientations more flexible and diverse. The building orientation determination of dwelling is impacted by the road, building base and river, etc. In addition, the distribution regularity and data statistics of building orientation for rural residences remain to be studied at a village-scale. Nevertheless, these data have an important role to play on the energy saving potential assessment and passive strategy implementation for the village. Therefore, this chapter is integrated with the real conditions of Chinese traditional dwellings, which have been representative of housing samples, to explore the impact of BA on energy consumption by varying its values within 360°.

The energy consumption of buildings varies with their BA principally via impacting their indoor temperature, natural ventilation and daylighting [57]. In accordance with Martin Marin’s research results [34], among all active systems, the energy consumption for space heating and cooling has the most dramatic fluctuation with varying BA, and that related to lighting and ventilating is in the second and third place, respectively. Whereas, the energy used for powering other electrical appliances is not affected by BA [34]. Thus, the energy consumption of AC (inclusion of the heating and cooling), electrical ventilation and artificial lighting was selected as the evaluation parameter in this chapter. A comparison of energy costs corresponding to the different BAs was performed to explore the best building orientation, which contributes to effectively promoting the energy saving of dwellings situated in the research region.

5.1.3 Scientific originality

The originality of this chapter is to estimate the thermal and lighting performances, as well as energy demands for the traditional dwellings located in East and Central China based on changes in BA, which are experiencing the harshly hot weather conditions over a long period of time. The evaluation of building energy cost for each of the test scenarios is based on the computational results of indoor thermal and visual performances. Also, the proposed analysis approach of BA can be regarded as a new research method for determining the optimal design option for the traditional dwelling. Application of this method can contribute to minimizing energy consumption and achieving energy saving in accordance with the data generated from the energy simulation, because a well-orientated building can efficiently reduce the equipment costs and time in operation of active systems. On the other hand, until very recently, related researches on the BA impacting energy consumption are often neglected to carry out in the traditional buildings [35]. Thus, the research results based on the case study of traditional dwellings in this chapter

may supply some new body of connection between BA and building energy consumption to fill in the knowledge gap in this field.

5.1.4 Research purpose

The purpose of this study is to research the impact that building orientation has on indoor environments (including air temperature, air velocity and illuminance), as well as on electricity consumption, based on the case study of Sizhai traditional dwellings. Furthermore, the BA statistics at a village-scale for Sizhai were carried out to evaluate its energy saving potential. The finding of this research may provide some suggestions on the building orientation determination for newly-built rural residences and proposes a method of assessing energy saving potential for the existing residences, taking the BA as the evaluation parameter.

5.2 Description of simulation tool and research flow

5.2.1 Division of dwelling subdomain for Sizhai village

According to the village geography and building typology, Sizhai village is considered as a typical mountainous traditional village. Observing the layout of village by G.E., almost all dwellings are situated in the flat basin area surrounded by mountains, and the scope of the building zone is highlighted by the red dashed line as shown in Fig. 5.1. By observing the remote image, there are totally 437 dwellings in this village.

In G.E. software, the longitude and latitude grid system covering remote sensing image can be automatically generated. By zooming the remote sensing image, the grid system intervals and dwelling sizes can be adjusted correspondingly. In this work, the intervals of grid system per unit are both set at 12.96’’ to create 10 dwelling subdomains (Fig. 5.1), of which the building density in NO. 2 dwelling subdomain is highest.

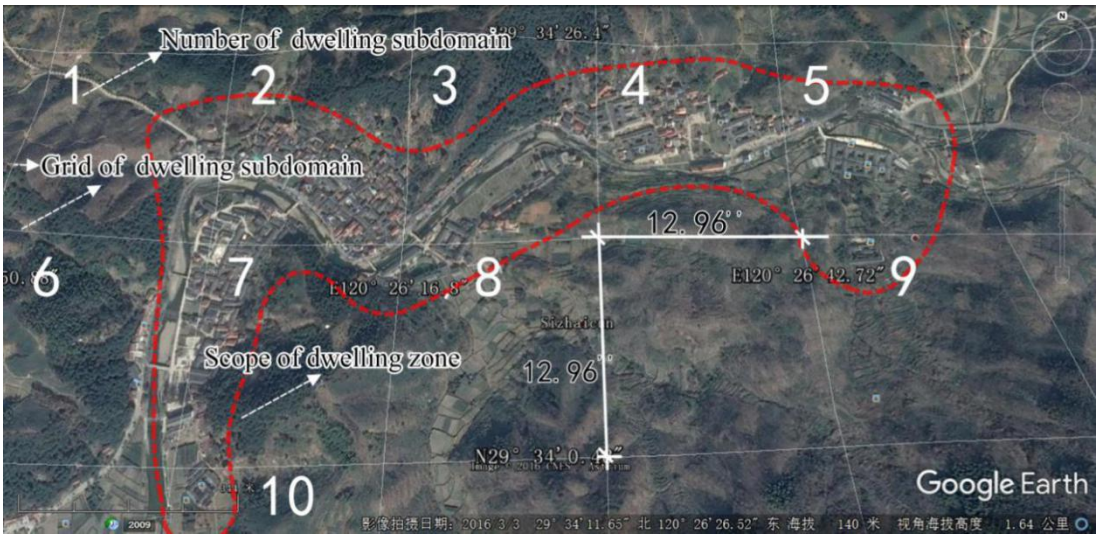

Fig. 5.1 Scope of building zone and division of dwelling subdomains in Sizhai village

5.2.2 Measurement method of building azimuth for dwelling

As shown in Fig. 5.2, by using the orientation measurement functionality in G.E. to click two terminal points of a building ridge, the BA of dwelling can be obtained. Since the value of BA for a building facing directly south is determined as 0° in this chapter, while the 0° in the G.E. represents facing directly north, the measurement data need to be converted, namely the measurement values plus 90°. The BA measurement was performed for all buildings located in the 10 dwelling subdomains of Sizhai village, and the analysis of percentage distribution corresponding to the 18 BA intervals was also conducted for each subdomain.

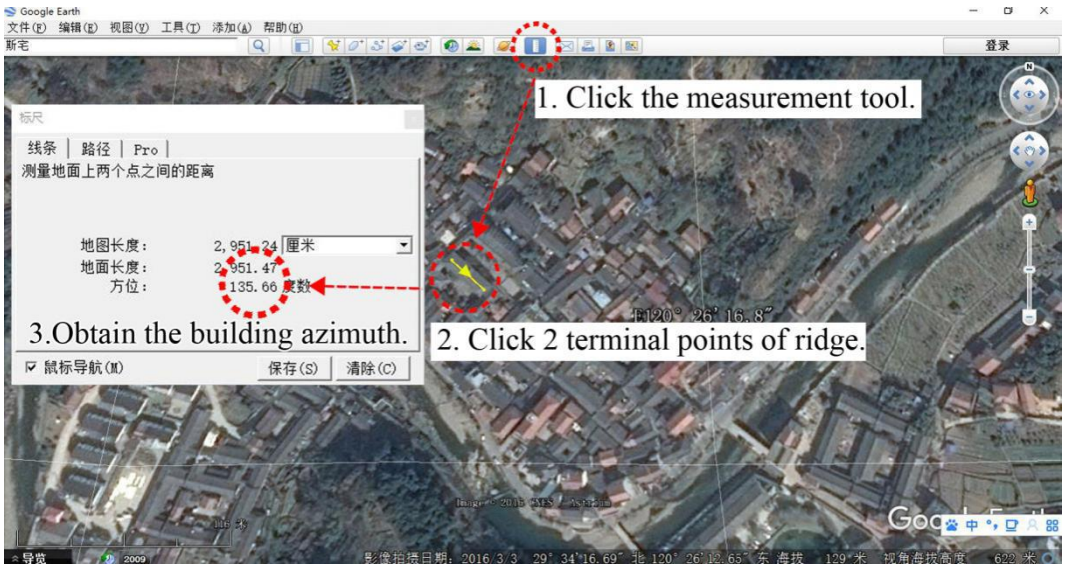

Fig. 5.2 Measurement method of building azimuth for dwelling in G.E.

5.2.3 Research flow descriptions

To simulate and compute the three evaluation parameters for the test scenarios at a series of BAs, software of ArchiWIZARD 3.1.1, PHOENICS 2009 and VELUX Daylight Visualizer 2 were used. In addition, through energy simulation in ArchiWIZARD 3.1.1 and Ecotect 2012, the energy consumption of AC, electrical ventilation and artificial lighting were computed, respectively. The total annual electricity consumption consumed in AC, electrical ventilation and artificial lighting was evaluated as well to explore the optimum BA for dwellings in the summer hot and winter cold climate zone of China. Together with on-site survey, the real data from electricity consumption bills obtained from 4 suites were used to compare with the computational results from software, aiming at verifying the computational result accuracy. Furthermore, using the evaluation parameter of BA, the energy saving potential of Sizhai village was assessed by observing the percentage distribution characteristics of all BAs at village-scale. To facilitate the understanding of the research methods framework, it is presented in Fig. 5.3.

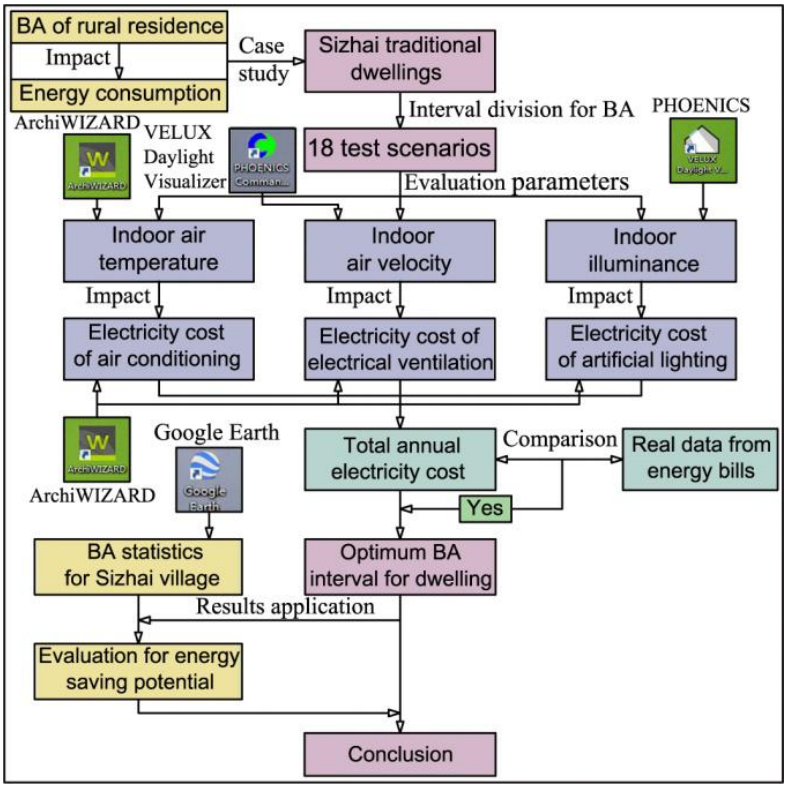

Fig. 5.3 Schematization of the proposed research method

5.3 Impact of building azimuth on the electricity consumption

5.3.1 Indoor temperature and electricity consumption of air conditioning with varying building azimuth

5.3.1.1 Air temperature in the internal space with varying building azimuth

The software of ArchiWIZARD 3.1.1 was applied to simulate and compute the average monthly indoor temperatures for the 18 test scenarios, aiming at evaluating the influence degree, for different BAs, on air temperatures. The geographic information of Sizhai village with latitude 29°34' North and 120°26' East was input into this software. Simultaneously, as the options of topography and meteorological files, countryside and Shaoxing climate were selected, respectively.

There are two ways in which the outdoor climate impacts indoor temperatures when the windows are under the condition of being closed, namely the heat transmission by temperature difference and solar radiation. As the facades facing different orientations possess the same WWR, the heat transfer through each window by the temperature difference between exterior and interior is the same as well, but that due to the solar radiation varies greatly depending on BA alterations. A building's capacity to receive naturally heat for the internal spaces relies on its external components and the way of its interaction with the sun [27]. Since the sunny weather conditions are related to a high intensity of solar radiation, it results in the facades obtaining different solar receptions, and evidently leads to

the difference in indoor temperatures with varying BA. On the other hand, although the orbit of the sun is symmetric with respect to north-south axis at 12 o'clock, the solar radiation level is constantly changing in the sky, which is impacted by the cloudage, dust level in air and air humidity, etc. In Sizhai, the magnitude of total solar radiation during the first half-day is generally greater than that during the second half-day [36, 37]. Besides, the earth's surface absorbs and retains solar heat during the forenoon, so the exterior temperatures during the afternoon are higher, which results in the fact that the heat transmissions performed on glazing of the test scenarios facing west are generally more drastic than those facing east, as listed in Table 5.1.

The mean monthly indoor temperatures for south are generally lower than those for north during January, because the test scenarios facing north lose a great quantity of solar reception. A mean monthly indoor temperature difference of 2.5 ℃ between the best (S-W20) and the worst (N) BAs of the test scenario was achieved. Since the solar azimuth becomes small in the morning of summer, which leads to the solar exposure time for the front facades facing south being short in June and July, the highest indoor temperatures both occur in the test scenario with N-W80. With solar azimuth increasing in August, the test scenario with S-W80 has the highest indoor temperatures. The mean monthly indoor temperature differences between the best and the worst BAs of the test scenarios in June, July and August are 1.8 ℃, 1.5 ℃ and 1.7 ℃, respectively. During these four months, the lowest indoor temperatures are kept in the test scenario with N.

Table 5.1 Mean monthly indoor temperatures in the 18 test scenarios during January, June, July and August

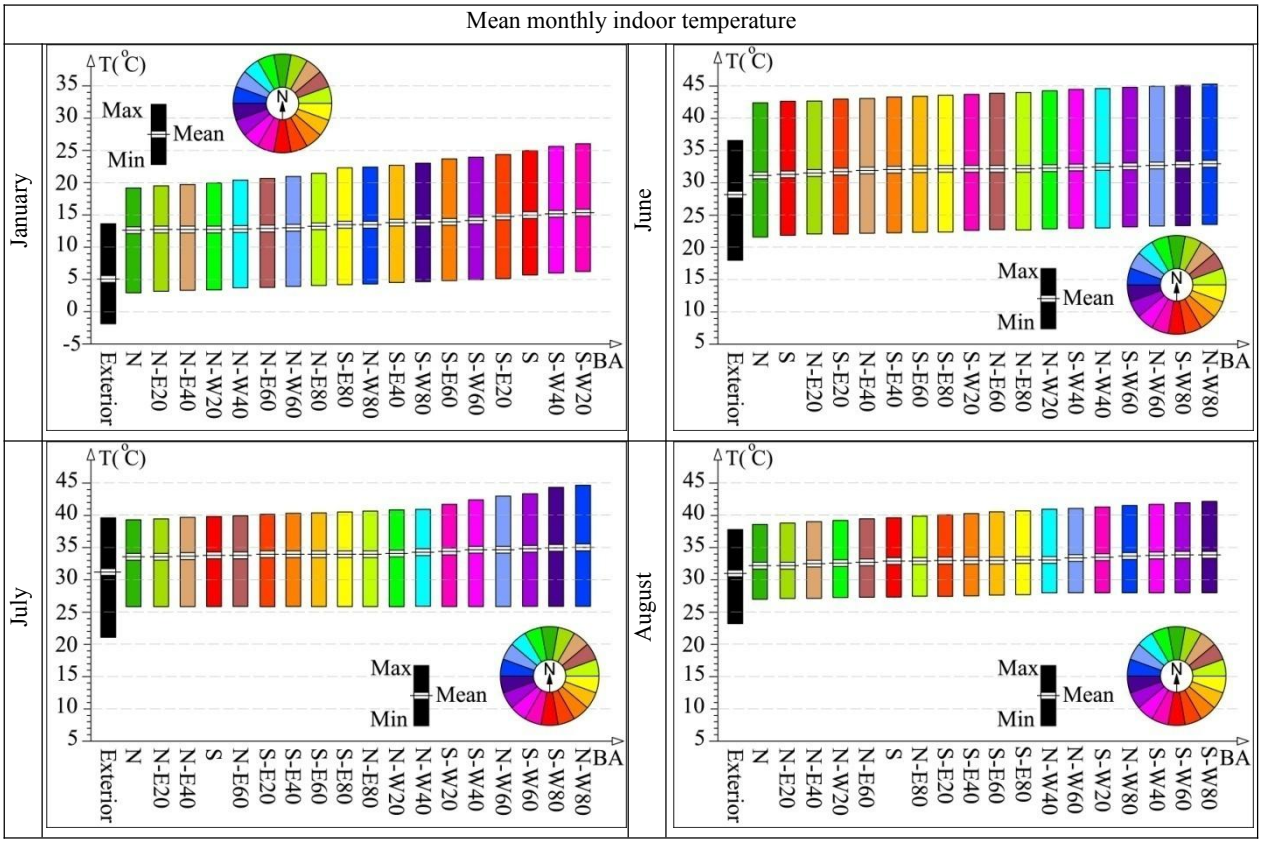

5.3.1.2 Impact of building azimuth on the energy consumption of air conditioning

During AC in operation, its action-points of heating and cooling temperatures should be controlled in appropriate scopes. The optimum scopes of AC action-points range from 26 ℃ to 28 ℃ during summer and from 18 ℃ to 20 ℃ during winter [38]. According to the recommended AC action-points and taking into consideration the habit of temperature setting for AC by occupants, the AC action-points were set at 27 ℃ and 18 ℃ in simulation for space heating and cooling, respectively.

Since the active system used for both cooling during summer and heating during winter for the internal spaces is AC in East and Central China, the electricity from power grid was chosen as the energy supply pattern in the simulation throughout the whole year. For improvement the accuracy of computational results from simulation, some set-points should be modified, in accordance with the real conditions of the air-conditioned conditions and occupancy schedules for dissimilar rooms. In consideration of the air-conditioned conditions and occupancy schedules for different rooms, the setting parameters in the simulation were adjusted as follows.

Since generally only bedrooms are equipped with AC in the Sizhai traditional dwellings, whose building area accounts for, approximately, 33% of a suite, the air-conditioned building area of the middle suite was set at 13.2 m^2 and the other four were all set at 7.99 m^2. Due to each suite being occupied by a small family with an average of two or three people, the population density of the bedroom was set at 0.221 in the simulation. Simultaneously, the probability of all five suites being simultaneously air-conditioned was set at 80%. In addition, the schedule assumed for the use of AC during weekdays is 7 hours daily, beginning at 22:00 p.m. and ending at 5:00 a.m. of the next day, accounting for a 29.17% of the whole day. Since the air temperatures are comparatively low during the forenoon in summer and the occupants' daily schedule is postponed in winter, the time of AC functioning during weekends was set at 15 hours daily, from 14:00 p.m. to 5:00 a.m. of the next day, accounting for 62.5% of the whole day.

By drawing an analogy between the electricity consumption for all the test scenarios, we found that the test scenario with N requires the lowest total electricity energy of AC (876.96 kW·h), despite it having the highest energy requirement (190.02 kW·h) for space heating during winter (Fig. 5.4). In general, the total electricity consumption of AC in the test scenarios facing west is higher than that of those facing east, of which the test scenario with N-W80 is assumed to be consumed the highest amount of electrical energy (979.87 kW·h). Moreover, a total electricity use difference of 102.91 kW·h throughout a year between N (the best BA) and N-W80 (the worst BA) of the test scenario is achieved. Furthermore, due largely to the climate in Sizhai, characterized by long summer and short winter, the impacts of BAs on the total electricity consumption of AC throughout a year are more related to the indoor temperatures in summer, by performing a comparison between Fig. 5.4 and Table 5.1.

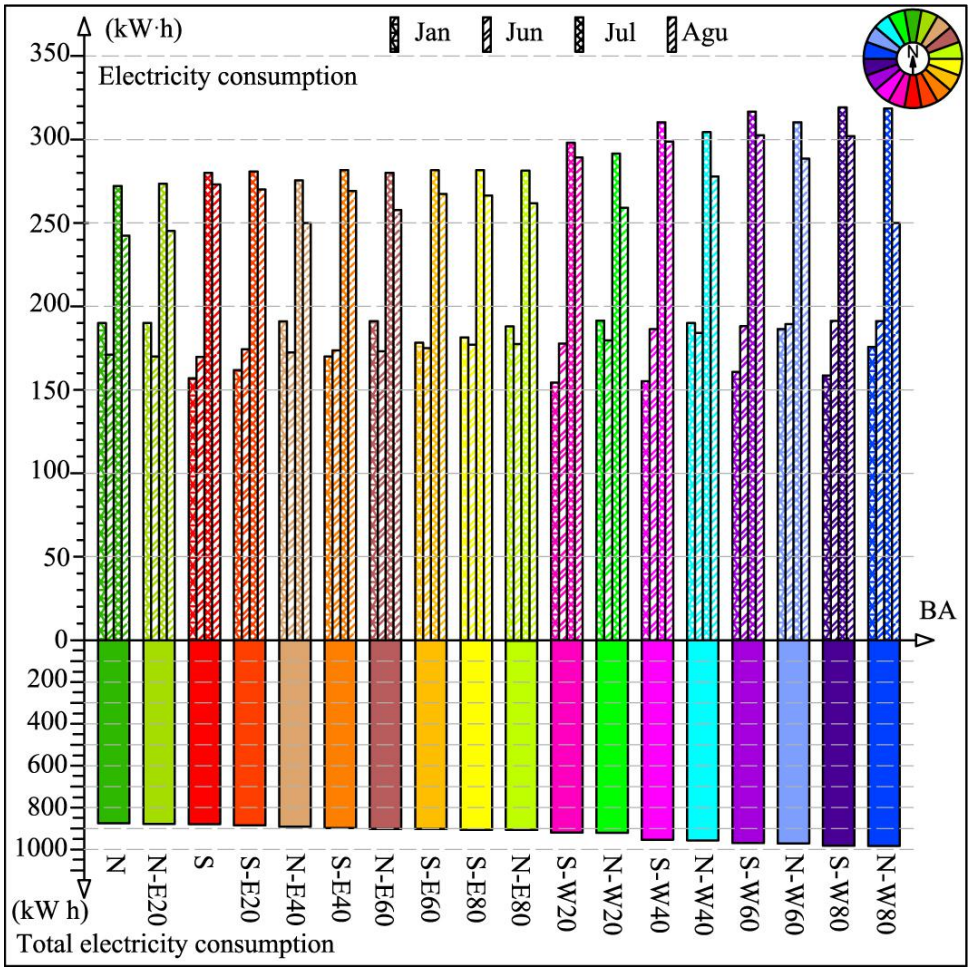

Fig. 5.4 Electricity consumption of air conditioning in January, June, July and August

and the total electricity consumption corresponding to different building azimuths

5.3.2 Indoor air velocity and electricity consumption of electrical ventilation with varying building azimuth

5.3.2.1 Natural ventilation in the internal space with varying building azimuth

Due to the Sizhai village characterized by the high air temperatures in summer with long period of time, the average monthly temperature of September is comparatively high in Sizhai, which is about 25℃. Therefore, the internal spaces require natural ventilation or electrical ventilation to expel the indoor heat, in order to mitigate the hot sensation for occupants. Through field investigation, it was found out that the occupants usually use electrical ventilators to make the indoor air flowing during this month. The prevailing wind directions in Sizhai are southeast and northwest, which accounts for 48.4% of the duration of the whole year. Under the influence of Siberian cold high pressure, the wind in winter is primarily from northwest. In contrast, due to the Northwest Pacific subtropical high pressure, the main wind orientation is southeast in summer. The mean air velocities in June, July, August and September are quite similar, approximately 2.1 m/s.

Because Sizhai is surrounded by mountains, the outdoor air velocity is relatively low in comparison with the average level of Shaoxing area. A field measurement was conducted to determine the set point of the incoming flow speed in the simulation. The outdoor air velocities in the three measurement points, as shown in Fig. 5.5, were measured during 3 days in a row from 4th to 6th of September, 2015, which were all days with sunny weather conditions. The selection principle of measurement points was to use the open spaces and to spread them throughout the village as much as possible. In detail, (1) Point 1 is near the mountain; (2) Point 2 is near the river; (3) P3 is near the building. The data logger (i.e., Anemograph with type 20100110, see Appendix 1-1) located 1.2 m above the ground level, recorded air velocity at 1 hour increments.

By taking an average for all the measurement data (Fig. 5.6), the means air velocity of the three measurement points during three days was calculated, which is 0.33 m/s. Thus, this mean air velocity with south by east 45° direction was chosen as a set point in the simulation. Because the height range within 2.00 m above ground is the major activity space for human beings, the simulation planes in the test scenarios were all set at 1.2 m above floor.

Fig. 5.5 Distribution of the three points for measuring air velocity in Sizhai village

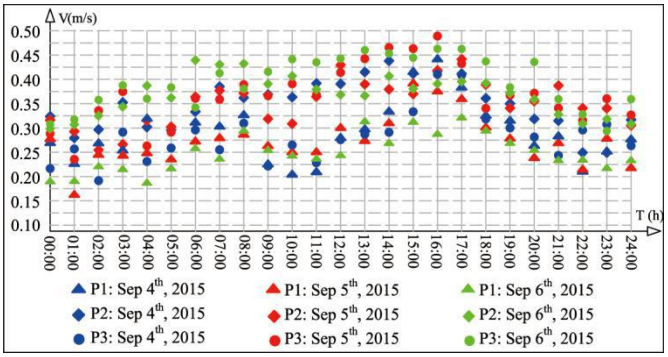

Fig. 5.6 Hourly air velocities at three measurement points for three days

As shown in Fig. 5.7, the magnitudes of mean indoor air velocities in test scenarios facing southeast are relatively large, because their glazed walls face the windward side. The test scenario with S-E40° has the maximum mean indoor air velocity, while the minimum air velocity occurs in the test scenario with S-E60°. The mean indoor air velocity difference between these two test scenarios is roughly 1.11 m/s.

According to the Chinese construction industry code of *Assessment Standard for Green Building* (GB/T 50378-2014), the evaluation parameters used for assessing indoor wind environments are the air velocity and the air pressure. When the indoor air velocity is lower than 1.00 m/s, it results in poor ventilation for the internal spaces. In contrast, if the indoor air velocity is higher than 5.00 m/s, it causes discomfort for humans. Hence, the optimum indoor air velocity ranges from 1.00 m/s to 5.00 m/s. Excluding the test scenarios with S, S-E20, S-E40 and S-E60,

the mean indoor air velocities for the other 14 BAs are all less than 1.00 m/s, which means they need to rely on the electrical ventilation systems to improve indoor thermal comfort in summer.

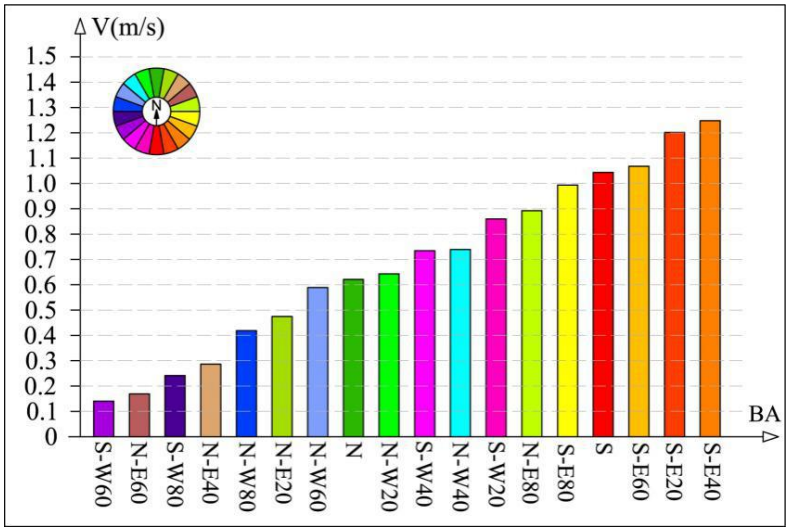

Fig. 5.7 Mean indoor air velocities in the 18 test scenarios with various building azimuth

5.3.2.2 Impact of BA on the energy consumption of electrical ventilation

For the mean indoor air velocity lower than 1.00 m/s in a test scenario, the schedule of electrical ventilation in operation during weekdays was assumed as to be of 11 hours, beginning at 18:00 p.m. and ending at 5:00 a.m. of the next day in the simulation, accounting for 45.83% of the whole day. For the weekends, it was set at 15 hours daily, from 14:00 p.m. to 5:00 a.m. of the next day. The situation of the cross ventilation being obstructed in the case of doors being closed after bedtime at night was also taken into consideration. Thus, the electrical ventilation was assumed to be working for 7 hours, from 22:00 p.m. to 5:00 a.m. of the next day in the test scenarios with S, S-E20, S-E40 and S-E60. Furthermore, although the mean air velocities in the test scenarios with these four BAs are above 1.00 m/s, the natural ventilation is characterized by intermittence and instability. Thus, the time of electrical ventilation system in operation for these four BAs, except for the bedtime period, was modified as half of that for the other orientations, which are 2 hours on weekdays and 4 hours on weekends, respectively.

Besides, the electrical ventilator is also assumed to be operating for the adjusting of the indoor thermal environments during weekdays for 4 hours, from 18:00 p.m. to 22:00 p.m. in the test scenarios with mean air velocity below 1.00 m/s during June, July and August. Furthermore, regarding those scenarios above 1.00 m/s, the time of electrical ventilator being in operation is set at 2 hours. Related to spatial division conditions in the Sizhai traditional dwellings, each suite is equipped with two electrical ventilators (i.e., fans with power of 35 W) in the bedroom and the living room, respectively.

The parameter settings in the simulation were optimized as follows: the probability of each fan being in operation was set as 75%, and the probability of the 5 suites being all under the mechanically ventilated conditions at the same time was set as 80%. The electricity consumption corresponding to different BAs is summarized in Fig. 5.8, of which the total annual electricity consumption of electrical ventilation for S, S-E20, S-E40 and S-E60 is all 82.05 kW·h and the others are all 130 kW·h.

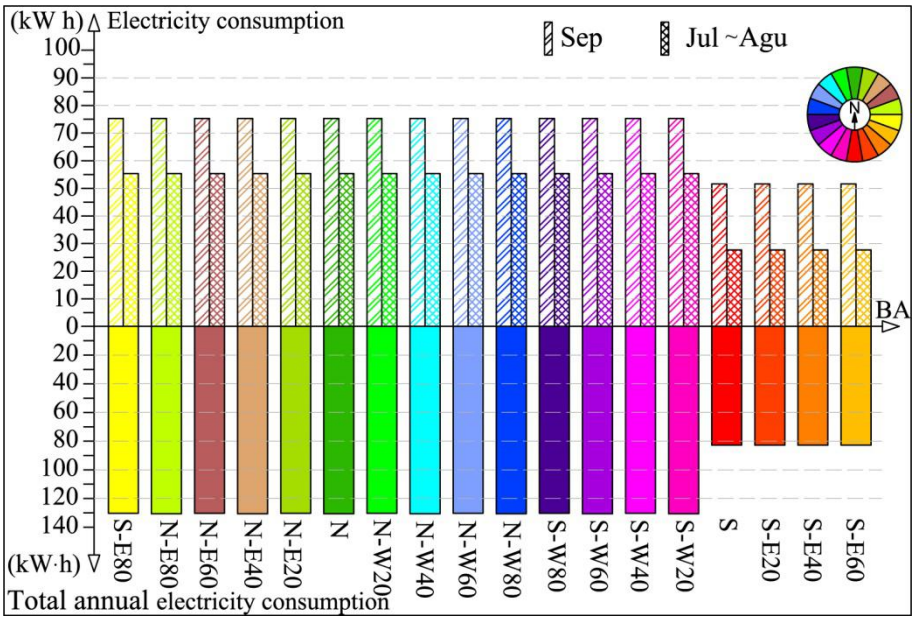

Fig. 5.8 Electricity consumption of electrical ventilation in the 18 test scenarios

5.3.3 Indoor daylighting and electricity consumption of artificial lighting with varying building azimuth

5.3.3.1 Daylighting in the internal space with varying building azimuth

The tool of VELUX Daylight Visualizer 2 was employed to simulate the indoor illuminance for the 18 test scenarios. Time spans of daytime and nighttime on the spring equinox are the same and the intensity of solar radiation is very close to the average value of the whole year. Regarding the set points in simulation, 21st March (i.e., the spring equinox) with sunny weather conditions was selected, and the computational result in each of the test scenarios was assumed to be 0.9 m above the floor level. In addition, the reflectance of walls, ground and ceiling was set at 0.75, 0.60 and 0.65, respectively. By altering the set point of the orientation value, the BA can be varied correspondingly without the need of rotation for the original model. Furthermore, by changing the time setting, the illuminance for internal spaces can be simulated and computed at any time-point.

As shown in Fig. 5.9, both the mean indoor illuminance at 1 hour time-step in the test scenarios with S and N presents symmetric distribution at 12 o'clock sharp. Besides, the mean indoor illuminance in the other test scenarios are roughly symmetric symmetrical with respect to the south-north orientation (e.g., the indoor mean illuminance for

S-W20 and SE-20, for S-W40 and SE-40, etc. is symmetrical with respect to the south-north orientation). In comparison with the north facing test scenarios, the illuminance magnitude in the south facing test scenarios is higher.

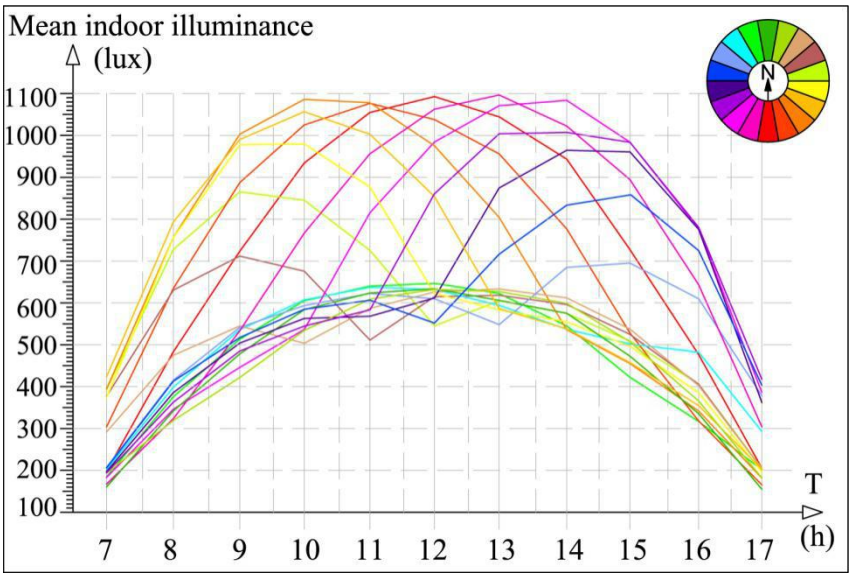

Fig. 5.9 Mean indoor illuminance at 1 hour time-step for in the 18 test scenarios

5.3.3.2 Impact of BA on the energy consumption of artificial lighting

The *Chinese Standard for Daylighting Design of Buildings* (GB 50033-2013) stipulates that the daylight factor in bedrooms, living rooms and kitchens should be greater than 2%, and the illuminance in these rooms should be above 300 lux. Ecotect 2012 software was applied to simulate the arrangement condition and the least quantity of lighting fixtures, as they satisfy the requirement of indoor illuminance being above 300 lux. As shown in Fig. 5.10, the minimal quantity of fluorescent lamps in each suite is three, with 0.04 kW.

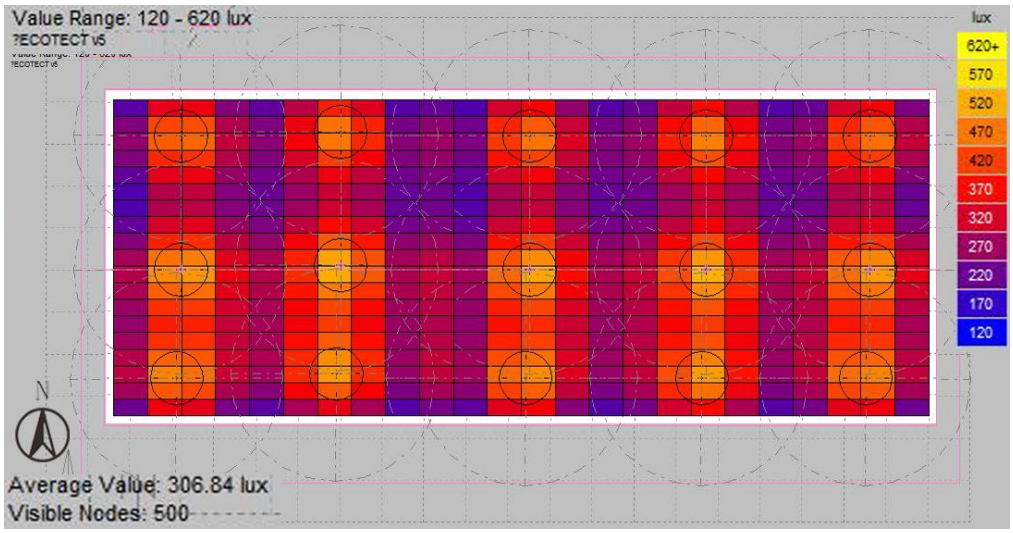

Fig. 5.10 Arrangement condition and quantity requirement of lighting fixtures over 300 lux

ArchiWIZARD 3.1.1 with the plug-in of EnergyPlus was used to compute the electricity consumption of artificial lighting for each of the test scenarios in this section. Through the questionnaire survey, we found that the wake-up time and bedtime for occupants are generally at 6:30 a.m. and 22:30 p.m., respectively. When the illuminance in each of the test scenario is lower than 300 lux, the lighting system is turned on to compensate the daylight illuminance to reach the desired value (i.e., 300 lux) on the work plane (0.9 m above floor). While in fact, not all lamps are in operation during nighttime generally, but according to occupancy conditions and lighting demand, a different quantity of lamps are switched on. Therefore, the parameter settings for the energy cost of artificial lighting in simulation also need to be optimized. The probability of all five suites being under the artificially lit conditions at the same time was set as 80%, and the average quantity of lamps in operation was set at 1.5 for each suite of the test scenario in this section.

As shown in Fig. 5.11, the time of artificial lighting being in operation is inversely proportional to the duration of visual comfort (i.e., ≥300 lux). The time of artificial lighting in operation for the test scenarios facing north are generally greater than of those facing south, of which the scenario with S-W40 requires the minimum artificial lighting time. In contrast, the artificial lighting time is directly proportional to its electricity consumption. The total annual electricity consumption of artificial lighting for south is generally lower than that for north, with a total electricity use difference of 14 kW·h throughout a year between S-W40 and N-E40 (Fig. 5.12).

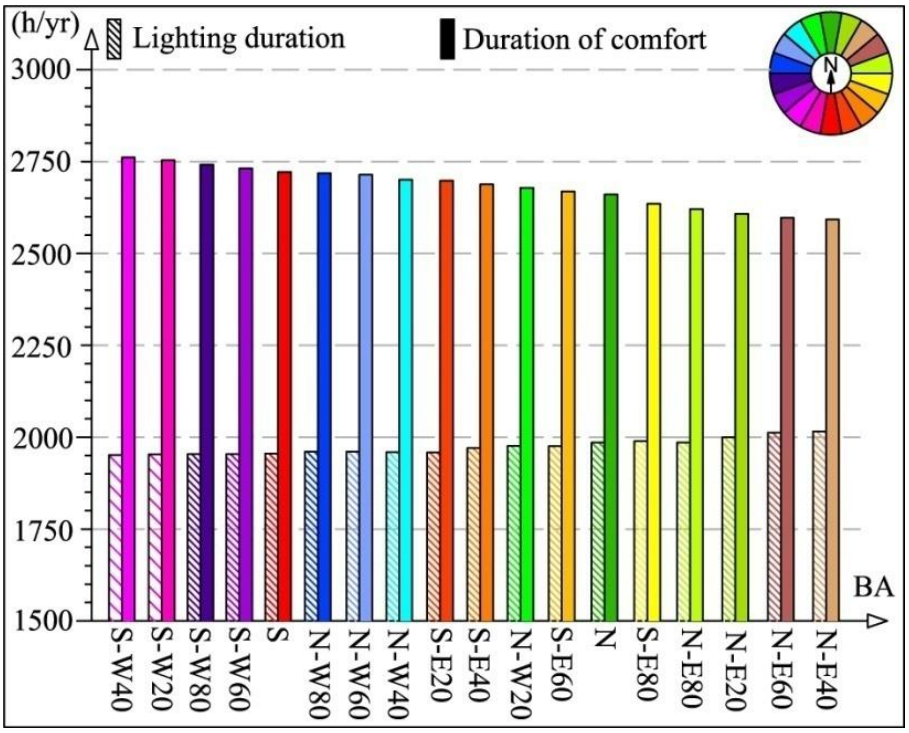

Fig. 5.11 Time of artificial lighting in operation and duration of visual comfort in the 18 test scenarios over a year

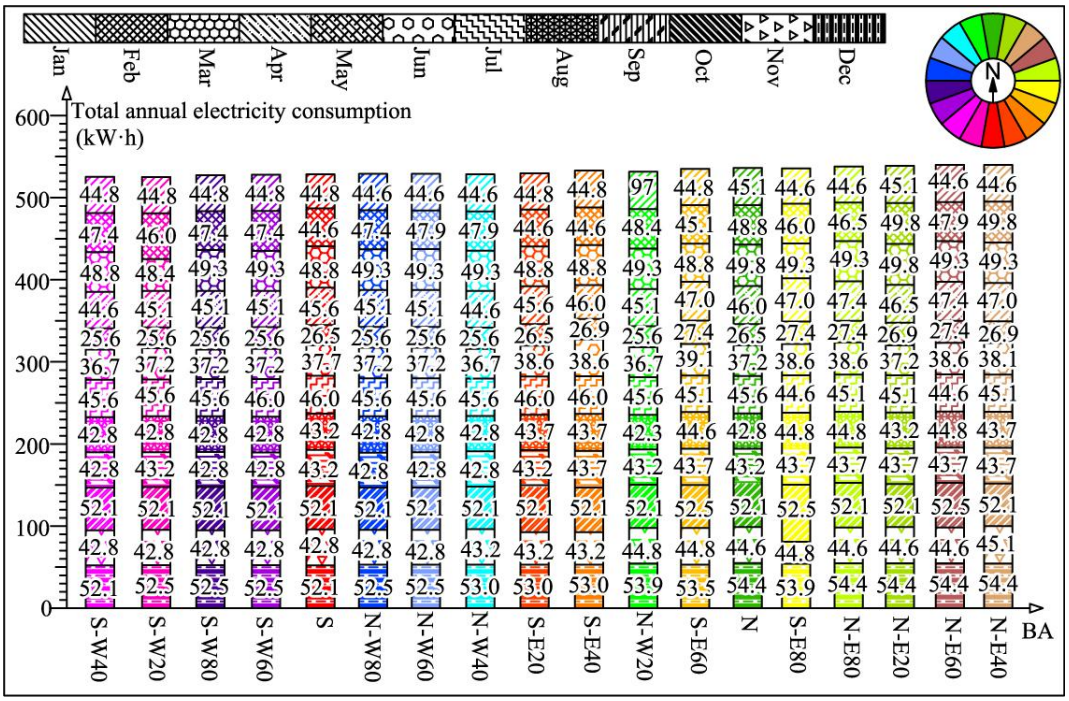

Fig. 5.12 Total annual electricity consumption of artificial lighting in the 18 test scenarios

5.4 Total annual electricity consumption and CO_2 emission

The total annual electricity consumption (the overall energy consumed by AC, electrical ventilation and artificial lighting per year) in the 18 test scenarios at a series of BAs are shown in Fig. 5.13.

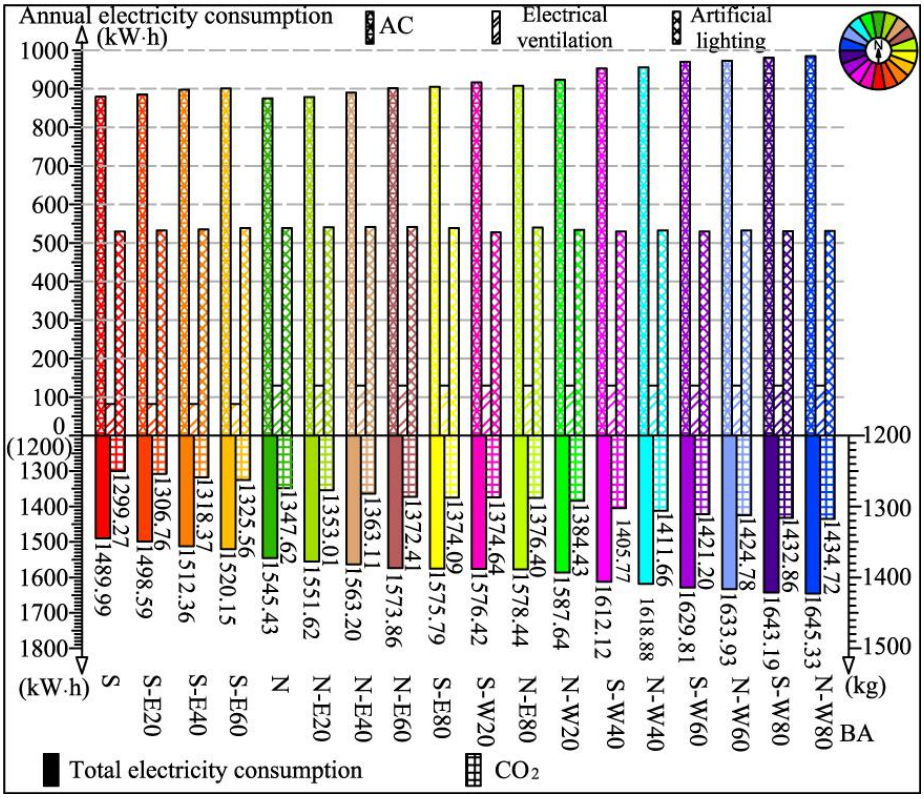

Fig. 5.13 Electricity consumption and CO_2 emissions in the 18 test scenarios

The total annual electricity consumption in the southerly orientated buildings is generally lower than those in northerly orientated buildings, of which the test scenario with S requires the minimal amount of energy (1489.99 kW·h). In contrast, the maximum energy consumption with 1645.33 kW·h occurs in the scenario with N-W80, which is about 1.1 times higher than that with S. Using the standard coal conversion coefficient, the consumption of 1 kW of electrical power requires to burn 0.404 kg of standard coal, which results in CO_2 emissions of 0.872 kg [39-40]. The CO_2 emissions corresponding to the 18 test scenarios are calculated in Fig. 5.13 as well, and range from a low of 1299.27 kg to a high of 1434.72 kg, with a total difference of 135.45 kg.

5.5 Validation of computational results: simulation tool versus real bills

Ryan etc. [41] suggested that computational results generated by building energy simulation software need to be validated by comparing with real energy consumed in actual building. Real energy bills are empirical, which are often called as “true data” and regarded as an extremely powerful validation proof, because they could be used to prove the accuracy of computational results [42].

Fig. 5.14 Positions of four reference buildings in Sizhai village

Fig. 5.15 Two reference suites orientated towards S in NO. 1 dwelling subdomain

Fig. 5.16 Two reference suites orientated towards N in NO. 4 dwelling subdomain

Based on the previous discussions, the total annual electricity consumed by AC, electrical ventilation and artificial lighting, which is generated by the energy simulation in software, is compared to that from the real electricity consumption bills to verify the computational accuracy in this chapter. Because of the building model with five suites was chosen in the simulation, the mean electricity consumption for each suite was calculated as one fifth of the total annual electricity use. There are two selection criteria for the real bills from reference suites: (1) the reference suite should be equipped with AC, fans and lamps, so that the energy consumption of AC, electrical ventilation and artificial lighting can be obtained from the bills; (2) the building area of the reference suite should be around 30 m^2 for fair comparison with the suite in the test scenario. Complying with these two conditions, the existing energy bills from four real suites (Fig. 5.14-5.16) are selected as the "true data", of which two are orientated towards S and the other two are orientated towards N. The details of the four reference suites are listed in Table 5.2. The E_{TAAEC} (total annual actual electricity consumption, kW·h) including AC, electrical ventilation and artificial lighting can be formulated as Equation (5.1).

$$E_{TAAEC} = E_T - E_O \qquad (5.1)$$

Where, E_T is the total annual actual electricity consumption including the all domestic electrical appliances, kW·h; E_O is the total annual actual electricity consumption of the all domestic electrical appliances except for AC, electrical ventilation and artificial lighting, kW·h. In accordance with the time in operation and quantity of domestic electrical appliances, the E_O can be calculated and listed in Table 5.2.

Table 5.2 List of domestic electrical appliances and details of the four reference suites

Domestic electrical appliance		EC	EK	Computer	Television	Refrigerator	Calorifier
Power (w)		500	800	200	100	100	1500
Operation period		Whole year	Whole year	Whole year	Whole year	Whole year	NANY
Use frequency per day during workday		1	1	1	1	1	1
Use frequency per day during weekend		2	3	3	3	1	1
Operation duration for each time (h)		0.33	0.17	2	2	24	1
Electricity cost per month (kW·h)		6.27	4.08	12	6	12	45
Annual electricity cost (kW·h)		75.24	48.96	144	72	144	270
Suite 1-S ($29.87\ m^2$)	Appliance	●	●	●	●	●	●
	E_O (kW·h)	754.2					
Suite 2-S ($29.87\ m^2$)	Appliance	●	●		●	●	●
	E_O (kW·h)	610.2					
Suite 1-N ($32.01\ m^2$)	Appliance	●	●	●	●	●	●
	E_O (kW·h)	754.2					
Suite 2-N ($32.01\ m^2$)	Appliance	●	●		●	●	●
	E_O (kW·h)	610.2					

Notes: 1. ● presents the suite equipped with of the given domestic electrical appliance; 2. EC: Electrical Cooker; EK: Electrical Kettle; NANY: from November to April of next year.

Table 5.3 Total actual annual electricity consumption of 2014 and 2015 in the four reference suites

Designation	E_T of 2014 (kW·h)	E_T of 2015 (kW·h)	E_{TAAEC} of 2014 (kW·h)	E_{TAAEC} of 2015 (kW·h)
S-House 1	1045.24	1028.76	277.04	259.56
S-House 2	909.72	906.61	289.52	283.41
N-House 1	1056.12	1045.45	294.92	279.25
N-House 2	910.04	892.69	275.84	269.49

The E_{TS} in the four reference suites throughout 2014 and 2015 are obtained from the monthly electricity consumption bills stored by homeowners. Using equation (5.1), the E_{TAAECS} are calculated and listed in Table 5.3. In 2014, the mean air temperature of January was 6.5℃, and that of three summer months, including June, July and August, was 28.7 ℃. With regard to 2015, the corresponding mean air temperatures were 6 ℃ and 28.3 ℃, respectively. Because the mean temperature in summer of 2014 was higher than 2015, the electricity consumption of 2014 was also higher than that of 2015 in the four reference suites.

The total annual electricity consumption in a suite with S and N from software is 294.95 and 309.09 kW·h, respectively. By conducting a comparison between the electricity consumption obtained from real bills and software, the average bias error of the four group data is 0.08, and the details are presented in Fig. 5.17.

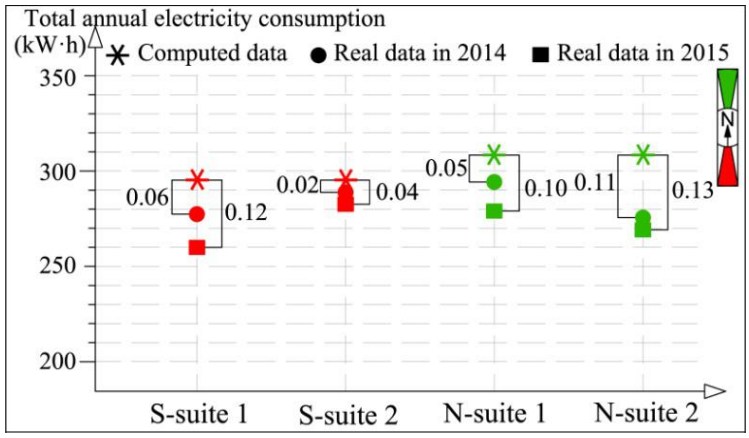

Fig. 5.17 Comparison of the total annual electricity consumed by air conditioning, fans and lamps from real bills and simulation

According to the criteria indicated by Reeves et al. [43] and Maamari et al. [44], the accepted percentage of bias error between real data and computational results should range in the scope of ±15% for the software simulation results to be considered accurate.

The computed percentage of bias errors for the four group data and their average values are both below 15% (Fig. 5.16), which are clearly within the accepted range. Hence, the computational results are of a comparatively high reliability, which can be regarded as a criterion for assessing energy saving potential of dwellings with different BAs.

The possible sources of bias error which can impact the computational results are important to highlight: (1) The BA is difficult to precisely measured for real dwelling, therefore the BAs used to conduct simulation test in software can not precisely represent the actual BAs for dwellings. (2) A substantial quantity of assumptions were made in software computation. The U-values of fabrics and materials used in the actual building may be not consistent with the assumed value adopted in the software. (3) Software simulation estimates the amount of energy consumption based on a fixed schedule, but the real conditions of occupancy times may differ from day to day throughout a year. (4) The accuracy of computational results may be correlated to human behavior. As stated by Ryan and Sanquist [40], the occupant behaviors are the common source leading to bias errors in the energy simulations, since they are highly variable resulting in being almost impossible to model them accurately. Besides, the life-style and behavior of each occupant is different, but the set points in the simulation are the same for each of the test scenario, which may also cause bias errors. (5) Weather data is another factor that influences the accuracy of computational results. The meteorological data used in simulation are collected from the whole Shaoxing city, but the case study in the mountainous area is easily impacted by a micro-climatic environment, which may causes bias errors for the computational results. (6) Some simplifications in the geometric model may be another source of bias error for the computational results, such as the dwellings in Sizhai are surrounded by mountains and vegetation in fact, which influences the intensity of solar radiation covering the walls.

5.6 Frequency distribution characteristics of BAs in Sizhai

5.6.1 Type classification of dwelling subdomain

In order to reveal the frequency distribution characteristics for all BAs in Sizhai village, the methodology of frequency statistics [45] are adopted in this chapter. Based on observation and measurement results, the dwelling subdomains in Sizhai village are classified into three categories, that is, the main uni-directional subdomain, the main bi-directional subdomain and the multi-directional subdomain.

5.6.1.1 Definition of the main uni-directional subdomain type

The BA measurement for all dwellings located in the 10 subdomains was performed to analyze their BA frequency distribution characteristics. If the summation of frequency values for two BA intervals that are vertically opposite angles (i.e., $P_n + P_{n+9}$, $n \leq 9$, P and n represent the frequency value for a certain BA interval and number of a certain BA interval, respectively), namely the sum of percentage for two BA intervals of [a, a+20°] and [a+180°, a+200°] (a is the initial value of each BA interval, $a \in [10°, 30°...350°]$), is equivalent to or greater than 70%, or the frequency value for one BA interval is equivalent to or greater than 50%, a dwelling subdomain with the

characteristic of BA frequency distribution matching with anyone of the above two conditions is classified as the main uni-directional subdomain.

5.6.1.2 Definition of the main bi-directional subdomain type

Concerning the BA frequency distribution in a certain dwelling subdomain, if its summation of frequency values for four BA intervals, of which two and two are both vertically opposite angles (i.e., $P_m+ P_{m+9}+P_n+ P_{n+9}$, $m\leq9$, $n\leq9$, $m\neq n$, m is the number of a certain BA interval), is equivalent to or greater than 70%, and the frequency values for these two pairs of vertically opposite angles satisfies the condition of $1/2\leq(P_m+ P_{m+9})/(P_n+ P_{n+9})\leq2$, this dwelling subdomain is classified as the main bi-directional subdomain.

5.6.1.3 Definition of the multi-directional subdomain type

Except for the previous two cases, if the BA frequency distribution of a dwelling subdomain is presents other patterns, this dwelling subdomain is classified as the multi-directional subdomain. Obviously, the frequency distribution in the multi-directional subdomain is without distinct peak value for any BA interval. This is because the building orientations in the multi-directional subdomain show scattered distribution, which are usually due to the building site shape in the irregular mountain terrain.

5.6.2 Factors of impacting three dwelling subdomain types

5.6.2.1 Factors of impacting main uni-directional subdomain

Resorting to the remote sensing image with high definition provided by G.E. to observe the BA distribution features of dwellings in the main uni-directional subdomain, we found that the BAs are principally determined by roads and streams. On the whole, dwellings in the area being adjacent to roads and streams are orientated along them, resulting in their ridges generally paralleling with the borders of the road or stream (Fig. 5.18). For instance, the BAs within NO. 6 dwelling subdomain generally range in [190°, 210°], which are close to the road direction of 198°. Moreover, the solar radiation is another driving factor that leads to most of the dwellings facing southward to improve the natural daylighting efficiency.

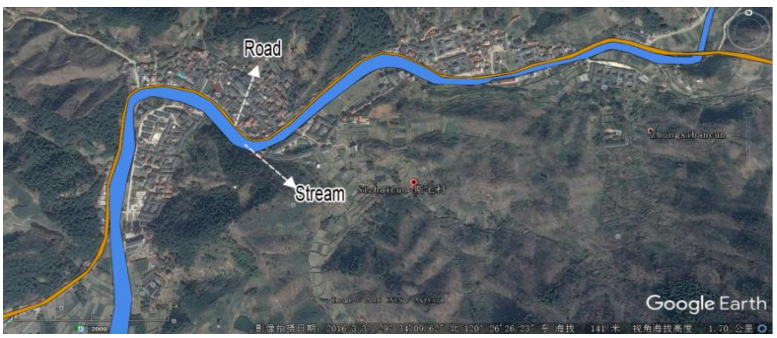

Fig. 5.18 Distribution of road and stream in the Sizhai traditional village

5.6.2.2 Factors of impacting main bi-directional subdomain

There are principally two dwelling typologies in Sizhai village, which are the detached dwelling and the courtyard dwelling. The special configuration of courtyard dwelling, which is featured by four buildings as a group centered around a patio, leads to its individual buildings presenting perpendicular correlation. Therefore, exclusion of roads, streams and solar radiation, the configuration characteristic of courtyard dwelling is another significant factor, which results in its BAs presenting a main bi-direction distribution. For instance, the NO. 10 dwelling subdomain belonging to the type of main bi-directional subdomain is attributed to it just containing a huge courtyard dwelling.

5.6.2.3 Factors of impacting multi-directional subdomain

In the BAs within the multi-directional subdomain it is difficult to spot their main orientation. Through the remote sensing image, we found that the dwelling distribution in the multi-directional subdomain is incompact, resulting from the lack of uniform planning. The BA determinations for dwellings are usually restricted by the conditions of their building sites, rather than affected by roads, streams and solar radiation. However, the south facing buildings account for relatively large percentage, in general.

5.6.3 Building azimuth frequency distribution and assessment of energy saving potential for Sizhai village

By using the orientation measurement functionality of G.E., the quantity statistics and frequency distribution analysis for all BAs scattered in the 10 dwelling subdomains were conducted. As shown in Table 5.4, among the 10 subdomains, the quantity and frequency for BAs within S interval, which has the highest energy saving potential, in NO. 5 and NO. 1 dwelling subdomain are the largest, which are 10 and 33%, respectively. On the contrary, in NO. 7 dwelling subdomain, those within the worst BA interval of N-W80 are both the largest, 8 and 17% respectively.

From the viewpoint of statistics at a village-scale, all the BAs in Sizhai present a multi-directional distribution, as shown in Fig. 5.19. The frequencies for the BA intervals of [190°, 210°], [310°, 330°], [330°, 350°] , [10°, 30°] and [30°, 50°] account for comparatively high proportion of them, 11%, 15%, 14% , 10% and 12% respectively.

The quantity and frequency for BAs within the three BA intervals of S, S-E20 and S-E40, with the highest energy saving potential, are 17 and 4%, 59 and 14%, 66 and 15%, respectively. Those for the worst three BA intervals of S-W80, N-W80 and N-W60 are only 3 and 1%, 17 and 4%, 7 and 2%, respectively.

Based on the evaluation parameter of BA statistics, the sunmation of frequency for three kinds of BAs with the highest energy saving potentials is 33% in Sizhai village, while that of frequency for three kinds of BAs with the lowest energy saving potentials is 7%. Thus, Sizhai village is estimated to be in possession of a high level of energy saving potential in general.

Table 5.4 Quantity statistics and frequency distribution of all building azimuths scattered in the 10 dwelling subdomains

Designation	NO. 1 dwelling subdomain	NO. 2 dwelling subdomain
Legend		
Frequency	Quantity and frequency distribution of dwellings	Quantity and frequency distribution of dwellings
Diagram	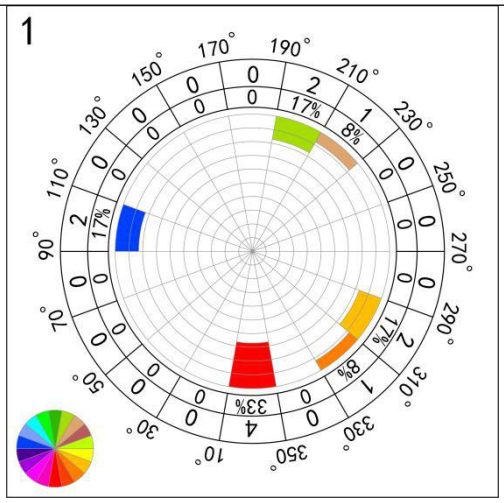	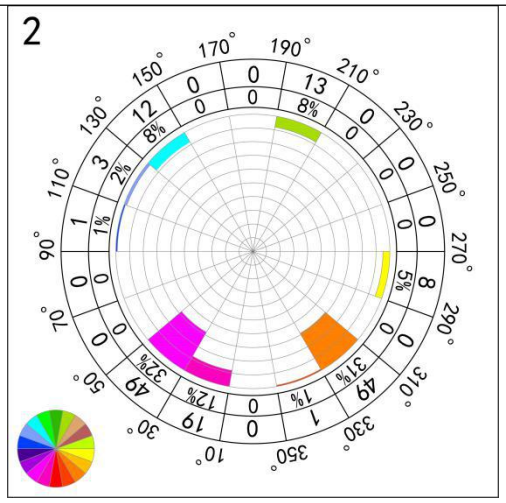
Type	Multi-directional subdomain	Multi-directional subdomain
Designation	NO. 3 dwelling subdomain	NO. 4 dwelling subdomain
Legend		
Frequency	Quantity and frequency distribution of dwellings	Quantity and frequency distribution of dwellings
Diagram	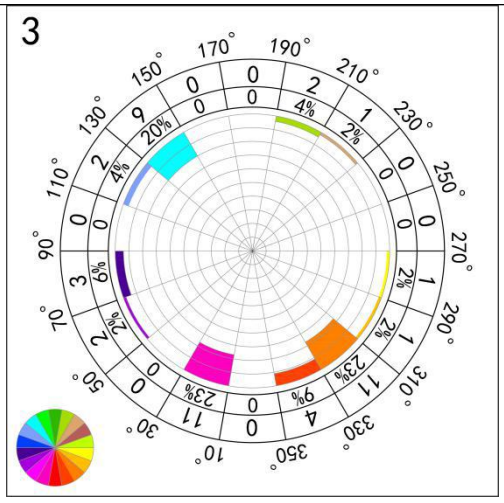	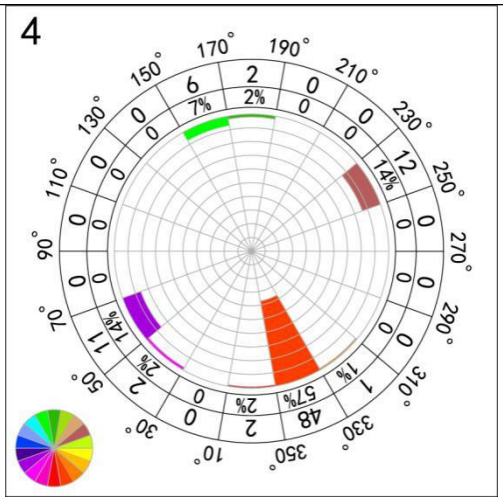
Type	Main bi-directional subdomain	Main uni-directional subdomain

Designation	NO. 5 dwelling subdomain	NO. 6 dwelling subdomain
Legend		
Frequency	Quantity and frequency distribution of dwellings	Quantity and frequency distribution of dwellings
Diagram	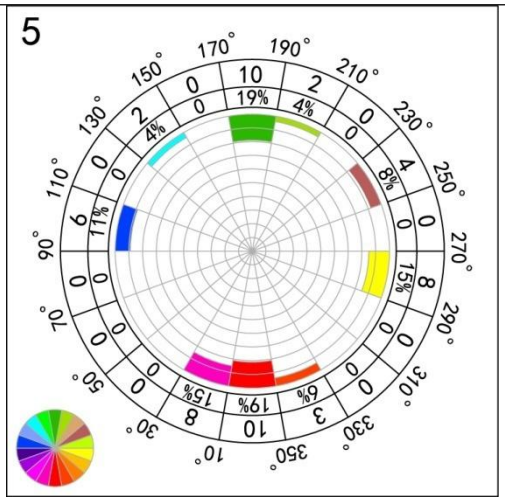	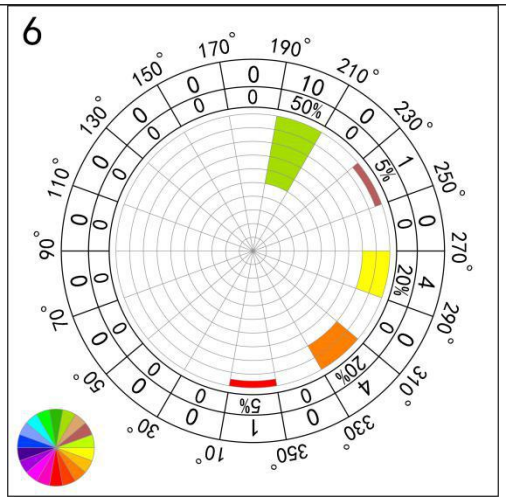
Type	Multi-directional subdomain	Main uni-directional subdomain
Designation	NO. 7 dwelling subdomain	NO. 8 dwelling subdomain
Legend	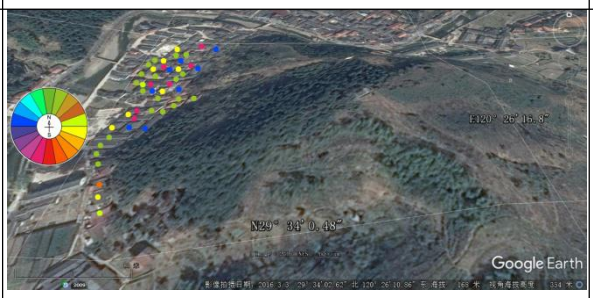	
Frequency	Quantity and frequency distribution of dwellings	Quantity and frequency distribution of dwellings
Diagram	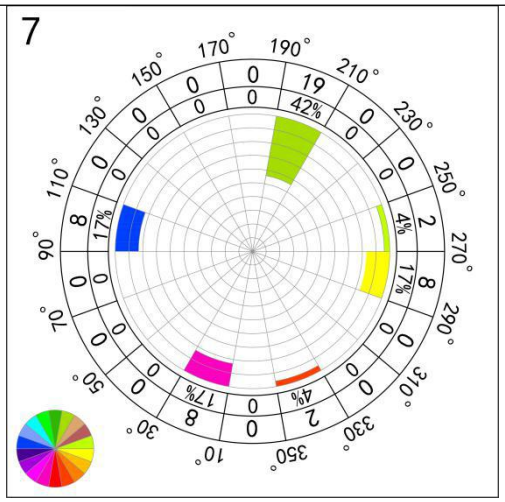	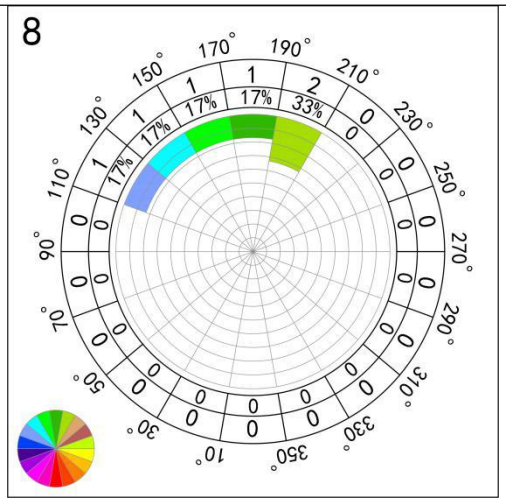
Type	Main uni-directional subdomain	Multi-directional subdomain
Designation	NO. 9 dwelling subdomain	NO. 10 dwelling subdomain

Legend		
Frequency	Quantity and frequency distribution of dwellings	Quantity and frequency distribution of dwellings
Diagram	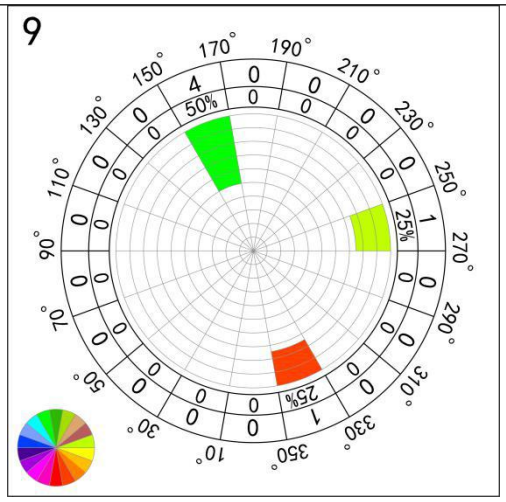	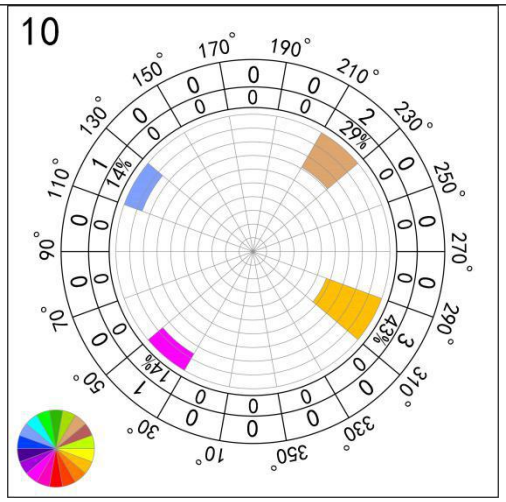
Type	Main uni-directional subdomain	Main bi-directional subdomain

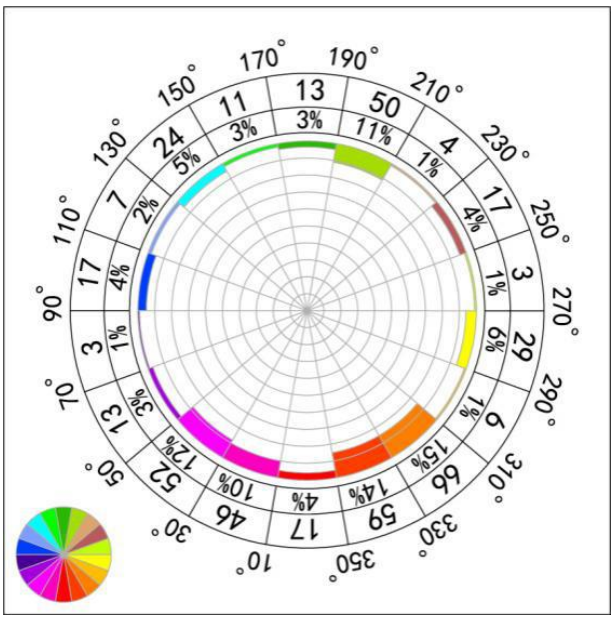

Fig. 5.19 Quantity and frequency distribution of building azimuths for all dwellings at village-scale

5.7 Finding and discussion

Taking the front facade equipped with glazing as reference, the BAs of dwellings are measured in G.E.. The building model was rotated at 20° increments clockwise to create a total of 18 test scenarios in this work. By using

software simulations, the thermal and daylighting performances in 18 test scenarios were created to assess their indoor comfort levels, based on the three evaluation parameters of indoor temperature, air velocity and illuminance. Furthermore, the electricity consumption of AC, electrical ventilation and artificial lighting, as well as the total annual electricity consumption were computed by software to explore the optimal BAs for dwellings corresponding to various BAs in the summer hot and winter cold climate zone of China. The finding of this research is summarized as follows.

(1) The test scenario with N requires the minimum total electricity consumption of AC. In general, the total electricity consumption of AC in the test scenarios orientated west is greater than those of the east, of which with the maximum electricity consumption (979.87 kW·h) was assumed to be the test scenario with N-W80.

(2) The total annual electricity consumption of electrical ventilation systems for the test scenarios with S, S-E20, S-E40 and S-E60 is all 82.05 kW·h, and that with the other 14 BAs is all 130 kW·h.

(3) The total annual electricity consumption of artificial lighting for south is generally lower than for north, where a total electricity use difference of 14 kW·h throughout a year between S-W40 (the best BA) and N-E40 (the worst BA) of the test scenario is achieved.

(4) The test scenario requiring the minimal amount of energy is orientated towards S, which is 1489.99 kW·h. In contrast, the maximum energy demand, with 1645.33 kW·h, occurs in the alternative with N-W80, which is about 1.1 times greater than that orientated towards S.

(5) By performing the quantity statistics and frequency distribution analysis for the all BAs at a village-scale, in Sizhai village, the quantities and frequencies for BAs within the best three BA intervals of S, S-E20 and S-E40 are 17 and 4%, 59 and 14%, 66 and 15%, respectively. Those within the worst three BA intervals of S-W80, N-W80 and N-W60 are merely 3 and 1%, 17 and 4%, 7 and 2%, respectively. From the viewpoint of BA, Sizhai village has a high level of energy saving potential in general.

References

[1] R. Pacheco, J. Ordóñez, G. Martínez. Energy efficient design of building: a review [J]. *Renewable and Sustainable Energy Reviews*, 2012, 16 (6): 3559-3573.

[2] Zhao L L. The current situation analysis of building energy consumption in China [J]. *Housing and Real Estate*, 2016, 30(10): 25.

[3] Wang X, Ren H, Cai W W, et al. The change trend and impact factors of time series of energy consumption in China [J]. *Journal Heating Ventilating and Air conditioning*, 2017, 47(11): 21-26, 93.

[4] Building Energy Conservation Research Center of Tsinghua University. The annual development report of China building energy conservation [R]. Beijing: China building industry press, 2012.

[5] Lu J F. The development inevitable trend of China's low carbon building and its future prospects [J]. *Productivity Research*, 2013(12): 72-74.

[6] Bynum P, Issa R, Olbina S. Building information modelling in support of sustainable design and construction [J]. *Journal of Construction Engineering and Management*, 2013, 139(1): 24-34.

[7] Caldera M, Corgnati SP, Filippi M. Energy demand for space heating through a statistical approach: application to residential buildings [J]. *Energy and Buildings*, 2008, 40(10):1972-1983.

[8] Tiberiu C, Virgone J, Blanco E. Development and validation of regression models to predict monthly heating demand for residential buildings [J]. *Energy and Buildings*, 2008, 40(10): 1825-32.

[9] Windows and Building Envelope Research and Development A Road map for Emerging Technologies, United States. Dept. of Energy. Office of Energy Efficiency and Renewable Energy, Washington, D.C., 2014.

[10] R.M.J. Bokel. The effect of window position and window size on the energy demand for heating, cooling and electric lighting, Proceedings [J]. *Building Simulation*, 2007(10): 117-121.

[11] A.M. Koohsari, R. Fayaz, B.M. Kari, The Influence of Window Dimensions and Location on Residential Building Energy Consumption by Integrating Thermal and Lighting Analysis in a Mild and Humid Climate, BRIS Journal Of Advances in Science and Technology 3, 2015: 187-194.

[12] N.A.M. Al-Tamimi, S.F.S. Fadzil, W.M.W. Harun, The Effects of Orientation, Ventilation, and Varied WWR on the Thermal Performance of Residential Rooms in the Tropics, JSD Journal Of Sustainable Development 4, 2011.

[13] AlAnzi A, Seo D, Krarti M. Impact of building shape on thermal performance of office building in Kuwait [J]. *Energy Convers Manag*, 2009, 50(3): 822-828.

[14] Catalina T, Virgone J, Lordache V. Study on the impact of building form on the energy consumption. In: Proceedings of Building Simulation 2011: 12th Conference of International Performance Simulation Association, Sydney, 14-16, November. Romania: Technical University of Civil Engineering Bucharest, 2011.

[15] Faizi F, Noorani M, Ghaedi A, Mahdavinejad M. Design an optimum pattern of orientation in residential complexes by analyzing the level of energy consumption (case study: Maskan Mehr Complexes, Tehran, Iran) [J]. *Procedia Engineering*, 2011, 21(12): 1179-87.

[16] Fallahtafti R, Mahdavinejad M. Optimization of building shape and orientation for better energy efficient architecture [J]. *International Journal of Energy Sector Management*, 2015, 9(4): 593-618.

[17] Mardookhy M, Sawhney R, Ji S, Zhu X, Zhou W. A study of energy efficiency in residential buildings in Knoxville, Tennessee [J]. *Journal of Cleaner Production*, 2014, 85(12): 241-9.

[18] S. Attia, E. Gratia, A. De Herde, et al. Simulation-based decision support tool for early stages of zero-energy building design [J]. *Energy and Buildings*. 2012, 49(2): 2-15.

[19] Leth-Petersen S, Togeby M. Demand for space heating in apartment blocks: measuring effect of policy measures aiming at reducing energy consumption [J]. *Energy Economics*, 2001, 23(4): 387-403.

[20] Morrissey J, Moore T, Horne RE. Affordable passive solar design in a temperate climate: an experiment in residential building orientation [J]. *Renewable Energy*, 2011, 36(2): 568-577.

[21] J. Straube, BSD-200. Low-energy commercial and institutional buildings: Top ten smart things to do for cold climates, Building Science Corporation (BSC), 2014

[22] Correia-Guedes sustainable architecture in Africa, in: A. Sayigh (Ed.), Sustainability, Energy and Architecture: Case Studies in Realizing Green Buildings, Elsevier Inc, Oxford, 2014, pp. 432-444.

[23] DianaÜrge-Vorsatz, Luisa F.Cabeza, SusanaSerrano. Heating and cooling energy trends and drivers in buildings [J]. *Renewable and Sustainable Energy Reviews*, 2015, 41(1): 85-98

[24] F.H. Abanda, L. Byers. An investigation of the impact of building orientation on energy consumption in a domestic building using emerging BIM (Building Information Modelling) [J], *Energy*. 2016, 97(2): 517-527.

[25] Wang KD, Fan Q. Building information modelling (BIM) for sustainable building design [J]. *Facilities*, 2013, 31(3/4): 138-57.

[26] Daniele Torreggiani, Alberto Barbaresi, Francesca Dallacasa, et al. Effects of different architectural solutions on the thermal behaviour in an unconditioned rural building. The case of an Italian winery [J]. *Journal of Agricultural Engineering*, 2018, 49 (1): 52-63.

[27] A. Al-Anzi, O. Khattab, Solar conscious house design in Kuwait [J]. *Kuwait Journal of Science & Engineering*, 2010, 37(2): 59-72.

[28] K.M. Odunfa, T.O. Ojo, V.O. Odunfa, O.S. Ohunakin. Energy efficiency in building: case of buildings at the University of Ibadan [J]. *Journal of Building Construction and Planning Researc*h, 2015 (3): 18-26.

[29] O. Koranteng, E.G. Abaitey. Simulation based analysis on the effects of orientation on energy performance of residential buildings in Ghana [J]. *Journal of Science and Technology (Ghana)*, 2009, 29 (3): 86-101.

[30] A.L.S. Chan, Effect of adjacent shading on the thermal performance of residential buildings in a subtropical region [J]. *Applied Energy*, 2012, 92 (4): 516-522.

[31] Aksoy U, Inalli M. Impacts of some building passive design parameters on heating demand for a cold region [J]. *Building and Environment*, 2006, 12(41): 1742-54.

[32] Ignacio Acosta, Miguel Ángel Campano, Juan Francisco Molina. Window design in architecture: Analysis of energy savings for lighting and visual comfort in residential spaces [J], *Applied Energy*. 2016, 168(2): 493-506.

[33] Ana Brandãode Vasconcelos, António Cabaço , Manuel Duarte Pinheiro, et al. The impact of building orientation and discount rates on a Portuguese reference building refurbishment decision [J], *Energy policy*. 2016, 91(1): 329-340.

[34] Daniel Martin Marin. The impact on building orientation on energy use [D].Gavle: University of Gavle, 2017: 20-24.

[35] Sonia Longo, Francesco Montana, Eleonora Riva Sanseverino. A review on optimization and cost-optimal methodologies in low-energy buildings design and environmental considerations [J]. *Sustainable Cities and Society*, 2019, 45 (1): 87-104.

[36] Ma X W, Fan Y Y, Hou Y B. Experiment of natural ventilation for residential buildings during summer time in Shenzhen [J]. *Journal Heating Ventilating and Air conditioning*, 2003, 33(5): 115-118.

[37] Guo L M. Calculation and distribution of solar radiation on the wall in Zhejiang Province [J]. *Energy Engineering*, 1984, (4): 27-30.

[38] Li Wenjie. A Thesis Submitted to Chongqing University in Partial Fulfillment of the Requirement for the Degree of Doctor of Engineering [D]. Chongqing: Chongqing University, 2010: 3.

[39] Takebayashi, H., Ishii, E., Moriyama, M., Ai, S., Nakajima, S., et al. Study to examine the potential for solar energy utilization based on the relationship between urban morphology and solar radiation gain on building rooftops and wall surfaces [J]. *Solar Energy*, 2015, 119: 362-369.

[40] Liang Chenga, Shuyi Lid, Hao Xud, et al. Calculating potential of solar energy and CO_2 emissions reduction for city scale buildings based on 3D remote sensing technologies [J]. *Remote Sensing of Environment*, 2018, 209(3): 612-632.

[41]Ryan EM, Sanquist TF. Validation of building energy modeling tools under idealized and realistic conditions [J]. *Energy and Buildings*, 2012, 47(4): 375-82.

[42] Jensen SO. Validation of building energy simulation programs: a methodology [J]. *Energy and Buildings*, 1995, 22: 133-44.

[43] Reeves T, Olbina S, Issa R. Validation of building energy modeling tools: Ecotect™, Green Building Studio™ and IES™. In: Laroque C, Himmelspach J, Pasupathy R, Rose O, Uhrmacher AM, editors. Proceedings of the 2012 Winter Simulation Conference. Berlin: Germany; 2012.

[44] Maamari F, Andersen M, de Boer J, Carroll W, Dumortier D, Greenup P. Experimental validation of simulation methods for bi-directional transmission properties at the daylighting performance level [J]. *Energy and Buildings*, 2006, 38(7): 878-89.

[45] Lu Wen long, Zhang Wei chen, Qi Feng, et al. Statistical analysis of rural house plane dimensions: a case study of Shao xing area [J]. *Building Energy Efficiency*, 2017(6): 109-113.

Chapter 6

Impact of shading devices with various shading depth and building azimuth combinations on the energy consumption

6.1 Introduction

6.1.1 Motivation

The building energy consumption rapidly increases, and now it accounts for approximately 32% of the total final energy cost and 40% of the total primary energy cost in the world [1]. To address this issue, a large quantity of studies have focused on how to create the energy efficient building with high level of thermal and visual comfort, by adopting the passive strategies [2], use of renewable energy [3], suitable building materials [4], smart building automation systems [5] and advanced building information technologies [6], etc.

China is the largest CO_2 emission country in the world currently, of which the building sector accounts for 19%. What's more, the proportion of building energy consumption has reached 27.6% of the total in China, with the trend of continuous growth [7]. Especially, the summation of Chinese rural residences is large, with a total building area of approximately 24 billion m^2, accounting for more than 60% of the national total and it keeps growing at increments of 700~800 million m^2 per year [8]. Furthermore, the energy consumption per unit area in rural residences has also been increasing in the recent years, rising from 3.02 kW·h/ m^2 in 2001 to 13.23 kW·h/m^2 in 2017, which is approximately a 3.4 times increase in a 16 years period [9]. Furthermore, due to yearly air temperatures rising due to the global climate change, the Air Conditioning (AC) usage time is expected to increase as well, due largely to the improvement of the living level. Consequently, there is an inevitable tendency to advocate and to develop the energy efficient buildings [10].

Window is an integral component of the building, which usually brings solar radiation into the buildings as it allows sunlight infiltration. Solar heat can improve the thermal comfort levels for the building's interiors during the cold months, which helps to reduce the heating requirements. In addition, solar radiation is a renewable resource useful for the internal space daylighting, which can cut down the time of artificial lighting in operation to achieve energy saving.

Whereas, an opposite effect occurs in summer, since too much solar energy is transmitted through glazing, this will cause over heat and glare inside. Aiming at creating an indoor environment with thermal and visual comfort for occupants, installing appropriate shading device is an efficient way to avoid the excessive solar heat gain and to improve the thermal and daylighting performances in buildings [11]. For instance, reduction in the solar gain as much as of 80% can be achieved in a building, with glazed areas that are fully shaded by an external shading device system [12]. Thus, as an indispensable component, the shading device is used by the fenestration systems to reduce the building energy consumption, as well as to avoid the uncomfortable glare [13].

6.1.2 Scientific originality

In the research field of residential buildings, there are also numerous studies focused largely on the influence of solar shading on the building energy consumption and daylighting performances conducted by O'Brian et al. [14], Arasteh et al. [15], Mavrogianni et al. [16], J. Karlsson [17], Sullivan et al. [18], S. Firlag et al. [19], Kim et al. [20], Vanhoutteghem [21]. Besides, the shading system also plays an important role in improving the occupants' productivity and health [22]. Due to the shading device having many advantages, it has become a passive strategy commonly applied in both newly-built construction and in retrofit projects. On the other hand, the total energy cost consumed by heating, cooling and lighting systems is responsible for a large proportion of the total in buildings [23]. Thus, the topic of improving the energy saving potential by means of the shading devices has become a major issue for buildings at present, where the internal environment and the energy consumption need to be coupled together to be analyzed in depth [24].

The traditional dwellings in East and Central China place a large emphasis on shading, as a result of the intense solar radiation and high outside air temperatures in summer. The roof eaves and corridor roofs in these buildings are characterized by the large tilt angles and large Shading Depths (SDs), aiming at providing a noticeable shading performance to lower the solar exposures and at covering walls on the second floor and first floor, respectively. Furthermore, since the building orientation determination for the traditional dwelling complies with the rule of "adaptation to building site conditions" in East and Central China, the BAs vary considerably depending on the building site. The present research mainly focuses on the impacts that the shading devices facing a limited quantity of orientations have on the energy consumption and on indoor daylighting performance, while few studies are based on the study of multiple orientations [13, 25]. In addition, many studies related to the influences of shading devices on the building energy consumption are based on changes in shading depth within a relatively small scope [14, 26]. Whereas, the studies about the impact on the energy consumption performance at a series of SDs, from providing full shading to no shading for glazing, are rather scarce. What's more, the related researches, in particular with regards to the impact of shading device on the energy consumption, have often been neglected to get carried out in the traditional buildings [27].

Based upon the afore-mentioned discussion, the originality of this chapter is to estimate the performances of solar energy management devices installed in the traditional dwellings of East and Central China. Rather than focus on the performances of certain evaluation parameters, the shading performance, indoor daylighting and thermal conditions, as well as energy behaviors were analyzed step by step, and the four kinds of evaluation parameters generated by simulation tools were all compared with the in-situ measurement data to verify the computational results accuracy.

After coupling the shading devices based on changes in depths with the angle rotations of Building Azimuths (BA) in the test scenarios, the total energy consumption including artificial lighting and AC is proven to vary under reasonable assumptions in the basis of energy simulation. Then the proposed models of shading devices with various SD-BA combinations can be used to explore the optimum shading depths for various BAs, in consideration of the energy consumption and indoor visual comfort. Also, the proposed SD-BA combinations can be regarded as a new method for determining the best final designs of SDs for the traditional dwellings with different building orientations. Furthermore, an evaluation criterion based on the energy saving potential and visual comfort was proposed. Then it was used to assess the energy saving potentials for three given specific dwellings to prove the applicability of the proposed evaluation criterion for the existing residences. On the other hand, until very recently, big attention, in terms of the shading performance, has been given to the contemporary buildings, rather than the traditional buildings. Thus, the traditional dwellings that were adopted as case studies in this chapter, can supply some new body of knowledge on the shading, to fill in the gap in this field. The research results can be used in any country to explore the optimum SDs for various BAs, by using the corresponding geometric model and local climate data instead of the original ones used in simulation.

6.1.3 Research purpose

In this chapter, a small-scale traditional dwelling was taken as the study building, situated in the Sizhai village, Zhuji city, Zhejiang Province, China. The roof eave and the exterior corridor installed on facade, both belong to the external fixed shading device system. This chapter focuses on the impacts of shading devices with different depths, based on changes in BAs on the indoor daylighting, air temperatures and building energy consumption. The recommended SD for each BA was summarized, in accordance with the daylighting standard issued by the Ministry of Housing and Urban-Rural Development of China, and the energy consumption performance. Since the building energy saving can be achieved by selecting shading device of a proper depth, this study results aim at providing some reference on SD determination to both newly-built constructions and to retrofit projects of the rural residences. Furthermore, an evaluation parameter based on SD was proposed, for the sake of supplying a new approach to estimate the energy saving potential of a building.

6.2 Research process and research flow

Taking into consideration the combination of SD and BA, there are a total of 180 simulation samples in this chapter. The evaluation parameter of Solar Heat Gain Coefficient (SHGC) [28] was employed to assess the shading

performances of configurations for the windows, which is defined as the ratio of solar radiation that enters a building through the window with a shading device to that without a shading device. Furthermore, the SHGC has a negative correlation with the Shading-to-Window Ratio (SWR) [29]. To simulate the SHGC and SWR, the software of ArchiWIZARD [30] (version 3.1.1) and Sketchup were adopted, respectively.

The Sketchup [31] can allow end-users and professionals to virtually learn the shading performance on window, before the real building is constructed on site. The ArchiWIZARD is compliant with the code of CSTB (Central Scientific Technological Building), which could be used as a plug-in installed in the software of Sketchup to perform the energy simulation in the Sketchup interface. Aiming at learning the correlation between the SHGC and SWR, the Sketchup 7 [32] program was used. By changing the set points of time and date in the simulation tool, the shading conditions could be simulated at any time-step throughout the whole year. Using the distance measurement tool in Sketchup 7, the percentage of shade coverage area on the glazing can be calculated, namely the SWR. In this chapter, the evaluation parameter of Mean Shading-to-Window Ratio (MSWR) during daytime was selected to estimate the shading performances for the test scenarios. The validation of computational results from the Sketchup 7 was conducted, by comparing with the calculation data using equations which are originally formulated by authors.

Besides, the two other simulation tools of VELUX Daylight Visualizer 2 and Ecotect 2012 were used in this work. The VELUX Daylight Visualizer 2 [33] is a professional lighting simulation tool for the analysis of daylight conditions in buildings. And Ecotect 2012 [34] is a whole building simulation tool that can used to predict the thermal, acoustic and visual performances of the buildings, where the thermal performance analysis in is based on the Chartered Institution of Building Services Engineers (CIBSE), and is suitable to perform indoor air temperature simulation. Obviously, the solar radiation reception and the solar heat gain influence the visual and thermal environments of the internal spaces [15,35]. Thus, the VELUX Daylight Visualizer 2 and Ecotect 2012 were selected to simulate the indoor illuminance and air temperatures in the test scenarios with different SD-BA combinations, respectively. To validate the computational results, a courtyard consisting of four detached buildings in the Thousand Pillar Dwelling located in the eastern Sizhai village, was chosen as the reference building to conduct the field measurements of the indoor illuminance and air temperature. The BAs of the four buildings range within the intervals of S, N, N-W80 and S-E80 respectively, and the depths of the external corridors mounted on the front facades, are all approximately 1.6 m through field measurements.

The solar radiation reception and the indoor solar heat gain impact the indoor visual and thermal comfort, and also impact the energy costs due to the artificial lighting and air conditioning [36]. To this end, the ArchiWIZARD was used again to compute the three parameters of solar radiation reception, indoor solar heat gain and energy loads of

artificial lighting and AC in each of the test scenarios, to explore their impact trends. Aiming at verifying the accuracy of computational results from the ArchiWIZARD, the data were compared with those from the real energy bills. In addition, coupling the energy load and the daylighting quality, the overall best SDs are recommended and applied to evaluating the current dwellings in Sizhai. To facilitate understanding the research methods framework, it is presented in Fig. 6.1

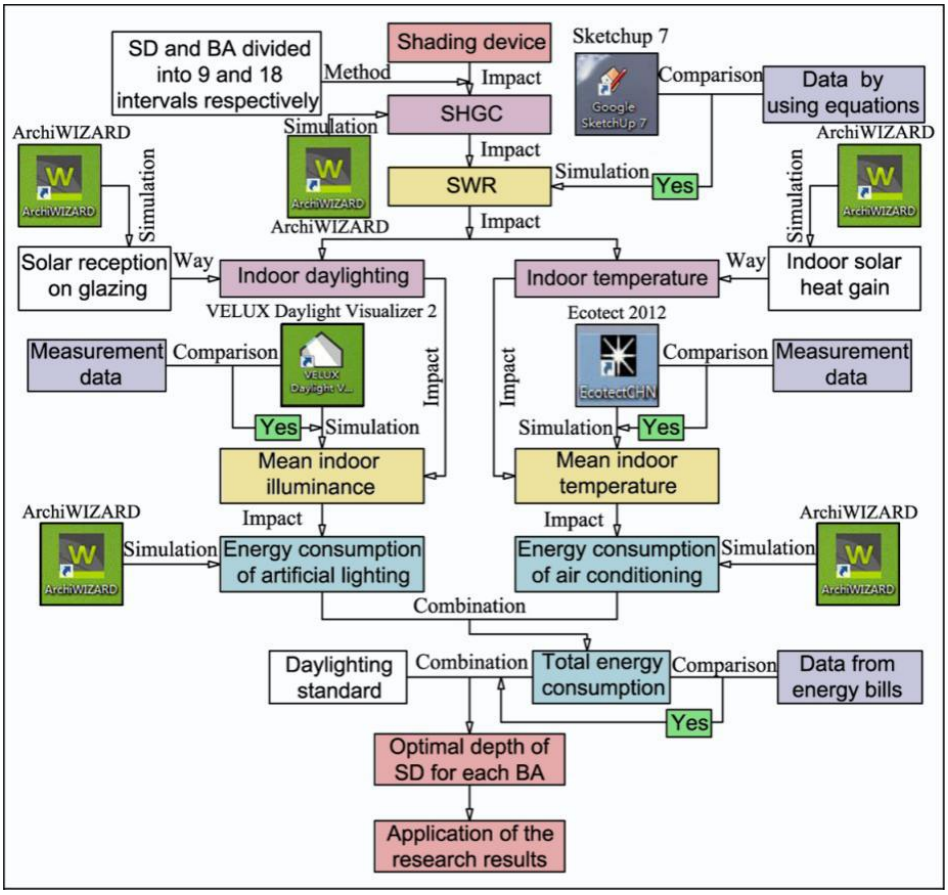

Fig. 6.1 Research methods framework

6.3 Impact of shading depth on SHGC and MSWR based on changes in building azimuth

The SHGCs for various SD-BA combinations can be generated by virtual simulation in software. Regarding the SWR, it can be obtained by means of two approaches, the equation calculation and the virtual simulation. The positive points of software computation are convenience and time-saving, so Sketchup 7 was adopted to simulate the SWRs in this chapter. Because the summer solstice and the winter solstice are usually considered as the representative days and are used as the design reference data for simulation setting in many papers [37], these two days were chosen as the date set points in this work as well. Formulating the equations for SWR is the second way to obtain the desired data. Throughout a whole year, the south facade is covered by the sunlight for the longest period

of a day precisely during the winter solstice. Therefore, the SWR on this day was calculated to verify the accuracy and to be compared with the computational results from the simulation tool.

6.3.1 Impact of shading devices with different orientations on SHGCs for windows

It can be seen from Fig. 6.2 that the SHGCs are inversely proportional to the SDs, because the deeper SD can intercept more solar radiation. Since the northerly oriented windows are covered by sunlight at the early morning and the end of afternoon in summer, when the solar rays are characterized by low solar altitudes, the SHGCs with the same SDs at x-axis present a decreasing trend while being rotated from the N to S clockwise and anticlockwise. With the SDs increasing, the gaps of SHGCs become larger. Furthermore, the inflexion points for the 18 polylines are all at 0.62 and 1.87 of the x-axis, between which the slopes of polylines are higher in comparison with their edge segments.

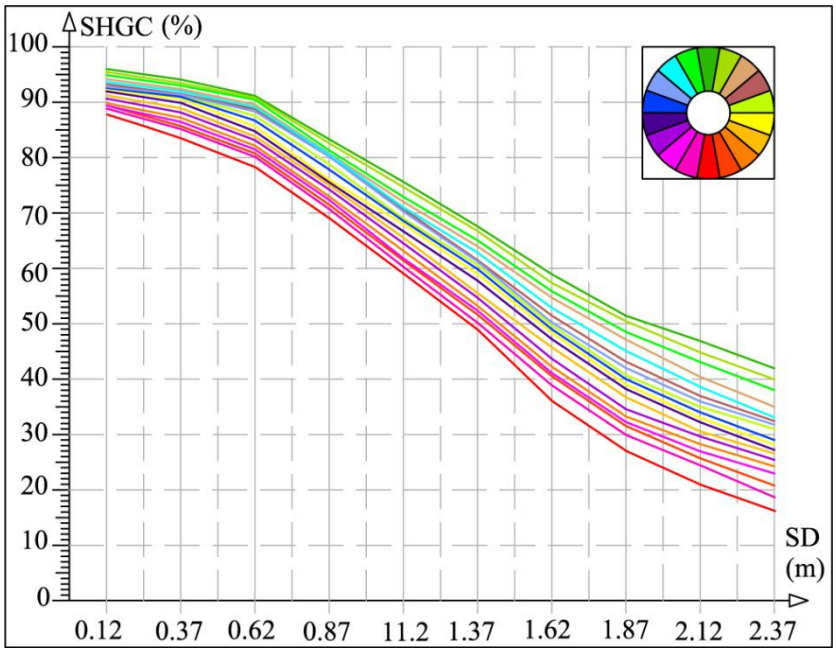

Fig. 6.2 Impact of shading devices with various shading depth and building azimuth combinations on SHGC

6.3.2 Impact of shading devices with different orientations on MSWRs for windows

For the southerly oriented and northerly oriented test scenarios, the SWRs are symmetrical with the south-north axis at 12 o'clock. For instance, the SWRs for S-E20 and S-W20 are symmetrical at 12 o'clock throughout the year. Therefore, to get the full picture, simulating the half-circle of BA intervals is enough. In this chapter, the test scenarios with 10 BAs from N to S clockwise were chosen as the study cases to investigate the impact tendencies of SD on the SWR. Due to the winter solstice being characterized by the minimal solar azimuth, approximately of 63°

at sunrise, the facades for N and N-E 20 are covered by no sunlight, which results in only eight sets of data on this day (Fig. 6.4).

As shown in Fig. 6.3, both the MSWRs on the summer solstice and winter solstice increase with the SDs increasing. The dispersion of polylines during the summer solstice is greater than that of the winter solstice. Moreover, the MSWRs on the summer solstice are roughly concave functions, which are characterized by the decreasing slopes of polylines with the SD increasing. Among the 10 polylines, the MSWRs for S and S-E 20 are much higher and present more significant fluctuations in comparison with the other 8 BAs, which contribute to their excellent shading performance for the windows.

During the winter solstice, the MSWRs for northeast orientation present the concave functions, while those for southeast and south are roughly convex functions (Fig. 6.4). The test scenario with N-E 40 is the closest to the direct north orientation among the 8 BAs, leading to no sunlight coverage on the facades near noon. Besides, due to the low solar intensity at the early forenoon, the MSWRs for N-E 40 remain low over this day.

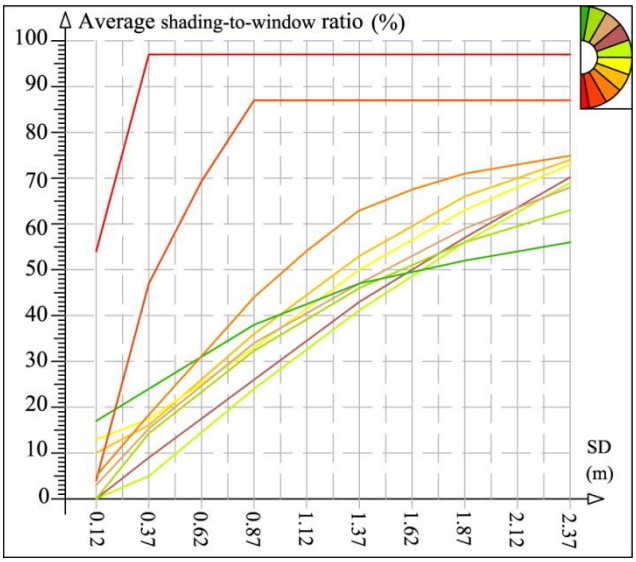

Fig. 6.3 MSWRs on the summer solstice corresponding to the circle of building azimuth intervals

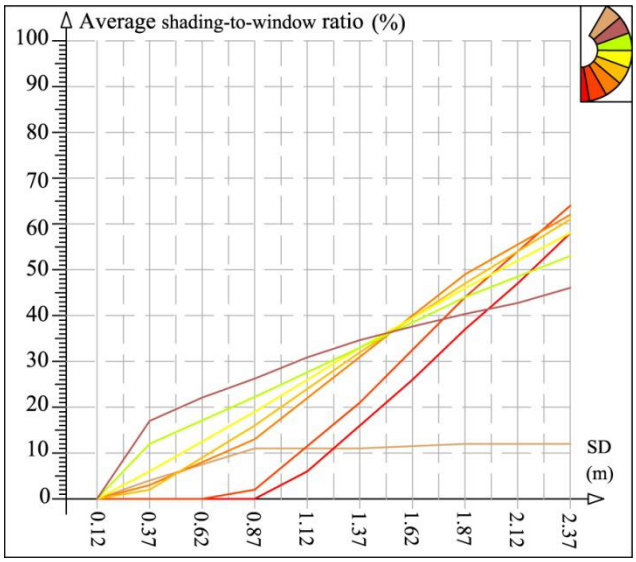

Fig. 6.4 MSWRs on the winter solstice corresponding to the half-half-circle of building azimuth intervals

6.3.3 Equation formulation of shading-to-window ratio

The geometric model facing the direct south was selected to formulate the SWR equations in this chapter, due largely to the fact that the included angles in relation to the window and the sun are comparatively simple for the southerly oriented model. With given data of the model details, solar altitudes and solar azimuths, the SWRs can be calculated. There are two solar shading conditions for the windows illustrated as following:

6.3.3.1 When $H_3<H_2$

According to the trigonometric functions, tangent b_2 is formulated as equation (6.1).

$$\tan b_2 = \frac{\tan a_2}{\cos(90°-a_4)} = \frac{\tan a_2}{\cos(90°-|180°-a_1|)} \tag{6.1}$$

Where, b_2 (Fig. 6.5) is the included angle between the vertical projection line of solar radiation on the south wall and bottom edge of window. The WSR (R_1) can be formulated as equation (6.4), based on the equation (6.2) and equation (6.3).

$$S_1 = \left(L_1 \times \cos c_1 \times \frac{\tan a_2}{\cos|180°-a_1|} - 1.1 + L_1 \times \sin c_1\right) \times \left(B_1 - \frac{\left(L_1 \times \cos c_1 \times \frac{\tan a_2}{\cos|180°-a_1|} - 1.1 + L_1 \times \sin c_1\right)}{\frac{\tan a_2}{\cos(90°-|180°-a_1|)}} \times \frac{1}{2}\right) \tag{6.2}$$

$$S = (B_1 \times H_2) \tag{6.3}$$

$$R_1 = \frac{S_1}{S} = \left(L_1 \times \cos c_1 \times \frac{\tan a_2}{\cos|180°-a_1|} - 1.1 + L_1 \times \sin c_1\right) \times \left(B_1 - \frac{\left(L_1 \times \cos c_1 \times \frac{\tan a_2}{\cos|180°-a_1|} - 1.1 + L_1 \times \sin c_1\right)}{\frac{\tan a_2}{\cos(90°-|180°-a_1|)}} \times \frac{1}{2}\right) / (B_1 \times H_2) \tag{6.4}$$

Where, S_1 is the shading areas covering the windows, m^2; S is the total window area on the first floor, m^2.

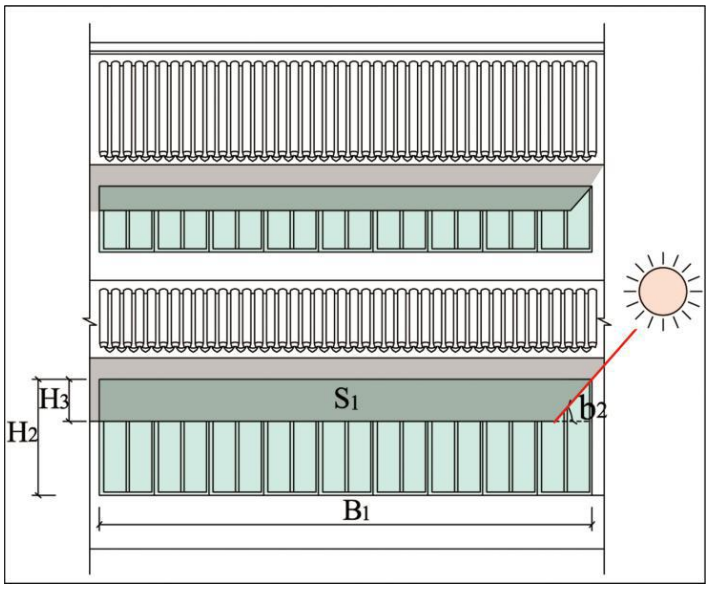

Fig. 6.5 Schematic 1: windows shaded by the shading device of corridor in traditional dwelling

6.3.3.2 When $H_3>H_2$

According the Fig. 6.6, the WSR (R_2) can be derived as equation (6.5).

$$R_2 = \frac{S_2}{S} = \left(B_1 - \frac{H_2}{\frac{\tan a_2}{\cos(90°-|180°-a_1|)}} \times \frac{1}{2}\right) / B_1 \tag{6.5}$$

Where, S_2 is the shading areas covered on the windows, m^2.

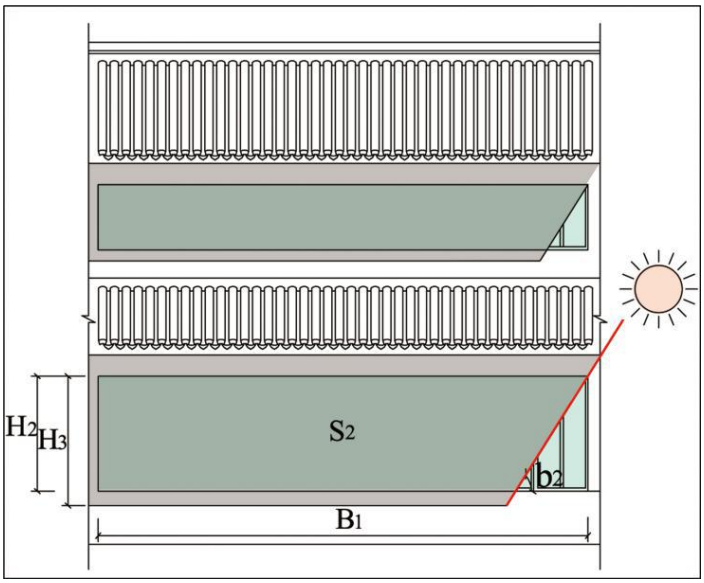

Fig. 6.6 Schematic 2: windows shaded by the shading device corridor in traditional dwelling

6.3.4 Validation of shading-to-window ratio: software versus equation

The time period, taken by software to compute the SWRs for a test scenario facing south, is from 7 a.m. to 5 p.m., with set points defined at intervals of 1 hour. The SWRs are kept at 0 for SDs shorter than 1.2 m, due to the winter solstice presenting lower solar altitudes. Therefore, the SDs ranged from 1.12 m to 2.37 m were chosen as the given data to calculate the SWRs, which are considered as the baseline in the validation. As shown in Fig. 6.7, the bias errors between the computational results and the calculation data are very slight, with average percentage of error between the six sets of data of approximately 1.2%.

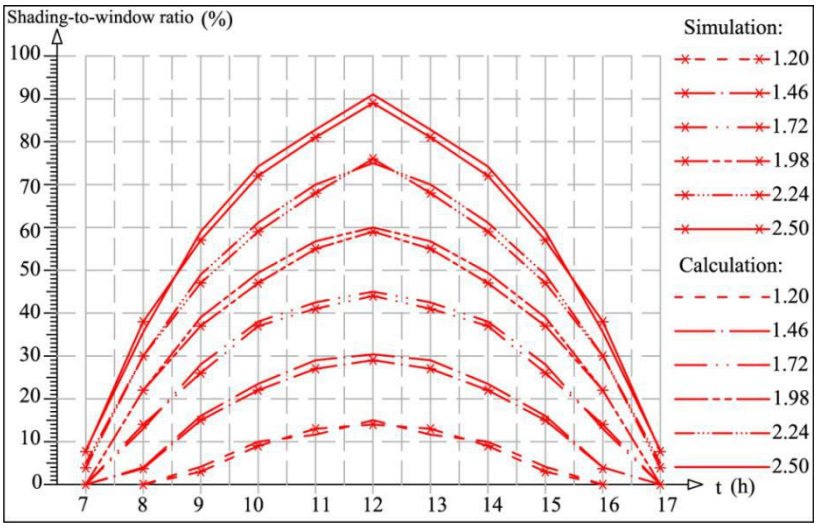

Fig. 6.7 Comparison of shading-to-window ratios obtained from simulation tool and equations

According to Reeves et al. [36] and Maamari et al. [38], the accepted percentage of error between the real data and the computational results should range in the scope of ±15%, for the data from the simulation tool to be considered accurate. Therefore, the computational results from Sketchup 7 are of a comparatively high reliability.

6.4 Impact of shading depth on the indoor daylighting and artificial lighting energy consumption based on changes in building azimuth

The visual comfort of the internal spaces is receiving increasing attention as the environmentally friendly buildings become popular [39]. Using an appropriate shading device can lead a to reduction in the energy consumption of artificial lighting, since the illumination levels in rooms are remain within a desirable range, with no or little glare [40].

Building envelope consists of the opaque and glazing elements, of which the glazing part is the channel allowing the daylight to penetrate inside. The ArchiWIZARD was used to analyze the solar radiation reception levels on the windows for the test scenarios, which is the factor that has the major impact on the internal daylighting performance [28]. Based on the computational results, another piece of software, VELUX Daylight Visualizer 2, was adopted to analyze the indoor daylighting performances and variation trends. To validate the accuracy of the data from the VELUX Daylight Visualizer 2, the field measurements of the diurnal indoor illuminance were performed in the chosen courtyard dwelling. Furthermore, the energy requirements of artificial lighting vary greatly depending on the indoor illuminance level [41]. To this end, the ArchiWIZARD was adopted again to compute the energy costs for each of the test scenarios corresponding to different illuminance magnitudes generated by the VELUX Daylight Visualizer 2.

6.4.1 Impact of shading devices with different orientations on the solar radiation reception levels for windows

Solar radiation reception is a relatively common and simple parameter to estimate the shading performance [42]. The solar radiation consists of direct radiation and diffuse radiation. Although the orbit of the sun is symmetrical with the north-south axis, the solar radiation magnitude is constantly changing in the sky, which is impacted by the cloudage, dust level in the air and air humidity, etc. In Sizhai, the total solar radiation levels in the afternoon are generally larger than that of the forenoon [43].

As presented in Fig. 6.8, the direct radiation reception levels that are indicated by solid lines for south, vary notably with the BAs. Moreover, the values facing west are generally higher than those facing east. Obviously, the inflexion points of the polylines for south are at approximately 0.62 of the x-axis, after which the slopes start to

decrease. In contrast with the test scenarios facing south, the major solar receptions on the windows facing north are due to diffuse radiation, so the slopes of these lines remain relatively low. In addition, the polylines' dispersion of diffuse radiation receptions, indicated by dashed lines, is negligible, which demonstrates that the BA has a negligible impact on the diffuse radiation receptions for windows.

While comparing the dispersion of polylines for the direct radiation receptions with those of total solar radiation receptions (Fig. 6.9), both sets of polylines present significant differences as the SDs at low x-axis. Obviously, their gaps decrease with the SD increasing, which means that the influence of shading devices on these two kinds of solar radiation reception levels becomes weaker with SDs increasing. In addition, among the 18 test scenarios, the southwest facing building models gain the highest levels of total solar radiation receptions.

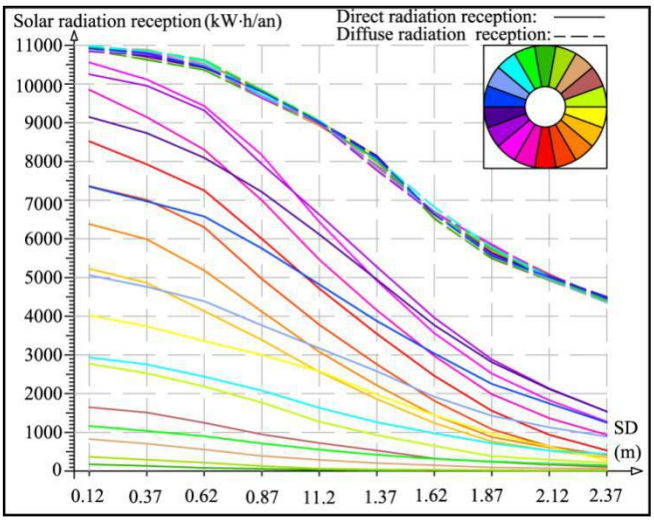

Fig. 6.8 Direct and diffuse radiation receptions for windows integrated with various shading devices

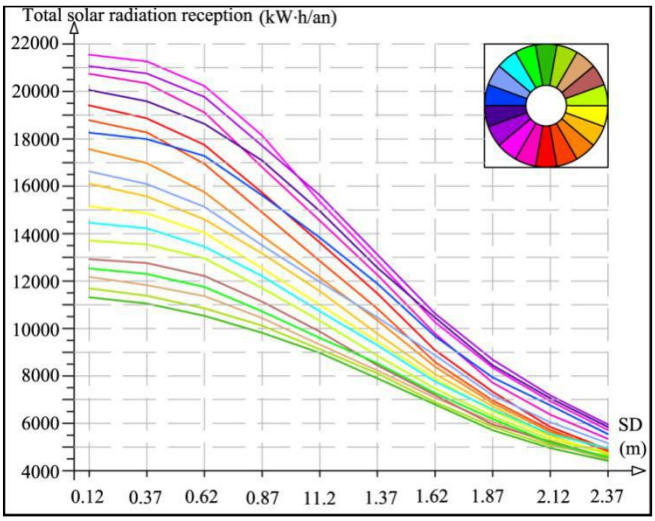

Fig. 6.9 Total solar radiation reception for windows integrated with various shading devices

6.4.2 Impact of shading devices with different orientations on the mean indoor illuminance

To simulate the indoor daylighting performance for the test scenarios, the VELUX Daylight Visualizer 2 was adopted in this section. The two representative days, both with sunny weather conditions, were assumed to be the setting parameters in simulation. The reflectance of the wall, the flooring and the ceiling is set at 0.75, 0.60 and 0.65, respectively.

In VELUX Daylight Visualizer 2, the value of orientation facing directly north is set at 0°. By altering the orientation value, the BA can be adjusted correspondingly, without the need to rotate the original model. Furthermore, the mean indoor illuminance can also be simulated at different times, by changing the set point of time.

Drawing an analogy between Fig. 6.10 and Fig. 6.11, we found that the dispersion of the 18 polylines during winter is greater compared with summer, thanks to the windows receiving larger shading coverage during summer. As obvious, the slopes and dispersion of polylines for the south are greater than those for the north in winter, which is due to the availability of substantial quantity of solar radiation covering the south facade. In contrast, the slopes of the 18 polylines are generally similar, and their dispersion is small in summer. Considering their common features on these two days, the dispersion of polylines and the mean indoor illuminance for the 18 BAs are both inversely proportional to SD. Moreover, the inflexion points of the polylines are both at 0.87 of the x-axis, after which the mean indoor illuminance levels start to drop dramatically.

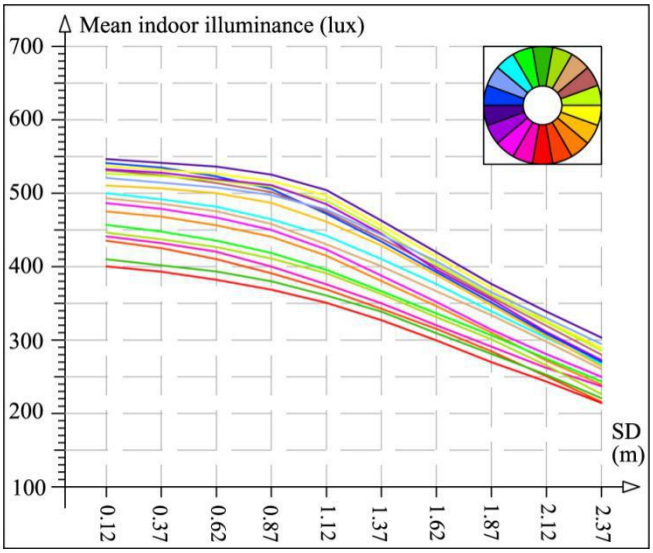

Fig. 6.10 Mean indoor illuminance in the test scenarios mounted with various shading devices on the summer solstice

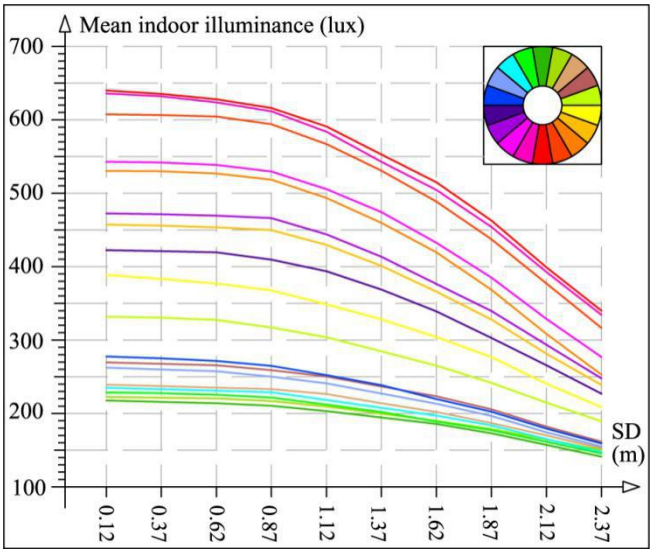

Fig. 6.11 Mean indoor illuminance in the test scenarios mounted with various shading devices on the winter solstice

6.4.3 Validation of illuminance data: simulation tool versus field measurements

The real measurement data are empirical, and are often called as “true data” and considered to be an extremely powerful validation proof, which could be used to compare with the computational results [44]. In addition, Ryan et al. [45] suggested that the computational results, generated by the energy simulation tools, need to be compared with the “true data” to verify their accuracy. Based on the preceding arguments, the data from field measurement conducted in the chosen courtyard dwelling were compared to the computed data obtained from the software.

According to the weather forecast, the dates selected to carry on the measurements were on July 25th, 2015 and December 27th, 2015, both with sunny conditions. The measurement period of time lasted from sunrise to sunset at 1 hour increments. The indoor illuminance was recorded by a data logger of Illuminometer (Type 061206363,

Accuracy: ±3%; Range of the measurement: 1~100000 lux), which was operated at three positions: in a line covered by the shadow near the window, at the center of the room and near the back wall respectively, at a height of 0.9 m above ground.

The measurement data, shown in Fig. 6.12, are the average values measured at the three positions. Among the four sets of data, the percentages of errors in the afternoon are larger than those in the forenoon. Since the climatic feature of Sizhai is that the solar radiation levels for the second half of the day are generally greater than those during the first half-day, it leads to the fact that the internal spaces corresponding to S and N presenting higher illuminance levels during afternoon. Therefore, the measurement data differ from the computational results, where the mean indoor illuminance for the direct S, direct N, S-E 80 and N-W 80 generated by simulation tool is all symmetrical at 12 o'clock. Taking an average for the 4 sets of data, their mean percentage of error is 7.5%, which is less than 15%, so the computational results are acceptable.

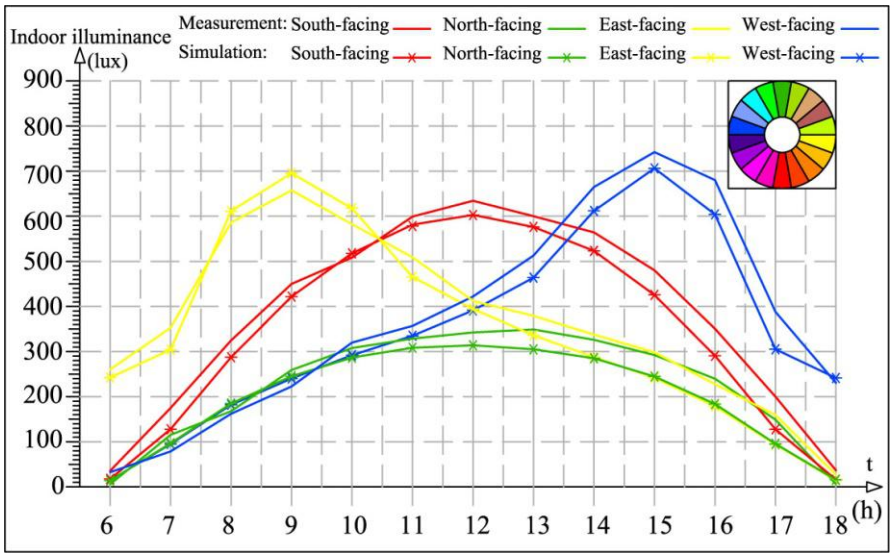

Fig. 6.12 Comparison of illuminance obtained from simulation tool and field measurements

6.4.4 Impact of shading devices with different orientations on the energy consumption of artificial lighting

Through the questionnaire survey, we found that the wake-up time and the bedtime for occupants are generally at 6:30 a.m. and 22:30 p.m., respectively. When the illuminance in each test scenario is lower than 300 lux, the lighting system is turned on to compensate the daylight illuminance and to reach the desired value (i.e., 300 lux) on the work plane (0.9 m above floor). While in fact, not all lamps are in operation during nighttime, but according to occupancy conditions and lighting demand, a variable quantity of lamps is switched on. Therefore, the parameter settings for the energy cost of artificial lighting in the simulation also needs to be optimized. The probability of all five suites being

under the artificially lit conditions at the same time was set at the 80%, and the average quantity of lamps in operation was set at 1.5 for each suite of the test scenario.

The trends of correlation of lighting demands with increasing SD differ from those of the mean indoor illuminance, by drawing an analogy between Fig. 6.10, Fig. 6.11 and Fig. 6.13. The energy consumption of artificial lighting presents decreasing trend, rotated from N to S-W 40 clockwise and anticlockwise for each SD at x-axis. In addition, all the 18 polylines represent concave functions with a similar slope. In other words, the fluctuation amplitudes of lighting energy consumption for different BAs are similar, varying by the SD. The dispersion of polylines for north is smaller than that for south, which means that the lighting energy consumption in buildings facing north is more sensitive to the changes in BAs. The inflexion point for most polylines is observed at 1.87 of x-axis, after which their slopes start to increase.

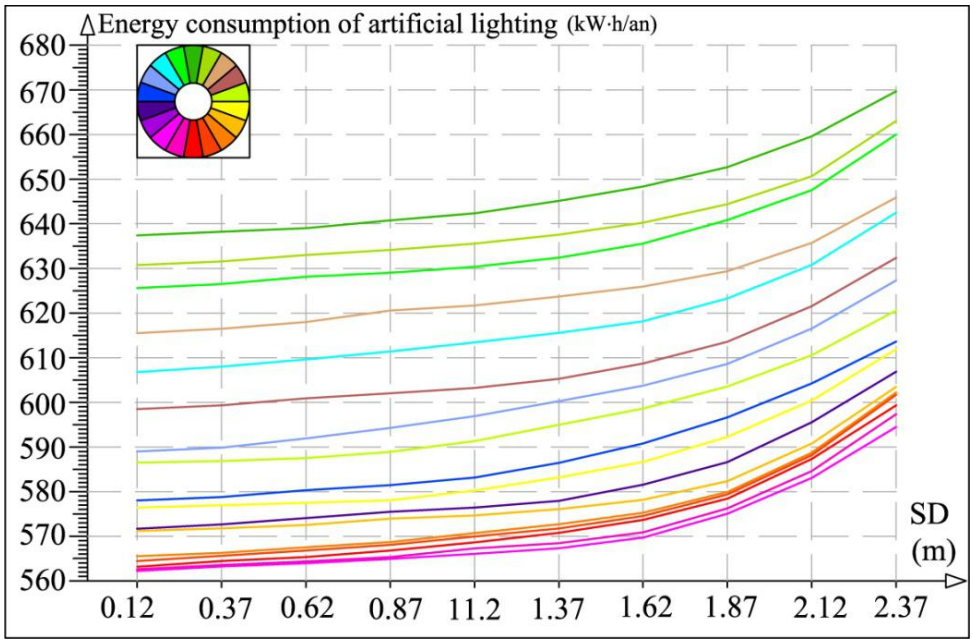

Fig. 6.13 Energy consumption of artificial lighting in the test scenarios mounted with different shading devices

6.5 Impact of shading depth on the indoor temperature and air conditioning energy cost

The depth of shading device is one of driving factors that affects the solar heat gain for internal spaces, as well as the indoor temperature [28]. The shading device of an appropriate depth not only provides the sufficient shading for windows in summer, but also allows solar radiation to penetrate into building's internal spaces. By using the Ecotect 2012, the indoor temperature in each of the test scenarios was computed to research the impact that shading devices with various SD-BA combinations have on the indoor temperature. Aiming at validating the computational results, a comparison between air temperatures generated by Ecotect 2012 and obtained from the on-site measurements was

carried out. Furthermore, the ArchiWIZARD was used to compute the total cooling and heating demands throughout the year for all the test scenarios, in order to conclude the variation trends of the AC energy consumption according to the shading device, changes in SDs and BAs.

6.5.1 Impact of shading devices with different orientations on the indoor solar heat gain

As shown in Fig. 6.14, the fluctuation trends of indoor solar heat gain for all the 18 BAs are similar, they decrease with SD increasing because more solar radiation is blocked by a larger SD. Under the condition of same SDs for variable BAs, the slopes of polylines present an increasing trend while being rotated from the true N to S-W 40 clockwise and anticlockwise. In other words, the indoor solar heat gains facing south are more susceptible to the SD variations than those facing north, due largely to windows in the test scenarios orientated towards south receiveing more solar contributions.

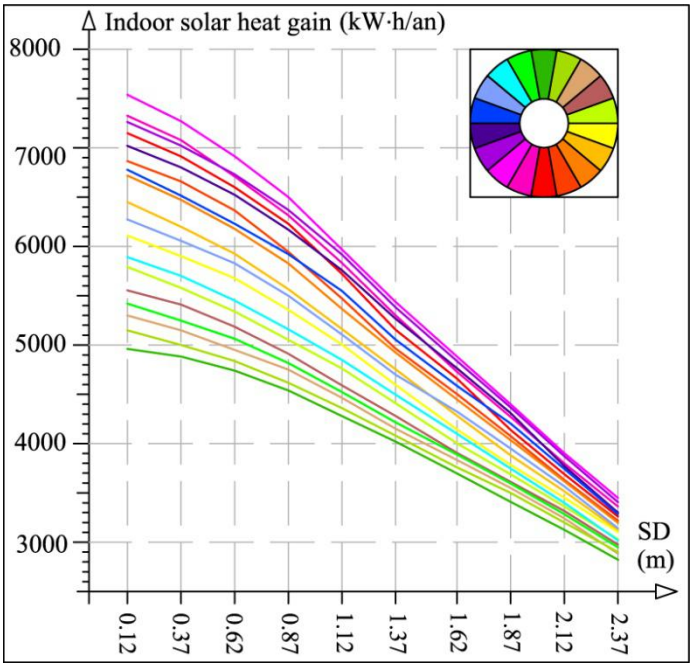

Fig. 6.14 Indoor solar heat gains in the test scenarios mounted with different shading devices

6.5.2 Impact of shading devices with different orientations on the indoor temperature

When the windows are in a closed position (i.e., convection was blocked), there are two ways in which the outdoor climate impacts indoor temperatures, namely the heat transmission by the temperature difference (i.e., heat conduction) and solar radiation (i.e., radiation). As the BA changes, a different facade of building will face the sun. The capacity of a building to receive the solar heat relies greatly on its external components and on the way it interacts with the sun [44]. Under the condition of walls with the same window-wall ratio, the heat transfer due to temperature difference between the exterior and interior, for a window facing any direction is almost identical, but

that by solar radiation varies heavily depending on the BA. Since the sunny weather is related to high intensity of solar radiation, which leads to consequent indoor temperate fluctuation, “sunshine” was selected as the weather condition in the simulation. The mean diurnal indoor temperature generated by Ecotect 2012 is adopted as the evaluation parameter to analyze the indoor thermal performances for each of the test scenarios. The summer solstice and winter solstice, when the sun is in the highest and lowest positions of sky, were used as the study dates for simulation in the software. The mean diurnal outdoor temperatures on these two days were 32.0 ℃ and 18.33 ℃ respectively, according to the simulation results.

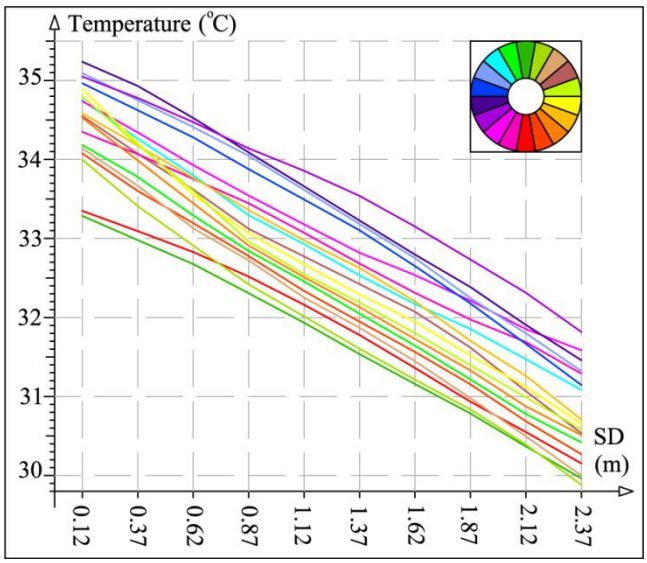

Fig. 6.15 Mean diurnal indoor temperatures the in the test scenarios mounted with various shading devices on the summer solstice

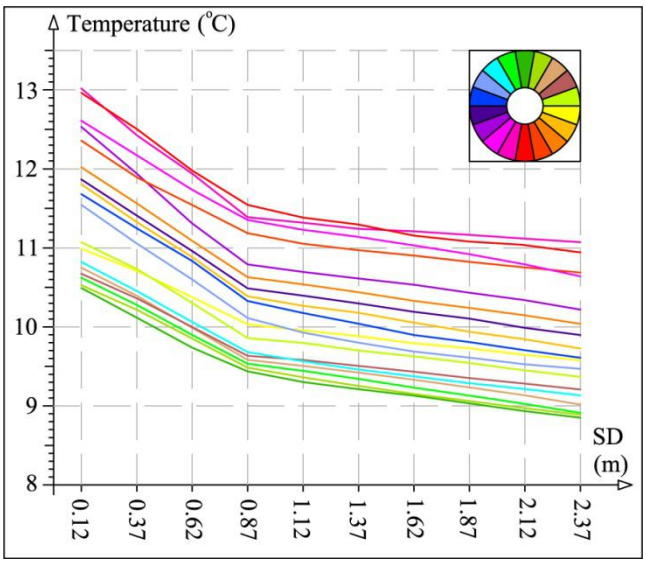

Fig. 6.16 Mean diurnal indoor temperatures the in the test scenarios mounted with various shading devices on the winter solstice

As shown in Fig. 6.15, the mean diurnal indoor temperatures for the southwest orientation are higher than those of the other BAs in summer. While in winter, the mean diurnal indoor temperatures for south are comparatively higher in comparison with those for north (Fig. 6.16). Regarding the slope, the mean diurnal indoor temperatures in summer are more sensitive to the variations in SD than those in winter, with a variation amplitude of over 3 ℃ correlated to SD increase from 0.12 m to 2.37 m. The 18 polylines in Fig. 6.15, with similar negative slopes of about -1.5, have no obvious inflexion point. In contrast, the polylines in Fig. 6.16 there is a clear inflexion point at 0.87 of the x-axis, after which the slopes start to increase, approximately at a rate of -0.3. Because the slopes of mean diurnal indoor temperatures for 18 BAs in both summer and winter are very similar, the polylines are aligned in parallel bands as shown in Fig. 6.15 and Fig.6.16. Whereas, the dispersion of polylines in summer is lower than that in winter, due largely to the higher solar altitudes in summer leading to higher SWRs.

6.5.3 Validation of air temperature data: simulation tool versus in-situ measurements

The on-site measurements of indoor temperature were performed in the chosen courtyard dwelling, and a point outside the buildings was selected to conduct the outdoor temperature measurement. According to the weather forecast, both days selected to perform the measurements (which were on July 25th, 2015 and December 27th, 2015) presented sunny conditions. The outdoor air temperatures on the two measurement days, ranged from 26~36 ℃ and 2 ~12 ℃, and are both consistent with the set points in the simulation for the summer solstice and winter solstice, respectively. The measurement time period lasted from the sunrise to the sunset, at 1 hour increments. The air temperatures were recorded by a data logger of Hygrothermograph (Type 20100117, Accuracy of temperature measurement: ±1 ℃; Range of the temperature measurement: -10 ℃~50 ℃), which operated at a height of 0.9 m above the floor/ground, and was placed in the shaded spaces of both the interiors and the exterior.

After modeling the same building geometry as the chosen courtyard dwelling in the Ecotect 2012, the indoor temperatures were computed for the south-facing and north-facing buildings on the summer solstice and on winter solstice, respectively. As shown in Fig. 6.17, the six sets of data are all reasonably fitting, whose average percentage of error is about 6.5%, less than 15%.

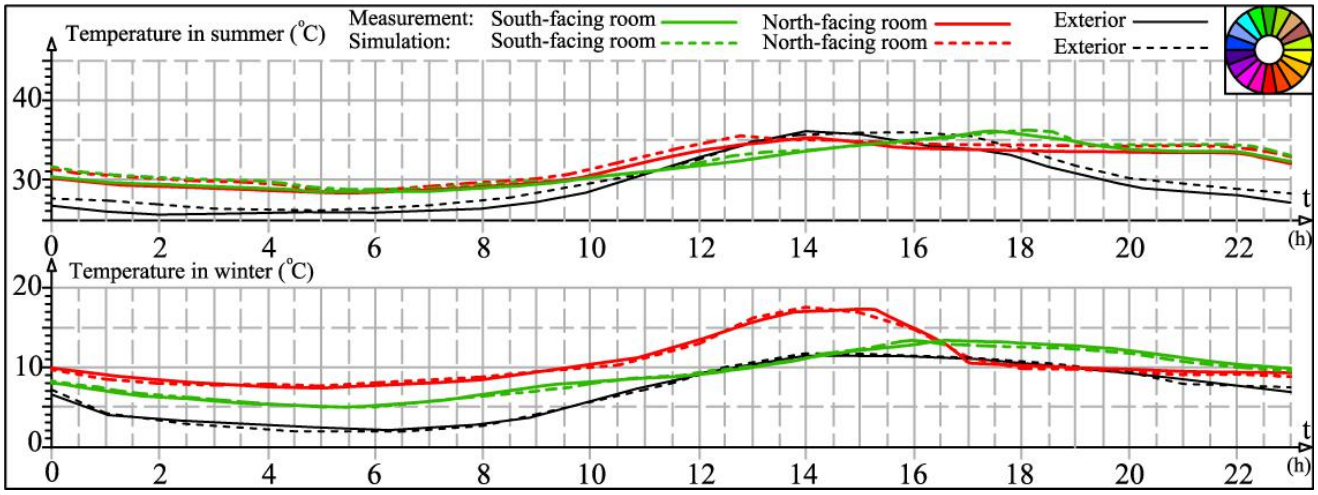

Fig. 6.17 Comparison of air temperatures obtained from the simulation tool and real measurements

6.5.4 Impact of shading devices with different orientations on the energy consumption of air conditioning

During AC in operation, its action-points of heating and cooling temperatures should be controlled in appropriate scopes. The optimum scopes of AC action-points range from 26 ℃ to 28 ℃ during summer and from 18 ℃ to 20 ℃ during winter [46]. According to the recommended AC action-points and taking into consideration the habit of temperature setting for AC by the occupants, the AC action-points were set at 27 ℃ and 18 ℃ in the simulation for

space heating and cooling, respectively. Furthermore, because the active system used for both cooling during summer and heating during winter for the internal spaces is AC in East and Central China, the electricity from power grid was chosen as the energy supply source in the simulation throughout the whole year. Considering the air-conditioned conditions and the occupancy schedules for various rooms, the setting parameters in the simulation need to be adjusted.

Since generally only bedrooms are equipped with AC in the Sizhai traditional dwellings, whose building area accounts for, approximately, a 33% of a suite, the air-conditioned building area of the middle suite was set at 13.2 m^2 and that of the other four were all set at 7.99 m^2. Due to each suite being occupied by a small family with an average of two or three people, the population density of the bedroom was set at 0.221 in the simulation. Simultaneously, the probability of all five suites being simultaneously air-conditioned was set at 80%. In addition, the schedule assigned to run the AC in the test scenarios during weekdays is 7 hours daily, beginning at 22:00 p.m. and ending at 5:00 a.m. of the next day, accounting for a 29.17% of the whole day. Since the air temperatures are comparatively low during the forenoon in summer and the occupants' daily schedule is postponed in winter, the time of AC functioning during weekends was set at 15 hours daily, from 14:00 p.m. to 5:00 a.m. of the next day, accounting for 62.5% of the whole day.

It can be deduced from Fig. 6.18 that the energy consumption for the space heating in winter is lower than that for space cooling in summer, due to the dwellings in Sizhai belonging to the cooling-load dominated buildings. This reason also leads to the fact that the polylines' dispersion for heating energy consumption is smaller than that for the cooling energy consumption. Furthermore, the variations in heating consumption for the north orientation are comparatively less dependent on the SD variations, due largely to no interaction with the sun.

For the cooling loads, as shown in Fig. 6.19, most of the polylines fit the characteristics of a convex function, unlike the heating loads. The slopes of polylines depicting cooling energy consumption show a decreasing trend from the southwest to the north clockwise and anticlockwise, while those for the heating requirements present an opposite increasing trend. The dispersion of the 18 polylines corresponding to the cooling loads, the heating loads and the total energy consumption (Fig. 6.20), are all inversely proportional to SD, which means that the impact of BA on the energy consumption diminishes with the SD increasing. Among the 18 polylines in Fig. 20, the test scenario with N-W 80 presents the most dramatic variation in the total energy consumption, of about 198.42 kW·h/an. Inversely, the alternative with the slightest variation can be observed for the scenario facing S, about 105.71 kW·h/an.

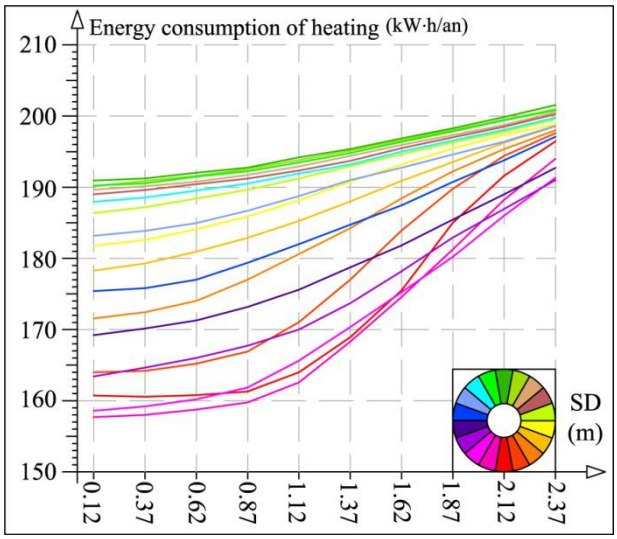

Fig. 6.18 Heating energy consumption in the test scenarios mounted with different shading devices

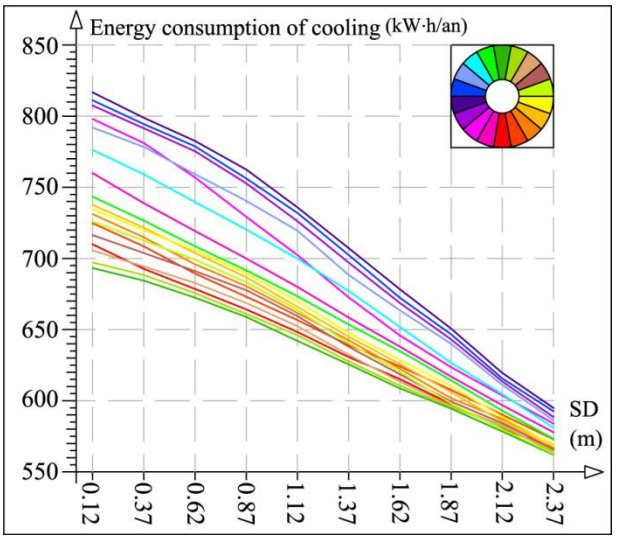

Fig. 6.19 Cooling energy consumption in the test scenarios mounted with different shading devices

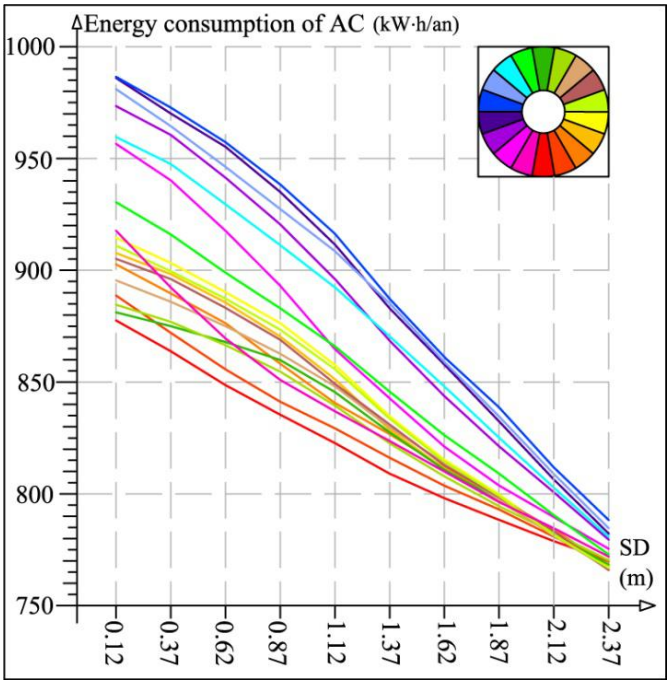

Fig. 6.20 Energy consumption of air conditioning in the test scenarios mounted with different shading devices

6.6 Total energy consumption including artificial lighting and air conditioning

The shading device can reduce the indoor solar heat gain contributing to the reduction in the cooling load. However, it can also lead to some negative effects in terms of the visual discomfort and insufficient solar heat gain in winter, which in turn results in an increase of the heating consumption. Therefore, the optimal SD for each BA needs to be investigated critically and carefully.

By summing up both the artificial lighting and AC demands, the total energy consumption in buildings can be calculated. As shown in Fig. 6.21, the total energy costs in the northerly oriented buildings are generally higher than those in the southerly oriented buildings. In addition, the energy costs in most of the south facing buildings present concave functions, while those in most of the north facing buildings present convex functions. The energy cost for S-W 80 is the most sensitive to changes in SD (which ranges from 0.12 to 2.37), with an increase in amplitude of approximately 155 kW·h/an. In contrast, the minimal fluctuation in total energy cost occurs in the test scenario with N, about 63 kW·h/an. With the change in BA, a different projected area of facade is orthogonal to the sun's radiation. Due to the shadow being cast by the south facing shading devices for a longer period in summer, as well as to availability of larger amount of solar radiation penetrating the southerly oriented windows, the values and variation amplitudes for S, S-E20, S-E40 and S-W 2 are comparatively low.

The building energy requirements for seven BA intervals from S-W 40 to N-W 20 are more susceptible to the SD in comparison with the others. As obvious, the inflexion points of polylines for S and S-E 20 are 1.46 m and 1.72 m respectively, and that for S-E 40, S-E 60, S-E 80, S-W 20 and S-W 40 are all at 2.24 m, after that point their energy consumption starts to increase. In addition, the optimal SDs in terms of the energy consumption recommended for the other 11 BAs are all at 2.37 m.

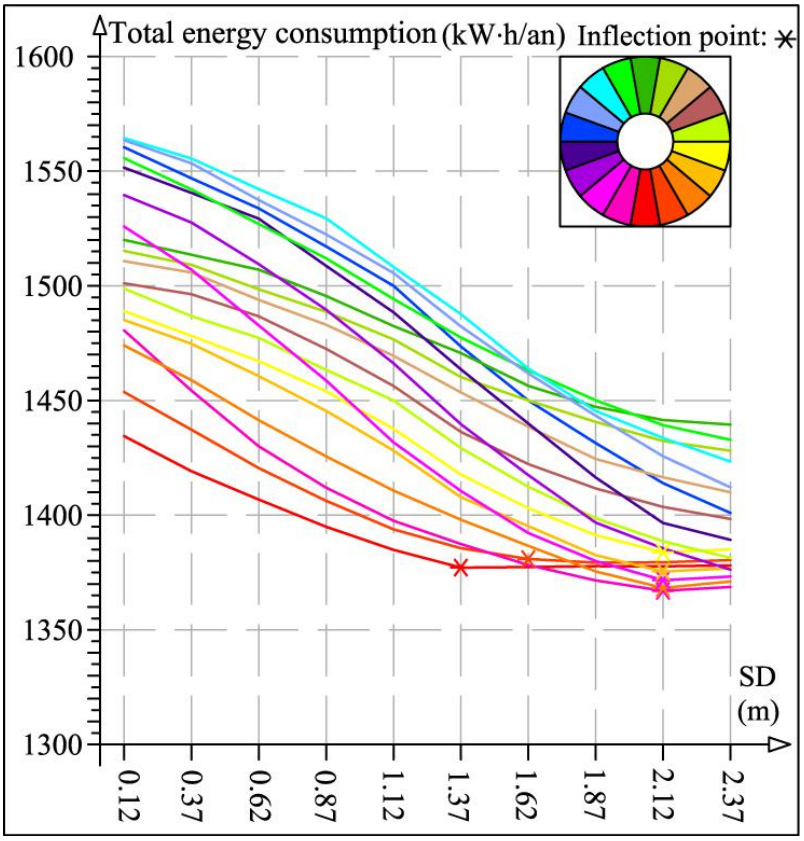

Fig. 6.21 Total energy consumption in the test scenarios mounted with various shading devices

6.7 Validation of the energy consumption data: simulation tool versus real bills

6.7.1 Energy consumption in the real traditional dwellings obtained from bills

Real energy bills are empirical, also often called “true data” and are regarded as an extremely powerful validation proof [44]. With this in mind, the total annual electricity consumed by the artificial lighting and AC, which is generated by simulation tool, is compared to that from the real electricity consumption bills to verify the computational accuracy in this chapter. Because the building model type with five suites was chosen in the simulation, the mean electricity consumption for each suite was calculated as one fifth of the total annual electricity use. There are two selection criteria for choosing the real bills from reference suites: (1) the reference suite should be equipped with AC and lighting fixtures; (2) the building area of the reference suite should be around 30 m^2 for fair comparison with the suite in the test scenario. Complying with these two conditions, the existing energy bills from four real suites (Fig. 22, Table 6.1) are selected as the “true data”, of which two are within S interval and the other two are within N interval. The domestic electrical appliances and details of the four reference suites are listed in Table 6.2. The E_{TAAEC} (the total annual actual electricity consumption, kW·h) including the artificial lighting and AC can be formulated as equation (6.6).

$$E_{TAAEC} = E_T - E_O \qquad (6.6)$$

Where, E_T is the total annual actual electricity consumption including the all domestic electrical appliances, kW·h; E_O is the total annual actual electricity consumption of the all domestic electrical appliances except for the artificial lighting and AC, kW·h. In accordance with the time in operation and the quantity of domestic electrical appliances, the E_O can be calculated and listed in Table 6.3.

Fig. 6.22 Positions of four reference buildings in Sizhai village

Table 6.1 Four reference suites in Sizhai chosen to collect the real energy bills

BA	Within S interval		Within N interval	
SD	0.36 m	1.33 m	0.38 m	1.34 m
Diagram				

Table 6.2 List of domestic electrical appliances and details of the four reference suites

Domestic electrical appliance		EC	WM	EV	EK	Com	T	R	Cal
Power (w)		500	210	50	800	200	100	100	1500
Operation period		Whole year	Whole year	JO	Whole year	Whole year	Whole year	Whole year	NANY
Use frequency per day during workday		1	1	1	1	1	1	1	1
Use frequency per day during weekend		2	1	2	3	3	3	1	1
Operation duration for each time (h)		0.33	0.3	6	0.17	2	2	24	1
Electricity cost per month (kW·h)		6.27	1.89	9	4.08	12	6	12	45
Annual electricity cost (kW·h)		75.24	22.68	46.29	48.96	144	72	144	270
Suite 1-S (28.56 m^2)	Appliance	●	●	●	●	●	●	●	●
	E_O (kW·h)	823.17							
Suite 2-S (33.87 m^2)	Appliance	●		●	●		●	●	●
	E_O (kW·h)	656.49							
Suite 1-N (30.53 m^2)	Appliance	●	●	●	●	●	●	●	●
	E_O (kW·h)	823.17							
Suite 2-N (32.01 m^2)	Appliance	●	●	●	●		●	●	●
	E_O (kW·h)	679.17							

Notes: 1. ● presents the suite equipped with the given domestic electrical appliance; 2. EC: Electrical Cooker; WM: Washing Machine; EV: Electrical Ventilator; EK: Electrical Kettle; Com: Computer; T: Television; R: Refrigerator; Cal: Calorifier. Whole year: WY; JO: from June to October; NANY: from November to April of next year.

Table 6.3 Total actual annual electricity consumption of 2014 and 2015 in the four reference suites

Designation	E_T of 2015 (kW·h)	E_T of 2016 (kW·h)	E_{TAAEC} of 2015 (kW·h)	E_{TAAEC} of 2016 (kW·h)
S-House 1	1079.40	1071.73	256.23	248.56
S-House 2	918.20	909.27	261.71	252.78
N-House 1	1102.59	1096.08	279.42	272.91
N-House 2	968.15	948.04	288.98	268.87

The E_Ts in the four reference suites throughout 2014 and 2015 are obtained from the monthly electricity consumption bills stored by homeowners. Using equation (6.6), the E_{TAAEC}s are calculated and listed in Table 6.3. In 2014, the mean air temperature of January was 6.5℃, and that of three summer months, including June, July and

August, was 28.7 ℃. As for 2015, the corresponding mean air temperatures were 6 ℃ and 28.3 ℃, respectively. Because the mean temperature in summer of 2014 was higher than that of 2015, the electricity consumption of 2014 was also higher than in 2015 in the four reference suites.

6.7.2 Comparison of total energy consumption obtained from simulation tool and bills

The total annual electricity consumption in S-House 1, S-House 2, N-House 1 and N-House 2 generated by the software is 284.74, 276.46, 303.15 and 294.29 kW·h, respectively. By drawing a comparison between the electricity consumption obtained from the simulation tool and from the real bills, the percentage of bias error for the eight sets of data on average is equivalent to 0.08, and the details are depicted in Fig. 6.23.

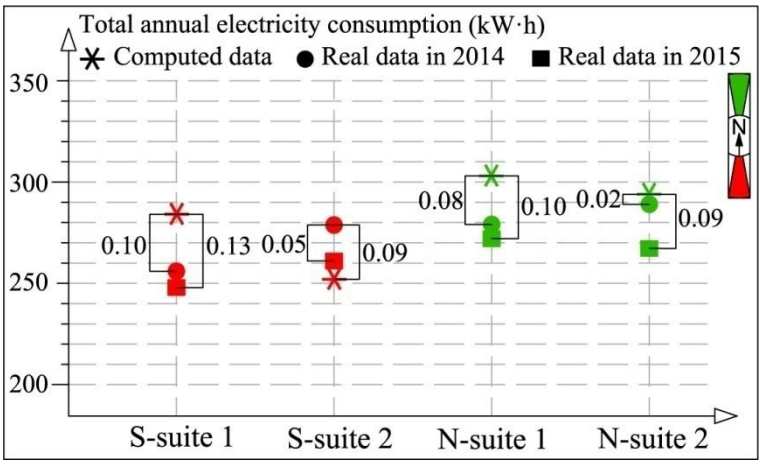

Fig. 6.23 Comparison of the total annual electricity use obtained from simulation tool and real bills

The possible sources of bias error which can impact the computational results are important to highlight: (1) It is difficult to precisely measure the BA for real dwellings, therefore the BAs used to conduct the simulation test in software cannot accurately represent the actual BAs for dwellings. (2) A substantial quantity of assumptions were made in software computation. The U-values of fabrics and materials used in the actual buildings may be not consistent with the assumed value adopted in the software. (3) Software simulation estimates the amount of energy consumption based on a fixed schedule, but the real conditions of occupancy times may differ from day to day throughout a year. (4) The accuracy of computational results may be correlated to human behavior. As stated by Ryan and Sanquist [45], the occupant behaviors are the common cause leading to bias errors in the energy simulations, since they are highly variable, resulting in being almost impossible to model them accurately. Besides, the life-style and behavior of each occupant is different, but the set points in the simulation are the same for each of the test scenario, which may also cause bias errors. (5) Weather data is another factor that influences the accuracy of computational results. The meteorological data used in simulation are collected from the whole Shaoxing city, but

the case study in the mountainous area is easily influenced by a local micro-climatic environment, which may cause bias errors for the computational results. (6) Some simplifications in the geometric model may be another source of bias error for the computational results, because the real dwellings in Sizhai are surrounded by mountains and vegetation, which influences the intensity of solar radiation covering the walls.

6.8 Optimal shading depths recommended for the 18 building azimuth intervals based on the energy consumption and Daylighting Standard

6.8.1 Daylight factor corresponding to 10 shading depths

Levels for daylighting are generally described as preferred or recommended, either by specific illuminance (lux) levels on a workplane or by daylight factor (DF). For evaluation of the quantity of indoor illumination inside a room, daylight factor is the most recognized performance indicator used at present. The *Chinese Standard for Daylighting Design of Buildings* (GB 50033-2013) is recommended that the mean daylight factor in bedroom, living room and kitchen should be above 2%, or the mean illuminance in these rooms should be higher than 300 lux on the work plane for the building design.

In Ecotect, the most basic data for lighting calculations is the daylight factor, and all other parameters (e.g., illuminance) are obtained applying calculations based on the daylight factor. Therefore, the evaluation parameter of daylight factor was used to estimate the indoor daylighting performances for each of the test scenarios.

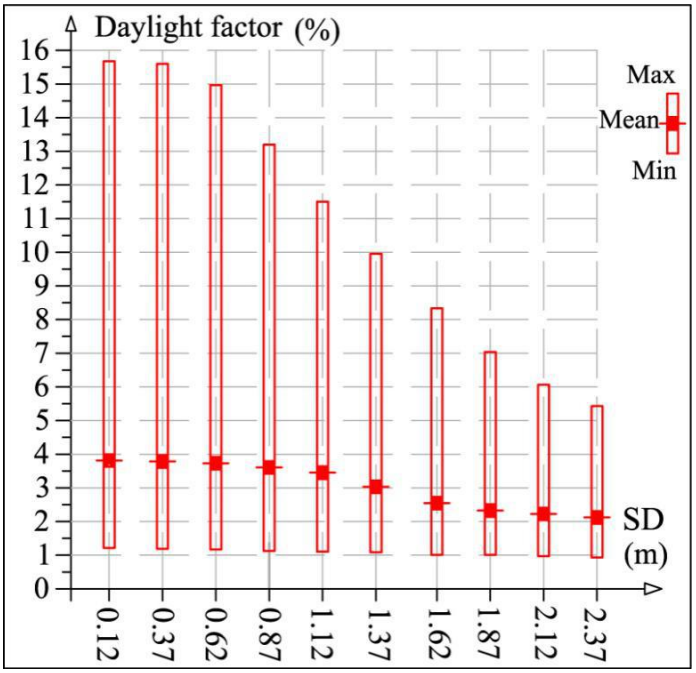

Fig. 6.24 Daylight factor for directly south (S) based on changes in shading depth

According to the Standard, the daylight climate of Sizhai is located in the fourth zone, where the natural illuminance of overcast sky is assigned to be of 13500 lux. The overcast weather is characterized by a uniform and stable diffuse radiation in the sky, which leads to the indoor daylighting performances corresponding to different orientations to be very similar. In this chapter, the test scenario with S was chosen as the case study. As shown in Fig. 6.24, the all shading depths are satisfied to the Standard.

6.8.2 Recommendation of the optimal shading depth to each building azimuth interval

The optimal SDs for each BA is summarized in the Fig. 6.25, based on the criteria of the total building energy cost and the daylight factor. Due largely to Sizhai experiencing the long summer with high air temperatures, the optimal SDs recommended for each of the test scenarios are relatively large. Obviously, the optimal SDs for S and S-E 20 are 1.46 m and 1.72 m respectively, and those for S-E 40, S-E 60, S-E 80, S-W 20 and S-W 40 are all 2.24 m, as well as those for the other 11 BAs are all 2.50 m.

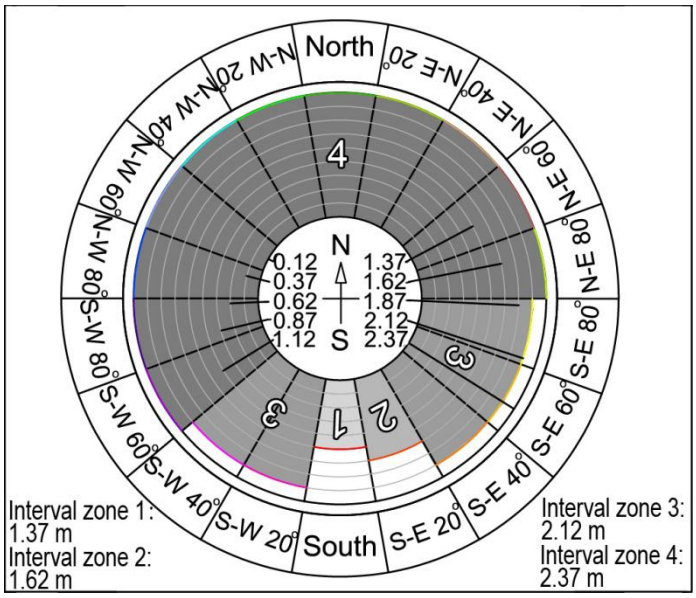

Fig. 6.25 Recommendation of the optimum shading depth to each building azimuth interval

6.9 Application of the research results

6.9.1 Definition of evaluation score of shading depth

To apply the research results, the Evaluation Score of Shading Depth (ESSD) was put forward in this work. According to the recommendation of the optimum SDs to the buildings with various BAs, the ESSD is defined as that it is used to assess the optimum level of a SD applied to building facing a certain direction by the value of score. The ESSDs assigned to the SD interval close to its optimal values for each BA are assumed to be 1. Furthermore, the

ESSDs assigned to the other SD intervals present descending trends at 0.1 increments, with values set apart from its optimum depicted in Fig. 6.26.

Regarding dwellings consisting of some stand-alone buildings, the equation (6.7) is formulated to calculate the average ESSD (Sa) for them.

$$S_a = \sum (SD \times ESSD) / \sum SD \qquad (6.7)$$

The construction approach of traditional dwellings in East and Central China complies with the professional standard of *Ying Zao Fa Yuan*, which leads to the components used in dwellings to be characterized by the modularization. Thus, the tilt angle, the shading type, window height above the floor, and window dimensions are very similar, and the ESSD is assumed to be suitable for each building in Sizhai village.

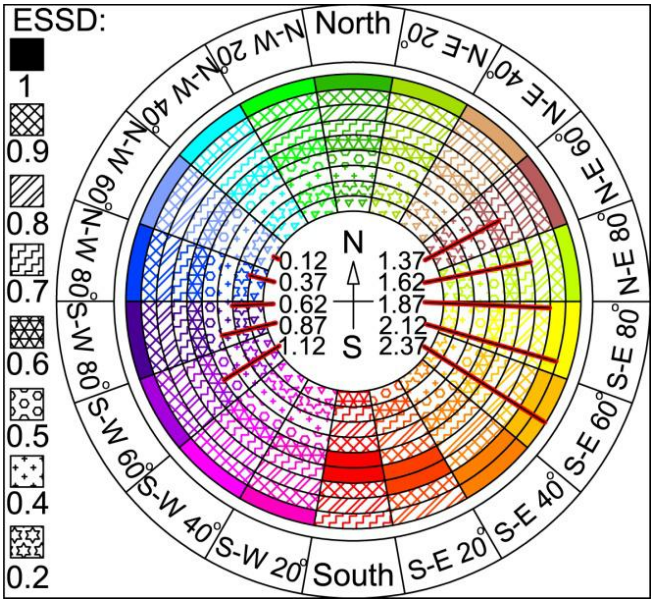

Fig. 6.26 Evaluation score of shading depth assigned to the 9 shading depth intervals corresponding to 18 building azimuths

6.9.2 Application of the evaluation score of shading depth to three courtyard dwellings

As shown in Table 6.4, three traditional dwellings in Sizhai are selected to estimate their ESSDs, in which the courtyard dwelling of Fa xiang ju (Fig. 6.27) is considered as the baseline case. The other two, case 1 (Shang xin ju) and case 2 (Xia men qian fan), within the same and with different BA comparing to the baseline case respectively, are chosen as the target buildings. The courtyard dwelling has comparatively complicated configuration, which results in the complex calculation of its ESSD. Therefore the building type of courtyard dwelling was chosen to conduct the calculation of ESSD for fully explanation.

Fig. 6.27 Three dwellings selected to assess their building energy saving potentials by the evaluation score of shading depth

The configurations of these three buildings with courtyard are quite complex, in order to explain the comparison procedures in detail. By using equation (6.7), the ESSDs of the three chosen dwellings are calculated, which are 0.77, 0.81 and 0.88 for the baseline case, the case 1 and the case 2, respectively. Thus, the dwelling with the highest energy saving potential is deemed to be the case 2, based on the evaluation parameter of SD. By repeating the previous procedures, the ESSD of each dwelling in the village can be obtained.

Table 6.4 Evaluation score of shading depths calculated for the three study dwellings

D	Fa xiang ju (Base case)	Shang xin ju (Case 1)	Xia men qian fan (Case 2)
Remote sensing images in G.E.			
BA	SE-20	SE-20 (the same with base case)	NW-60 (differing from base case)
SDs for three buildings	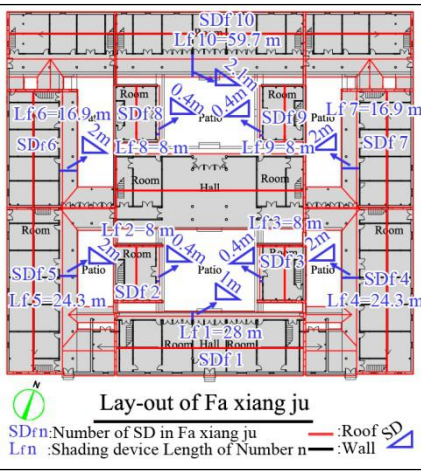	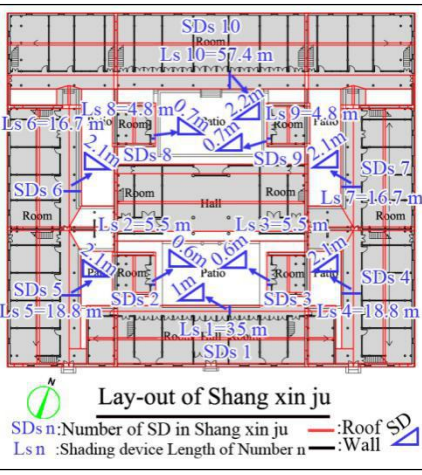	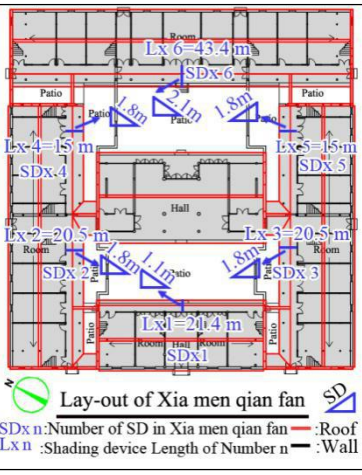
ES	0.77	0.81	0.88

Notes: 1. D represents designation; 2. ES represents ESSD.

6.10 Finding and discussion

This chapter focuses on the impacts of shading devices with different depths based on changes in building azimuths on the performances of indoor daylighting and air temperatures, as well as on building energy loads in the traditional dwellings. Taking into consideration the combinations of different shading depths and building azimuths, there are 180 test scenarios being simulated in several pieces of software. The evaluation parameters of the solar heat gain coefficient and mean shading-to-window ratio are used to assess the shading performances of shading devices by varying the building azimuth. Furthermore, the energy costs of artificial lighting and air conditioning were computed for each of the test scenarios.

(1) The solar heat gain coefficients are all inversely proportional to the shading devices length, and present a decreasing trend while being rotated from the S to N clockwise and anticlockwise if we maintain the same shading device depth.

(2) The mean shading-to-window ratios on both the summer solstice and on winter solstice increase with the shading depth increasing. On the summer solstice, the mean shading-to-window ratios for S and S-E 20 present larger fluctuations in comparison with the other alternatives.

(3) The annual reception amounts of direct radiation for south vary significantly with the building azimuth. In contrast, the dispersion of polylines for the diffuse radiation reception, is negligible. Regarding the total solar radiation reception, its correlation with shading depths increases is similar to that of the direct radiation reception.

(4) The dispersion of polylines and the mean indoor illuminance for the 18 building azimuths on the summer solstice and the on the winter solstice are both inversely proportional to shading depths. As for the differences, their dispersion of polylines in winter is greater than in summer, while the slopes of polylines in winter are lower than in summer.

(5) For a given shading device, the energy loads of artificial lighting present a descending trend while being rotated from the N to S-W 40 clockwise and anticlockwise. In addition, the 18 polylines are all presented the concave functions with a similar slope. The inflexion points for the most of polylines are at 1.87 of x-axis, after which the slopes of polylines start to become large.

(6) Under the condition of windows with the same shading devices, the slopes of polylines for the internal solar heat gains present an increasing trend while being rotated from the N to S-W 40 clockwise and anticlockwise. The internal solar heat gains for the 18 building azimuths are all the inversely proportional to shading depths. Thus, the longer shading depth contributes to more desirable thermal comfort in rooms.

(7) The mean diurnal indoor temperatures in the test scenarios for south and north are both generally lower than those for east and west during summer. In winter, the mean diurnal indoor temperatures in the test scenarios for south and southwest are comparatively high, and those for northeast are relatively low.

(8) The dispersion of the 18 polylines for the cooling loads, heating loads and the total energy consumption are all inversely proportional to the shading depth. Among the 18 polylines, the test scenario with N-W 80 presents the most dramatic variation in the total energy consumption, and the alternative with the slightest variation can be observed in the scenario facing N-E 20.

(9) The shading depths leading to the minimal total energy costs for S and S-E 20 are 1.37 m and 1.62 m respectively, and that for S-E 40, S-E 60, S-E 80, S-W 20 and S-W 40 are all 2.12 m. In addition, the optimum SDs recommended for the other 11 BAs are all 2.37 m.

To apply the research results, the Evaluation Score of Shading Depth was put forward in this work. Three traditional dwellings in Sizhai were selected to estimate their Evaluation Score of Shading Depths. Based on the calculated results, the dwelling with the highest energy saving potential was observed for the case 2. By repeating the previous procedures, the ESSD of each dwelling in the village can be obtained.

References

[1] Yilong Han, John E. Taylor, Anna Laura Pisello. Exploring mutual shading and mutual reflection inter-building effects on building energy performance [J]. *Applied Energy*, 2015, (10): 1-30.

[2] DESOGUS Giuseppe, CANNAS Leonardo Giuseppe Felice, SANNA Antonello. Bioclimatic lessons from Mediterranean vernacular architecture: The Sardinian case study [J]. *Energy and Buildings*, 2016, 129(6): 574-588.

[3] D. Connolly, H. Lund, B.V. Mathiesen, M. Leahy. The first step towards a 100% renewable energy-system for Ireland [J]. *Appl. Energy*, 2011, 88(2): 502-507.

[4] U. Berardi, A. Ghaffarian Hoseini, A. Ghaffarian Hoseini. State-of-the-art analysis of the environmental benefits of green roofs [J]. *Appl. Energy*, 2014, 115: 411-428.

[5] J. Široký, F. Oldewurtel, J. Cigler, S. Prívara. Experimental analysis of model predictive control for an energy efficient building heating system [J]. *Appl. Energy*, 2011, 88(9): 3079-3087.

[6] T. Hong, S. Chou, T. Bong, Building simulation: an overview of developments and information sources [J]. *Build. Environ.*, 2000, 35(4): 347-361.

[7] Building Energy Conservation Research Center of Tsinghua University. The annual development report of China building energy conservation [R]. Beijing: China building industry press, 2012.

[8] ZHAO L L. The current situation analysis of building energy consumption in China [J]. *Housing and Real Estate*, 2016, 30(10): 25.

[9] WANG X, REN H, CAI W W. The change trend and influence factors of time series of energy consumption in China [J]. *Journal Heating Ventilating and Air conditioning*, 2017, 47(11): 21-26, 93.

[10] Lu J F. The development inevitable trend of China's low carbon building and its future prospects [J]. *Productivity Research*, 2013(12): 72-74.

[11] Kirimtat, A., Koyunbaba, B.K., Chatzikonstantinou, I., Sariyildiz, S.. Review of simulation modeling for shading devices in buildings [J]. *Renew. Sustain. Energy Rev.*, 2016, 53: 23-49.

[12] ASHRAE Handbook. Fundamentals. Atlanta: American Society of Heating [J]. *Refrigeration and Air-Conditioning Engineers*, 1997.

[13] Ramkishore Singh, I.J. Lazarus, V.V.N. Kishore. Uncertainty and sensitivity analyses of energy and visual performances of office building with external venetian blind shading in hot-dry climate [J]. *Applied Energy*, 2016, 184(10):155-170.

[14] W. O'Brian, A. Athienitis, T. Kesik. Thermal zoning and inter zonal airflow in the design and simulation of solar houses: a sensitivity analysis [J]. *J. Build. Perform. Simul.*, 2011,4: 239-256.

[15] J. Apte, D. Arasteh, Y.J. Huang. Future Advanced Windows for Zero-Energy Homes. ASHRAE Transactions 109 Part 2 (2003). Lawrence Berkeley National Laboratory Report LBNL-51913.

[16] A. Mavrogianni, M. Davies, J. Taylor, Z. Chalabi, P. Biddulph, E. Oikonomou, P.Das, B. Jones. The impact of occupancy patterns: occupant-controlled ventilation and shading on indoor overheating risk in domestic environments [J]. *Build. Environ.*, 2014, 78: 183-198.

[17] J. Karlsson, B. Karlsson, A. Roos. Control strategies and energy saving potentials for variable transmittance windows versus static windows, in: Proceedings of Euro sun, 19-22 June, Copenhagen, Denmark, 2000.

[18] R. Sullivan, F. Beck, D. Arasteh, W. Selkowitz. Energy Performance of Evacuated Glazings in Residential Buildings. Report LBL-37130, Lawrence Berkeley Laboratory, 1995.

[19] S. Firlag, M. Yazdanian, C. Curcija, C. Kohler, S. Vidanovic, R. Hart, S. Czarnecki. Control algorithms for dynamic windows for residential buildings [J]. *Energy Build.*, 2015, 109: 157-173.

[20] G. Kim, H.S. Lim, T.S. Lim, L. Schaefer, J.T. Kim. Comparative advantage of an exterior shading device in thermal performance for residential buildings [J]. *Energy Build.*, 2012, 46: 105-111.

[21] L. Vanhoutteghem, S. Svendsen, Modern insulation requirements change the rules of architectural design in low-energy homes [J]. *Renew. Energy*, 2014, 72: 301-310.

[22] M.C. Dubios. Solar Shading and Building Energy Use, Lund University, Lund, 1997.

[23] Goyal S, Ingley HA, Barooah P. Occupancy-based zone-climate control for energy-efficient buildings: complexity vs. performance [J]. *Appl. Energy*, 2013, 106: 209-221.

[24] S. Citherlet, J.A. Clarke, J. Hand. Integration in building physics simulation [J]. *Energy Build.*, 2001, 33: 451-461.

[25] F.H. Abanda, L. Byers. An investigation of the impact of building orientation on energy consumption in a domestic building using emerging BIM (Building Information Modelling) [J]. *Energy*, 2016, 97(2): 517-527.

[26] Marco Manzan. Genetic optimization of external fixed shading device [J]. *Energy and Buildings*, 2014, 72: 431-440.

[27] Sonia Longo, Francesco Montana, Eleonora Riva Sanseverino. A review on optimization and cost-optimal methodologies in low-energy buildings design and environmental considerations [J]. *Sustainable Cities and Society*, 2019, 45 (1): 87-104.

[28] Kun Lai, Wen Wang, Harry Giles. Solar shading performance of window with constant and dynamic shading function in different climate zones [J]. *Solar Energy*, 2017, 147(3): 113-125.

[29] Li Li, Ming Qu, Steve Peng. Performance evaluation of building integrated solar thermal shading system: Building energy consumption and daylight provision [J]. *Energy and Buildings*, 2016, 113(12):189-201.

[30] Tanja Siems, Katharina Simon, Maria Wall. State-of-the-Art of Education on Solar Energy in Urban Planning, Part I: Approaches and Methods in Education, Katharina Simon, University of Wuppertal, Institute for urban design and urban research, 2017, 05: 67.

[31] Yuan Gao, Jianfei Dong, Olindo Isabella, Rudi Santbergen, Hairen Tan, Miro Zeman, Guoqi Zhange. A photovoltaic window with sun-tracking shading elements towards maximum power generation and non-glare daylighting [J]. *Applied Energy*, 2018, 228 (7): 1454-1472.

[32] Chopra A. Introduction to Google sketchup. John Wiley & Sons; 2012.

[33] Ignacio Acosta, Carmen Munoz, Miguel Angel Campano, Jaime Navarro. Analysis of daylight factors and energy saving allowed by windows under overcast sky conditions [J]. *Renewable Energy*, 2015, 77(5):194-207.

[34] Jinkyun Cho, Changwoo Yoo, Yundeok Kim. Viability of exterior shading devices for high-rise residential buildings: Case study for cooling energy saving and economic feasibility analysis [J]. *Energy and Buildings*, 2014, 82(8): 771-785.

[35] F. Mazzichi, M. Manzan. Energy and daylight interaction in offices with shading devices, in: Proc. of 1st IBPSA Italy Conference, Bolzano, IT, 2013,

[36] Reeves T, Olbina S, Issa R. Validation of building energy modeling tools: Ecotect™, Green Building Studio™ and IES™. In: Laroque C, Himmelspach J, Pasupathy R, Rose O, Uhrmacher AM, editors. Proceedings of the 2012 Winter Simulation Conference. Berlin: Germany; 2012.

[37] Ana I. Palmero-Marrero, Armando C. Oliveira. Effect of louver shading devices on building energy requirements [J]. *Applied Energy*, 2010, 87(6): 2040-2049.

[38] Maamari F, Andersen M, de Boer J, Carroll W, Dumortier D, Greenup P. Experimental validation of simulation methods for bi-directional transmission properties at the daylighting performance level [J]. *Energy and Buildings*, 2006, 38(7): 878-89.

[39] C. Brunsgaard, M.-A. Knudstrup, P. Heiselberg. Occupant experience of every day life in some of the first passive houses in Denmark [J]. *Hous. Theory Soc.*, 2012, 29: 223-254.

[40] Hashemi, A., Khatami, N.. Effects of solar shading on thermal comfort in low-income tropical housing [J]. *Energy Proc.*, 2017, 111: 235-244.

[41] I.H. Yang, E.-J. Nam. Economic analysis of the daylight-linked lighting control system in office buildings [J]. *Sol. Energy*, 2012, 84: 1513-1525.

[42] A. Atzeri, F. Cappelletti, A. Gasparella. Internal versus external shading devices performance in office buildings [J]. *Energy Procedia*, 2014, 45: 463-472.

[43] GUO L M. Calculation and distribution of solar radiation on the wall in Zhejiang Province [J]. *Energy Engineering*, 1984, (4): 27-30.

[44] Jensen SO. Validation of building energy simulation programs: a methodology [J]. *Energy and Buildings*, 1995, 22: 133-44.

[45] Ryan EM, Sanquist TF. Validation of building energy modeling tools under idealized and realistic conditions [J]. *Energy and Buildings*, 2012, 47(4): 375-82.

[46] Li Wenjie. A Thesis Submitted to Chongqing University in Partial Fulfillment of the Requirement for the Degree of Doctor of Engineering [D]. Chongqing: Chongqing University, 2010: 3.

Chapter 7

Impact of windows with various window-to-wall ratio and building azimuth combinations on the energy consumption

7.1 Introduction

7.1.1 Motivation

Indoor environmental quality (IEQ) is an important factor that impacts occupants' comfort and well-being [1]. To compensate the interiors' lighting, approximately 19% of electricity is consumed by the artificial lighting worldwide, which accounts for 2.4% of the total primary electricity consumption [2]. For adjusting the indoor temperature, the Air Conditioners (AC) used to remain internal spaces cool or warm are responsible for about 40% of the global building energy consumption [3].

The summation of building area in terms of the all rural residences in China is roughly 24 billion m^2, accounting for over 60% of the national total [4]. Building energy is primarily consumed for heating, cooling, lighting, cooking, and domestic appliance utilizing in the rural residences, of which ACs (inclusion of heating and cooling) consume approximately 20% of the total building energy use in China [5]. Regarding the energy cost of artificial lighting, it is responsible for 7~8% [5]. Taking into account the energy consumption of electric ventilator and humidifier, etc., the energy used for enhancing the indoor thermal and visual comforts accounts for approximately 30% of the national building energy consumption [6].

To address these issues, many researches have focused on how to create the energy efficient building with high comfort level by means of the passive strategy [7], suitable building material [8], smart building automation system [9], advanced building information technology [10]. The indoor thermal and visual comforts are greatly related to the magnitude of solar radiation passing through the transparent parts of building [11]. Solar heat gain can improve the thermal comfort level in the internal space during cold months, which contributing to reduction in heating demand. Moreover, using the passive strategy of natural daylighting not only achieves the building energy saving, but contributes to improvement in the productivity and visual comfort for occupants [12]. However, design of buildings with thermal and visual comforts requires the analysis of building components. The control of glazing proportion for the facade is a technique, aiming at allowing a proper amount of solar radiation and airflow penetrating into the buildings. As obvious, WWR has a significant influence on the indoor daylighting and air temperature, and affects the building energy consumption [13]. Additionally, the fenestration system possesses a function of offering the exterior view [14]. However, building integrated with a large glazing will results in some side effects, such as increase in the energy load for space cooling during summer and reduction in the insulation property of envelope [15]. Besides, window is usually regarded as the main passage for heat loss during winter, since its heat transfer coefficient is relatively high in comparison to the other building components under interaction with the exterior, such as roof and external wall [16]. Therefore, the fenestration system needs to be designed in well-dimensioned conditions, in order to

provide a comfortable external view, as well as enhance the building energy efficiency. Furthermore, the WWR is determined in the first stage of architecture design based on an energy-wise approach usually, which is so important that this selection needs to be made carefully.

7.1.2 Scientific originality

Since the building orientation determination for the traditional dwelling complies with the rule of "adaptation to building site conditions" in East and Central China, the BAs vary considerably depending on the building site. The present research mainly focuses on the impacts that the windows facing a limited quantity of orientations or based on changes in WWR at large increments have on the energy consumption and indoor daylighting performances, while few studies are on the basis of the multiple combinations of WWR and orientation [17-18]. What's more, the related researches, in particular with regards to the impact of window on the energy consumption, have often been neglected to get carried out in the traditional buildings up to now [19].

Based upon the afore-mentioned discussion, the originality of this study is to estimate the performances of solar energy management for windows installed in the traditional dwellings located in the research region og this work, which experiences the harshly hot climates over a long period of time. Rather than focus on the performances of scarce evaluation parameters, the solar heat gain, solar radiation reception, indoor daylighting and thermal conditions, as well as energy behaviors were analyzed step by step. After coupling the windows based on changes in WWR with the diverse Building Azimuths (BA) in the test scenarios, the total energy consumption including artificial lighting and AC is proven to vary under reasonable assumptions. Then the proposed models of windows with various WWR-BA combinations can be used to explore the optimum glazing ratios for various BAs, in consideration of the energy consumption and indoor satisfactory comfort conditions. Also, the proposed WWR-BA combinations can be regarded as a new method to determine the best final designs of WWRs for the traditional dwellings with different building orientations. Furthermore, an evaluation criterion based on the energy saving potential and visual comfort was proposed. Then it was used to assess the energy saving potentials of three given specific dwellings to prove the applicability of the proposed evaluation parameter for the existing residences.

On the other hand, until very recently, extensive attention, in terms of the energy behavior impacted by WWR, has been given to the contemporary buildings, rather than the traditional buildings. Therefore, the traditional dwellings that were adopted as case studies in this chapter, can supply some new body of knowledge on the WWR, to fill in the gap in this field. The research methodology can be used in any country to explore the optimum WWRs for various building orientations, by using the corresponding geometric model and local climate data instead of the original ones used in simulation.

7.1.3 Research purpose

In this chapter, a small-sized traditional dwelling was taken as study building, situated in the Sizhai village, Zhuji city, Zhejiang Province, China. Since the thermal and visual comfort levels in the internal spaces can be enhanced by choosing appropriate WWRs [20], this study aims at providing some advice on WWR decision to both newly-built construction and retrofit of rural residences in the hot summer and cold winter climate zone of China. Moreover, the optimization of WWRs corresponding to different building orientations in this work was discussed in order to achieve a deeper energy saving.

7.2 Research process and research flow

Simulate the Building models with different BA-WWR combinations, giving a total of 162 simulation runs. The evaluation parameters of solar heat gain, air temperature, solar radiation reception, visual comfort rate and energy consumption were employed to evaluate the effects of WWR variations on the indoor environments and energy requirements in the test scenarios facing different orientations.

The ArchiWIZARD is a piece of building energy assessment software integrated with the Energy Plus plug-in, especially worked for the BIM models [21]. As obvious, the solar heat gain and solar radiation reception will influence the indoor air temperatures and illuminance, respectively [22]. To this end, the ArchiWIZARD integrated with the Energy Plus in-plug, characterized by time saving during running, is suitable to be adopted in this work.

Besides, the other two simulation tools of VELUX Daylight Visualizer 2 and Ecotect 2012 were used in this work. The VELUX Daylight Visualizer 2 [23] is a professional lighting simulation tool for the analysis of daylight conditions in buildings, which was used to analyze the visual comfort rate in each of the test scenarios in this work. Besides, the Ecotect 2012 [24] is a piece of whole building simulation tool, which can be used to predict the thermal, acoustic and visual performances in buildings. The thermal performance analysis method in this tool based on the Chartered Institution of Building Services Engineers (CIBSE) is fitted to perform indoor air temperature simulation in this chapter. Since the indoor illuminance and air temperature can impact the energy demands of artificial lighting and AC [25], to research their correlations, the software of ArchiWIZARD (version 3.1.1) was adopted.

Aiming at verifying the accuracy of computational results from the ArchiWIZARD, the data were compared with those from the real energy bills. In addition, combining the total energy consumption (including AC and lighting) with the daylighting quality, the compromised WWRs are recommended for each BA. In addition, an evaluation parameter of Evaluation Score of Window-to-Wall Ratio (ESWWR) was proposed to evaluate the energy saving

potential of current dwellings in Sizhai. To facilitate understanding the research methods framework, it is presented in Fig. 7.1.

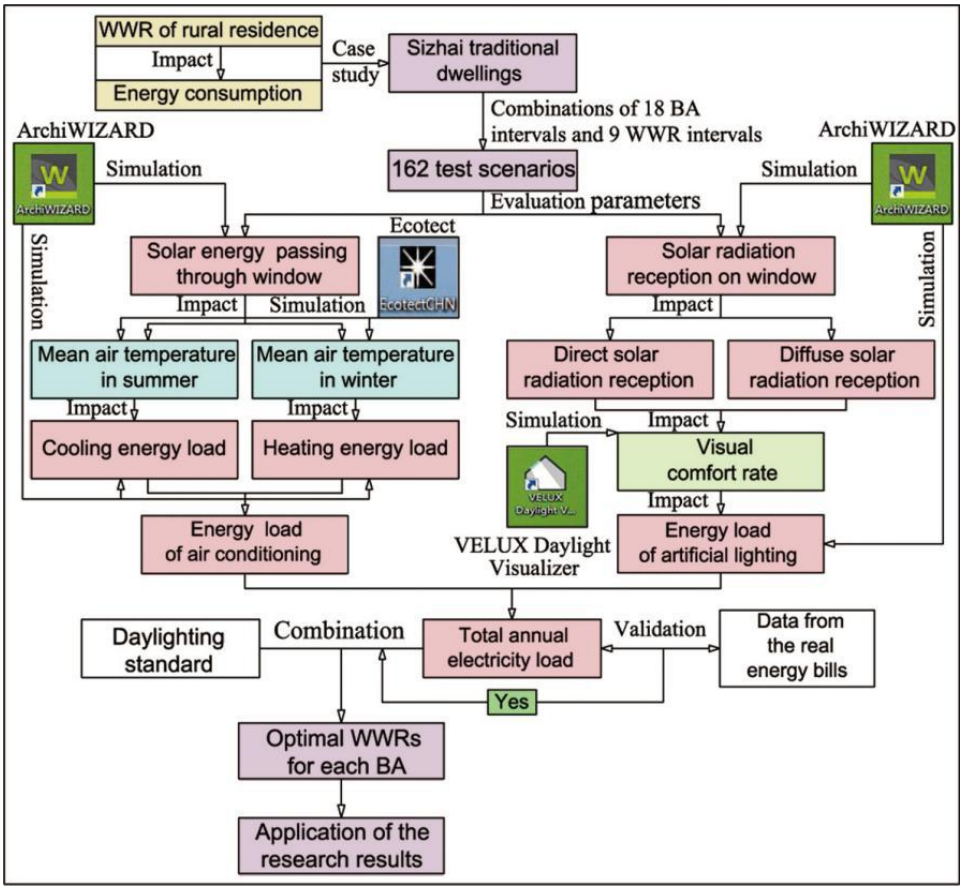

Fig. 7.1 Research methods framework

7.3 Impact of window-to-wall ratio on the indoor temperature and air conditioning energy consumption based on changes in building azimuths

WWR is a driving factor that affects the solar heat gain of internal space, as well as indoor temperature [26]. Furthermore, WWR is an important variable affecting energy performance in a building, such as, the building's heating, cooling, and lighting, as well as relating it to the natural environments. On the contrary, the window is the important factor resulting in the indoor energy leak, due to with high heat transmission.

By using the Ecotect 2012, the indoor temperatures in each of the test scenarios were simulated, respectively. Furthermore, the ArchiWIZARD was adopted to compute the cooling and heating loads, as well as the total energy consumption of space heating and space cooling (i.e., the energy consumption of AC, due to both space heating and space cooling achieved by AC in East and Central China) throughout the year, in order to conclude the impact rules of windows with different WWR-BA combinations on the energy consumption of AC.

7.3.1 Energy Differences between solar heat gains and indoor heat losses passing through windows with different window-to-wall ratio and building azimuth combinations

7.3.1.1 Energy differences between solar heat gains and indoor heat losses in winter

The solar heat gain of internal space is mainly yielded from the solar radiation penetrating glass, resulting in the change trends and rules of solar heat gains for all BAs, with increasing WWR, to be similar. As shown in Fig. 7.2, the total solar heat gains for 18 BAs in winter (i.e., January) are all directly proportional to the increase in WWRs, because a greater WWR leads to the room obtaining more solar contribution. The slopes of polylines present increasing trend rotated from the N to S-W 20 clockwise and anticlockwise (see cycle legend in Fig. 7.2). In other words, the solar heat gains at a series of south orientations are more susceptible to the WWR variations than those for north, which could be a result of availability of solar radiation, covering the windows of test scenarios facing south, for a longer period than those facing north. The polylines' dispersion of solar heat gains exists slight differences, as the values at x-axis are low. With WWR increasing, the dispersion increases gradually, which means that the impact of BA on solar heat gain shows strong dependency on the increase of glazing area.

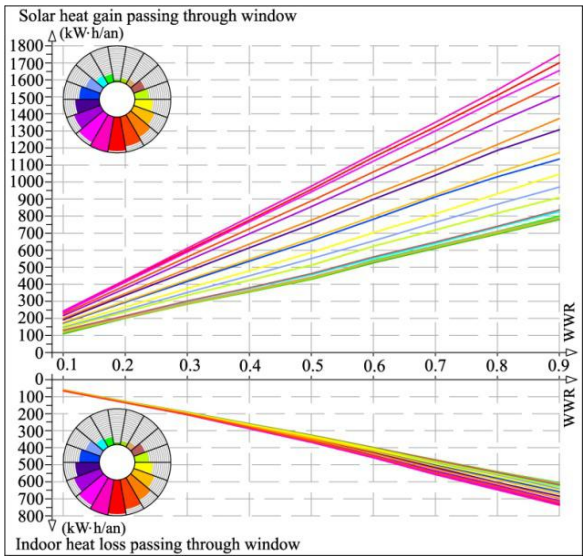

Fig. 7.2 Solar heat gains and indoor heat losses passing through windows in winter

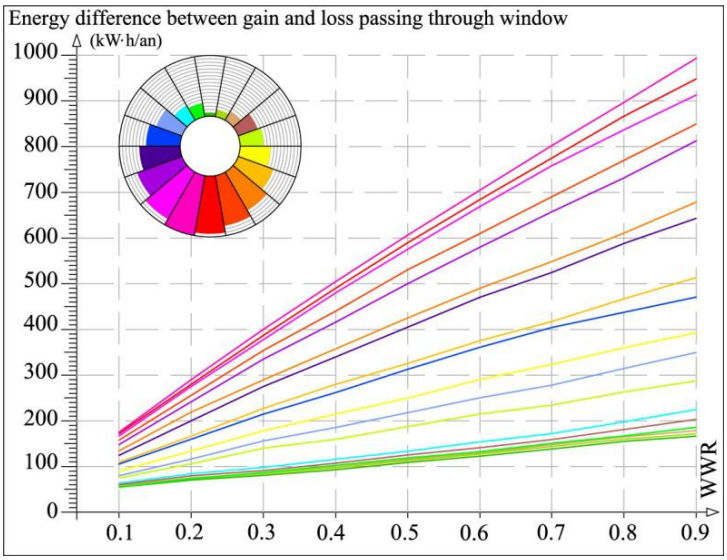

Fig. 7.3 Energy differences between solar heat gains and indoor heat losses passing through windows in winter

In contrast, glazing is particularly leading to large heat loss in a building, since it is characterized by comparatively less thickness, as well as high heat transfer coefficient and air leakage (infiltration), compared to wall [15]. As shown in Fig. 7.2, the total indoor heat losses passing through windows for the 18 BAs in January are all directly proportional to the WWRs. In comparison to magnitude of solar heat gain, the values of indoor heat losses

are comparatively low, which is helpful for maintaining the indoor temperatures stable in winter. The energy differences between solar heat gain and indoor heat loss passing through windows are shown in Fig. 7.3. The polylines' distribution characteristics of energy difference in January are consistent to those of solar heat gain.

7.3.1.2 Energy differences between solar heat gains and indoor heat losses in summer

As shown in Fig. 7.4, the total solar heat gains for the 18 test scenarios in summer (i.e., from June to August) are all directly proportional to the WWRs increasing. Although the orbit of sun is symmetrical with north-south axis, solar radiation level is constantly changing in the sky, which is impacted by the cloudage, dust level in air and air humidity, etc. In Sizhai, the total solar radiation level for the second half day during one year is generally greater than that for the first half day throughout the year [27]. The slopes of polylines show increasing trend rotated from the N to S-W 80 clockwise and anticlockwise, which means that the internal solar heat gains at a series of east orientations are less than west orientations.

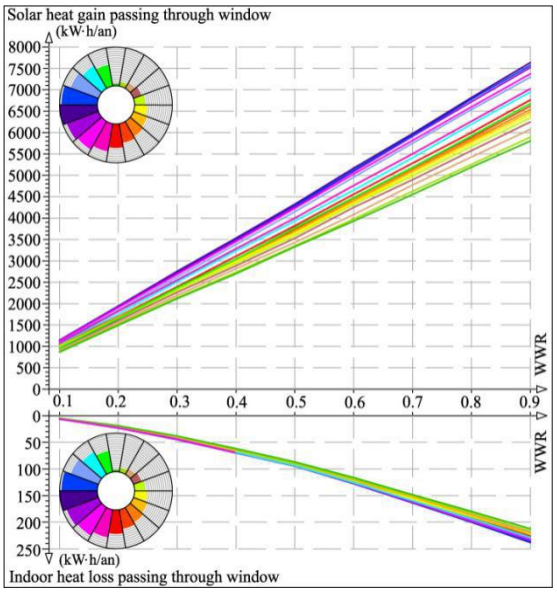

Fig. 7.4 Solar heat gains and indoor heat losses passing through windows in summer

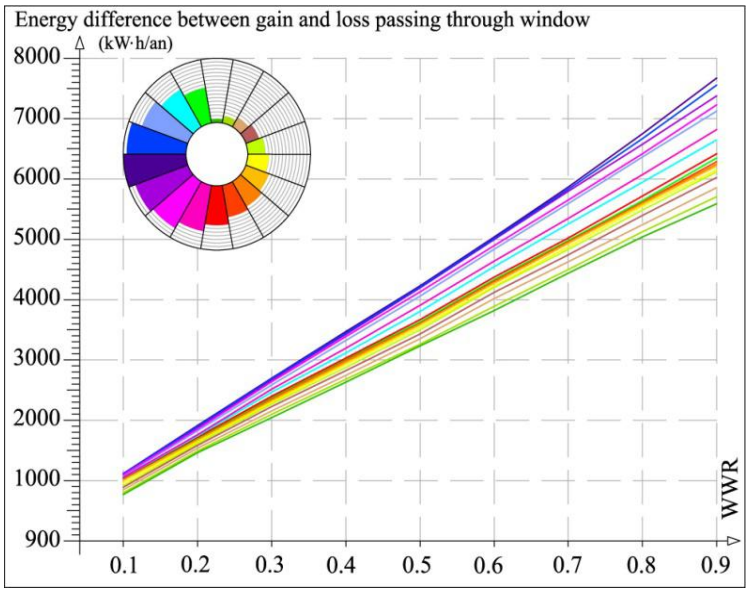

Fig. 7.5 Energy differences between solar heat gains and indoor heat losses passing through windows in summer

In comparison with winter (Fig. 7.3), the magnitudes of energy differences between solar heat gains and indoor heat losses passing through windows in summer (Fig. 7.5) are much greater. Furthermore, it can be seen from Fig. 7.5 that the polylines' dispersion of energy differences, between solar heat gain and indoor heat loss passing through windows, increases when the WWR grows. Furthermore, the energy differences are very close to the solar heat gains in each of the test scenarios, due largely to the heat losses with relatively low magnitudes compared to solar contributions.

7.3.2 Impact of windows with different window-to-wall ratio and building azimuth combinations on the mean indoor temperatures

When the windows are in a closed condition (i.e., heat convection is blocked), there are two ways that the outdoor climate impacts indoor temperatures, namely the heat transmission by the temperature difference (i.e., heat conduction) and solar radiation (i.e., heat radiation). As the BA is changed, a different facade will face the sun. The capacity of a building to receive the solar heat relies heavily on the glazing system and the way interacting with the sun [28]. Under the condition of walls with the same WWR, the heat transfer due to temperature difference between the exterior and interior, for a window facing any direction is almost identical, but that by solar radiation varies greatly depending on the BA.

The mean indoor temperatures during winter (i.e., January) and summer (i.e., from June to August) generated by Ecotect 2012 are adopted as evaluation parameter to assess the indoor thermal performances for each of the test scenarios. The mean outdoor temperatures in these two periods of time were 5.13 ℃ and 30.34℃ from simulation, respectively.

7.3.2.1 Mean indoor temperature in each of the test scenarios during winter

As shown in Fig. 7.6, a similar variation tendency is observed for the mean indoor temperatures in comparison to the solar heat gains, because the solar contribution is a driving factor that keeps the indoor space warm in winter. The slopes of polylines present increasing trend rotated from the N to S-W 80 clockwise and anticlockwise, of which the slopes of polylines for south are greater than those for north.

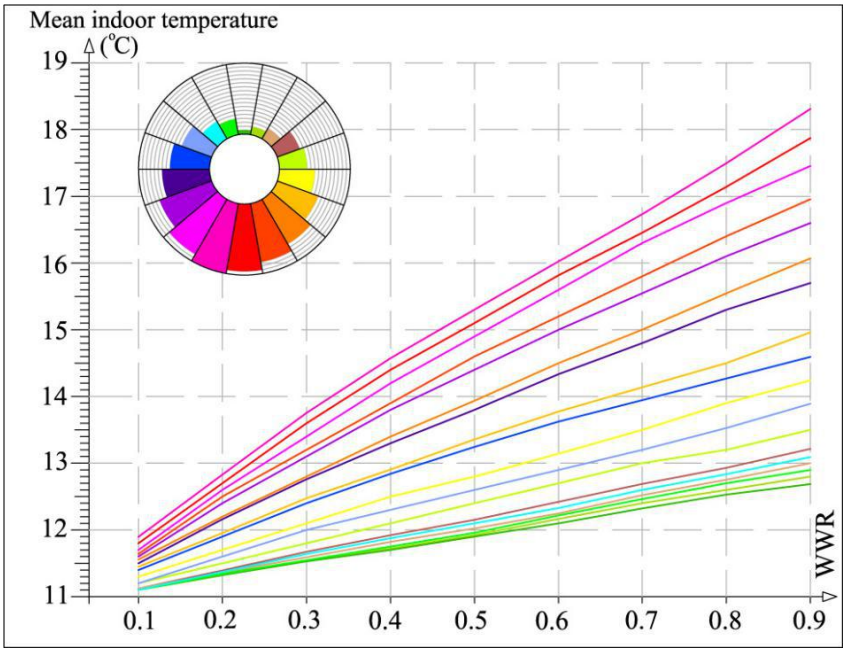

Fig. 7.6 Mean indoor temperatures for windows with different window-to-wall ratio and building azimuth combinations in winter

The mean indoor temperatures in southerly oriented test scenarios are generally greater than those in northerly oriented alternatives, thanks to the north facades without any availability of solar coverage in winter. Moreover, both the indoor temperatures and polylines' dispersion for south monotonically increase with WWR increasing, while those for north are kept relatively stable. With regard to 0.1 of WWR, the maximum difference of mean temperature between S-W 20 and N is negligible (0.9 ℃), but the value increases to 5.6 ℃ at 0.9 of x-axis.

7.3.2.2 Mean indoor temperature in each of the test scenarios during summer

By drawing an analogy between Fig. 7.6 with Fig. 7.7, the maximum differences of mean indoor temperatures between S-W 80 and N in summer at 0.1 and 0.9 of x-axis are 0.5 ℃ and 3.1 ℃ respectively, both lower than those in winter. This is primarily because that the solar shading performance of roof eave is more outstanding in summer featured by high solar altitudes, which is helpful for intercepting the solar radiation effectively.

The mean indoor temperatures for west are higher than east, due to the period of time for afternoon with higher solar radiation levels in Sizhai. Thanks to existing a wider-ranging outdoor temperature difference in summer, the variation amplitudes of mean indoor temperatures (7 ℃ on average for the 18 BAs) by varying WWR from 0.1 to 0.9 are larger in comparison to winter (3 ℃ on average for the 18 BAs), regardless of BAs. In other words, the mean indoor temperatures are more sensitive to variations in WWR during summer. Furthermore, the mean indoor temperatures directly proportional to the WWR, since greater glazed area in the wall can allow more solar radiation to penetrate into the internal spaces.

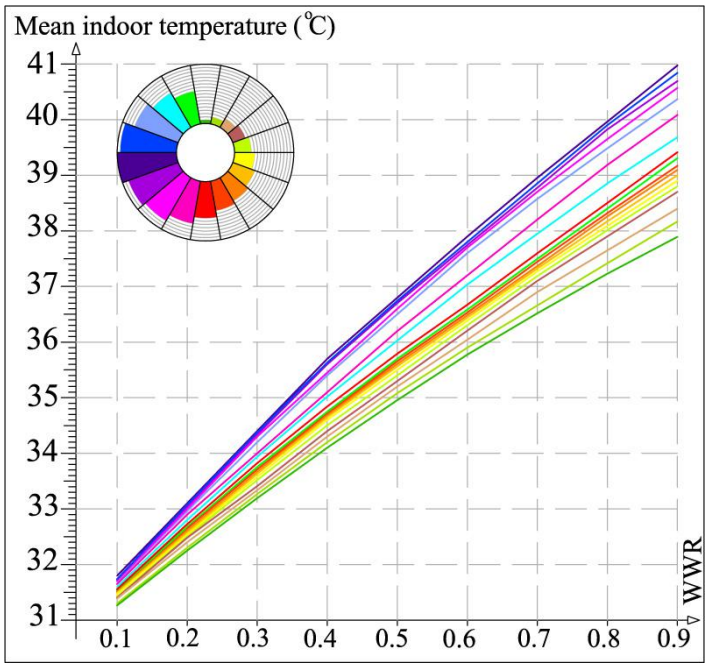

Fig. 7.7 Mean indoor temperatures for windows with different window-to-wall ratio and building azimuth combinations from June to August

7.3.3 Impact of windows with different window-to-wall ratio and building azimuth combinations on the air conditioning energy consumption

During AC in operation, its action-points of heating and cooling temperatures should be controlled in appropriate scopes. The optimum scopes of AC action-points range from 26 ℃ to 28 ℃ during summer and from 18 ℃ to 20 ℃ during winter [29]. According to the recommended AC action-points and taking into consideration the habit of temperature setting for AC by the occupants, the AC action-points were assumed to be 27 ℃ and 18 ℃ in the simulation for space heating and cooling, respectively.

Furthermore, because the active system used for both cooling during summer and heating during winter for the internal spaces is AC in East and Central China, the electricity from power grid was chosen as the energy supply source in the simulation throughout the whole year. In consideration of the air-conditioned conditions and the occupancy schedules for various rooms, the setting parameters in the building energy consumption simulation need to be adjusted for reduction in the bias error of computational results.

Since generally only bedrooms are equipped with AC in the Sizhai traditional dwellings, whose building area accounts for approximately 33% of a suite, the air-conditioned building area of the middle suite was set at 13.2 m^2 and that of the other four were all set at 7.99 m^2. Due to each suite being occupied by a small family with an average of two or three people, the population density of the bedroom was set at 0.221 in the simulation. Simultaneously, the probability of all five suites being simultaneously air-conditioned was set at 80%.

In addition, the schedule assigned to run the air conditioning in the test scenarios during weekdays was assumed to be 7 hours daily, beginning at 22:00 p.m. and ending at 5:00 a.m. of the next day, accounting for a 29.17% of the whole day. Since the air temperatures are comparatively low during the first half day in summer, and the occupants' daily schedule is postponed in winter, the time of air conditioning in operation during weekends was assumed to be 15 hours daily, beginning at 14:00 p.m. and finishing at 5:00 a.m. of the next day, which accounts for 62.5% of the whole day.

7.3.3.1 Energy consumption in each of the test scenarios during winter

As shown in Fig. 7.8, the heating loads for N, N-W 20°, N-E 20° and N-E 40° show to be kept increasing dependency upon the increase of WWR. While for the other orientations, the polylines firstly decrease and then increase with the WWR increasing, which with the obvious inflection points can be observed. The inflection points for south and west are observed at 0.8 of x-axis in general. The values of inflection points at x-axis present decreasing trend rotated from N-W 60 and S-E 60 to N clockwise and anticlockwise, respectively. Among the 18

polylines, the most dramatic and slight variations in the energy loads by varying WWR from 0.1 to 0.9 occur in the test scenarios with S-W 80 and N-E 80 respectively, 46.3 kW·h/an and 3.7 kW·h/an.

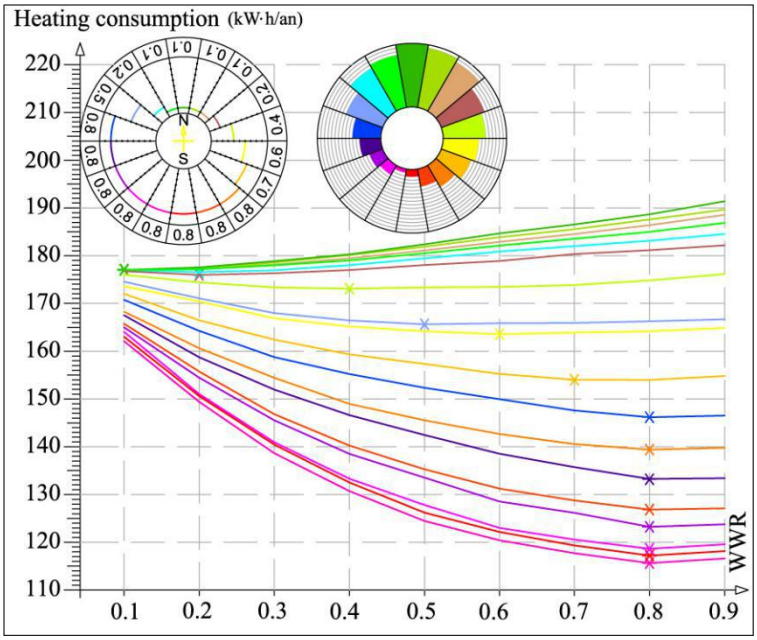

Fig. 7.8 Heating energy consumption for windows with different window-to-wall ratio and building azimuth combinations

7.3.3.2 Energy consumption in each of the test scenarios during summer

In comparison with the heating consumption in winter, the cooling consumption in the test scenarios during summer are much greater (Fig. 7.9), since Sizhai experiences a long summer period characterized by harshly hot weather conditions.

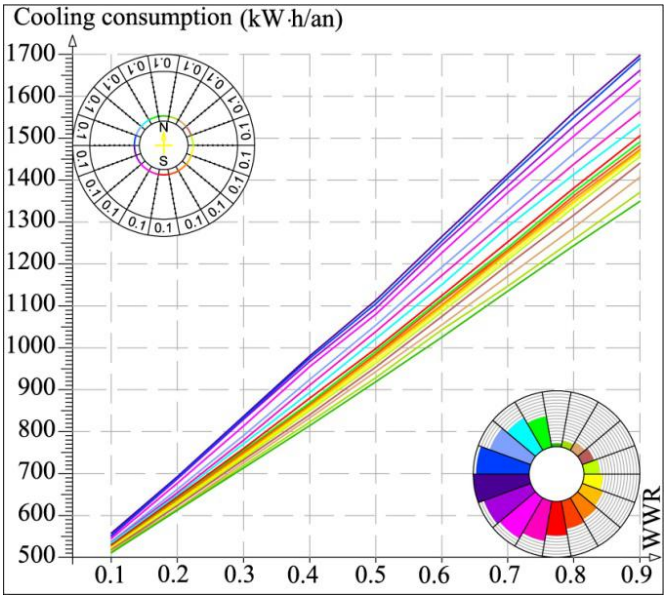

Fig. 7.9 Cooling energy consumption for windows with different window-to-wall ratio and building azimuth combinations

The polylines' dispersion of cooling consumption increases with varying window size, which is consistent with that of the mean indoor temperature. As WWR is equivalent to 0.1, the maximum difference of cooling load among the 18 polylines is 46 kW·h/an, while the difference increases to 346 kW·h/an at 0.9 of x-axis. Moreover, the slopes of polylines show an increasing trend rotated from the N to S-W 80 clockwise and anticlockwise. Furthermore, the test scenarios with S-W 80 and N have the most dramatic and slight variations in the total energy loads (1131 kW·h/an and 829 kW·h/an), respectively. Regarding the optimal WWRs, all the lowest cooling costs occur in the test scenarios with 0.1 of WWR.

7.3.4 Total energy consumption of air conditioning including space cooling and space heating

For any given value of WWR, the magnitude order of the total energy consumption of AC including heating and cooling for 18 BAs is distinct from both heating consumption and cooling consumption, with the sequence west, east, south and north as shown in Fig. 7.10.

Due largely to the dwellings in Sizhai belonged to the cooling-load dominated buildings, the increase in cooling consumption is greater than the reduction in heating consumption with WWR increasing. Therefore, the total energy consumption of AC for the 18 BAs is all directly proportional to the WWR. According to the distribution of polylines, the energy consumption of AC becomes sensitive to BA change with WWR increasing. Among the 18 polylines, the maximum differences at 0.1 and 0.9 of x-axis are 32 kW·h/an and 324 kW·h/an, respectively.

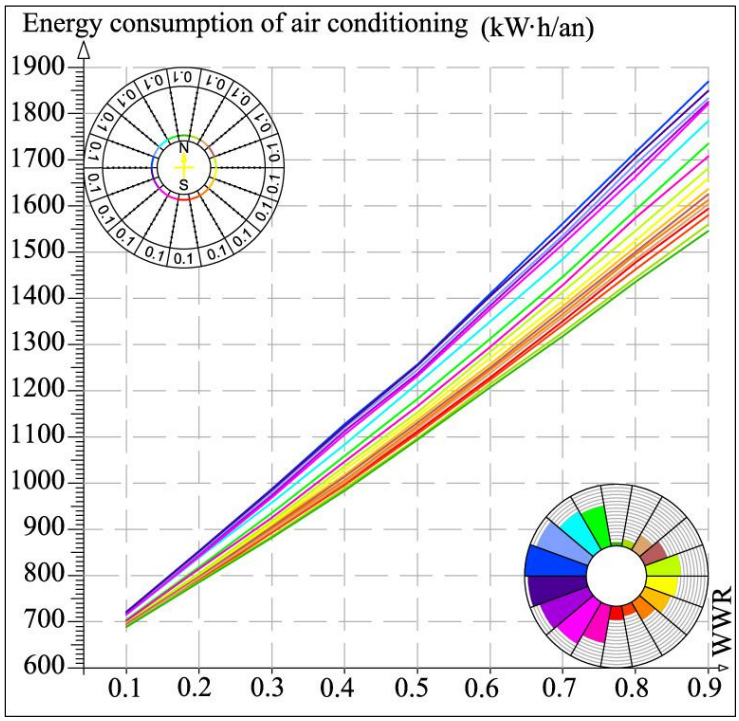

Fig. 7.10 Energy consumption of air conditioning for windows with different window-to-wall ratio and building azimuth combinations

The minimum energy consumption is observed for the test scenarios facing north, due to less solar coverage on its glazing. Furthermore, the energy consumption in southerly orientated test scenarios is lower than that in easterly orientated alternatives, since summer with high solar altitudes leads to little or no sunlight covering on the south-facing facades for longer period of time. In contrast, the internal spaces in southerly oriented test scenarios can yield a great quantity of solar heat in winter featured by low solar altitudes.

7.4 Impact of window-to-wall ratio on the solar radiation reception and energy consumption of artificial lighting based on changes in building azimuth

The visual comfort of internal spaces is receiving increasing attentions as the environmentally friendly buildings become popular [30]. Using optimal WWR can reduce the energy consumption of artificial lighting, because the illumination levels of interiors are kept within a desirable range with no or little glare [31].

Building envelope is comprised of the opaque and transparent elements, of which the glazing parts are the channels allowing the daylight to penetrate inside. ArchiWIZARD was used to simulate the solar radiation reception level of windows installed in the test scenarios, which is a major factor that has significant impact on the internal daylighting performance [32]. Based on the simulation results, another piece of software of VELUX Daylight Visualizer 2 was adopted to continue to analyze the indoor visual comfort rates and change trends. The energy requirement of artificial lighting varies greatly depending on the indoor natural daylight level [33]. To this end, the ArchiWIZARD was adopted again to compute the energy consumption for each of the test scenarios.

7.4.1 Impact of windows with different window-to-wall ratio and building azimuth combinations on the solar radiation reception

Solar radiation is a perpetual source of natural energy that has a great potential for a wide variety of applications, since it is accessible and abundant. Solar radiation reception is a relatively common parameter to estimate the solar control capacity of building component [34]. The solar radiation is consisted of direct radiation and diffuse radiation. As presented in Fig. 7.11, the direct radiation receptions of windows for west are generally greater than those for east, due to the afternoon periods with more intense solar radiation compared to the forenoon periods. Moreover, the direct radiation receptions for south vary notably with the WWRs increasing, due to the solar coverage on the south-facing facades for long period of time. In comparison with the southerly facing facades, the major solar contributions of windows facing north are the diffuse radiation, so their direct radiation receptions are kept relatively low. In contrast, the polylines' dispersion of diffuse radiation is negligible, which demonstrates that BA has a trivial impact on the diffuse radiation reception for window.

The total solar radiation receptions (i.e., the sum of direct radiation reception and diffuse radiation reception) are all directly proportional to increases in WWRs. Besides, the total solar radiation receptions exist wide-ranging differences at the high values of x-axis, which means that the impact of BA on the solar radiation reception starts to become obvious as the glazing area increases.

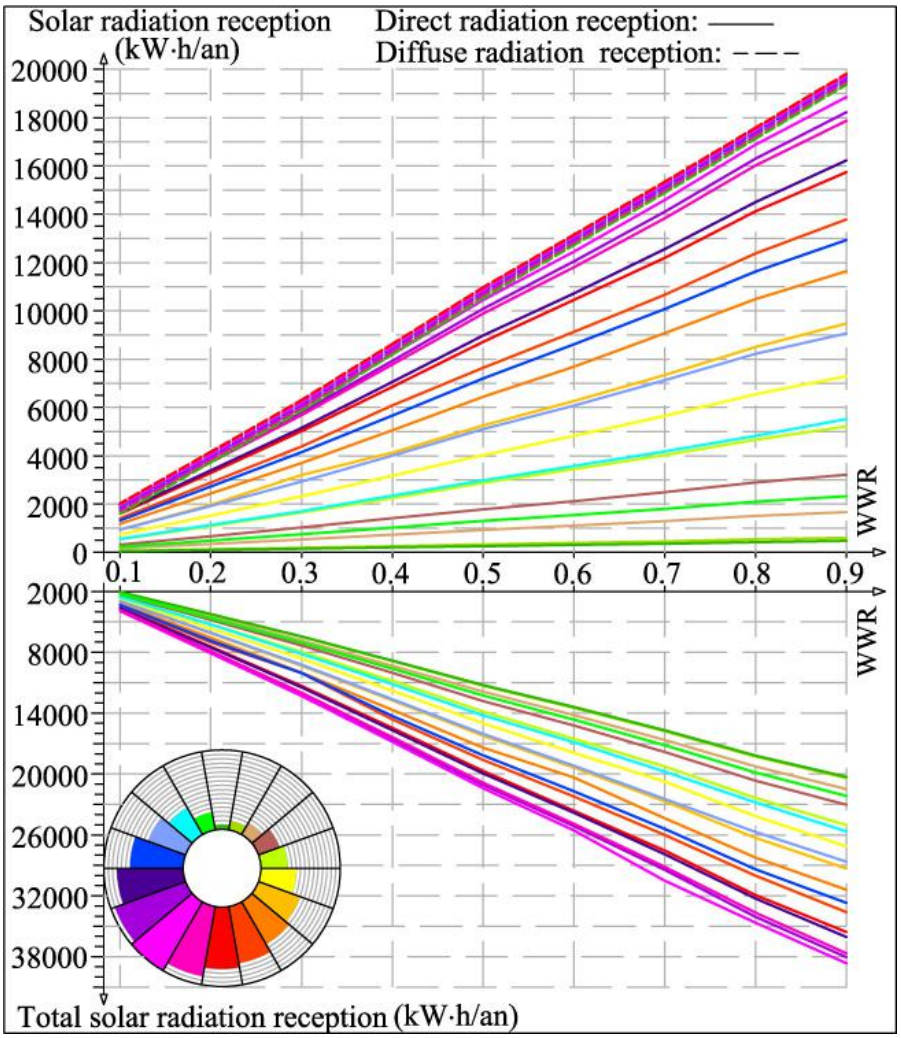

Fig. 7.11 Three kinds of solar radiation receptions for windows with different window-to-wall ratio and building azimuth combinations

7.4.2 Impact of windows with different window-to-wall ratio and building azimuth combinations on the indoor visual comfort rate

Levels for daylighting are generally described as preferred or recommended, either by specific illuminance (lux) levels on a work plane or by daylight factor (DF). The *Chinese Standard for Daylighting Design of Buildings* (GB 50033-2013) stipulates that the mean daylight factor in bedroom, living room and kitchen should be greater than 2%, or the mean illuminance in these rooms should be greater than 300 lux. Therefore, the term of visual comfort rate in this chapter is defined as the ratio of time for the internal space with mean illuminance greater than 300 lux by the

natural daylighting to a year period. To simulate the visual comfort rate for the test scenarios, the VELUX Daylight Visualizer 2 was adopted in this section. The reflectance of wall, flooring and ceiling was assumed to be 0.75, 0.60 and 0.65, respectively. The set-point of directly north is 0° in VELUX Daylight Visualizer 2. By altering this set-point, BA of the building geometry can be varied correspondingly without necessity to rotate the original model, which is helpful for the time-saving.

It can be seen from Fig. 7.12 that the visual comfort rates are directly proportional to the WWR. The polylines' dispersion decreases dependency on the WWR increasing, since the daylighting in the southerly oriented test scenarios derives from both the direct and diffuse radiations, while that in the alternatives facing north principally relies on the diffuse radiation resulting in being difficult to meet the demand of greater than 300 lux. With increase in WWRs, the northerly orientated test scenarios can prolong visual comfort time effectively by the diffuse radiation. Therefore, the visual comfort rate becomes to be not susceptible to the variation of BA at the high values of x-axis.

The visual comfort rates for south are greater than those for north, because the availability of substantial quantity of solar radiations covering the south-facing facades with longer period of time. The visual comfort rates display an increasing trend rotated from N to S-W 40 clockwise and anticlockwise, under the conditions of WWRs for 18 BAs with the same value.

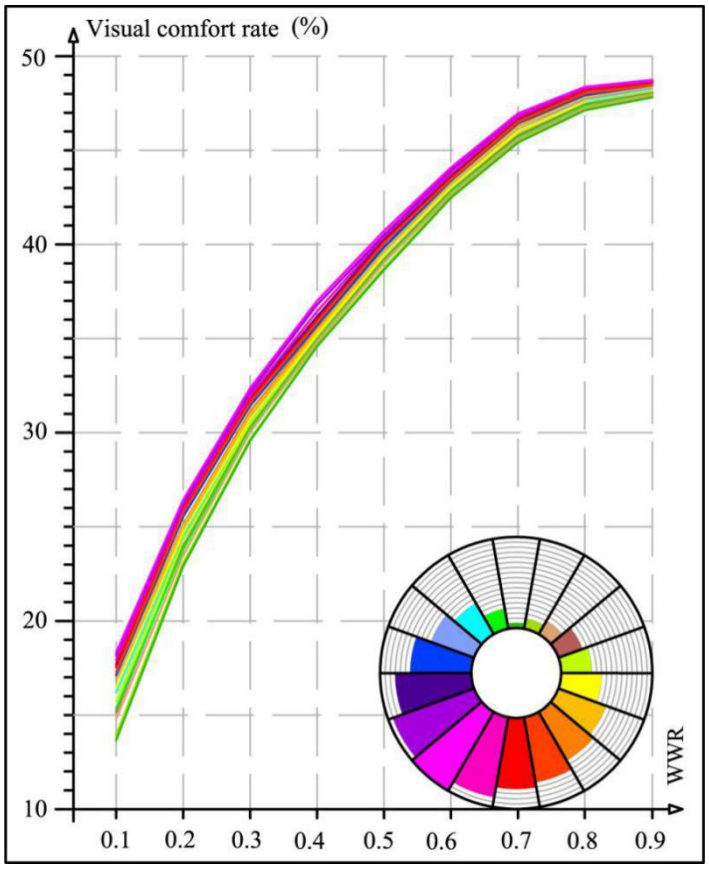

Fig. 7.12 Visual comfort rates for windows with different window-to-wall ratio and building azimuth combinations

7.4.3 Impact of windows with different window-to-wall ratio and building azimuth combinations on the energy consumption of artificial lighting

Through the questionnaire survey, we found that the wake-up time and the bedtime for occupants are generally at 6:30 a.m. and 22:30 p.m., respectively. When the illuminance in each test scenario is lower than 300 lux, the lighting system is turned on to compensate the daylight illuminance, aiming at reach the desired value (i.e., 300 lux) on the work plane (0.9 m above floor). Therefore, the schedule assigned to the artificial lighting system was assumed to be 7.5 h on workdays from 6:30 a.m. to 7:30 a.m. and from 6:00 p.m. to 22:30 p.m. in simulation, while during weekends, the time in running was set from 6:30 a.m. to 22:30 p.m.. In fact, not all lamps are in operation during nighttime, but according to occupancy conditions and lighting demand, a variable quantity of lamps is switched on. Therefore, the parameter settings in the simulation to compute the energy consumption of artificial lighting also need to be optimized. The probability of all five suites being under the artificially lit conditions at the same time was set at the 80%, and the average quantity of lamps in operation was set at 1.5 for each suite of the test scenarios.

Drawing an analogy between Fig. 7.12 with Fig. 7.13 can be seen that the polylines' sequence of the lighting energy consumption for 18 BAs is mutually inverse with that of the visual comfort rate, since the test scenarios with higher visual comfort rate need less artificial lighting compensation.

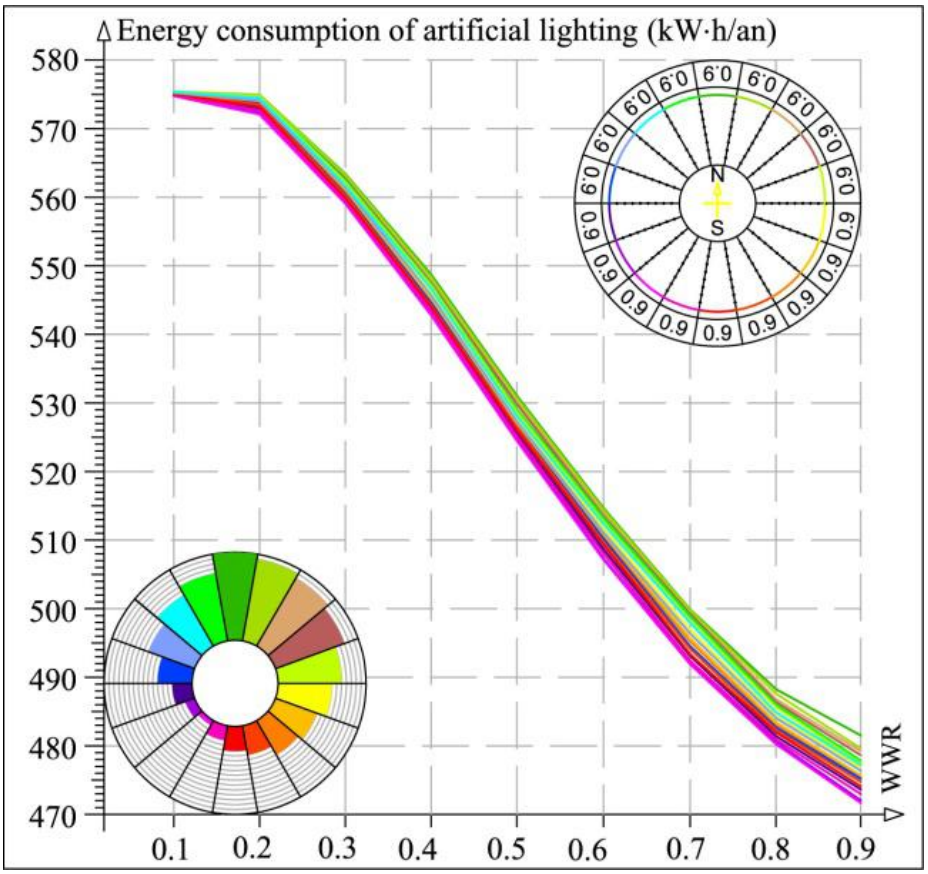

Fig. 7.13 Energy loads of artificial lighting for windows with different window-to-wall ratio and building azimuth combinations

The test scenarios with southwest orientations receive the highest solar radiation levels leading to the most notable reduction in the lighting energy loads. The inflexion points of polylines for 18 BAs are all at 0.2 of x-axis, after which the slopes start to increase. As WWR is assumed to be 0.1, the indoor illuminance in all of the test scenarios is difficult to reach 300 lux so that needs long period of artificial lighting compensation time, resulting in high energy costs and negligible differences. With increase of WWR, the dispersion of polylines increases as well, which means that the impact of BA on the energy consumption become evident. Therefore, the recommended WWRs for the 18 test scenarios are all observed for 0.9.

7.5 Impact of window-to-wall ratio on the total energy consumption including air conditioning and artificial lighting based on changes in building azimuth

As shown in Fig. 7.14, the polylines' sequence and distribution characteristics of the total energy consumption including cooling and heating (i.e., AC), as well as artificial lighting for windows with different WWR-BA combinations are consistent with the energy consumption of AC. The dispersion of polylines for west is greater than that for east at the high values of x-axis, which means that the total energy consumption in buildings orientated towards west is more sensitive to the BA changes.

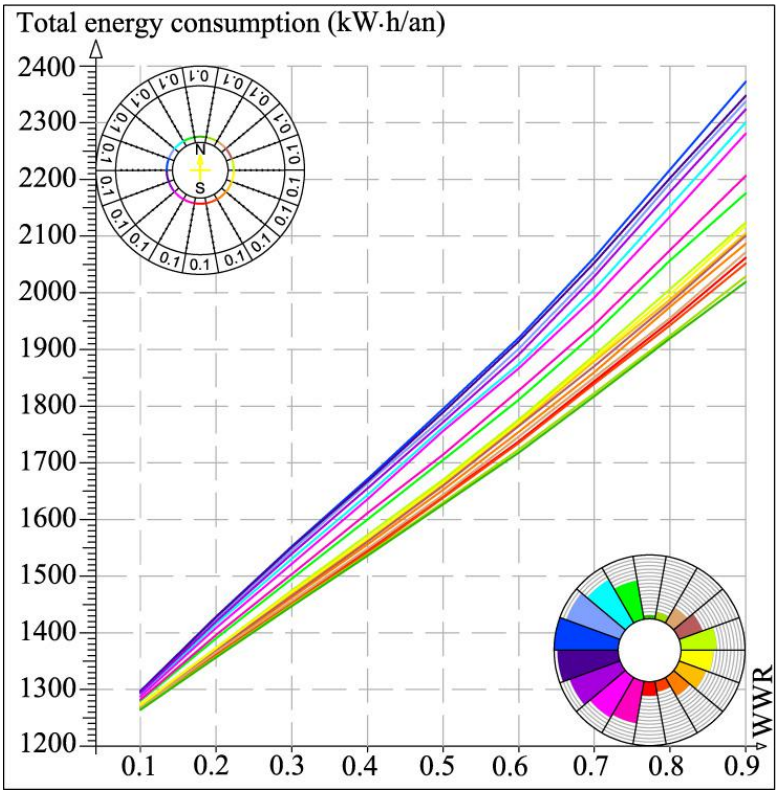

Fig. 7.14 Total energy consumption for windows with different window-to-wall ratio and building azimuth combinations

Among the three kinds of energy loads, the cooling energy consumption accounts for the highest proportions. Especially, when the WWR is assumed to be a high value, the proportion of cooling energy cost is up to approximately 70% in each of the test scenario. Therefore, the change trends and value order of total energy consumption are more close to those of cooling energy consumption. Besides, the WWRs recommended for all the test scenarios, in accordance with criterion of the total energy requirement, are 0.1, which is the same with the recommendation based on criterion of the cooling energy requirement. The maximum difference of total energy consumption among the 18 polylines is 31 kW·h/an when WWR is 0.1, while the value raises to 352 kW·h/an at 0.9 of x-axis.

7.6 Validation of the energy consumption results: simulation tool versus real bills

7.6.1 Energy consumption in the real traditional dwellings obtained from real bills

Real energy bills are empirical, also often called "true data" and are regarded as an extremely powerful validation proof [35]. With this in mind, the total annual electricity consumed by the artificial lighting and AC, which is generated by simulation tool, is compared to that from the real electricity consumption bills to verify the computational accuracy in this chapter. Because the building model type with five suites was chosen in the simulation, the mean electricity consumption for each suite was calculated as one fifth of the total annual electricity use. There are two selection criteria for choosing the real bills from reference suites: (1) the reference suite should be equipped with AC and lighting fixtures, so that the energy consumption of AC and artificial lighting can be obtained from the bills; (2) the building area of the reference suite should be around 30 m^2 for fair comparison with the suite in the test scenario. In compliance with these two conditions, the existing energy bills from four real suites (Fig. 7.15, Table 7.1) are selected as the "true data", of which two are within S interval and the other two are within N interval. The domestic electrical appliances and details of the four reference suites are listed in Table 7.2. The E_{TAAEU} (total annual actual electricity use, kW·h) including and the artificial lighting and AC in a bay can be formulated as Equation (7.1).

$$E_{TAAEU} = E_T - E_O \qquad (7.1)$$

Where, E_T is the total annual actual electricity use including the all domestic electrical appliances, kW·h; E_O is the total annual actual electricity use of the all domestic electrical appliances except for the artificial lighting and AC, kW·h. In accordance with the time in operation and the quantity of domestic electrical appliances, the E_O can be calculated and listed in Table 7.3.

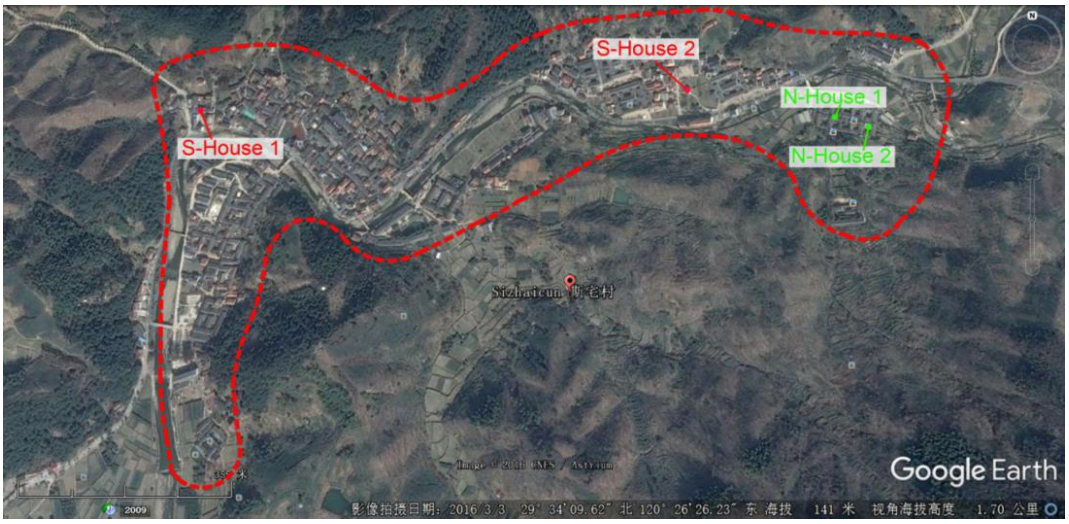

Fig. 7.15 positions of four reference buildings in Sizhai village

Table 7.1 Four reference suites in Sizhai chosen to provide real energy bills

BA	Within S interval		Within N interval	
WWR	0.46	0.21	0.47	0.22
Diagram			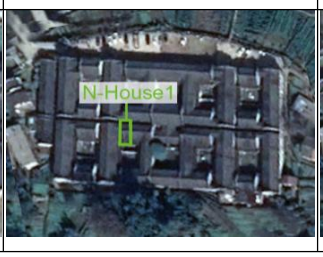	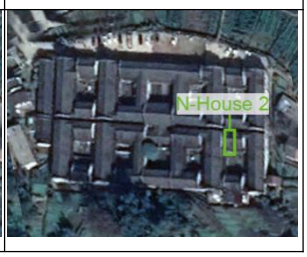

Table 7.2 List of domestic electrical appliances and details of the four reference suites

Domestic electrical appliance		EC	WM	EV	EK	Com	T	R	Cal
Power (w)		500	210	50	800	200	100	100	1500
Operation period		Whole year	Whole year	JO	Whole year	Whole year	Whole year	Whole year	NANY
Use frequency per day during workday		1	1	1	1	1	1	1	1
Use frequency per day during weekend		2	1	2	3	3	3	1	1
Operation duration for each time (h)		0.33	0.3	6	0.17	2	2	24	1
Electricity cost per month (kW·h)		6.27	1.89	9	4.08	12	6	12	45
Annual electricity cost (kW·h)		75.24	22.68	46.29	48.96	144	72	144	270
Suite 1-S (28.56 m^2)	Appliance		●	●	●		●	●	●
	E_O (kW·h)	603.93							
Suite 2-S (33.87 m^2)	Appliance		●	●	●	●	●	●	●
	E_O (kW·h)	747.93							
Suite 1-N (30.53 m^2)	Appliance	●		●	●		●	●	●
	E_O (kW·h)	656.49							
Suite 2-N (32.01 m^2)	Appliance		●	●	●	●	●	●	●
	E_O (kW·h)	747.93							

Notes: 1. ● presents the suite equipped with the given domestic electrical appliance; 2. EC: Electrical Cooker; WM: Washing Machine; EV: Electrical Ventilator; EK: Electrical Kettle; Com: Computer; T: Television; R: Refrigerator; Cal: Calorifier. Whole year: WY; JO: from June to October; NANY: from November to April of next year.

Table 7.3 Total actual annual electricity consumption of 2014 and 2015 in the four reference suites

Designation	E_T of 2015 (kW·h)	E_T of 2016 (kW·h)	E_{TAAEU} of 2015 (kW·h)	E_{TAAEU} of 2016 (kW·h)
S-House 1	864.27	856.01	260.34	252.08
S-House 2	996.36	1028.65	306.24	280.72
N-House 1	904.92	899.46	248.43	242.97
N-House 2	1042.24	1026.36	294.31	278.43

The E_{TS} in the four real suites throughout 2014 and 2015 are obtained from the monthly electricity consumption bills stored by homeowners. Using equation (7.1), the calculated E_{TAAEUS}, listed in Table 7.3, are regarded as the baselines used to conduct the comparison with computational results. In 2014, the mean air temperature of January was 6.5℃, and that of three summer months (i.e., June, July and August) was 28.7 ℃. As for 2015, the corresponding mean air temperatures were 6 ℃ and 28.3 ℃, respectively. The mean temperature in summer of 2014 was higher than 2015, resulting in the electricity use of 2014 greater than 2015 in the four reference suites.

7.6.2 Comparison of the total energy consumption obtained from simulation tool and real bills

The total annual electricity uses in the S-House 1, S-House 2, N-House 1 and N-House 2 generated by the software is 274.42, 319.27, 273.75 and 320.21 kW·h, respectively. By drawing a comparison between the electricity consumption obtained from the simulation tool and from the real bills, the percentage of bias error for the eight sets of data on average is equivalent to 0.09 (within the acceptable range), and the details are depicted in Fig. 7.16.

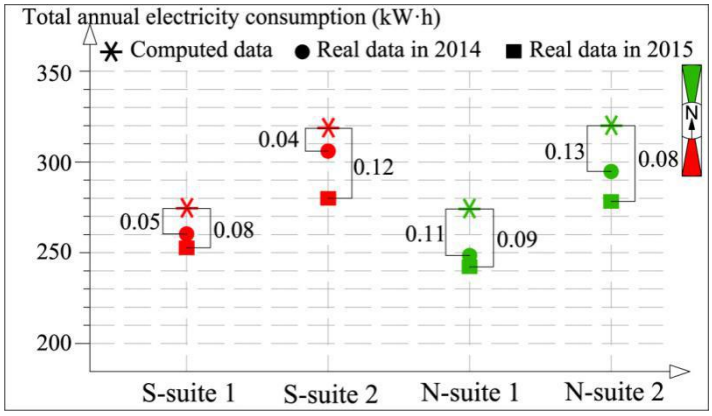

Fig. 7.16 Comparison of the total annual electricity consumed by lamps and air conditioning obtained from simulation tool and real bills

The possible sources of bias error which can impact the computational results are important to highlight: (1) The BA is difficult to precisely measured for the real dwelling, therefore the BAs used to conduct simulation test in software can not precisely represent the actual BAs for dwellings. (2) A substantial quantity of assumptions made in software computation. The U-values of fabrics and materials used in the actual building may be not consistent with the assumed value adopted in the software. (3) Software simulation estimates the amount of energy consumption

based on a fixed schedule, but the real conditions of occupancy times may differ from day to day throughout a year. (4) The accuracy of computational results may be correlated to human behavior. As stated by Ryan and Sanquist [36], the occupant behaviors are the common source leading to bias errors in the energy simulations, since they are highly variable resulting in being almost impossible to model them accurately. Besides, the life-style and behavior of each occupant is different, but the set points in the simulation are the same for each of the test scenario, which may also cause bias errors. (5) Weather data is another factor that influences the accuracy of computational results. The meteorological data used in simulation are collected from the whole Shaoxing city, but the case study in the mountainous area is easily impacted by a micro-climatic environment, which may causes bias errors for the computational results. (6) Some simplifications in the geometric model may cause another source of bias error for the computational results, such as the dwellings in Sizhai are surrounded by mountains and vegetation in fact, which influences the intensity of solar radiation covering the walls.

7.7 Optimal window-to-wall ratio recommended for each building azimuth interval

Levels for daylighting are generally described as preferred or recommended, either by specific illuminance (lux) levels on a work plane or by daylight factor (DF). For evaluation of the quantity of indoor illumination inside a room, daylight factor is the most recognized performance indicator used at present. The *Chinese Standard for Daylighting Design of Buildings* (GB 50033-2013) is recommended that the mean daylight factor in bedroom, living room and kitchen should be above 2%, or the mean illuminance in these rooms should be higher than 300 lux on the work plane for the building design.

The daylighting mode of fenestration system used in Sizhai traditional dwellings belongs to side daylighting. In Ecotect 2012, the most basic data for lighting calculations is the daylight factor, and all other parameters (e.g., illuminance) are obtained applying calculations based on the daylight factor. Therefore, the evaluation parameter of daylight factor was used to estimate the indoor daylighting performances for each of the test scenarios with different shading depth and building azimuth combinations.

According to the Standard, the daylight climate of Sizhai is located in the fourth zone, where the natural illuminance of overcast sky is assigned to be of 13500 lux. The overcast weather is characterized by a uniform and stable diffuse radiation in the sky, which leads to the indoor daylighting performances corresponding to different orientations to be very similar. In this chapter, the test scenario with S was chosen as the case study. As shown in Fig. 7.17, excluding the 0.1 of WWR resulting in the indoor daylight factor of less than 2%, the other WWRs are all satisfied to the Standard.

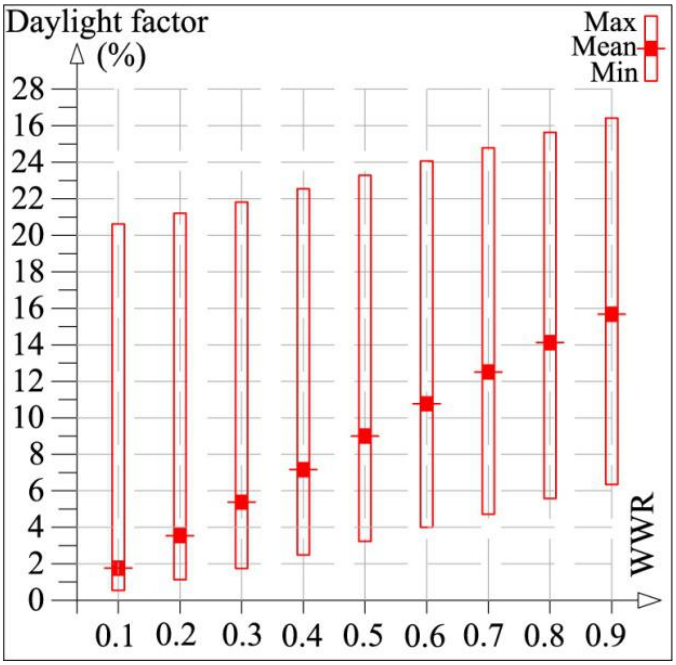

Fig. 7.17 Daylight factor for directly south (S) by varying window-to-wall ratio

The compromised WWRs recommended for each BA are depicted in Fig. 7.18, based on the total building energy consumption and indoor daylight factor standard. Because the increases in cooling loads in each of test scenarios are greater than the reductions in the sum of heating and lighting loads, the recommendations of WWRs for all the test scenarios are the same, 0.2. This research results meet the requirements from *Code for Thermal Design of Civil Building* (GB50176-2016), which stipulates that the north-, east-, west-, and south-facing facades of residences should be not greater than 0.25, 0.3, 0.3 and 0.35, respectively.

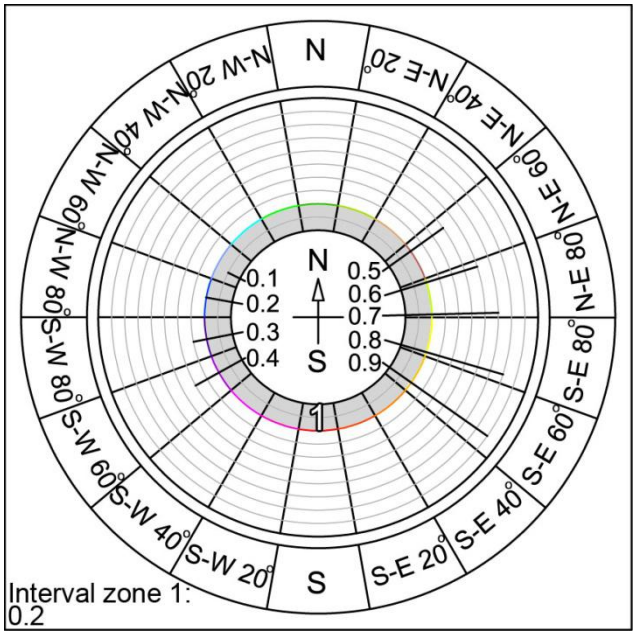

Fig. 7.18 Recommendation of the optimum window-to-wall ratio for each building azimuth interval

7.8 Application of the research results

7.8.1 Definition of Evaluation Score of Window-to-Wall Ratio

To apply the research results, the Evaluation Score of Window-to-Wall Ratio (ESWWR) was put forward in this work. The ESWWRs assigned to the WWR interval close to its optimal values for each BA are assumed to be 1. Since the indoor daylight factor in the building with WWR of less than 0.2 is not meet the code of visual comfort, the ESWWR is not assigned to WWR of less than 0.2. As depicted in Fig. 7.19, the ESWWRs assigned to the other WWR intervals present descending trends at 0.1 increments, with being apart from its optimum.

With respect to the courtyard dwellings consisted of some stand-alone buildings, the equation (7.2) is formulated to calculate the average ESWWR (Wa) for them.

$$W_a = \sum (WWR \times ESWWR) / \sum WWR \qquad (7.2)$$

The construction approach of traditional dwellings in East and Central China is compliant to with the professional standard of *Ying Zao Fa Yuan*, which leads to the building components used in dwellings characterized by the modularization. Thus, the height of window above the floor and height of window are greatly similar, the ESWWR is deemed to be applicable for each building in Sizhai village to analyze its energy saving potential.

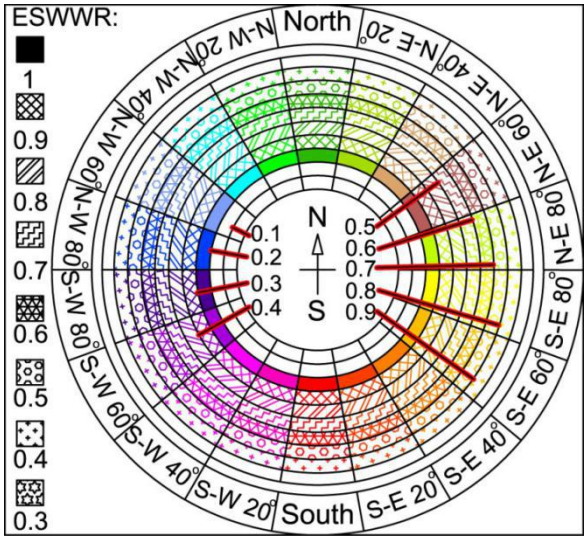

Fig. 7.19 Evaluation score of window-to-Wall ratio assigned to 8 window-to-wall ratio intervals for 18 building azimuth intervals

7.8.2 Application of the evaluation score of window-to-Wall ratio to three courtyard dwellings

As shown in Table 7.4, three traditional dwellings in Sizhai are selected to estimate their ESWWRs, of which the courtyard dwelling of Fa xiang ju (Fig.7.20) is considered as the baseline case. The other two, case 1 (Shang xin ju)

and case 2 (Xia men qian fan), within the same and different BA intervals comparing to the baseline case respectively, are chosen as the target buildings. Due largely to the hall buildings in three courtyard dwellings with only a storey, there are not corridor constructed for them. This work is focused on the shading performance of corridor in traditional dwellings, so the ESWWRs of hall buildings were not considered.

The configurations of these three buildings with courtyard are quite complex, in order to explain the comparison procedures in detail. By using equation (7.2), the ESWWRs of the three chosen dwellings are calculated, which are 0.86, 0.84 and 0.85 corresponding to the baseline case, the case 1 and the case 2, respectively. Thus, the dwelling with the highest energy saving potential is deemed to be the case 1, based on the evaluation parameter of WWR. By repeating the previous procedures, the ESWWR of each dwelling in the village can be obtained. Also, this new evaluation of building energy saving potential can be applied to assess the energy efficiency of the traditional dwellings in East and Central China, thanks to having the same classification of the traditional dwelling, building materials and building structure.

Table 7.4 Evaluation score of window-to-Wall ratios calculated for the three study dwellings

D	Fa xiang ju (Base case)	Shang xin ju (Case 1)	Xia men qian fan (Case 2)
Remote sensing images in G.E.			
BA	SE-20	SE-20 (the same with base case)	NW-60 (differing from base case)
SDs for three buildings	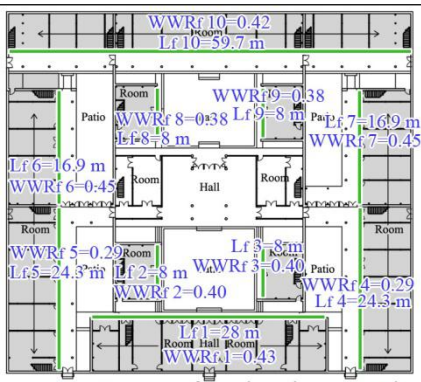	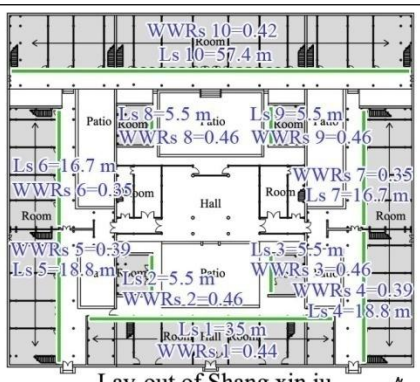	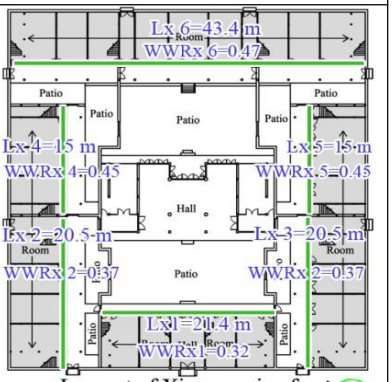
Wa	0.86	0.84	0.85

Notes: 1. D is the abbreviation of designation.

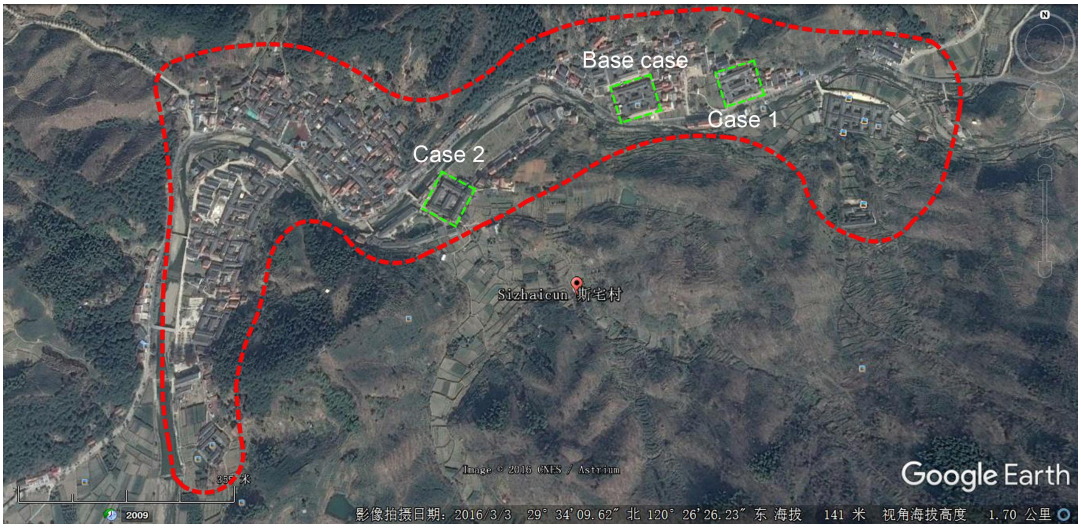

Fig. 7.20 Three dwellings selected to assess their building energy saving potentials

7.9 Finding and discussion

Since the glazing and opaque areas on facade has significant impact on the indoor visual and thermal comfort as well as energy cost, the optimal WWR is necessary to be explored for the rural residences with a large quantity in China. Take into consideration the different combinations of BAs and WWRs, giving a total of 162 simulation runs in this chapter. Through software simulation, the evaluation parameters of solar heat gain, air temperature, solar radiation reception, visual comfort rate and energy consumption were employed to assess the effects of WWRs on indoor environments and energy consumption performances in each of the test scenarios with different WWR-BA combinations.

(1) The total indoor heat losses passing through windows for the 18 BAs in January are all directly proportional to the WWRs increasing. In comparison to magnitude of solar heat gain, the values of indoor heat losses are comparatively low. The polylines' distribution characteristics of energy difference in January are consistent to those for solar heat gain.

(2) The polylines' dispersion of energy differences, between solar heat gain and indoor heat loss passing through windows, increases when the WWR grows in summer. Furthermore, the energy difference in each of the test scenarios is very close to its solar heat gain, due largely to the heat loss with relatively low magnitudes compared to solar contribution.

(3) The heating loads show the continuously increasing trends for north and northeast dependency on WWR increasing. While for the other orientations, the polylines firstly decrease and then increase with WWR increasing after the infection points.

(4) The cooling demands in the test scenarios during summer are much higher, since Sizhai experiences a long summer period characterized by harshly hot weather conditions. The polylines' dispersion of cooling loads dramatically increases by varying window dimensions.

(5) The magnitude order of the total energy consumption of AC for 18 BAs is west, east, south and north orientations. Among the 18 polylines, the maximum differences at 0.1 and 0.9 of x-axis are 32 kW·h/an and 324 kW·h/an, respectively.

(6) The polylines' sequence of the lighting energy consumption for 18 BAs is mutually inverse with that of the visual comfort rate. Moreover, the test scenarios facing southwest receive higher solar radiation levels leading to slight reduction in the energy requirements of artificial lighting.

(7) The percentage of bias error on average for the total energy consumption is 9%, which is ranged within the acceptable scope, so the research results have reliability.

(8) Based on the total energy cost (including AC and artificial lighting) and indoor daylight factor standard, the recommendations of WWRs for all the test scenarios are the same, 0.2.

To apply the research results, the Evaluation Score of Window-to-Wall Ratio was put forward in this work. Three traditional dwellings in Sizhai were selected to estimate their energy saving potentials. Based on the calculated results, the dwelling with the highest energy saving potential was observed for the case 1. By repeating the previous procedures, the Evaluation Score of Window-to-Wall Ratio of each dwelling in the village can be obtained.

References

[1] Yousef Al horr, Mohammed Arif, Martha Katafygiotou, et al. Impact of indoor environmental quality on occupant well-being and comfort: A review of the literature [J]. *International Journal of Sustainable Built Environment*, 2016, 5(1): 1-11.

[2] Hans-peter Brikhofer. SSL lighting hype or the only solution in future lighting with respect to specification and application, Proceedings, Balkan Light 5th International Banlkan Conference on Lighting, October 3-6, 2012: 8-13.

[3] DianaÜrge-Vorsatz, Luisa F.Cabeza, SusanaSerrano. Heating and cooling energy trends and drivers in buildings [J]. *Renewable and Sustainable Energy Reviews*, 2015, 41(1): 85-98.

[4] ZHAO L L. The current situation analysis of building energy consumption in China [J]. *Housing and Real Estate*, 2016, 30(10): 25.

[5] Lu J F. The development inevitable trend of China's low carbon building and its future prospects [J]. *Productivity Research*, 2013(12): 72-74.

[6] JIANG Y, PENG Z, HU S. The classification of energy consumption in China [J]. *Construction Science and Technology*, 2015(14): 22-26.

[7] DESOGUS Giuseppe, CANNAS Leonardo Giuseppe Felice, SANNA Antonello. Bioclimatic lessons from Mediterranean vernacular architecture: The Sardinian case study [J]. *Energy and Buildings*, 2016, 129(6): 574-588.

[8] U. Berardi, A. Ghaffarian Hoseini, A. Ghaffarian Hoseini. State-of-the-art analysis of the environmental benefits of green roofs [J]. *Appl. Energy*, 2014, 115: 411-428.

[9] J. Široký, F. Oldewurtel, J. Cigler, S. Prívara. Experimental analysis of model predictive control for an energy efficient building heating system [J]. *Appl. Energy*, 2011, 88(9): 3079-3087.

[10] T. Hong, S. Chou, T. Bong. Building simulation: an overview of developments and information sources [J]. *Build. Environ.*, 2000, 35(4): 347-361.

[11] SAÁ C., M ÍGUEZ J.L, MORÁN J.CC. A study of the influence of solar radiation and humidity in a bioclimatic traditional Galician agricultural dry storage structure (horreo) [J]. *Energy and Buildings*, 2012, 55(5): 109-117.

[12] E. Rautkyla, M. Puolakka. Alerting effects of daytime light exposure a pro-posed link between light exposure and light mechanisms [J]. *Lighting Research and Technology*, 2012, 44: 238-252.

[13] C. Marino, A. Nucara, M. Pietrafesa. Does window-to-wall ratio have a significant effect on the energy consumption of buildings? A parametric analysis in Italian climate conditions [J]. *Journal of Building Engineering*, 2017, 13(8): 169-183.

[14] C. Cuttle. People and windows in workplaces. in: Proceedings of the People and Physical Environment Research Conference, Wellington, 1983.

[15] V.B. Moorjani, S. Asadi, Assessing the effects of glazing type on optimum dimension of windows in office buildings. in: Proceedings of the 50th ASC Annual International Conference Proceedings, Associated Schools of Construction, 2014.

[16] S. Nikoofard, V.I. Ugursal, I. Beausoleil-morrison. Effect of window modifications on household energy requirement for heating and cooling in Canada. in: Proceedings of the eSim 2012: the Canadian Conference on Building Simulation. 2012, p. 324-337.

[17] Ramkishore Singh, I.J. Lazarus, V.V.N. Kishore. Uncertainty and sensitivity analyses of energy and visual performances of office building with external venetian blind shading in hot-dry climate [J]. *Applied Energy*, 2016, 184(10): 155-170.

[18] Peizheng MA, Linshu WANG, Nianhua GUO. Maximum window-to-wall ratio of a thermally autonomous building as a function of envelop U-value and ambient temperature amplitude [J]. *Applied Energy*, 2015, 146: 84-91.

[19] Sonia Longo, Francesco Montana, Eleonora Riva Sanseverino. A review on optimization and cost-optimal methodologies in low-energy buildings design and environmental considerations [J]. *Sustainable Cities and Society*, 2019, 45 (1): 87-104.

[20] CHANG J, LI Y A. Study on the influence of window area ratio of residential building on heating energy consumption [J]. *Journal Heating Ventilating and Air conditioning*, 2008, 38(5): 109-113.

[21] Fumo N, Mago P, Luck R. Methodology to estimate building energy consumption using Energy Plus Benchmark Models [J]. *Energy Build*, 2010, 42(7): 2331-2347.

[22] F. Mazzichi, M. Manzan. Energy and daylight interaction in offices with shading devices, in: Proc. of 1st IBPSA Italy Conference, Bolzano, IT, 2013.

[23] Ignacio Acosta, Carmen Munoz, Miguel Angel Campano, Jaime Navarro. Analysis of daylight factors and energy saving allowed by windows under overcast sky conditions [J]. *Renewable Energy*, 2015, 77(5): 194-207.

[24] Jinkyun Cho, Changwoo Yoo, Yundeok Kim. Viability of exterior shading devices for high-rise residential buildings: Case study for cooling energy saving and economic feasibility analysis [J]. *Energy and Buildings*, 2014, 82(8): 771-785.

[25] Reeves T, Olbina S, Issa R. Validation of building energy modeling tools: Ecotect™, Green Building Studio™ and IES™. In: Laroque C, Himmelspach J, Pasupathy R, Rose O, Uhrmacher AM, editors. Proceedings of the 2012 Winter Simulation Conference. Berlin: Germany; 2012.

[26] Liwei Wena, Kyosuke Hiyamab, Makoto Koganei. A method for creating maps of recommended window-to-wall ratios to assign appropriate default values in design performance modeling: A case study of a typical office building in Japan [J]. *Energy and Buildings*, 2017, 145 (4): 304-317.

[27] GUO L M. Calculation and distribution of solar radiation on the wall in Zhejiang Province [J]. *Energy Engineering*, 1984(4): 27-30.

[28] F.H. Abanda, L. Byers. An investigation of the impact of building orientation on energy consumption in a domestic building using emerging BIM (Building Information Modelling) [J]. *Energy*, 2016, 97(2): 517-527.

[29] Li Wenjie. A Thesis Submitted to Chongqing University in Partial Fulfillment of the Requirement for the Degree of Doctor of Engineering [D]. Chongqing: Chongqing University, 2010: 3.

[30] C. Brunsgaard, M.-A. Knudstrup, P. Heiselberg. Occupant experience of every day life in some of the first passive houses in Denmark [J]. *Hous. Theory Soc.*, 2012, 29: 223-254.

[31] Hashemi, A., Khatami, N.. Effects of solar shading on thermal comfort in low-income tropical housing [J]. *Energy Proc.*, 2017, 111: 235-244.

[32] Kun Lai, Wen Wang, Harry Giles. Solar shading performance of window with constant and dynamic shading function in different climate zones [J]. *Solar Energy*, 2017, 147(3): 113-125.

[33] I.H. Yang, E.-J. Nam. Economic analysis of the daylight-linked lighting control system in office buildings [J]. *Sol. Energy*, 2012, 84: 1513-1525.

[34] C.F. Reinhart, K. Voss. Monitoring manual control of electric lighting and blinds [J]. Light. *Res. Technol.*, 2003, 35(3): 243-260.

[35] Jensen SO. Validation of building energy simulation programs: a methodology [J]. *Energy and Buildings*, 1995, 22: 133-44.

[36] Ryan EM, Sanquist TF. Validation of building energy modeling tools under idealized and realistic conditions [J]. *Energy and Buildings*, 2012, 47(4): 375-82.

Chapter 8

Impacts of walls with various construction type and building azimuth combinations on the energy consumption

8.1 Introduction

8.1.1 Motivation

Today, due to population growth, global warming and environmental issues, as well as energy crisis, reduction in energy consumption becomes increasingly important [1]. The operation and construction of buildings account for approximately 25-40% of the total energy consumption in the world, and result in around 25% of the total CO_2 emissions [2]. Also, building sector is one of the largest energy consumers in China, responsible for approximately 25-30% of the total national energy consumption. This is due largely to the substantial amount of energy used for space heating and space cooling, which accounts for about 40% of the total energy use in China, in order to achieve the desired levels of thermal comforts in building interiors [3]. What's more, thanks to the rapid economy development and raising requirement for the indoor thermal comfort by occupants, the energy cost in the building sector will reach a higher magnitude [4].

Energy efficiency and energy saving are commonly considered as the cheapest and the most effective methods to conquer the challenge of energy crisis in building sector. With increasingly serious of global warming, the concept of energy saving and low carbon has been widely realized worldwide. At present, various energy-efficient technologies and environmental protection methods used in buildings can now be found worldwide. Furthermore, many countries have already adopted some mechanisms, such as regulations, laws, building standards and codes, to decrease the energy consumption in both the refurbishment and newly-built buildings.

Most of energy consumed in buildings is greatly associated with building components. In particular, the exterior wall is responsible for roughly 29-59% of the total heat loss [5]. The wall system is a driving factor that influences the indoor thermal performances, as a buffer element between the outside and inside of building. The above highlighted issues need to be emphasized and to be solved by alternative solutions, based on investigations of the thermal performances and construction characteristics of wall systems. Nowadays, building envelopes are generally designed and constructed, in accordance with the energy saving measures. In the cold climate zone, integration of the thermal insulation materials into walls is one of common methods to reduce the energy loss [6]. Due to the high quality thermal insulation materials used in building envelopes, heat transfer through the external walls has been evidently reduced. The thermal insulation materials, such as the expanded polystyrene (EPS) and extruded polystyrene (XPS), are widely used to play their roles in decrease of the air conditioning energy consumption. Furthermore, Trombe wall with air layer has been gained growing attentions, due to its passive heating functionality by utilizing solar radiation. Besides, cavity wall consisting of two "skins" separated by a hollow space is a conventional method to enhance the thermal insulation of building envelopes, which is suitable to be used under both hot and cold climate conditions.

The cavity brick walls with double layers, widely applied in the Chinese traditional dwellings, have an outstanding performance in terms of thermal insulation, so as to mitigate the thermal transmission in walls [7]. However, concerning the hot climate zone, the primary task of building design is heat dissipation of the external walls, in consideration of thermal insulation at the same time, aiming at cutting down the cooling load [8]. The traditional solution dissipate the internal heat of buildings is increase in opening areas on facades. Due to without or less consideration of wall's thermal insulation, the air conditioning energy load will be significantly raised. However, the tendency of the increasing quantity of air-conditioned residential buildings is remained in China. In doing so, a novel method on improving the wall properties in terms of heat dissipation and thermal insulation for buildings in the hot climate zone need to be urgently proposed.

Up to Dec 31st, 2017, the summation of administrative villages in China was 691510, which was comprised of 2617000 natural villages [9]. At present, there are approximately 13100 of the traditional villages, accounting for 1.9% of the total administrative villages. The traditional dwellings situated in East and Central China are characterized by the cavity brick wall construction, aiming at improving the thermal insulation effectiveness. Through the field investigations, we found that the thermal property of cavity brick walls need to be further improved. Thus, this chapter focuses on the heat dissipation in consideration of thermal insulation for the cavity brick walls of traditional dwelling in East and Central China, where climate is characterized by the harshly hot weather conditions with long summer period.

8.1.2 Scientific originality

In East and Central China, buildings are characterized by the long cooling period and short heating period throughout the year. Furthermore, with raising of the living standard, increasing number of the traditional dwellings with brick-wood structure are air-conditioned. Unlike the previous studies, here, the vented cavity brick wall was focused to evaluate its passive cooling property for buildings under the hot weather conditions. Then, the comparisons of wall surface temperatures and air temperatures, through in-situ measurements, between conventional cavity brick wall and vented cavity brick wall were conducted in this chapter, to investigate the passive cooling effect of vented wall. Since the energy efficiency of conventional cavity brick wall does not meat the current China's energy saving demand, here, we proposed another two novel designs for vented cavity brick wall, in consideration of the cooling performance and thermal insulation at the same time. By coupling between the vents and increased wall thickness, the two novelly-designed walls are the vented cavity brick wall with increased inner layer thickness, and vented cavity brick wall with increased outer layer thickness, respectively. Through the building energy simulation, the most outstanding performance of wall type in terms of energy saving was recommended in this chapter. Also,

instead of limited wall orientations, the analyses of walls' passive cooling performances were based on 18 building azimuth intervals, and also the optimum building orientations were determined in this chapter.

On the other hand, until very recently, numerous attentions have been given to the energy performance of building envelopes in the contemporary buildings, instead of the traditional buildings. Thus, the research results on the energy saving potentials of diverse wall construction types incorporated into the traditional dwellings situated in East and Central China in this chapter, can supply a new body of wall system study to fill the knowledge gap in this field.

8.1.3 Aim of this study

In this chapter, the prototype of geometric models used to run energy simulation was derived from the traditional dwellings in Sizhai village, Zhejiang Province, China. This chapter focuses on the impact of passive cooling performances of cavity brick walls with four types of constructions on the indoor air temperatures and energy consumption, based on changes in building azimuth. Furthermore, the optimum wall construction type (i.e., the kind of wall construction type used in building models with the maximum energy saving potentials) were recommended in this chapter, aiming at acceleration of heat dissipation as well as improvement of thermal insulation at the same time for the cavity brick walls in traditional dwellings.

The research results are thus expected to contribute to some state-of-the-art knowledge and facilitate the further researches on improving the passive cooling efficiency and enhancing thermal insulation property of walls in cooling-load dominated buildings. Furthermore, based on this research, we aim at providing some advice on wall construction design decisions to both newly-built construction and retrofit of the rural residences with various building orientations.

8.2 Research methodology

8.2.1 Research subject

The traditional dwellings are the representative and typical house samples among the rural residences, whose structures, lay-out, indoor comfort and energy consumption are the driving factors influencing the sustainable development of villages. Therefore, the traditional dwellings situated in Sizhai village (East China), with longitude of 120°26' East and latitude of 29°34' North, were chosen to be the target buildings in this chapter. According to the criteria of traditional village category based on the building typology and village geography, Sizhai is regarded as a mountainous traditional village.

In compliance with the Köppen-Geiger Climate Classification, Sizhai is located in the humid subtropical climate (Cfa) zone. The average annual air temperature here is in the range of 16.5-17.5 ℃. January with mean air

temperature of 5.5 ℃ and average diurnal temperature variation of 6 ℃ is the coldest month throughout the year. In contrast, the hottest month is July with mean air temperature of 31.7℃, experiencing approximately 8 ℃ of daily temperature variation. Besides, the average annual relative humidity, precipitation days, sunshine duration per year and annual precipitation are 82%, 158.3 d, 1887.6 h and 1373.6 mm, respectively.

The building material of back walls and gable walls in Sizhai village is the sintered clay brick (see Fig. 8.1). The total thickness of external cavity brick wall is approximately 340 mm, of which 300 mm of thickness is the rowlock cavity wall consisted of two layers with an air layer inside, and 40 mm of thickness is two mortar layers brushed on outer and inner wall surfaces, respectively (Fig. 8.1).

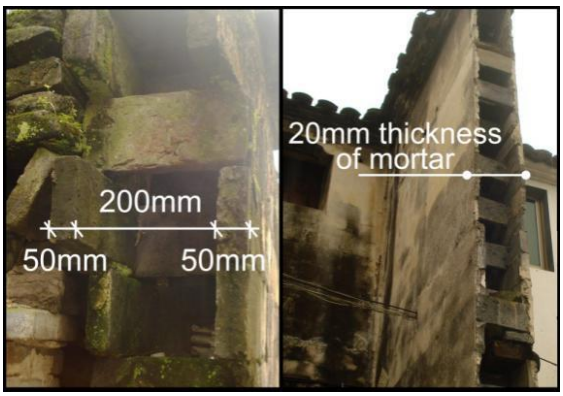

Fig. 8.1 Construction of the external cavity brick wall in Sizhai traditional dwelling

8.2.2 Description of in-situ measurement

As shown in Fig. 8.2, two dwellings in Sizhai village were chosen as the base building and test building respectively, to collect the measurement data. These two buildings are both built in brick and wood, within the same building azimuth interval of N-E 20. In base building, we found a small crack in the cavity wall between bricks located 0.9 m above the outdoor ground (Table 8.1.7), which can provide the passage for thermometer sonde to measure the air layer temperature inside the wall.

Fortunately, another building with upper and lower vents in a cavity brick wall were found in this village (Table 8.1.8-8.1.9), so we could conduct the air temperature measurements to observe the passive cooling effectiveness of vented cavity brick wall. The two vents' sizes are both of 0.24 m (Height) × 0.24 m (Width), which are above 0.3 m and 3.6 m of the outdoor ground, respectively.

Three measurement points were placed in the wall of base building (Table 8.1.1), aiming at observing the outer layer surface temperatures contacted outdoor air (i.e., T_{s1}) (Table 8.1.3), the inner layer surface temperatures

contacted indoor air (i.e., T_{s2}) (Table 8.1.5), and the air layer temperatures inside wall (i.e., T_{al}) (Table 8.1.7). All measurement points were located 0.9 m above the outdoor ground. Regarding the test building, four measurement points were set in the vented cavity wall (Table 8.1.2). They are the outer layer surface temperature contacted outdoor air (i.e., T_{vs1}) (Table 8.1.4), the inner layer surface temperature contacted indoor air (i.e., T_{vs2}) (Table 8.1.6), as well as the air temperature in lower vent (i.e., T_{v1}) (Table 8.1.8) and upper vent (i.e., T_{v2}) (Table 8.1.9). The heights of measurement points of Tvs1 and Tvs2 are the same with the corresponding points in base building (i.e., 0.9 m), and the points of T_{v1} and T_{v2} are placed at the middle of vents, with 0.4 m and 3.7 m of heights, respectively. Furthermore, an another measurement point (P_o, 1.5 m above ground) was placed in outdoor space to collect the air temperature data during the testing days, where is spatial and without any obstacles near it.

As highlighted by purple dotted line in Fig. 8.2, a bay in base building was selected to conduct a measurement of indoor air temperature (measurement point positioned 0.9 m above the flooring at the center of the room), and to perform an experiment of air conditioning energy consumption. The results from measurement and experimentation were considered as baseline to verify the accuracy of the computational results from simulation in chapter 5.

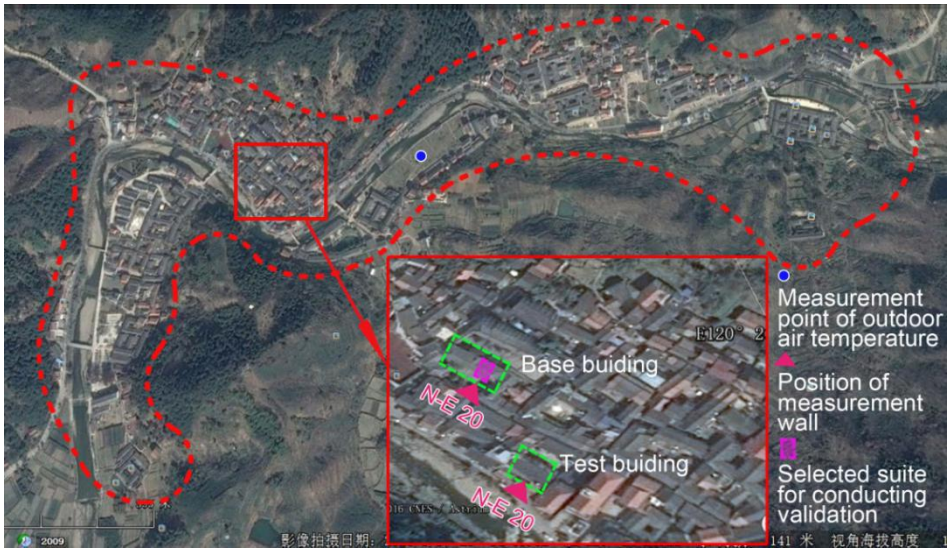

Fig. 8.2 Distribution of measurement walls and point as well as selected suite in Sizhai village

During the measurements, thermometers (type: M0101T2CS, accuracy of ±0.2 ℃, rang of -40-60℃) were employed to measure air temperatures in vents and indoor space, as well as outdoor space. The measurement data were recorded by data acquisition system at 10 min of increments. All the measurement sensors were placed in shaded spaces during the measurement period of time. Furthermore, infrared thermometers (type: AS530, accuracy of ±0.2 ℃, rang of -32-380℃) were used to measure the wall surface temperatures at intervals of 10 min. The measurement time is one week in summer, from Aug 4th, 2018 to Aug 10th, 2018.

Table 8.1 Details of measurement points and measurement methods in base building and test building

8.1.1 Base building	8.1.2 Test building
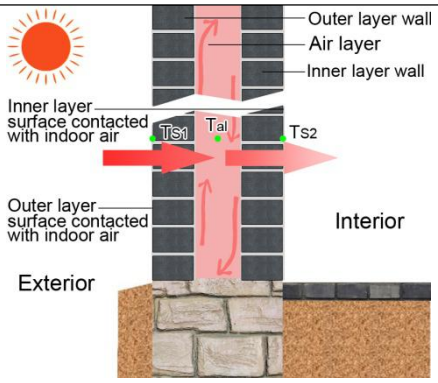	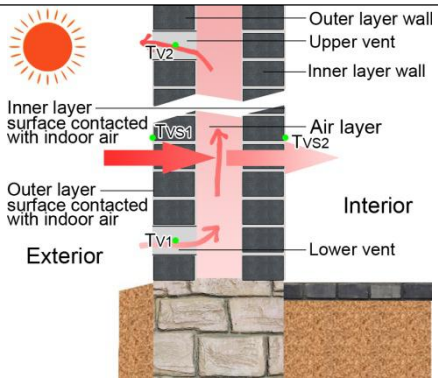
8.1.3 Measurement of Ts1	8.1.4 Measurement of Ts1
8.1.5 Measurement of Ts2	8.1.6 Measurement of Ts2
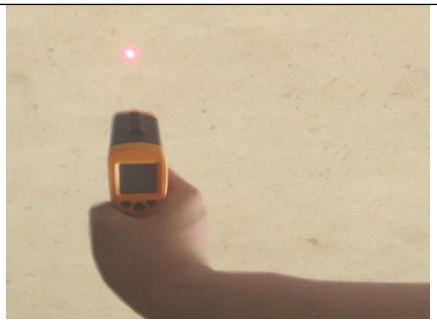	
8.1.7 Measurement of Tay	8.1.8 Measurement of Tv1 / 8.1.9 Measurement of Tv1
	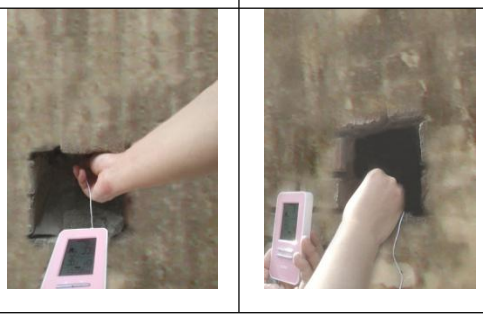

8.2.3 Research flow description

The vented cavity brick wall was focused to evaluate its passive cooling property for buildings under the hot weather conditions. Then, the comparisons of wall surface temperatures and air temperatures, through in-situ

measurements, between conventional cavity brick wall and vented cavity brick wall were conducted in this chapter, to investigate the passive cooling effect of vented wall.

Simulate the Building models with different wall type-building azimuth combinations, giving a total of 72 simulation runs. The evaluation parameters of air temperature and energy consumption were employed, to estimate the effect of diverse wall construction types on the indoor thermal environments and energy requirements in the all building models facing different orientations. Ecotect 2012, whose thermal performance analysis method used in this tool is based on the Chartered Institution of Building Services Engineers (CIBSE), is suitable to conduct the indoor air temperature simulation in this chapter. Obviously, air temperature is a driving factor impacting the energy consumption in a building [10]. To this end, the ArchiWIZARD integrated with the Energy Plus in-plug, characterized by time saving during running, is suitable to be adopted in this chapter.

Aiming at verifying the accuracy of computational results from Ecotect and ArchiWIZARD, the data were compared with those from the field measurements and real experimentation. In addition, based on the air conditioning energy consumption, the optimal wall construction type and building azimuth were recommended in this chapter. To facilitate understanding the research methods framework of this chapter, it is shown in Fig. 8.3.

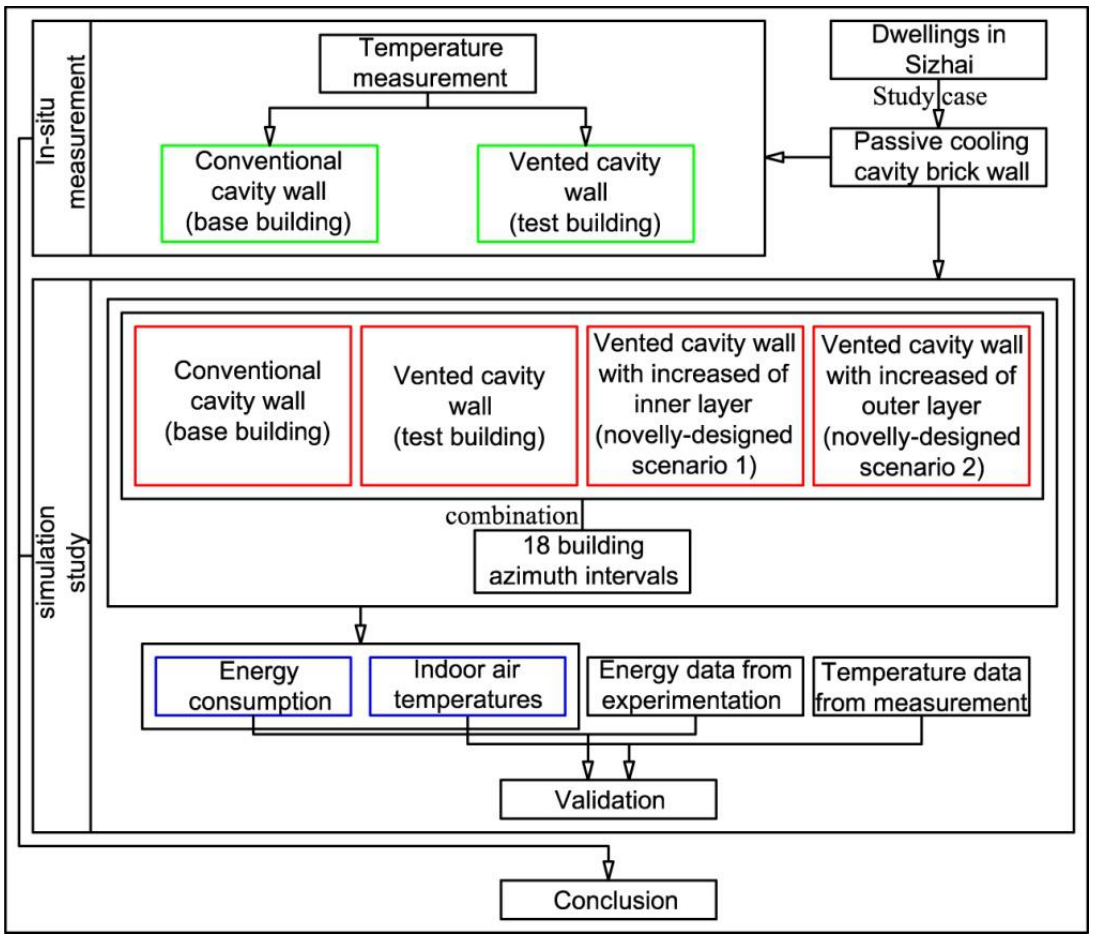

Fig. 8.3 Research methods framework of this chapter

8.3 Field measurements for walls in base building and test building

8.3.1 Meteorological data of Sizhai during testing days

The most significant impact factor on the indoor thermal comfort is air temperature. The air temperature data and solar intensity data was collected from the field measurement and obtained from an automatic meteorological observation station with approximately 3 km as the crow flies away from Sizhai village.

It can be seen from Fig. 8.4 that the solar intensities were comparatively low in the early forenoon and late afternoon, and then turned to zero after sunset. Obviously, the magnitudes of solar intensity were very high during most of the testing days, which was expected to observe the passive cooling effect of vented cavity walls under the harshly hot weather conditions. Concerning the outdoor air temperature, it was fluctuated in synchronization with the solar intensity's variation. The sunny weather conditions without clouds on Aug 6th, lead to the highest outdoor air temperatures (28.6-36.9 ℃) during the testing days. In addition, the outdoor air temperatures during the other testing days were also comparatively high, within range of 26.9-35.9 ℃. In the testing days, the highest outdoor temperatures always emerged between 13:00 p.m. and 14:00 p.m., which were 1-2 h later than the peaks of solar intensities, due largely to the solar heat absorption of the earth. The lowest outdoor temperatures were always occurred at before sunrise, between 5:00 a.m. and 6:00 a.m..

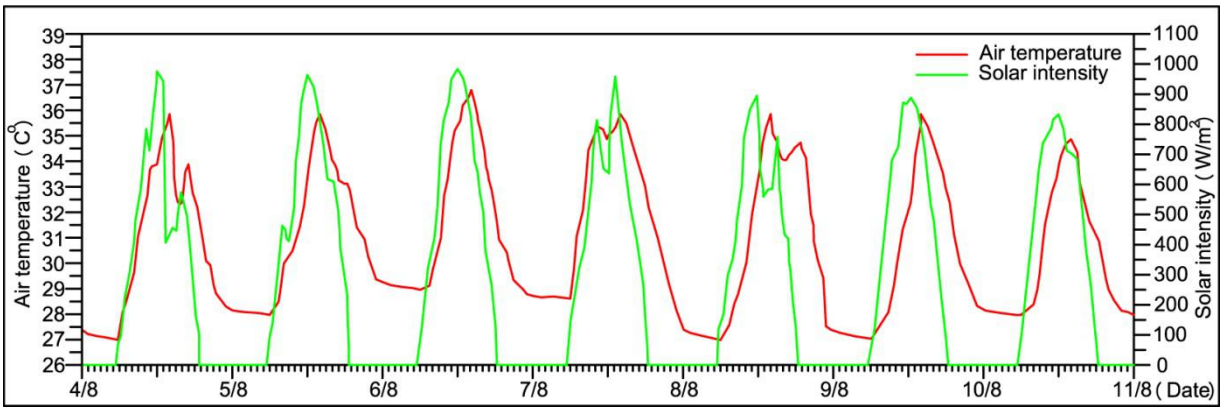

Fig. 8.4 Meteorological data of solar intensity and air temperature during the testing days

8.3.2 Wall surface temperatures in base building and test building

As shown in Fig. 8.5, both T_{s1} and T_{sv1} were distinctly higher than the outdoor air temperatures during most of daytime on the testing days. The reason is associated with the absorption of solar radiation by walls. Draw an analogy between Fig. 8.4 with Fig. 8.5, the change trends of wall surface temperatures of outer layers follow those of solar intensity. The higher of the solar radiation intensity, the more solar heat gains are received in the cavity walls,

and thus lead to higher the outer layer surface temperatures. Furthermore, the wall surface temperatures of outer layers always drop to the minimum values around daybreak. Concerning the maximum values, they emerge at between 14:00 p.m. and 15:00 p.m. in general, later about 1 h of the peak values of outdoor temperatures, as a result of walls' solar radiation absorption.

The vented walls depend on the heat pressure (i.e., thermal plume) in air channel and the natural ventilation can realize heat convection. This is because that the low-temperature air is imported into the air channel through lower vent and is expelled from upper vent can dissipate the stored heat of brick wall to exterior. Thus, the vented wall contributes to reduction in the heat flowing through wall, resulting in T_{sv1} always lower than T_{s1}. This means that the vented wall is more outstanding in terms of heat dissipation.

The maximum differences between T_{s1} and T_{sv1} occur at the same time of the highest surface temperatures, with average 2.8 ℃ during the testing period. Furthermore, the difference values are directly proportional to the solar intensity. During nighttime, the differences are close to zero. Regarding the T_{s2} and T_{sv2}, the maximum differences between them occur at around 16:00 p.m., with average 2.1 ℃ during the testing period. Moreover, the maximum differences always occur at the time of approximately 1 h later than the peak values of outer layer surface temperatures, thanks to the continuous heat reception from outer layer.

T_{sv2} become stable from approximately 21:00 p.m. to sunrise, which differs from T_{s2} beginning at approximately 23:00 p.m. and finishing at sunrise. Regarding T_{sv1}, it has relatively negligible variation during nighttime, in comparison with T_{s1}. This is because that the cavity wall without vent in base building has better heat insulation property, resulting in extending the heat dissipation time.

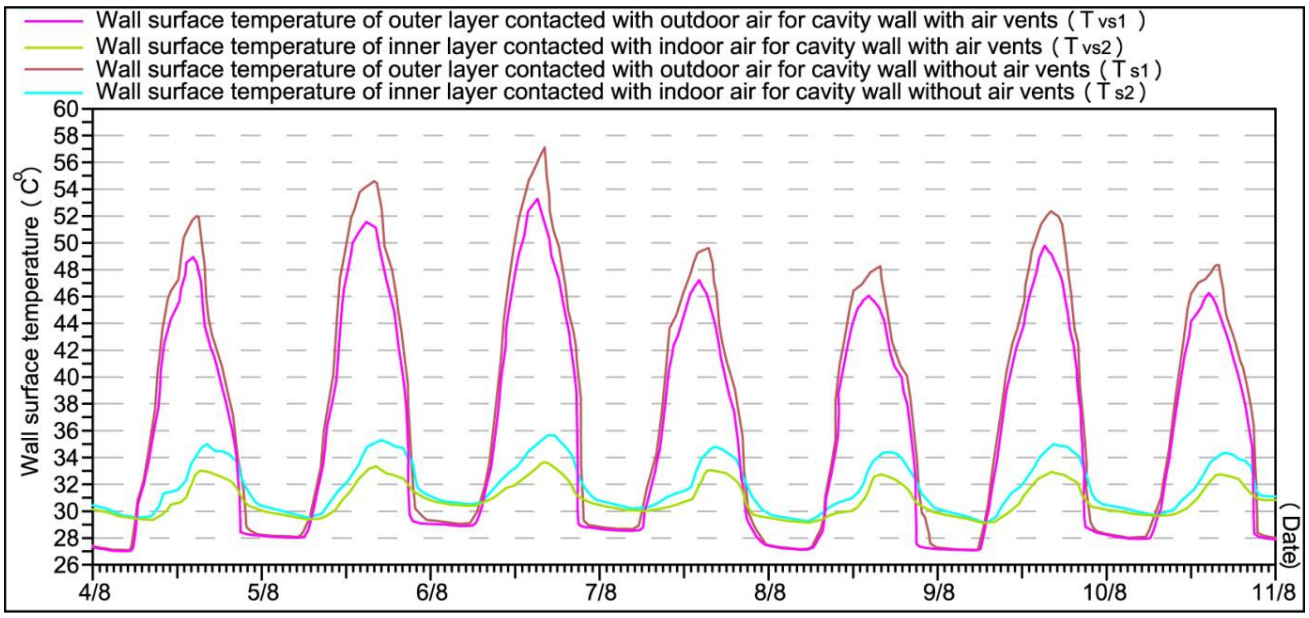

Fig. 8.5 Inner layer and outer layer surface temperatures of cavity wall in case building and test building

8.3.3 Air temperatures in cavity of base building and in vents of test building

Fig. 8.6 shows the air temperatures inside the wall of base building and in vents of test building. As seen, except for a small proportion of the testing periods after sunrise, T_{al} in the case building is always greater than T_{v1} and T_{v2} in the test building. This is because that the heat in air channel of base building is obtained from heat transportation through wall, while for the air temperatures vent in upper and lower vent of test building, they are impacted by both the outdoor air temperatures and heat transportation through wall. After sunrise, the outdoor air temperatures are rising gradually, but the heat transmission in outer layer of cavity walls is not notable at the beginning, due to the sintered clay brick with comparatively high thermal resistance and solar absorption capacity. This results in higher air temperatures in vents of test building, compared with those in the channel of base building, during some time after sunrise.

The maximum air temperatures in these three points always emerged at between 15:00 p.m.-17:00 p.m.. However, the time of peak values for vents are earlier than those for channel. As the air in channel was heated and expanded, and integrate with natural ventilation, the upward airflow was formed. The hot air was expelled to the outdoor space through the upper vent, and cool air from outside flowed into the channel, leading to evident cooling effect in the wall of test building.

The average maximum difference values during the seven testing days between T_{al} and T_{v1}, as well as between T_{al} and T_{v2} were 1.8 ℃ and 3.7 ℃, respectively. At the time before sunrise, the difference values reached the minimum in general. Moreover, the second half days with larger difference values were visible, compared with that in the first half day, due to afternoon with higher levels of solar intensity. Furthermore, we found that the differences between T_{al} and T_{v1}, as well as between T_{al} and T_{v2} are larger in the second half days than those in the first half days, and the peak values were emerged at around 14:00 p.m., during the testing period. Since the second half days have higher levels of solar intensity, this means that the higher solar intensity leads to more notable effect of passive cooling.

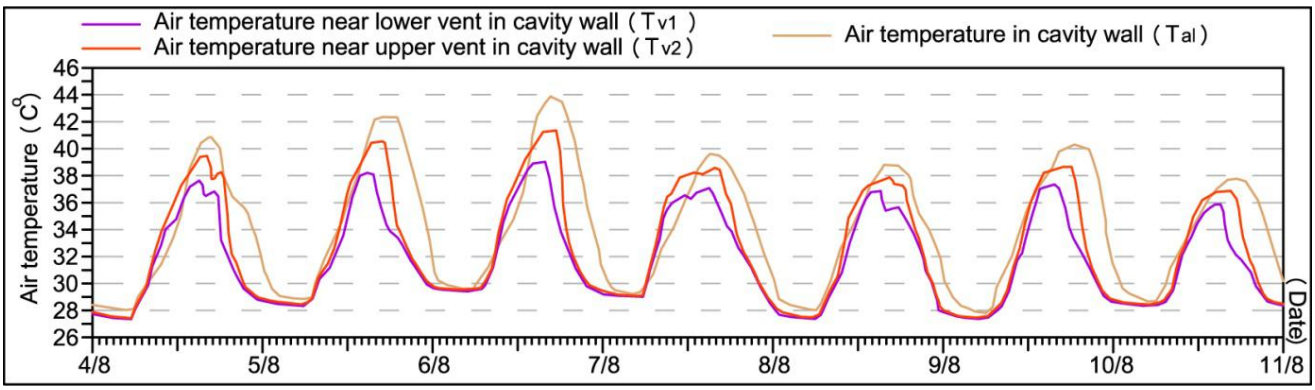

Fig. 8.6 Air temperature in channel of base building and vents of test building during the testing days

8.4 Air temperature and energy consumption obtained from simulation

8.4.1 Air temperatures for four wall types based on changes in building azimuth

8.4.1.1 Air temperatures in each building model during summer

Fig. 8.7 shows the mean indoor air temperatures during summer (i.e., June, July and August) in the building models with different wall type-building azimuth combinations. The mean indoor air temperatures for east orientations are lower than those for west orientations. The reason is associated with less solar heat receptions of the easterly oriented walls. Although the movement trajectory of the sun is symmetrical with the north-south orientation in the earth, the solar radiation level is constantly changing in the sky, which is influenced by the air humidity, dust level in the air and cloudage, etc. In Sizhai, the magnitudes of solar radiation in the second half day are greater than those in the first half day throughout the year in general [11].

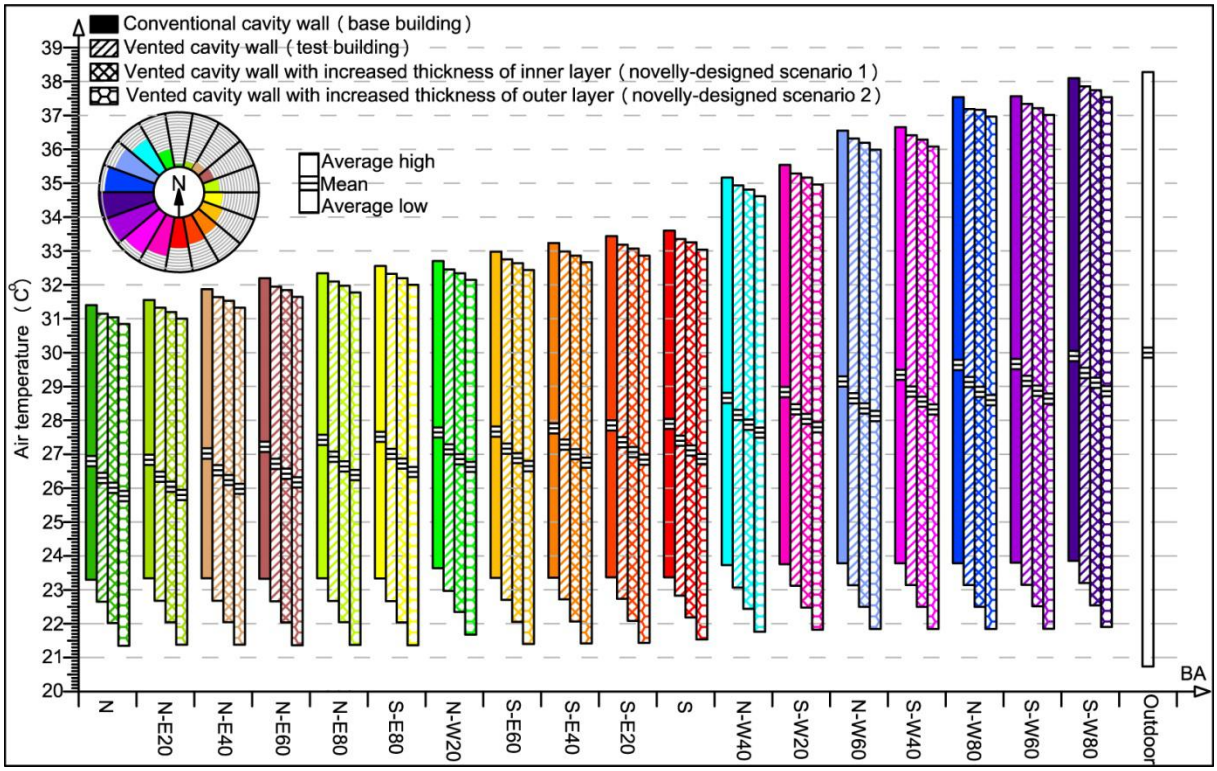

Fig. 8.7 Air temperatures in each of the building models with various wall type-building azimuth combinations in summer

During summer, low air temperatures are desired in the building interiors. Thus, the three recommended building azimuth intervals for the buildings with four wall types are all observed for N, N-E 20, S-E 40. Furthermore, the lowest air temperatures are always observed for novelly-designed scenario 2 with various building azimuths, attributing to their outstanding passive cooling performance. The average low temperatures are remained stable, with varying the building azimuth for various wall construction types. However, in comparison to east-facing building

models, the average high temperatures in west-facing alternatives with a larger magnitude are observed. A total mean air temperature difference of about 3 ℃ corresponding to four wall construction types between the worst (i.e., S-W 80) and best (i.e., N) azimuths of the buildings was achieved.

8.4.1.2 Air temperatures in each building model during winter

For improving heat insulation of walls, all vents in building models of test buildings and novel scenarios were sealed by bricks in winter. Regarding the indoor air temperatures in this season, those for south orientations are higher than north orientations. This is because the solar azimuth during winter is low in Sizhai village, resulting in no solar exposure on the northerly oriented walls. During winter, the high indoor air temperatures are expected, so the three best building azimuth intervals for the buildings with four types of wall constructions are all observed for S-W20, S, S-W40, as shown in Fig. 8.8.

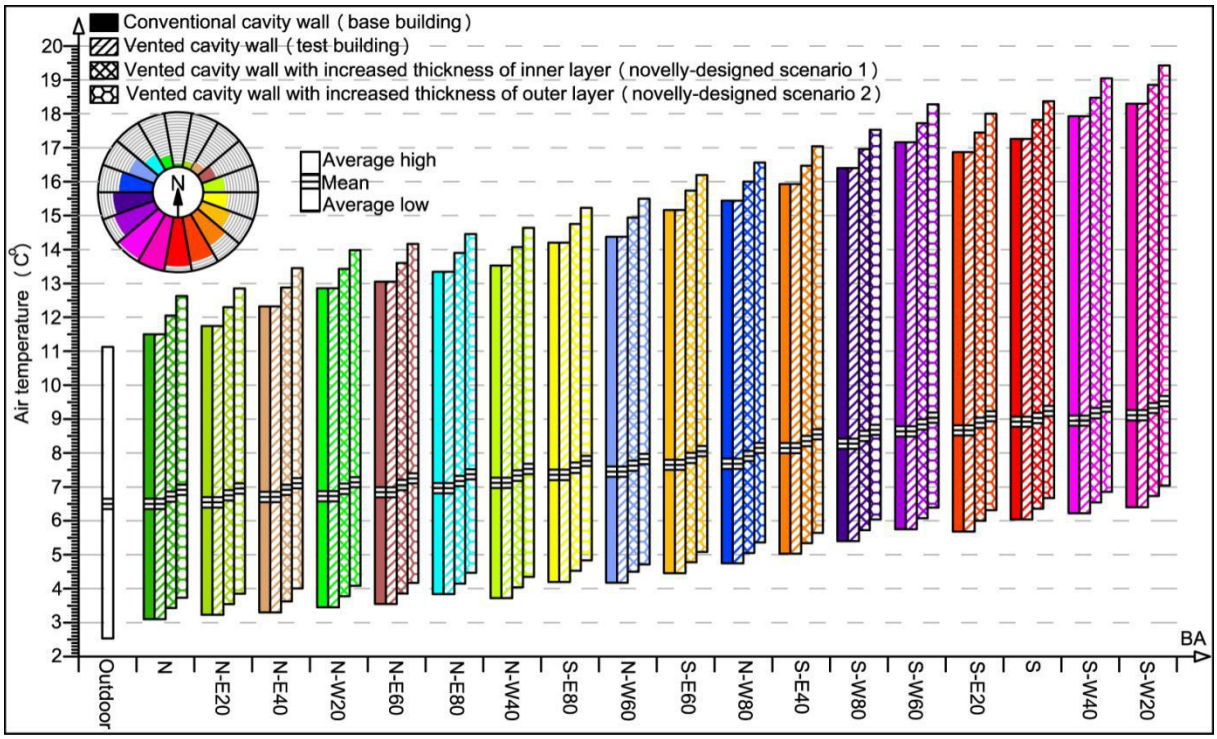

Fig. 8.8 Air temperatures in each of the building models with various wall type-building azimuth combinations in winter

As opposed to the change trends of air temperatures in summer, both the average low and high temperatures are experienced notable variations, when the building models were rotated. For the buildings with high mean indoor air temperatures, the differences between their average high temperatures and mean temperatures are larger. On the contrary, the differences of air temperatures between the average low and mean are larger in buildings with low mean indoor air temperatures. Moreover, A total mean air temperature difference of about 2.6 ℃ corresponding to four wall construction types between the worst (i.e., N) and best (i.e., S-W 20) azimuths of the buildings was

achieved. Also, among these four wall types, the walls in the novelly-designed scenario 2 can create the most desirable indoor air temperatures for occupants in winter.

8.4.2 Energy consumption for four wall types based on changes in building azimuth

During ACs in running, their action-points of cooling and heating temperatures should be set within proper scopes, in consideration of thermal comfort and energy saving [7]. The optimal scopes of AC action-points are within ranges of 18-20 ℃ and 26-28 ℃ in heating and cooling seasons, respectively [12]. In addition, taking into consideration the temperature setting styles for ACs by local occupants, the AC action-points were assumed to be 18 ℃ and 27 ℃ for space heating and space cooling in simulation, respectively. Moreover, because the active equipment system used for both heating and cooling in buildings located in East and Central China is AC, the energy supply model of "electricity from power grid" was chosen in simulation for whole year.

Considering the occupancy schedule and air-conditioned conditions for various rooms, some setting parameters need to be modified in simulation. In the Sizhai traditional dwellings, usually only the bedrooms are installed air conditioner, whose building areas account for approximately 33% of suites. Thus, the building areas of middle suite and the other four served by AC were set at 13.2 m^2 and 8.0 m^2 respectively, and each bedroom was equipped one air conditioner. Since each suite is generally occupied by a family with two or three people, the population density of bedroom was assumed to be 0.22. Furthermore, the probability of five air conditioners in operation at the same time was assumed to be 80%. In addition, the schedule was assigned to run AC in the building models during weekdays was 7 h daily, lasting from 22:00 p.m. to 5:00 a.m. of the next day. Since the occupants' daily schedules are postponed in winter and air temperatures are relatively low during the first half days in summer, the schedule of AC in operation for weekends was assumed to be 15 h daily, beginning at 14:00 p.m.and finishing at 5:00 a.m. of the next day.

8.4.2.1 Energy consumption of space cooling in each building model

Fig. 9 shows the cooling energy consumption in the each of the building models with different wall type-building azimuth combinations. The cooling energy consumption is directly proportional to the indoor air temperatures, comparing the circle legends between Fig. 8.7 and Fig. 8.9. As shown in Fig. 8.9, the magnitudes of cooling costs for building azimuths from N to S are obviously lower than the rest alternatives, as a result of less solar radiation receptions.

Since the vents in test building and novel scenarios were opened in summer, the cooling energy costs in all buildings with vented wall have different levels of reduction in relation to the corresponding base buildings. The novelly-designed scenario 2 consumed less cooling energy compared with the novelly-designed scenario 2. It can be

seen as a result of the scenario 2 with thinner inner layer of wall, which leads to smaller cool energy storage capacity. Thus, the inner wall layer absorbs less cool energy from the internal space, contributing to higher energy saving potential of building. Furthermore, the cooling energy saving levels in testing buildings compared with baselines of base buildings, present increasing change trends from N to S and from N-W 40 to S-W 80, as shown in Fig. 8.9.

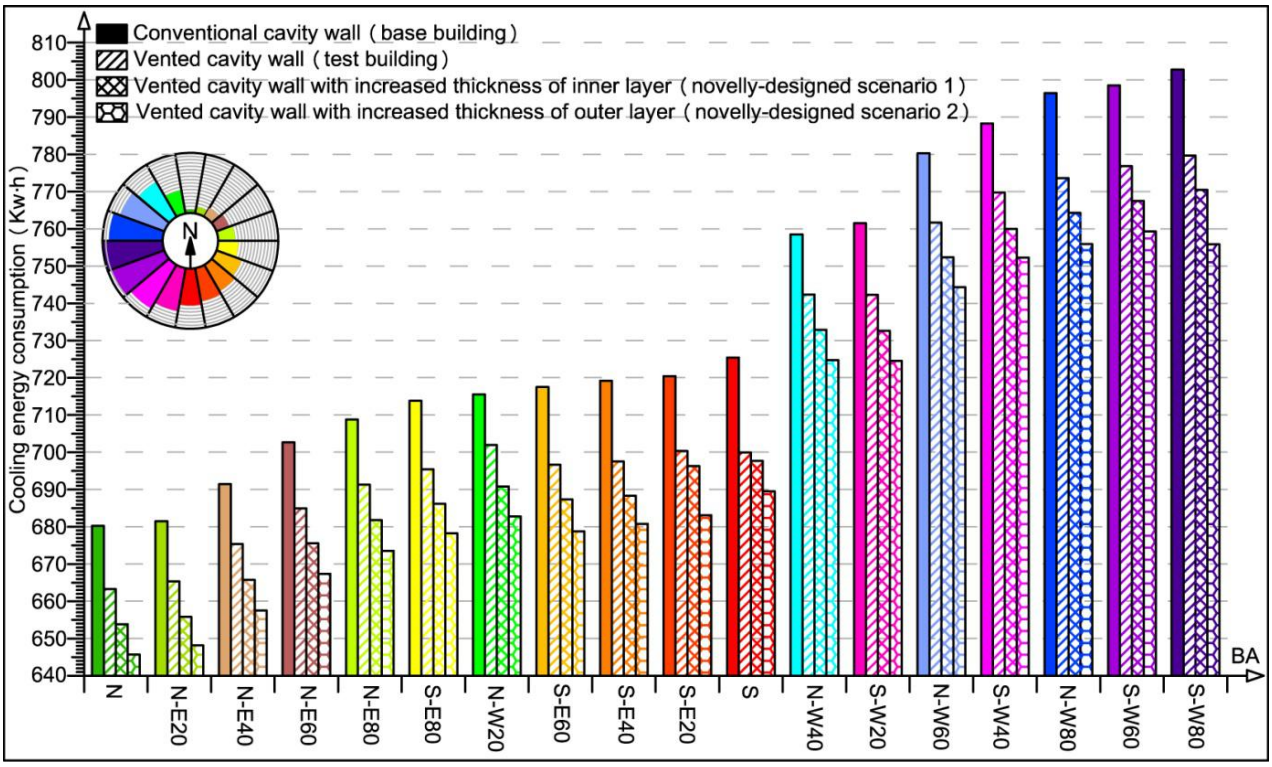

Fig. 8.9 Cooling energy consumption in each of the building models with various wall type-building azimuth combinations in summer

8.4.2.2 Energy consumption of space heating in each building model

As opposed to cooling energy consumption, an inverse order of circle legend in Fig. 8.10 was observed in comparison with Fig. 8.8, which means that the heating energy consumption is inversely proportional to the indoor air temperatures. The heating costs present increasing trend rotated from the S-W 20 to N clockwise and anticlockwise (see cycle legend in Fig. 8.10).

As shown in Fig. 8.10, the growth rate of heating costs for building azimuths from N-E 60 to N is larger than that from S-W 20 to N-W 40, which could be a result of availability of direct radiation over the glazing of building models facing south for a longer period of time than those facing north. In other words, the heating costs for a series of south orientations in buildings with various wall types are more susceptible to the variations in building azimuth. Since the vents in test buildings were sealed in winter, their heating energy costs for all building azimuths are the same with those in base buildings. Due to the same reason, the novelly-designed scenario 1 consumes more heating

energy in comparison with the novelly-designed scenario 2, because the thicker inner layer of wall has larger capacity to store heat obtain from room.

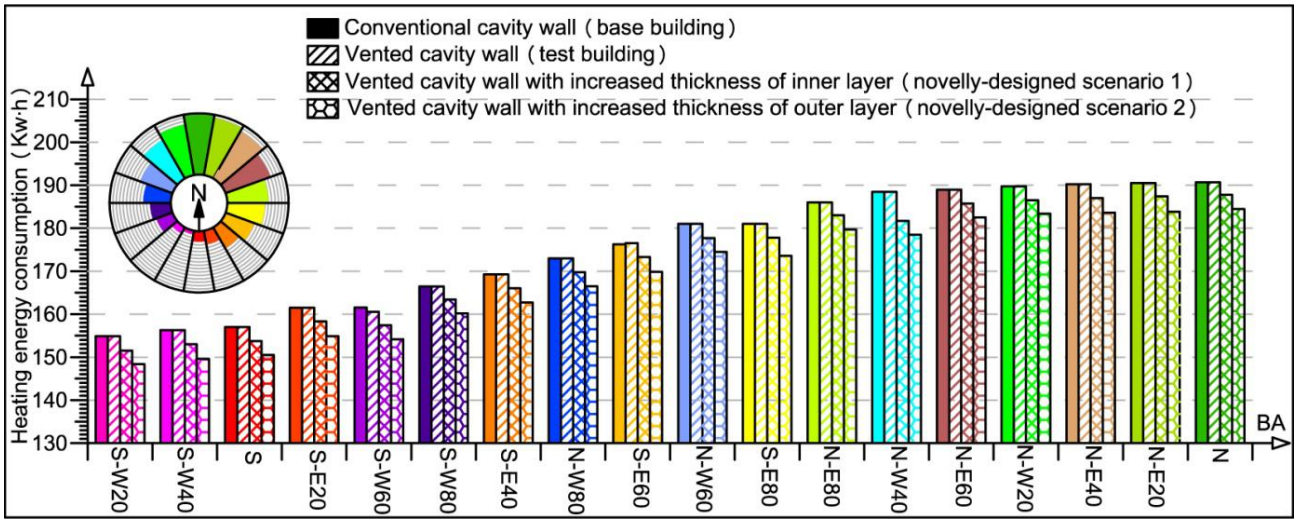

Fig. 8.10 Heating energy consumption in each of the building models with various wall type-building azimuth combinations in winter

8.4.2.3 Total Energy consumption including cooling and heating in each building model

Regarding Fig. 8.11, it shows the total energy consumption including space heating and space cooling throughout the year. Due largely to the dwellings in Sizhai village belonged to the cooling-load dominated buildings, the change trend and order in terms of the total energy consumption in each of the building models are more close to the cooling energy consumption. The three best building azimuth intervals are observed for N, N-E 20 and S-E 20, while the worst three are N-W 60, S-W 80 and N-W 80, based on the criteria of total energy consumption.

Among the four wall types, the maximum total energy consumption for various building azimuths always occurs in base buildings. In contrast, the minimum values are always observed for the novelly-designed scenario 2, thanks to the vented cavity wall with increased outer layer having outstanding heat dissipation performance and favourable heat insulation capacity. The total energy consumption in each building model of the test building and the novelly-designed scenario 1 are in the second and third places, respectively. Furthermore, the energy consumption difference of them for each building azimuth is relatively stable, about 12 kW·h. Although increase in the inner layer thicknesses of walls results in storing more cool or heat energy from rooms, this method contributes to less total energy cost in each of the building models of novelly-designed scenario 1, compared with test buildings and base buildings, due to improvement of the heat insulation property. Furthermore, a total energy consumption difference of approximately 100 kW·h corresponding to four wall construction types between the worst (i.e., S-W 80) and best (i.e., N) azimuths of the buildings was achieved.

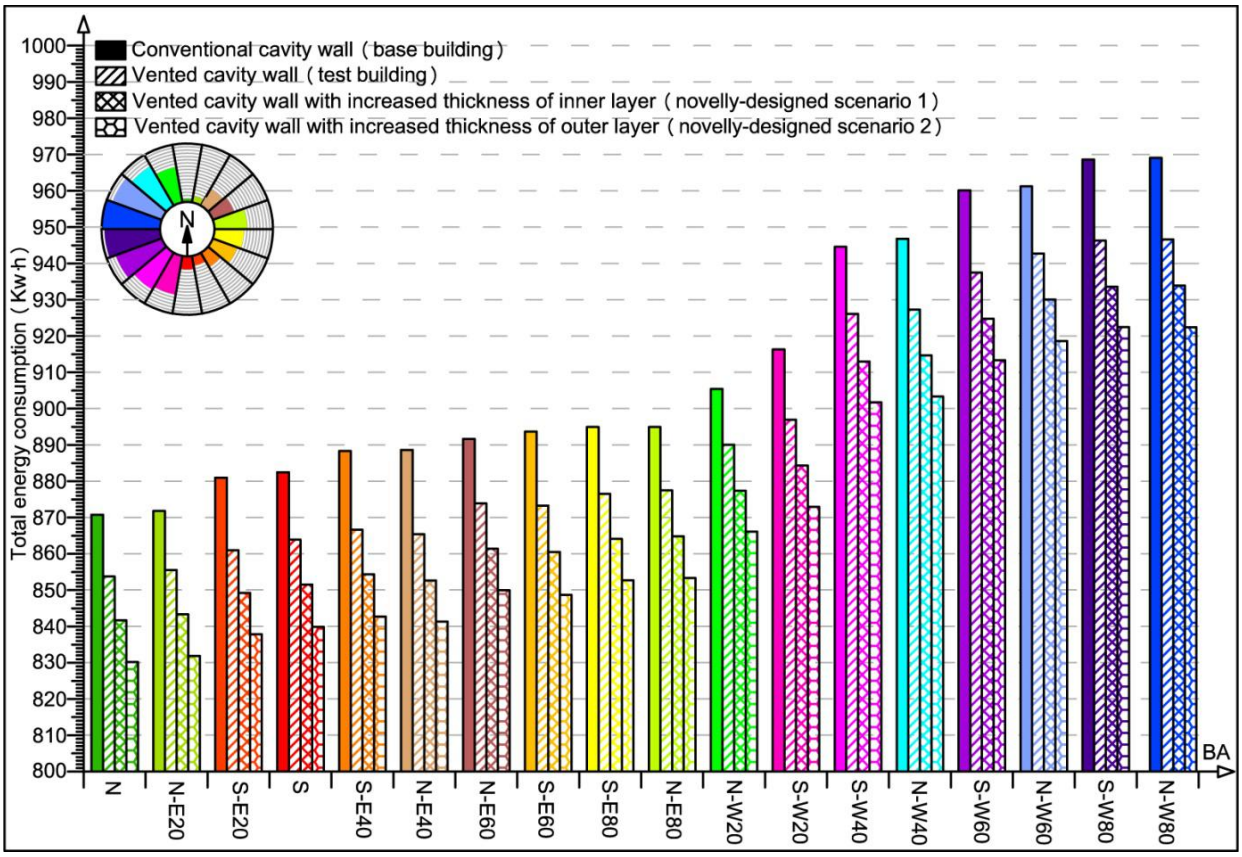

Fig. 8.11 Total energy consumption in each of the building models with various wall type-building azimuth combinations

8.5 Validation of computational results

In this chapter, the accuracy of computational results were verified by two validation techniques. The first is validation of air temperature accuracy, by comparing them with data obtained from field measurements. Another accuracy validation was conducted for energy consumption, which are compared with data generated from experimentation in a real dwelling.

8.5.1 Validation of air temperature: Ecotect versus filed measurement

For verifying the computational accuracy of air temperature from Ecotect, the computed results were compared with the measurement data. The real building selected to perform the indoor air temperatures is base building (Fig. 8.2). As shown in Fig. 8.12, both the indoor air temperatures and outdoor temperatures from Agu 4th, 2018 to Agu 11th, 2018 were compared. The biases of these two sets of data are slight in general, especially two sets of outdoor air temperature data. While, for the different percentage between two sets of the indoor air temperature is lager compared with that of the indoor air temperature. The average deviation during the testing days of outdoor temperatures is 2.1% and that of indoor temperatures is 1.4%.

In accordance with suggestion from Reeves et al. [13] and Maamari et al. [14], the accepted percentage of bias error should be ranged in the scope of ±15% for the simulation results to be regarded accurate. The percentages of bias errors for two sets of air temperature data are both less than 15%, which are clearly within the accepted range.

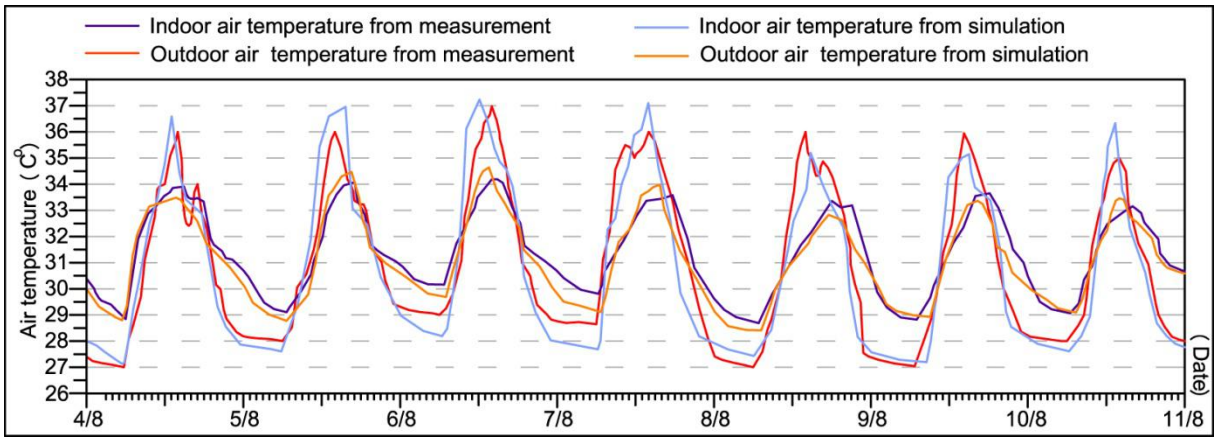

Fig. 8.12 Comparison of air temperature from Ecotect and filed measurement

8.5.2 Validation of energy consumption: ArchiWIZARD versus real experimentation

Also, the base building was chosen as the experimental building to investigate the air conditioning energy consumption from Agu 4th, 2018 to Agu 11th, 2018. Since the building model with five bays was selected in simulation, the average electricity use for each bay was calculated as 20% of the total electricity use. The real experimental dwelling in Sizhai village is facing north by east 20°. Thus, the air conditioning energy consumption for N-E 20 in simulation was chosen baseline.

In the experimental room, it was equipped with a hanging air conditioner with variable frequency model in terms of cooling-heating exchange (Type: F360, cooling power: 855(130-1360) W, heating power: 760 W) (Fig. 8.13), whose level of energy efficiency is the third grade in China. The running schedule assigned to this air conditioner was the same with that in simulation. The initial value in the electricity meter before running the air conditioner was 6.09 kW·h (Fig. 8.14), and it was read at 8:00 a.m. once a day during the experimental days. This is because after 8:00 a.m. in the morning, air conditioners were not turned on by occupants.

In can be seen from Fig. 8.15 that the percentage differences of energy consumption during the testing days between experimentation and simulation are comparatively slight, with 2 kW·h, 4 kW·h, 3 kW·h, 1 kW·h, -3 kW·h, 1,5 kW·h on Agu 4th, 2018 to Agu 11th, respectively. The average percentage difference of energy consumption during the testing days between experimentation and simulation is 7.8 %, which is also clearly within the accepted range in this chapter.

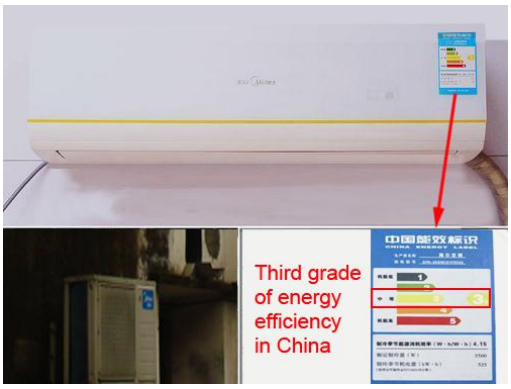

Fig. 8.13 Details of air conditioner used in the experimental building in Sizhai village

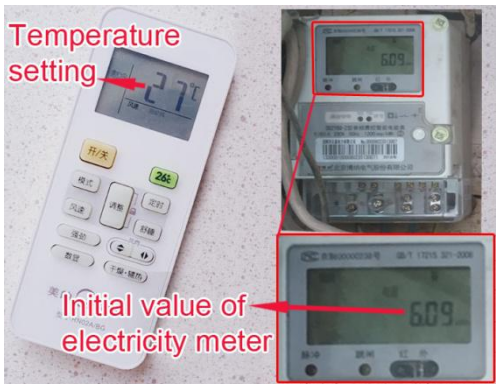

Fig. 8.14 Temperature setting of air conditioner and data collection from electricity meter

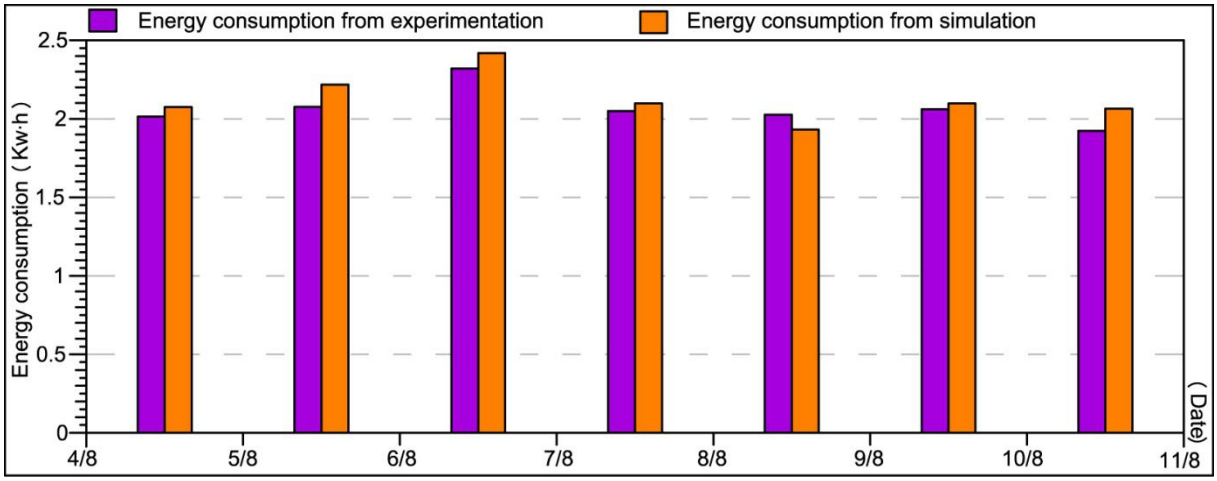

Fig. 8.15 Comparison of energy consumption from ArchiWIZARD and real experimentation

8.6 Conclusion

In this chapter, the vented cavity brick wall in the traditional dwellings situated in Sizhai vallage was researched, for assessing its passive cooling performance. Then, the comparison of wall surface temperatures and air temperatures, through in-situ measurements, between conventional cavity brick wall and vented cavity brick wall was conducted, to investigate the cooling effectiveness of vented wall. Furthermore, we proposed two another new designs for vented cavity brick wall, in consideration of thermal insulation performance. The prototype of geometric models used to perform energy simulation was derived from the traditional dwellings in Sizhai village. Through the building energy simulation, the most outstanding performance of wall type in terms of energy saving was recommended to be the vented cavity wall with increased outer layer thickness.

(1) The vented walls depend on the heat pressure in air channel and the natural ventilation can realize heat convection. This is because that the low-temperature air flows into the channel inside wall through lower vent and is

expelled from upper vent, which is helpful for dissipating the stored heat in brick wall to exterior. Thus, the vented wall contributes to reduction in the heat flowing through wall during summer.

(2) Except for a small proportion of the testing periods after sunrise, T_{al} in the case building are always greater than T_{v1} and T_{v1} in the test building. The maximum air temperatures in channel and two vents always emerged at between 15:00 p.m.-17:00 p.m.. However, the time of peak values of T_{v1} and T_{v1} are earlier than those of T_{al}.

(3) In summer, the mean indoor air temperatures for east orientations are lower than those for west orientations. The three recommended building azimuth intervals for the buildings with four wall types are all observed for N, N-E 20, S-E 40.

(4) Regarding winter, the mean indoor air temperatures for south orientations are higher than north orientations. The three best building azimuth intervals for the buildings with four types of walls are all observed for S-W20, S, S-W40.

(5) The cooling energy consumption is directly proportional to the indoor air temperatures. The cooling energy costs in all buildings with vented wall have different levels of reduction. Moreover, the novelly-designed scenario 2 consumed the least cooling energy.

(6) As opposed to cooling energy consumption, the heating energy consumption is inversely proportional to the indoor air temperatures. Since the vents in test buildings were sealed during winter, their heating energy costs for all building azimuths are the same with those in the base buildings. Also, the least heating energy consumption was observed for the novelly-designed scenario 2.

(7) Among the four wall types, the maximum total energy consumption for various building azimuths always occurs in base buildings, while the minimum values are observed for the novelly-designed scenario 2. Although increasing the inner layer thicknesses of walls results in storing more cool or heat energy from rooms, this method contributes to less total energy cost in each of the building models of novelly-designed scenario 1, compared with base buildings and test buildings.

The research results are thus expected to contribute to some state-of-the-art knowledge and facilitate the further researches on improving the passive cooling efficiency and enhancing thermal insulation property of walls in cooling-load dominated buildings. Furthermore, based on this research, we aim at providing some advice on wall construction design decisions to both newly-built construction and retrofit of the rural residences with various building orientations.

References

[1] A. Reilly, O. Kinnane. The impact of thermal mass on building energy consumption [J]. *Appl. Energy*, 2017, 198 (4): 108-121.

[2] M.K. Dixit, J.L. Fernández-Solís, S. Lavy, C.H. Culp. Identification of parameters for embodied energy measurement: A literature review [J], *Energy Build.*, 2010, 42(2): 1238-1247.

[3] F. Abbassi, N. Dimassi, L. Dehmani. Energetic study of a Trombe wall system under different Tunisian building configurations [J]. *Energy Build.*, 2014, 80: 302-308.

[4] K.K.W. Wan, D.H.W. Li, D. Liu, J.C. Lam. Future trends of building heating and cooling loads and energy consumption in different climates [J]. *Build. Environ.*, 2011, 46 (1): 223-234.

[5] Balaras CA, Droutsa K, Argiriou AA, Asimakopoulos DN. Potential for energy conservation in apartment buildings [J]. *Energy Build.*, 2000, 31(2): 143-154.

[6] A. Dombayci, Ö. Atalay, S. Güven Acar, E. Yilmaz Ulu, H. Kemal Ozturk. Thermoeconomic method for determination of optimum insulation thickness of external walls for the houses: Case study for Turkey [J]. *Sustain. Energy Technol. Assessments*, 2017, 22 (5): 1-8.

[7] Fang'ai Chi, Jianxun Zhang, Gaomei Li, Zongzhou Zhu, Dewancker Bart. An investigation of the impact of Building Azimuth on energy consumption in sizhai traditional dwellings[J]. *Energy*, 2019, 180(8): 594-614.

[8] Fang'ai Chi, Iryna Borys, Lei Jin, Zongzhou Zhu, Dewancker Bart. The strategies and effectiveness of climate adaptation for the thousand pillars dwelling based on passive elements and passive spaces [J]. *Energy and Buildings*, 2019, 183(1): 17-44.

[9] YANG R, LIU Y S, LONG H L, et al. Spatial distribution characteristics and optimized reconstructing analysis of rural Settlement in China [J]. *Scientia Geographica Sinica*, 2016, 36(2): 170-179.

[10] F. Mazzichi, M. Manzan. Energy and daylight interaction in offices with shading devices, in: Proc. of 1st IBPSA Italy Conference, Bolzano, IT, 2013.

[11] GUO L M. Calculation and distribution of solar radiation on the wall in Zhejiang Province [J]. *Energy Engineering*, 1984(4): 27-30.

[12] Li Wenjie. A Thesis Submitted to Chongqing University in Partial Fulfillment of the Requirement for the Degree of Doctor of Engineering [D]. Chongqing: Chongqing University, 2010: 3.

[13] Reeves T, Olbina S, Issa R. Validation of building energy modeling tools: Ecotect™, Green Building Studio™ and IES™. In: Laroque C, Himmelspach J, Pasupathy R, Rose O, Uhrmacher AM, editors. Proceedings of the 2012 Winter Simulation Conference. Berlin: Germany; 2012.

[14] Maamari F, Andersen M, de Boer J, Carroll W, Dumortier D, Greenup P. Experimental validation of simulation methods for bi-directional transmission properties at the daylighting performance level [J]. *Energy and Buildings*, 2006, 38(7): 878-89.

Chapter 9

Conclusion

9.1 Research results

In chapter 1, the rural residences in China were selected as the research subjects in this work. Then the intersection area of dwelling zone with brick-wood structure and hot summer and cold winter climate zone, which is within East and Central China, was chosen as the research region, thanks to the substantial quantity of traditional villages recorded in the Catalogs, high electricity use and complicated pattern of building energy consumption in the east of China. The Sizhai traditional village located in the east of Zhejiang Province was recorded in the First Edition of Traditional Villages' Catalog, with large scale and well-protected conditions, was chosen as the representative house samples for researching the energy consumption in the rural residences.

In chapter 2, the literature studies on characteristics of the traditional dwellings, impact of building azimuth on the energy consumption, impact of shading devices with various shading depth and building azimuth combinations on the energy consumption, and impact of shading devices with various window-to-wall ratio and building azimuth combinations on the energy consumption, as well as impact of walls with various wall construction type and building azimuth combinations on the energy consumption were performed in this section.

In chapter 3, the simulation model dimensions, division of building azimuth interval, division of shading depth interval, division of window-to-wall ratio interval, design of wall constructions, design day data assumed in simulation and selection of simulation tool were illustrated in this section.

In chapter 4, by taking the Thousand Pillars Dwelling situated in the Sizhai village as the study building, characteristics of the traditional dwellings in the research region were analyzed. The air temperatures, relative humidities, air velocities and illuminance in diverse parts of Thousand Pillars Dwelling were carried out to research their effectiveness of climate adaptation. The results show that passive elements and passive spaces are effective at mitigating the impact of outdoor climate on internal spaces, which is helpful for the Extension of Indoor Comfort Time by 3,472 h per year.

In chapter 5, the electricity consumption of air conditioning, mechanical ventilation and artificial lighting, as well as the total annual electricity consumption including air conditioning, mechanical ventilation and artificial lighting were computed by software to explore the optimum building azimuth. The results show that a total annual electricity cost difference of approximately 150 kW·h throughout a year between the best (S) and worst (N-W80) BA of the building was achieved. By performing building azimuth measurements for all dwellings in Sizhai village, the conclusion is that this village has a comparatively high energy saving potential.

In chapter 6, the total energy consumption, including the artificial lighting and air conditioning, in the test scenarios with different shading depth and building azimuth combinations was demonstrated to be disparate, under

reasonable assumptions in the energy simulation. Then the optimum shading depth was recommended for each building azimuth interval, based on the criteria of energy cost and indoor daylighting standard. Furthermore, a new evaluation method that assesses the energy saving potentials of buildings was proposed, taking the shading depth as evaluation parameter.

In chapter 7, the integrated models were first erected, which were coupled the various window-to-wall ratios with angle rotations in building azimuth, for the traditional dwellings. The total energy consumption, including the artificial lighting and air conditioning, in the test scenarios with different window-to-wall ratio and building azimuth combinations was demonstrated to be dissimilar. Then the optimum window-to-wall ratios were recommended for each building azimuth interval, based on the criteria of energy cost and indoor daylighting standard. Furthermore, a new evaluation method used for assessing the building energy saving potential was proposed, on the basis of the evaluation parameter of window-to-wall ratio.

In chapter 8, the cavity brick walls in were set two vents (i.e., upper vent and lower vent), aiming at accelerating their heat dissipation, as well as improving indoor thermal comforts and energy saving potentials. According to the in-situ measurements, the vented walls have better performance in terms of the passive cooling. Furthermore, based on the vented wall system, two novelly-designed scenarios were proposed, so as to enhance the walls' heat insulation property. Based on the research results, the most desirable of the wall construction type was recommended.

For facilitating to understand the research results of this work, the summaries were listed in Table 9.1 and Table 9.2. The optimum building orientation scope was observed for the S-E20, based on the 4 evaluation criteria of energy consumption impacted by building azimuth, shading depths window-to-wall ratios and wall construction type.

Table 9.1 Summary of search results based on four building parameters

Designation	**S-W80**	**S-W60**	**S-W40**	**S-W20**	**S**	**S-E20**	**S-E40**	**S-E60**	**S-E80**
Building azimuth					(1)	(2)	(3)		
Shading depth (m)	2.37	2.37	2.12	2.12	1.37	1.62	2.12	2.12	2.12
Window-to-wall ratio	0.2	0.2	0.2	0.2	0.2	0.2	0.2	0.2	0.2
Wall type	❹	❹	❹	❹	❹	❹	❹	❹	❹
Designation	**N-W80**	**N-W60**	**N-W40**	**N-W20**	**N**	**N-E20**	**N-E40**	**N-E60**	**N-E80**
Building azimuth									
Shading depth (m)	2.37	2.37	2.37	2.37	2.37	2.37	2.37	2.37	2.37
Window-to-wall ratio	0.2	0.2	0.2	0.2	0.2	0.2	0.2	0.2	0.2
Wall type	❹	❹	❹	❹	❹	❹	❹	❹	❹

Notes: 1. (1), (2) and (3) stand for the three building azimuth intervals with highest energy saving potential in sequence. 2. 1.37, 1.62, 2.12 and 2.37 are the shading depth for the corresponding building azimuth intervals. 3. 0.2 presents the window-to-wall ratio for the corresponding building azimuth intervals. 4. ❹ stands for the fourth designed wall type (i.e., vented cavity wall with increased outer layer thickness).

Table 9.2 Summary of optimum building azimuth interval recommend in this work

Designation	Building azimuth	Shading depth	Window-to-wall ratio	Wall construction
Optimum building azimuth interval	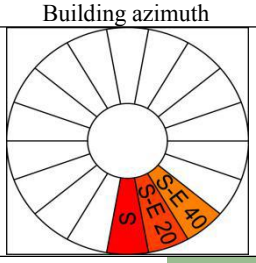	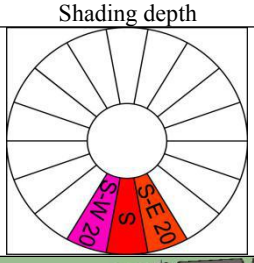	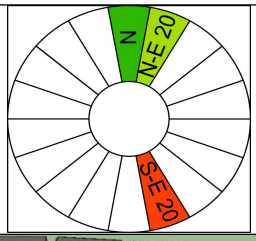	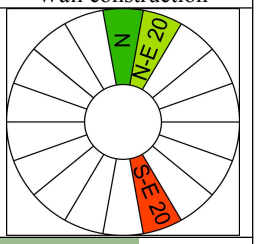
Optimum building azimuth interval based on the 4 parameters	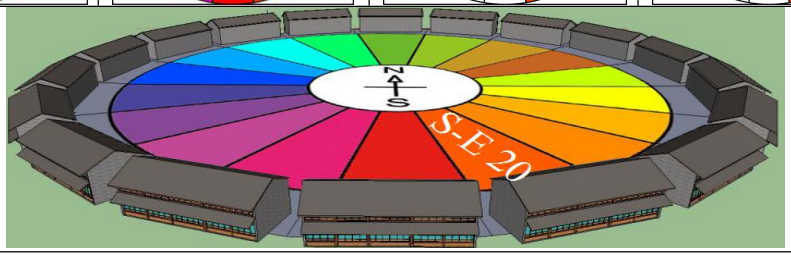			

9.2 Research findings

This study focuses on the impacts of building azimuth, shading device and window system on the indoor daylighting, air temperatures and building energy consumption. The optimum building azimuth interval, compromised depth of shading device for each building azimuth interval and compromised window-to-wall ratio for each building azimuth interval were summarized in this work, based on the daylighting standard issued by the Ministry of Housing and Urban-Rural Development of China, and the energy consumption performance.

9.2.1 Optimum building azimuth

The three building azimuth intervals with the highest energy saving potentials are observed for S, S-E20 and S-E40 in sequence.

9.2.2 Optimum shading depth recommended for each building azimuth interval

The optimal SDs for S and S-E 20 are 1.37 m and 1.62 m respectively, and those for S-E 40, S-E 60, S-E 80, S-W 20 and S-W 40 are all 2.12 m, as well as those for the other 11 BAs are all 2.37 m, based on the criteria of the energy consumption and lighting quality.

9.2.3 Optimum window-to-wall ratio recommended for each building azimuth interval

The optimal WWRs for 18 building azimuth intervals are all 0.2, based on the criteria of the energy consumption and lighting quality.

9.2.4 Optimum wall construction type recommended for each building azimuth interval

The indoor air temperatures and energy consumption behaviors in the novelly-designed scenarios 2 (i.e., vented wall with increased outer layer thickness) were the most desirable.

9.3 Contributions

Since the building energy saving can be achieved by selecting optimum building orientation, shading device with a proper depth and appropriate glazing area on the facade, this study results aim at providing some references on building azimuth's, depth of shading device's and window-to-wall ratio's determination to both newly-built constructions and to retrofit projects of the rural residences.

Furthermore, three evaluation parameters based on building azimuth, shading depth and window-to-wall ratio were proposed, for the sake of supplying some new approaches to estimate the energy saving potential of a building. Moreover, the traditional dwellings as case studies in this work, can supply some new bodies of knowledge to fill in the gap of this field.

9.3.1 Application of optimum building azimuth to both newly-built buildings and existing buildings

(1) Newly-built buildings: the optimum building orientations were recommended for them in the design phase, which are located in the research region.

(2) Existing buildings: the evaluation of the energy saving potential at village scale can be conducted, by measuring all the existing building's building azimuth in the target village.

9.3.2 Application of optimum shading depth to both newly-built buildings and existing buildings

(1) Newly-built buildings: the optimum shading depths were recommended for them with different building orientations in the design phase, which are located in the research region.

(2) Existing buildings: the evaluation of the energy saving potentials can be conducted for them, based on the evaluation parameter of shading depth.

9.3.3 Application of optimum window-to-wall ratio to both newly-built buildings and existing buildings

(1) Newly-built buildings: the optimum window-to-wall ratios were recommended for them with different building orientations in the design phase, which are located in the research region.

(2) Existing buildings: the evaluation of the energy saving potentials can be conducted for them, based on the evaluation parameter of window-to-wall ratio.

9.3.4 Application of optimum wall construction type to both newly-built buildings and existing buildings

(1) newly-built buildings, the optimum all construction is recommended for each of them with different building orientations, which are located in the research region.

(2) existing buildings: some suggestions on improvement of walls' thermal insulation can be supplied for existing buildings.

Acknowledgements

After three years' study for architecture design and building energy costs in the traditional dwellings, this dissertation was finally accomplished. Without of the help from many people, it could never be completed, thus here I would like to express my sincere gratitude towards them.

First and foremost, I owe my heartfelt appreciation to my distinguished and cordial supervisor, Professor Bart Dewancker, who influenced me by his insightful ideas and meaningful inspirations, and guided me by academic advice and feasible instructions, as well as enlightened me while I was confused during the writing process. His thought-provoking comments and patiently encouragements were indispensable for my accomplishment of this dissertation. My selection of the research direction that is the building energy costs in the traditional dwellings, as the research theme, is deeply motivated by his profound knowledge. Without his dedicated assistance and insightful supervision, this dissertation would have gone nowhere.

Then, my faithful appreciation also goes to the prestigious and distinguished teachers of Professor Weijun Gao, and Professor Hiroatsu Fukuda, whose splendid and diversified lectures have empowered me the building energy knowledge and upright academic attitude.

Ultimately, thanks go to my parents who are my mentors and guardians from the very beginning in primary school. Without their refined education and care, I could never grow up in such a joyous and cozy environment, nor have the courage to confront any obstacles on my way to success.